Emergency Musculoskeletal Imaging in Children

Leonard E. Swischuk
Siddharth P. Jadhav

Springer

Emergency Musculoskeletal Imaging in Children

Leonard E. Swischuk
Siddharth P. Jadhav

Emergency Musculoskeletal Imaging in Children

Springer

Leonard E. Swischuk, MD
Department of Radiology
University of Texas Medical Branch
Pediatric Radiology
Galveston, TX
USA

Siddharth P. Jadhav, MD
The Edward B. Singleton
Department of Pediatric Radiology
Texas Children's Hospital
Houston, TX
USA

ISBN 978-1-4614-7746-4 ISBN 978-1-4614-7747-1 (eBook)
DOI 10.1007/978-1-4614-7747-1
Springer New York Heidelberg Dordrecht London

Library of Congress Control Number: 2013946241

© Springer Science+Business Media New York 2014
This work is subject to copyright. All rights are reserved by the Publisher, whether the whole or part of the material is concerned, specifically the rights of translation, reprinting, reuse of illustrations, recitation, broadcasting, reproduction on microfilms or in any other physical way, and transmission or information storage and retrieval, electronic adaptation, computer software, or by similar or dissimilar methodology now known or hereafter developed. Exempted from this legal reservation are brief excerpts in connection with reviews or scholarly analysis or material supplied specifically for the purpose of being entered and executed on a computer system, for exclusive use by the purchaser of the work. Duplication of this publication or parts thereof is permitted only under the provisions of the Copyright Law of the Publisher's location, in its current version, and permission for use must always be obtained from Springer. Permissions for use may be obtained through RightsLink at the Copyright Clearance Center. Violations are liable to prosecution under the respective Copyright Law.
The use of general descriptive names, registered names, trademarks, service marks, etc. in this publication does not imply, even in the absence of a specific statement, that such names are exempt from the relevant protective laws and regulations and therefore free for general use.
While the advice and information in this book are believed to be true and accurate at the date of publication, neither the authors nor the editors nor the publisher can accept any legal responsibility for any errors or omissions that may be made. The publisher makes no warranty, express or implied, with respect to the material contained herein.

Printed on acid-free paper

Springer is part of Springer Science+Business Media (www.springer.com)

Preface

This book primarily addresses the detection of more subtle and frequently missed fractures. There is no attempt to cover all fractures, especially those that require imaging simply to confirm their presence or visualize the precise position of the fractured fragments. In keeping with this, there also is emphasis on evaluation of the soft tissues and periarticular fat pads, which can focus one's attention on the site of bony injury that is not readily apparent. The value of comparative views also is emphasized. Musculoskeletal MR is included to emphasize its futuristic and expanding role in the Emergency Room and acute care setting. The focus will be on what is different in children and not a simple replication of what occurs in adults. In particular, instances where MR imaging affects management will be discussed. Other pathologies, including infection and tumors that may present in the acute care setting will be briefly addressed.

Galveston, TX, USA — Leonard E. Swischuk, MD
Houston, TX, USA — Siddharth P. Jadhav, MD

Contents

1 General Considerations 1
What Views Should Be Obtained? 1
Utilizing the Soft Tissues 2
Significance of Intra-articular Fluid 2
Role of MRI 2
References 3

2 Infection/Inflammation and Infarction 5
Osteomyelitis, Pyomyositis, and Cellulitis/Fascitis 5
Bone Infarction 9
Pyomyositis 11
References 17

3 Tumors, Cysts, and Tumor Mimickers 19
References 29

4 Types of Fractures in Children 31
Types of Fractures Seen in Children 31
Role of MRI 35
Epiphyseal–Metaphyseal (Salter–Harris) Fractures 35
Stress Injuries and Fractures 35
References 38

5 Shoulder and Upper Arm 41
Normal Soft Tissues 41
Joint Fluid 41
Clavicular Injuries 41
Upper Humerus Injuries 42
Scapular Fractures 48
Normal Findings Causing Problems 58
Humeral Shaft Injuries 58
References 59

6 Elbow and Forearm 61
Normal Soft Tissues and Fat Pads 61
Elbow Fractures and Injuries 61
Injuries of the Distal Humerus 63
Injuries of the Proximal Radius 71
Injuries of the Proximal Ulna 75

Dislocation of the Elbow 79
Osteochondritis Dissecans of the Elbow 79
Normal Variations Causing Problems 80
Injuries of the Forearm. 80
Normal Variations Causing Problems 81
References 90

7 Wrist and Hand 91
Injuries of the Wrist 91
Evaluation of Fat Pads and Soft Tissues 91
Determining the Presence of Fluid in the Wrist Joint 91
Injuries of the Distal Radius and Ulna. 91
Injuries of the Carpal Bones 92
Carpal Bone Dislocation 96
Normal Findings Causing Problems 97
Injuries of the Hand 97
Evaluation of the Fat Pads and Soft Tissues 97
Detecting Fluid in the Small Joints of the Hand 100
Injuries of the Metacarpals and Phalanges. 100
Normal Findings Causing Problems 102
References 118

8 Pelvis and Sacrum 121
Fractures of the Sacrum 121
Fractures of the Pelvis 121
Normal Findings Causing Problems 122
References 128

9 Hip and Femur/Femoral Shaft 129
Normal Fat Pads and Joint Space. 129
Detecting Fluid in the Hip Joint. 129
Injuries of the Upper Femur. 129
Legg–Perthes Disease 131
Slipped Capital Femoral Epiphysis (SCFE) 133
MRI of the Hip and Thigh 134
Femoral Shaft. 135
References 139

10 Knee and Leg 141
Normal Fat Pads and Soft Tissues 141
Detection of Fluid in the Knee Joint 141
Injuries of the Distal Femur and Proximal Tibia and Fibula 141
Patellar Fractures and Dislocations 143
Normal Findings Causing Problems 162
Injuries of the Lower Leg (Midshafts of the Tibia and Fibula) . . . 165
Normal Findings Causing Problems 165
References 180

11 Ankle and Foot 183
Ankle 183
Normal Soft Tissues and Fat Pads of the Ankle 183
Detecting Fluid in the Ankle Joint 183
Injuries of the Distal Tibia and Fibula 183
Injuries of the Tarsal Bones 184
Sprained Ankle. 187
Achilles Tendonitis 187
Plantar Fasciitis and Stone Bruise 188
Osteochondritis Dissecans of the Tarsal Bones 191
Aseptic Necrosis of the Tarsal Bones 192
Normal Variations Causing Problems 192
Foot 193
Normal Soft Tissues and Fat Pads 193
Detecting Fluid in the Small Joints of the Foot 193
Injuries of the Metatarsals and Phalanges 193
Miscellaneous Injuries of the Foot. 203
Normal Findings Causing Problems 205
References 215

12 Battered Child Syndrome/Non-accidental Trauma 217
References 299

Index 231

General Considerations

1

What Views Should Be Obtained?

For the extremities, at least two views, usually at right angles to each other, are necessary and most often consist of frontal and lateral projections of the involved extremity. In addition, in some cases, for example, the wrist, ankle, hand, and the foot, a third oblique view is fairly well standard. In the shoulder, internal and external rotation views are obtained, while in the hip, AP and frog-leg views are standard. In addition, it is of considerable benefit to obtain comparative views of the other (normal) side. They are very useful for the detection of subtle findings and fractures [1–5].

Over the years, there has been some movement towards discouraging the routine use of comparative views, but in this regard, in a summary on the subject in a report by the Committee on Radiology of the American Academy of Pediatrics, so many loopholes in the premise that comparative views are not required were identified that the loopholes virtually destroyed the original premise. To this end, and quoting directly from their report [6], the following is presented.

"Injury to the hip joint" is a notable exception to the selective approach; at least one view should routinely include the normal hip, with the gonads shielded. *Hip injuries in children are most frequently associated with joint effusion*, *which can be detected only with comparing similar measurements of the opposite joint space*.

Other specific areas of the appendicular skeleton may require more comparative views. The elbow, with a relatively large number of ossification centers appearing at widely varying times, *may prove confusing even to the experienced radiologist*; *comparison view of this joint may be requested frequently*. *Detection of joint effusion in the knee and ankle may necessitate a comparison view*, *in at least one projection*. *Comparison views may also be helpful in evaluating the tissue planes and subcutaneous fat in suspected inflammatory conditions of the soft tissues or* "bones."

Finally, a conclusion from the same communication suggests that no one uniform policy can be expected for all individuals dealing with pediatric trauma: "A number of theoretical and practical considerations will continue to determine the use of comparison views. Personal conviction based on experience and training is the major theoretical consideration. Practical considerations include the availability of radiologic consultation, the expertise of the physician who initially interprets the study, and clinical demands. An individual's policy toward the use of comparison images is a balance of these considerations." This latter sentence is probably the most important in this ongoing controversy. Do what you have to do, but be sure in your mind that you will not miss any fractures when you obtain views of the injured side only. One might ask, "How sure am I that I am not missing a bending fracture, a subtle Salter–Harris type I injury, or a minimal buckle fracture?"

Now, what about cost and radiation exposure encumbered with the use of comparative views? In our study [1], it was demonstrated that the cost of obtaining hardcopy comparative views was

L.E. Swischuk, S.P. Jadhav (eds.), *Emergency Musculoskeletal Imaging in Children*,
DOI 10.1007/978-1-4614-7747-1_1, © Springer Science+Business Media New York 2014

negligible and so was the risk of radiation injury to the patient. Indeed, it is difficult to construct a case against comparative views if one wants to be able to detect subtle injuries. *This is especially true if one does not look at pediatric images on a full-time basis*. How did I (LES) come to use comparative views? A number of decades ago, I was placed in charge of pediatric radiology in a teaching hospital. One of the first things that came to my attention was that I was calling kids back for repeat X-rays or X-rays of the other extremity to decide whether a fracture was present. This seemed to be redundant and inconvenient and indeed, not necessary. So I decided that comparative views should be obtained during the first imaging encounter.

Utilizing the Soft Tissues

Evaluating soft tissue changes in trauma and infection of the extremities in childhood, and even in adulthood, is invaluable [7]. The findings one should look for include localized or generalized soft tissue swelling, obliteration of muscle/fat interfaces, and displacement or obliteration of the periarticular fat pads. Such evaluation of the soft tissues can serve to localize the site of injury or infection. More detailed discussion of the soft tissue changes for each joint/extremity is presented at subsequent points throughout this book.

Significance of Intra-articular Fluid

As a general rule in children, joint fluid in the absence of trauma should be presumed to be pus until proven otherwise. A common and important exception however is the hip joint where transient/toxic synovitis is the most common cause of joint fluid accumulation. In the elbow and ankle, fluid in the joint is manifest by outward displacement of the anterior and posterior fat pads. In the shoulder and hip, fluid accumulation causes lateral displacement of the humerus or the femoral head (more common). As a result there is concomitant joint space widening. This finding is more common in the hip in infants and young children where the ligaments and capsule are not as tight. In the older patient, this finding usually is not present. Knee fluid produces bulging of the suprapatellar bursa, just behind the quadriceps tendon. In the wrist joint, fluid has no specific imaging findings and simply consists of swelling around the wrist.

In the presence of trauma, fluid in the joint should cause one to look more diligently at the bones for evidence of a fracture. In some cases, however, even though the fat pads, soft tissues, and/or the joints spaces are abnormal, a fracture is not seen. In our study on this subject [8], the incidence of missed fracture was low except for the wrist where it was approximately 67 %. In the elbow, the incidence of missed fracture was 15 %. This was corroborated by another study on this subject [9]. However, in another recent article, the incidence of missed fracture in the elbow was said to be around 76 % [10]. This seemed to represent a significant disparity, but when examined, the authors did not use comparative views. As a result, my response to this article was that if you did not take comparative views, and if you did not know where to look for subtle fractures, then the result would be 76 % missed fractures [11]. If, on the other hand, one took comparative views, knew what to look for, and knew how to identify subtle buckle fractures, the result would probably be much more less and indeed around 15 %. Overall, our incidence of missed elbow fractures remains very low.

Role of MRI

The role of MRI in the ER setting is expanding with greater availability of equipment, shorter scan time, and personnel during the day and after hours. While it is important to utilize MRI when necessary, it is equally important not to go overboard with the capabilities of MR imaging. In this age of surging medical costs, use of MRI is justified only if it affects management. This is usually true with specific instances of acute trauma, infections, and pathologic fractures. These situations will be reviewed in subsequent chapters.

References

1. Swischuk LE. Comparative views in childhood fractures. Emerg Radiol. 1997;4:2.
2. John SD, Phillips WA. Imaging evaluation of pediatric extremity trauma, part I: injury patterns of the immature skeleton and imaging modalities. Intensive Care Med. 1998;13:124–34.
3. John SD, Phillips WA. Imaging evaluation of pediatric extremity trauma, part II: upper extremity. Intensive Care Med. 1998;13:184–94.
4. John SD, Phillips WA. Imaging evaluation of pediatric extremity trauma, part III: lower extremity and soft tissues. Intensive Care Med. 1998;13:241–52.
5. Chong-Han CH, Yngve DA, Lee JY, Hendrick EP, John SD, Swischuk LE. Comparison views for subtle physeal injury in the pediatric ankle. Emerg Radiol. 2001;8:207–12.
6. Committee on Radiology. Comparison radiographs of extremities in childhood: recommended usage. Pediatrics. 1980;65:646–7.
7. Curtis DJ, Downey Jr EF, Brower AC, Cruess DF, Herrington WT, Ghaed N. Importance of soft tissue evaluation in hand and wrist trauma: statistical evaluation. AJR Am J Roentgenol. 1984;142:781–8.
8. Swischuk LE, Hayden CK, Kupfer MC. Significance on intra-articular fluid without visible fracture in children. AJR. 1984;142:1261–2.
9. Connelly LF, Klostermeier TT, Klosterman LA. Traumatic elbow effusions in pediatric patients: are occult fractures the rule? AJR. 1998;171:243–6.
10. Skaggs DL, Mirzayan R. The posterior fat pad sign in association with occult fractures of the elbow in children. J Bone Joint Surg Am. 1999;81:A1429–33.
11. Swischuk LE, Skaggs DL, Mirzayan R. The posterior fat pad and use of comparison radiographs in the diagnosis of occult fractures, letter to the editor. J Bone Joint Surg Am. 2001;83:1435–6.

Infection/Inflammation and Infarction

2

Osteomyelitis, Pyomyositis, and Cellulitis/Fascitis

Roentgenographic bony changes in osteomyelitis take 10 days to 2 weeks to develop; therefore, in the early stages, one can only infer the diagnosis from soft tissue changes. Osteomyelitis manifests in deep soft tissue edema as does pyomyositis, while superficial cellulitis demonstrates findings reflecting superficial edema (Fig. 2.1). Because of this, deep edema should suggest the presence of osteomyelitis or pyomyositis until proven otherwise.

After 10–14 days, bony destruction is seen and can manifest as an acute destructive process or a low-grade smoldering problem (low-grade osteomyelitis), which frequently mimics entities such as Ewing's sarcoma and eosinophilic granuloma [1]. More aggressive permeative and "moth-eaten" changes are seen with the former, while with the latter, more reactive bone healing or sclerosis is seen. In addition, although osteomyelitis usually is a metaphyseal problem, it can involve the epiphysis [2, 3]. All of these variations are demonstrated in Fig. 2.2.

If one suspects the presence of osteomyelitis clinically but plain film changes do not support the diagnosis, one should turn to nuclear scintigraphy or MR. With nuclear scintigraphy, the findings are nonspecific but helpful. It should be remembered, however, that the pyrophosphate bone scan measures reactive (healing) bone activity and not bone destruction or the development of a purulent exudate. It is for this reason that in some cases imaging with gallium- or indium-labeled white blood cells [4] may be required to determine whether an infection is present. Finally it should be remembered that in many cases, the technetium bone scan, in the very early stages of the infection, may appear falsely normal [5]. The reason for this is that in such early stages of infection (osteomyelitis), there is so much congestion of the bone marrow by the developing infection that blood flow, and hence the delivery of isotope to the bone (marrow), is impaired. Usually within 24–48 h the bone scan becomes positive. Because of this, if one can make the presumptive diagnosis of osteomyelitis on the basis of clinical and plain film roentgenographic (deep edema) findings, one should assume that such infection is present and begin therapy. The bone scan, delayed a day or two, then will become positive [6].

Ultrasonography also has been used to detect osteomyelitis [7], but the changes demonstrable with ultrasound are usually late changes. They consist of purulent exudate elevating the periosteum from the cortex of the involved bone (Fig. 2.3). They are not very easy to demonstrate, and so overall, MR is becoming more and more popular for the evaluation of occult osteomyelitis where the normal high signal of marrow fat on T1-weighted images is lost, and on the proton-density and T2-weighted images, increased signal is seen (Fig. 2.4).

MRI not only confirms the presence of osteomyelitis but also assesses the extent of bone and soft tissue involvement and the presence of an

L.E. Swischuk, S.P. Jadhav (eds.), *Emergency Musculoskeletal Imaging in Children*,
DOI 10.1007/978-1-4614-7747-1_2, © Springer Science+Business Media New York 2014

abscess. MRI with intravenous contrast is essential to identify medullary, subperiosteal, and/or soft tissue abscess which in turn affects management. Presence of an abscess greater than 1.5 cm in size warrants either imaging-guided or surgical drainage. Smaller abscesses may resolve with antibiotic treatment. The presence and extent of subperiosteal abscess, presence of a sharp zone

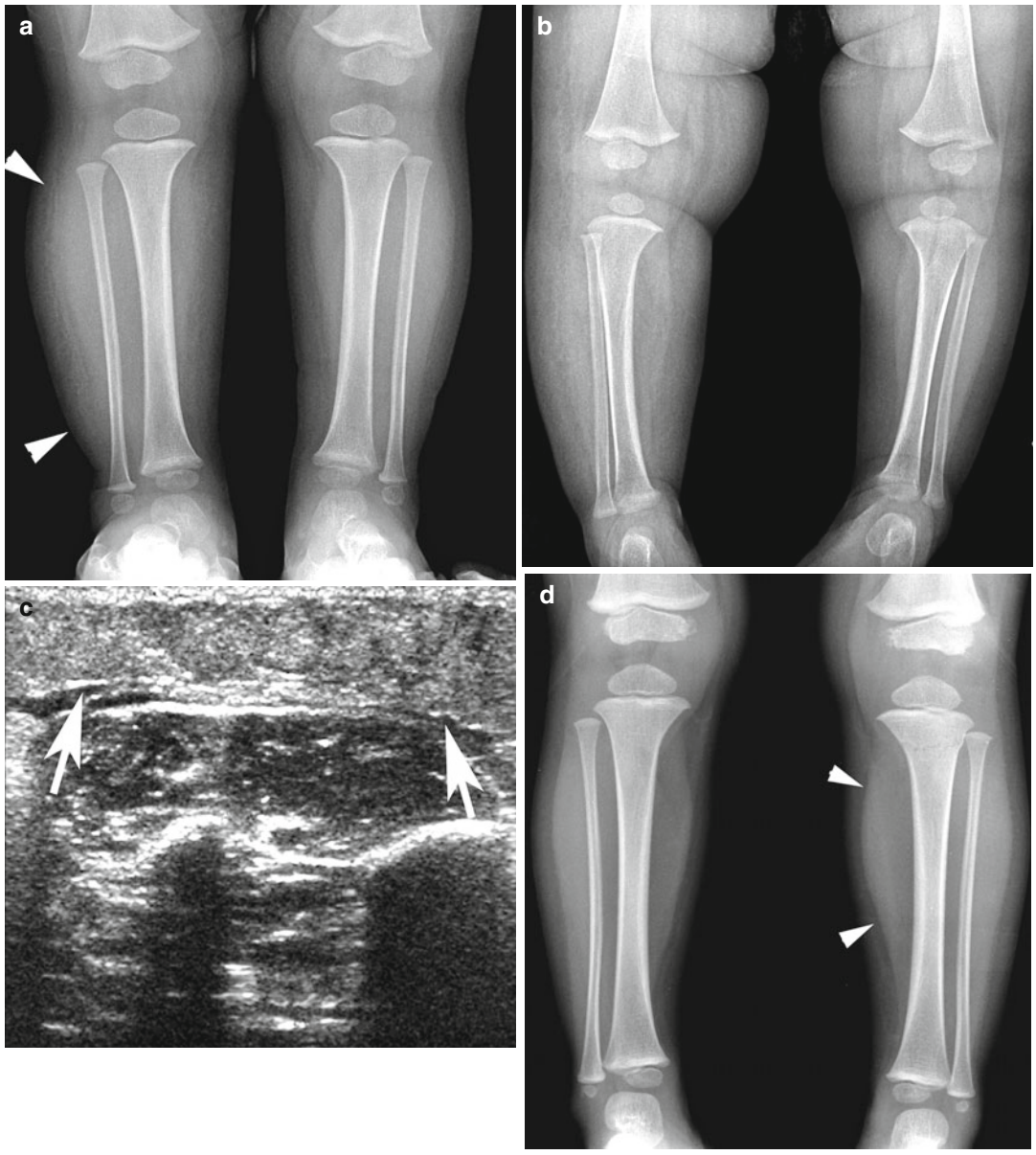


Fig. 2.1 Superficial versus deep edema. (**a**) Superficial edema. Cellulitis of right leg. Note the swollen leg (*arrowheads*). The subcutaneous soft tissues are reticulated but the muscle is still visible as a distinct structure. (**b**) Another patient with superficial edema/cellulitis. Note the swollen right leg, reticulated subcutaneous fatty tissue with preservation of the muscle. (**c**) Ultrasound in the same patient. Note the nodular, heterogeneous appearance of subcutaneous cellulitis (*arrows*). (**d**) Deep edema. Note the expanded deep muscle compartment (*arrowheads*) in the left leg. The subcutaneous soft tissues are intact. This patient had an upper tibial fracture, and the resultant bleeding and edema caused the deep compartment to expand

of abnormal bone marrow enhancement, and presence of intramuscular abscess at initial MRI in cases of acute *Staphylococcus aureus* osteomyelitis has been shown to predict patients at risk of pathologic fracture [8]. Transphyseal extension which is usually seen before 18 months of age or after physeal closure is also well depicted on MRI. This has prognostic implications in terms of early physeal fusion and resultant leg length discrepancy. On MRI, it may be difficult

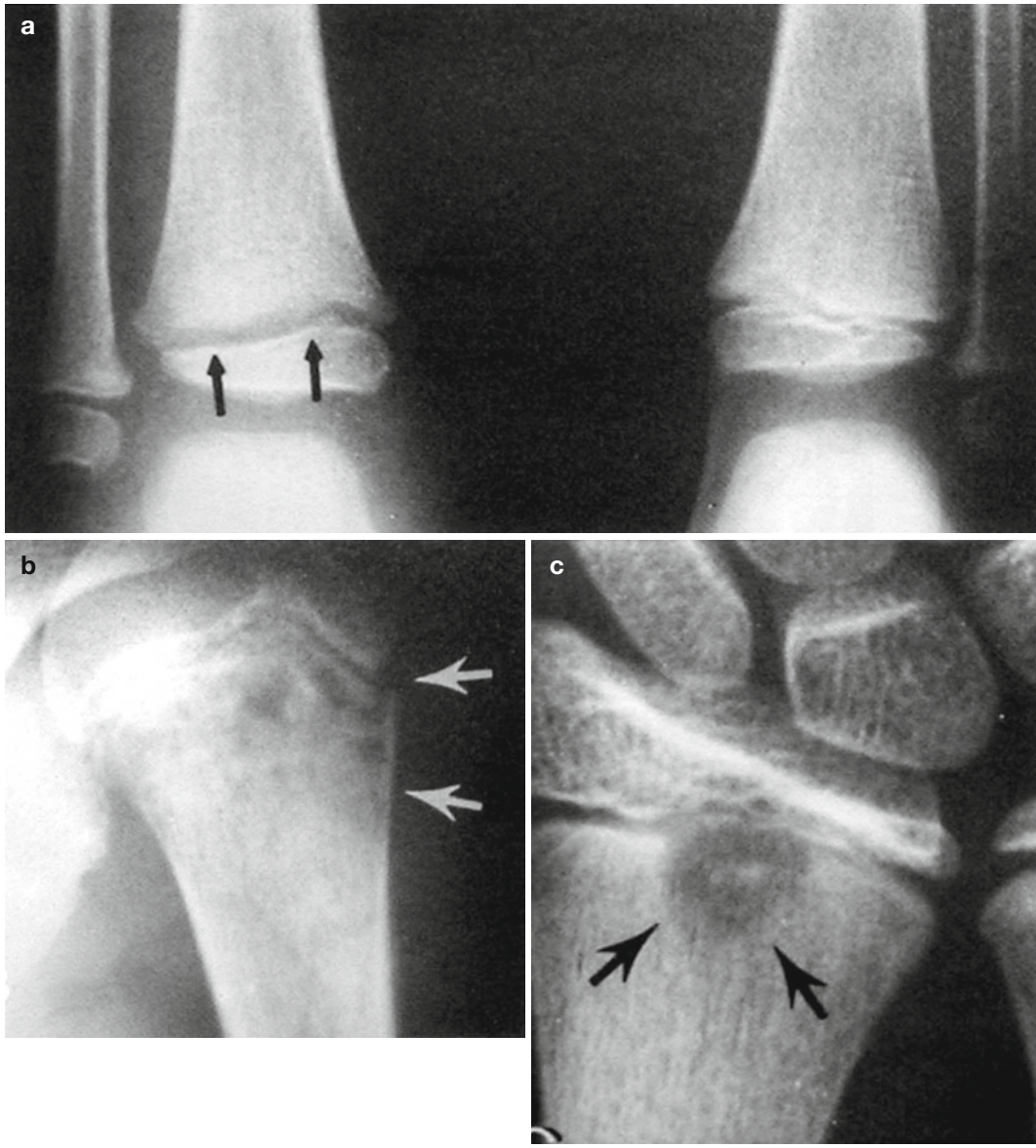


Fig. 2.2 Osteomyelitis, various configurations. (**a**) In this patient there is widening of the epiphyseal plate (*arrows*) due to juxta bony resorption without any significant metaphyseal destruction. (**b**) This patient demonstrates typical permeated metaphyseal bone destruction (*arrows*). (**c**) Less common presentation. Note the focal, relatively distinct area of bony destruction (*arrows*) extending into the epiphysis. (**d**) Low-grade osteomyelitis (*arrows*) mimicking a nonossifying fibroma or cyst. (**e**) Low-grade diaphyseal osteomyelitis. Note bony expansion, widespread destruction, and loss of cortex (*arrows*) in this patient with low-grade diaphyseal osteomyelitis. The findings mimic Ewing's sarcoma or eosinophilic granuloma

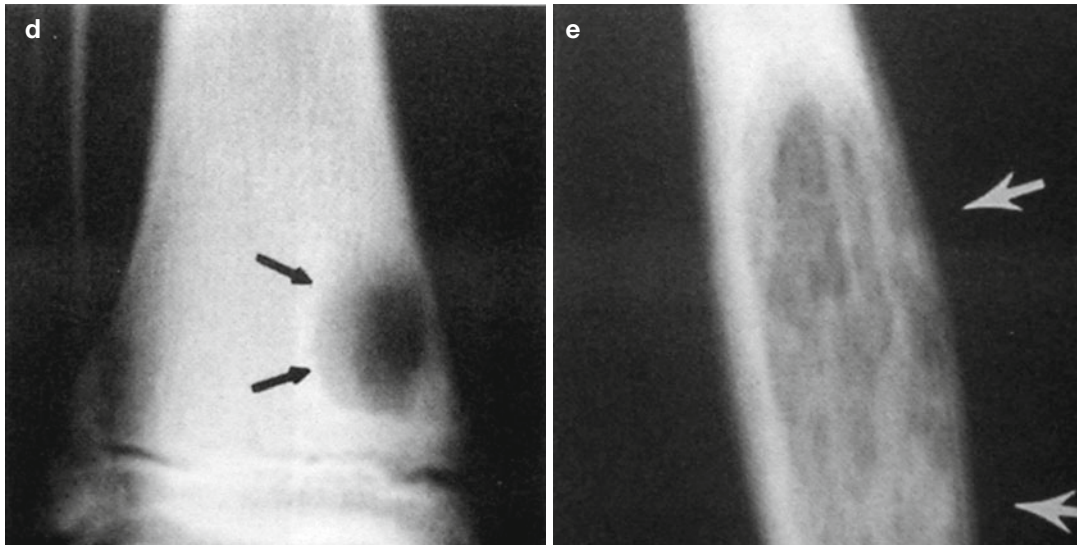


Fig. 2.2 (continued)

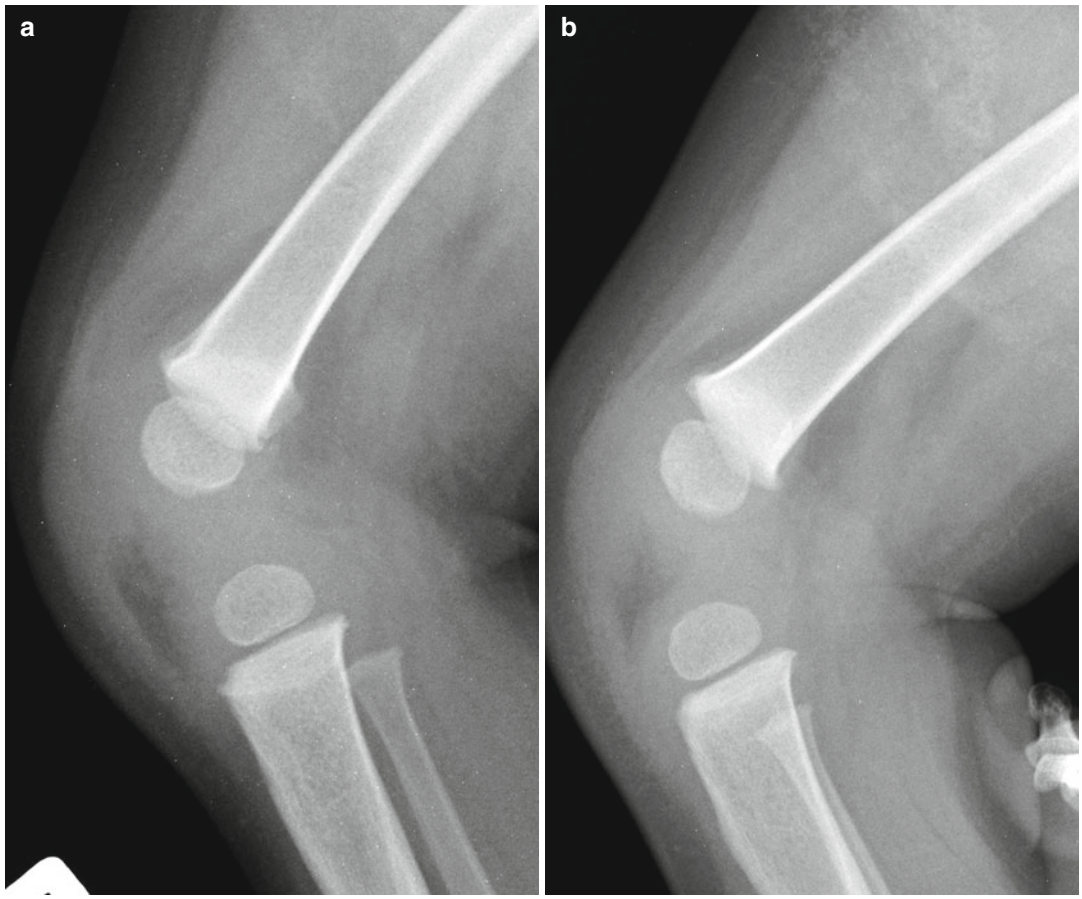


Fig. 2.3 Acute osteomyelitis. Note indistinct fat/soft tissue planes both anterior and posterior to the distal femoral metaphysis. This signifies deep edema. (**b**) Normal side. Compare the normal distinct fat pads with those in (**a**). (**c**) Ultrasound through the distal femur demonstrates a defect in the metaphysis (*arrow*) just above the epiphyseal plate. Also note the subperiosteal purulent material/abscess anterior to the distal cortex (*arrowheads*). (**d**) Later radiograph demonstrates typical bony destruction (*arrow*)

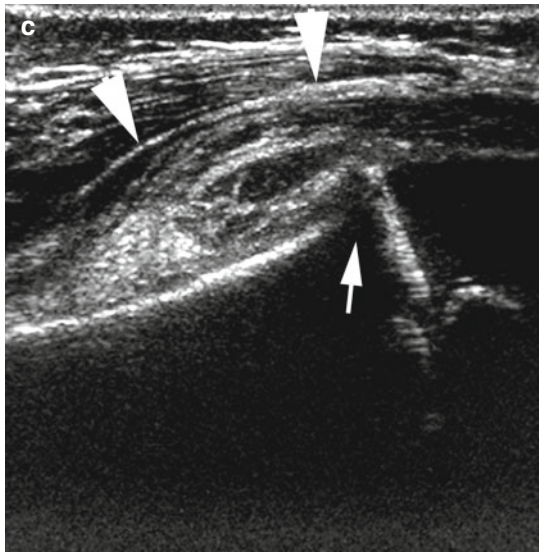




Fig. 2.3 (continued)

to differentiate osteomyelitis from leukemia/lymphoma, neuroblastoma metastasis, and Langerhan cell histiocytosis. Clinical and laboratory correlation and presence of abscesses are helpful in this situation.

Most cases of osteomyelitis in childhood are hematogenous in origin, but some result from puncture wounds, with secondary involvement of the underlying bone. A small number result from osteomyelitis superimposed on a previous fracture [9]. In any event, the bony changes are the same, but it should be noted that osteomyelitis in flat bones (i.e., pelvic bones, clavicle, ribs, scapula) is much more difficult to detect with plain films, and it is in these cases that nuclear scintigraphy, and MR imaging are more useful.

Bone Infarction

Bone infarction, usually a problem in sickle cell disease is difficult to evaluate with imaging. Generally speaking, there is less soft tissue swelling than with osteomyelitis, and on nuclear scintigraphy the area of interest may be negative. However, in the end, the findings often are confusing and close clinical/imaging correlation is required. One exception to the foregoing is the hand/foot syndrome. These patients, who have sickle cell disease, usually come to the attention of the physician because of painful swelling of the hands and/or feet. The swelling and bony changes on plain films can be quite dramatic



Fig. 2.4 Acute osteomyelitis, MR findings. (**a**) In this patient, there is subtle permeative bony destruction (*arrow*) in the distal tibia. (**b**) Coronal STIR MR image demonstrates increased signal in the distal tibia (*arrowhead*) and increased signal in subperiosteal fluid/exudate accumulation medially (*arrows*). (**c**) Coronal MR, gadolinium-enhanced image. Note high signal in the femoral shaft and in the surrounding soft tissues. The proximal epiphysis also has high signal all of which indicates inflammation. Loss of signal in the proximal tibia (X) indicates bone infarction and the arrow points to the early collection of associated subperiosteal purulent exudate. (**d**) Coronal MR, STIR image. Note high signal (*arrows*) in the purulent exudate collection

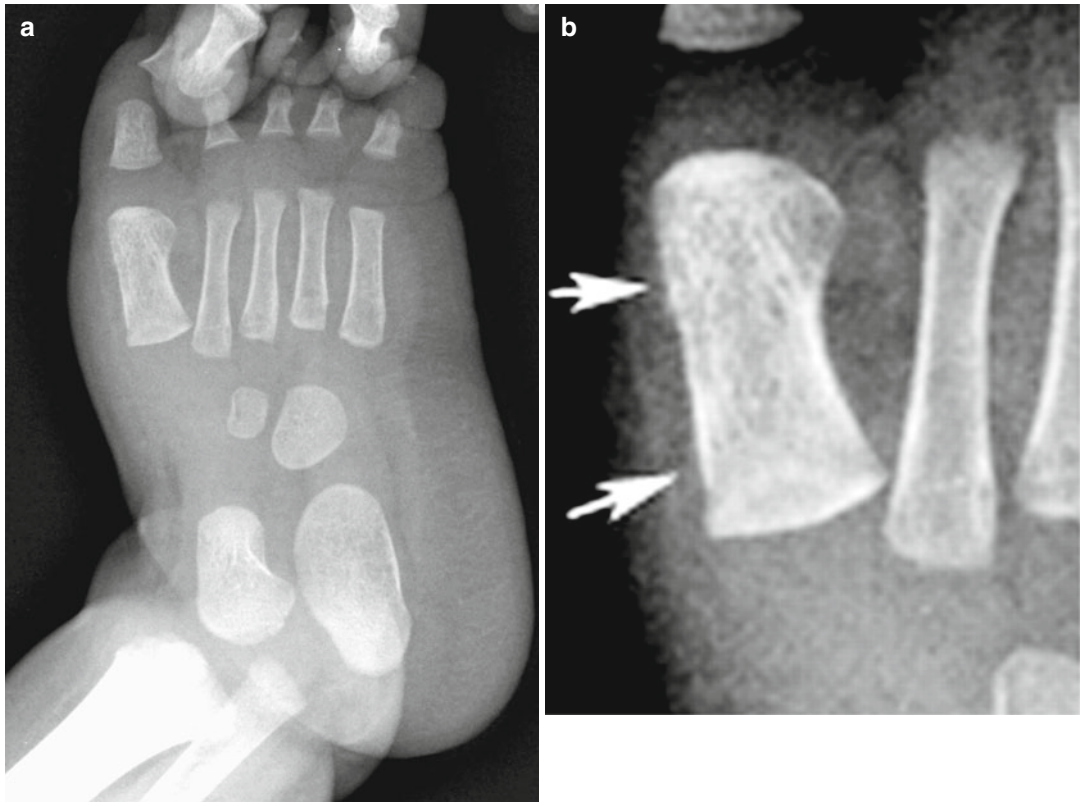


Fig. 2.5 Hand–foot syndrome. (**a**) Note that the foot is swollen. However, also note that there is subtle permeated destruction of the first metatarsal. (**b**) Magnified view of the first metatarsal more clearly demonstrates the mottled destruction (*arrows*) secondary to bone infarction/infection

(Fig. 2.5), and under these circumstances, further imaging usually is not required. Superimposed infection, that is, osteomyelitis, is common [10].

Pyomyositis

Pyomyositis in children is more common than generally believed [11, 12]. It can be confused with osteomyelitis, and in some cases, frank abscess formation ensues. Plain film findings in pyomyositis simply demonstrate soft tissue edema and expansion of the involved deep muscle compartment. In this regard, the findings are not very different from those seen with osteomyelitis. On ultrasound, if an abscess is present, it will become clearly visible as it will with magnetic resonance imaging which is becoming more and more the desired imaging modality for evaluating pyomyositis (Fig. 2.6).

With cellulitis, plain radiographs usually clearly demonstrate that the problem is limited to the subcutaneous soft tissues. However, when the problem is fascitis, then MR much more graphically demonstrates the extent of the infection (Fig. 2.7).

Adenopathy is usually readily demonstrable with ultrasound (Fig. 2.8). The enlarged nodes are easy to identify. In some cases they are very hypoechoic and then color flow Doppler will demonstrate that this is due to marked edema rather than suppuration (Fig. 2.9). In the elbow, epitrochlear adenitis is common (Fig. 2.9). Very often adenitis in this region as well as other areas in the upper extremity is due to cat scratch disease.

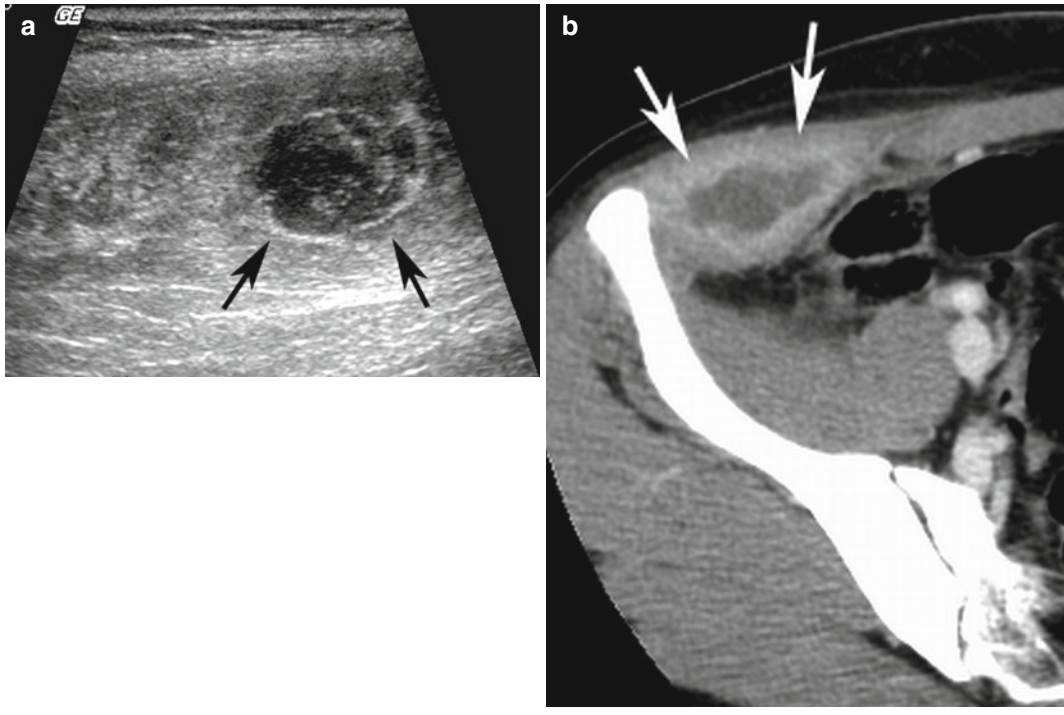


Fig. 2.6 Pyomyositis. (**a**) Ultrasound demonstrates an abscess (*arrows*) within muscle. (**b**) Subsequent CT study with contrast demonstrates the abscess (*arrows*) in the abdominal wall muscles



Fig. 2.7 Fascitis. (**a**) Note the markedly swollen left thigh. (**b**) Coronal MR, STIR image, demonstrates increased signal all along the soft tissues around the distal femur (*arrowheads*). The femur itself is normal. (**c**) Coronal MR, STIR image anterior to the femur. Note high signal in the fascial sheaths (*arrows*) surrounding the muscle. (**d**) Axial MR STIR image similarly demonstrates high signal in the fascial sheaths (*arrow*). The underlying muscle is normal

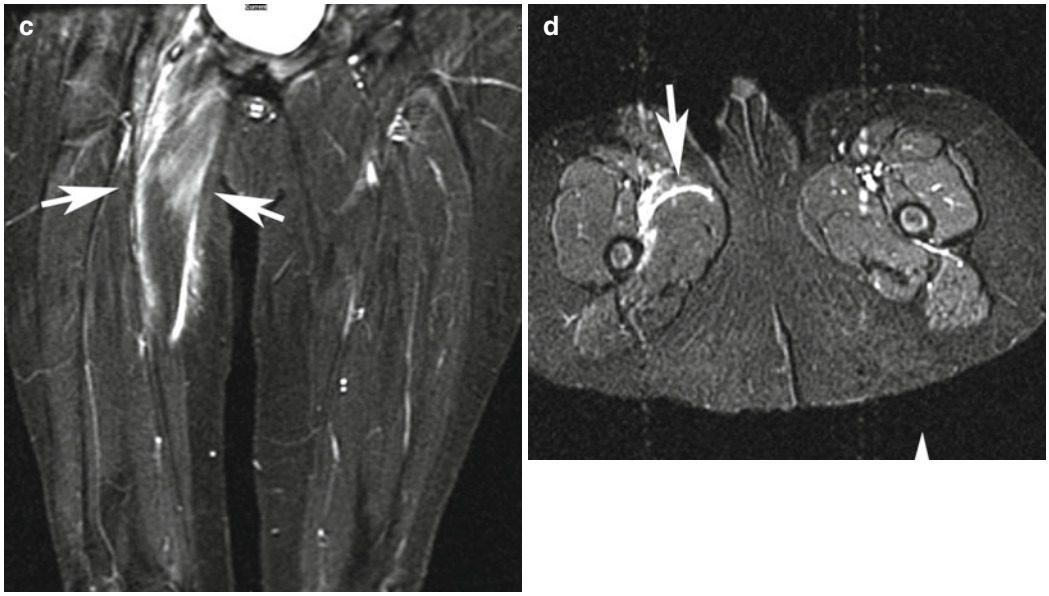


Fig. 2.7 (continued)

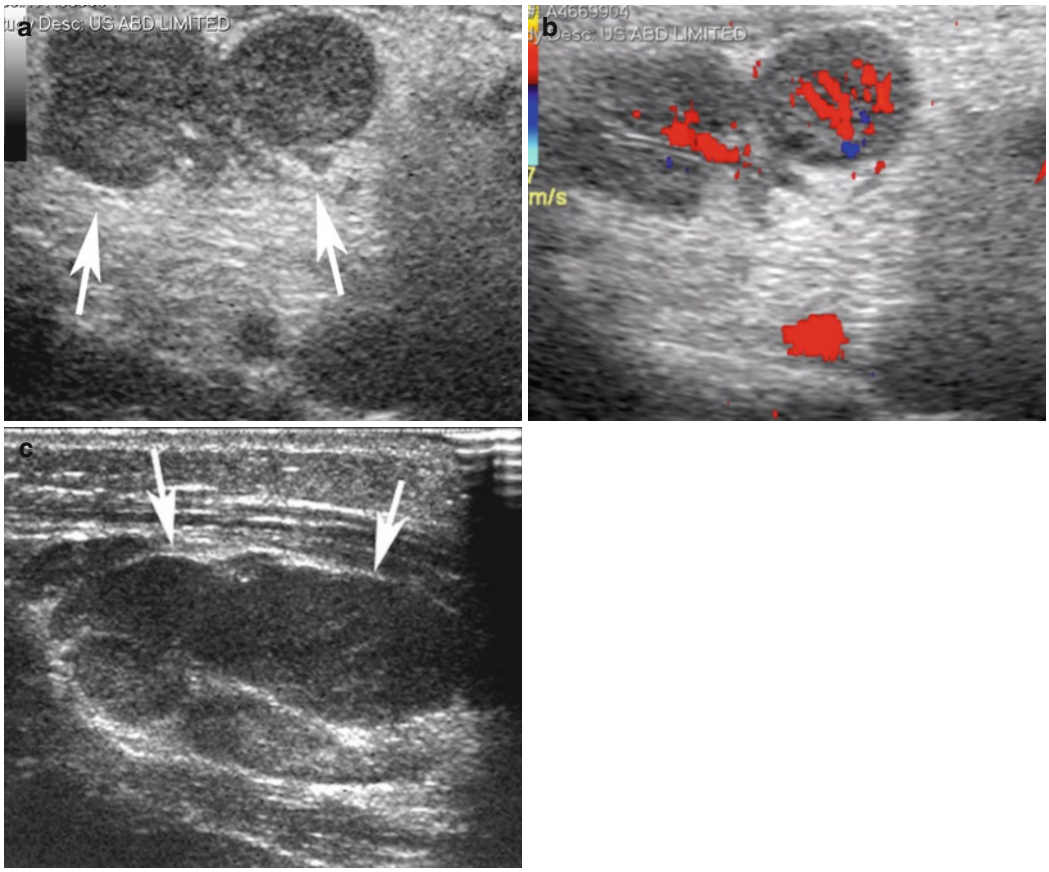


Fig. 2.8 Adenopathy. (**a**) Note hypoechoic/granular enlarged and inflamed lymph nodes (*arrows*). (**b**) Color Doppler demonstrates increased flow to the inflamed lymph nodes. If suppuration were present, no internal blood flow would be seen. (**c**) Another patient with a cluster of large elongated, inflamed lymph nodes (*arrows*)

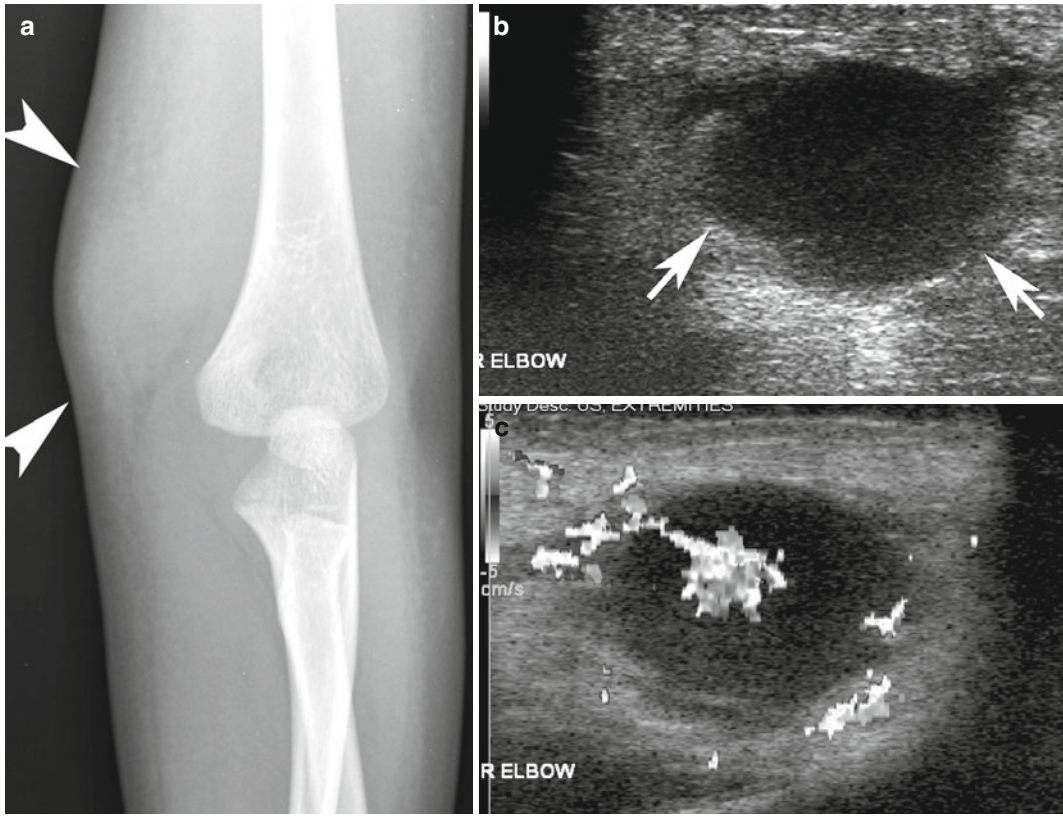


Fig. 2.9 Epitrochlear adenitis. (**a**). Note swelling (*arrowheads*) along the medial aspect of the elbow. (**b**) Ultrasound demonstrates a hypoechoic mass (*arrows*) in the area. At first, one might consider an abscess or a suppurated lymph node, but in (**c**), color flow Doppler demonstrates markedly increased flow to the lymph node, discounting the possibility of suppuration

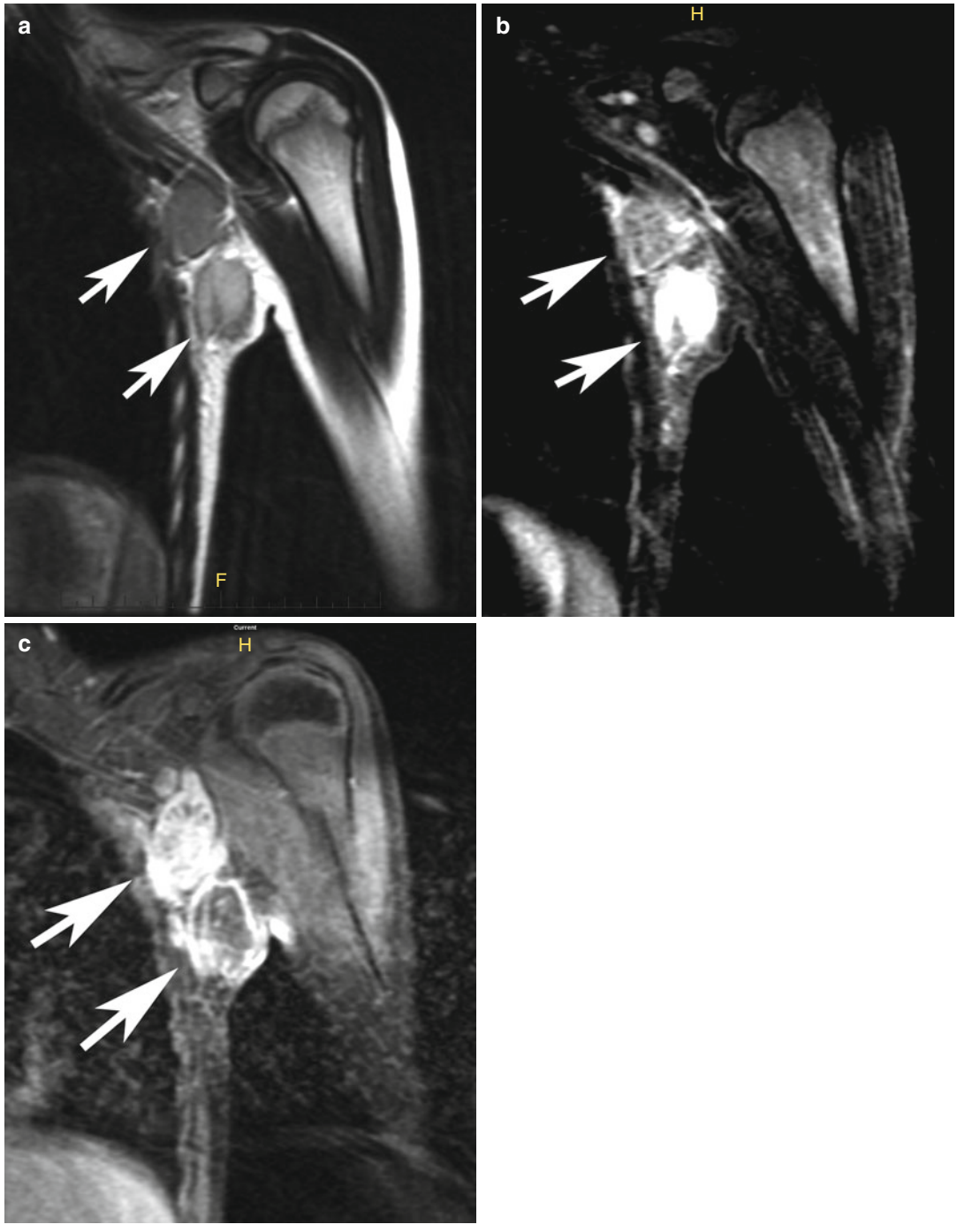


Fig. 2.10 Adenopathy with suppuration, MR findings. (**a**) Coronal MR, T1 coronal image. Note two enlarged lymph nodes (*arrows*). The lower one demonstrates slightly increased signal. (**b**) Coronal MR, STIR image. Both lymph nodes (*arrows*) demonstrate increased signal, but the lower demonstrates marked homogeneous increase in signal (fluid/exudate). (**c**) Coronal MR, gadolinium-enhanced. The upper lymph node (*upper arrow*), which is inflamed, enhances. The lower lymph node (*lower arrow*) enhances only around its periphery, indicating that suppuration in the center has occurred

Lymph nodes commonly undergo suppuration, and this can be identified with ultrasound but more vividly with MR imaging (Fig. 2.10).

References

1. Hernandez JA, Camacho A, Palacio D, Swischuk LE. Low-grade osteomyelitis (a diagnostic problem and/or a mimicker of tumor). Emerg Radiol. 2005;11:322–7.
2. Andrew TA, Porter K. Primary subacute epiphyseal osteomyelitis: a report of three cases. J Pediatr Orthop. 1985;5:155–7.
3. Rosenbaum DM, Blumhagen JD. Acute epiphyseal osteomyelitis in children. Radiology. 1985;156:89–92.
4. Raptopoulos V, Dohery PW, Goss TP, King MA, Johnson K, Gantz NM. Acute osteomyelitis: advantage of white cell scans in early detection. AJR. 1982;139:1077–82.
5. Berkwitz ID, Wenzel W. "Normal" technetium bone scans in patients with acute osteomyelitis. Am J Dis Child. 1980;134:828–30.
6. Dangman BC, Hoffer FA, Rand FF, O'Rourke EJ. Osteomyelitis in children: gadolinium enhanced MR imaging. Radiology. 1992;182:743–7.
7. Kaiser S, Sosenberg M. Early detection of subperiosteal abscesses by ultrasonography: a means for further successful treatment in pediatric osteomyelitis. Pediatr Radiol. 1994;24:336–9.
8. Belthur MV, Birchansky SB, Verdugo AA, Mason Jr EO, Hulten KG, Kaplan SL. Pathologic fractures in children with acute Staphylococcus aureus osteomyelitis. J Bone Joint Surg Am. 2012;94:34–42.
9. Morrissy RT, Haynes DW. Acute hematogenous osteomyelitis: a model with trauma as an etiology. J Pediatr Orthop. 1989;9:447–56.
10. Bennett OM. Salmonella osteomyelitis and the hand-foot syndrome in sickle cell disease. J Pediatr Orthop. 1992;12:534–8.
11. Renwick SE, Ritterbusch JF. Pyomyositis in children. J Pediatr Orthop. 1993;13:769–72.
12. Spiegel DA, Meyer JS, Dormans JP, Flynn JM, Drummond DS. Pyomyositis in children and adolescents: report of 12 cases and review of the literature. J Pediatr Orthop. 1999;19:143–50.

Tumors, Cysts, and Tumor Mimickers

3

Soft tissue tumors seldom present as an acute problem in the emergency room. Every so often, a hemangioma thromboses or bleeds and a cystic hygroma becomes infected or encounters a bleed, but otherwise soft tissue tumors are more indolent. For the most part, soft tissue tumors are first evaluated with plain films where deep edema will be seen and then with ultrasound. Ultrasound is especially useful for the evaluation of hemagiomas and cystic hygromas along with their complications [1, 2] (Fig. 3.1).

Also somewhat rare is the acute presentation of a malignant bone tumor. Once again, these entities are somewhat indolent but every so often a patient will present because of extremity pain, and imaging will demonstrate the presence of a bone tumor, occasionally with a pathologic fracture (Fig. 3.2). In the young pediatric patient, metastatic neuroblastoma is a common entity to encounter with unexplained pain. What one see in these cases is permeated bony destruction usually around the metaphysis (Fig. 3.2c). Much more commonly, however, one will encounter a pathologic fracture in a benign lesion such as a unicameral bone cyst (Fig. 3.3).

Most commonly the cysts occur in the proximal humerus and then the proximal femur, but they can occur almost anywhere in the extra-axial skeleton. Diagnosis usually is straightforward as they are located in the metaphysis or diaphysis, have distinct benign features, and when a fracture is present, a fragment of bone often is seen within the cyst leading to the "fallen fragment sign" or "tumbling bullet sign" (Fig. 3.3). A few of these cysts may appear malignant as their surrounding cortex is very thin and irregular (Fig. 3.4). In such cases, one may need to go on to CT or MR imaging to fully diagnosis the benign nature of the lesion (Fig. 3.4).

Even more common is the incidental benign cortical defect/nonossifying fibroma. These lesions may be single or multiple (Fig. 3.5) and are very common. Their eccentric cortical location along with their very benign appearance solidifies the diagnosis without further investigation required. Every so often however the cortex over the outer surface of the lesion may be pulled off by a muscle attachment (Fig. 3.6). Pain will be the problem and at first a malignancy might be suspected. In addition, a pathologic fracture occasionally can be the presenting feature (Fig. 3.6c) much as with a benign bone cyst.

Another benign tumor occasionally presenting in the emergency room is the osteochondroma. While fracture of a pedunculated osteochondroma can occur more often, the problem is bursitis as a result of a tendon/muscle attaching and pulling on the osteochondroma (Fig. 3.7) [3]. MR very clearly demonstrates the bursitis (Fig. 3.7d). Osteoidostema also can present with acute pain, and the imaging findings usually are typical (Fig. 3.8)

Finally eosinophilic granuloma (histiocytosis X) can present with acute problems resulting from pathologic fracture. The plain film appearance of eosinophilic granuloma is variable but generally more benign than malignant appearing (Fig. 3.9). If you have a bony lesion put

L.E. Swischuk, S.P. Jadhav (eds.), *Emergency Musculoskeletal Imaging in Children*,
DOI 10.1007/978-1-4614-7747-1_3, © Springer Science+Business Media New York 2014

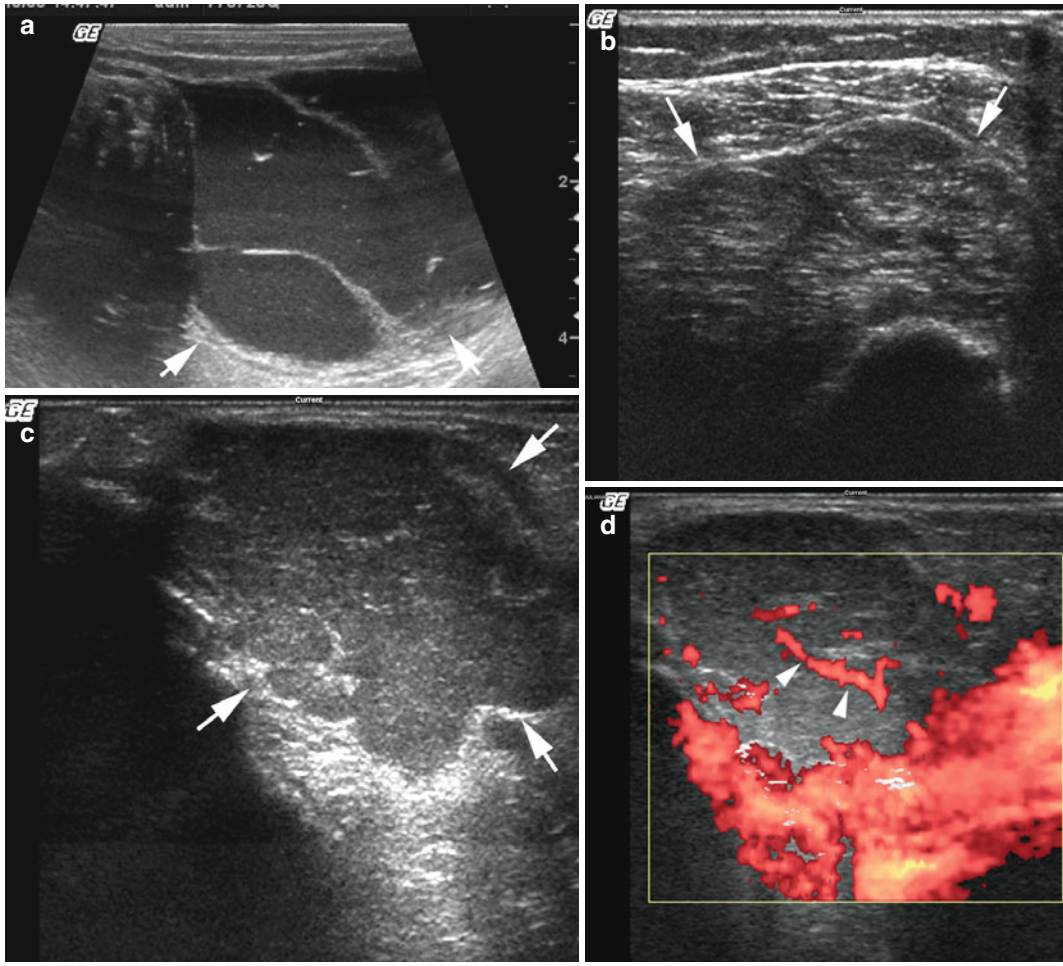


Fig. 3.1 Lymphangioma/hemangioma. (**a**) Cystic hygroma. Note the multiloculated fluid-filled mass (*arrows*) with septae. The fluid is dirty because bleeding into the cystic hygroma occurred and brought the patient to the ER. (**b**) Hemangioma. Note the multilobulated coarsely echogenic mass (*arrows*). The echogenic arc at the lower end of the image is the humerus. This hemangioma was located over the patients shoulder. (**c**) Capillary hemangioma. Note the multilobulated coarsely echogenic mass (*arrows*). This is typical for a hemangioma. (**d**) Color flow Doppler demonstrates increased flow and feeders (*arrowheads*) to and within the hemangioma

medullary bony lesion. However, this is not always the case, and many times, further imaging with CT/MR is required. Finally, the diagnosis of eosinophilic granuloma frequently is made only after biopsy for it does mimic both benign and malignant bony lesions. For this reason, I have always said "if you have a bony lesion in the pediatric skeleton, no matter what it looks like, always put eosinophilic granuloma in the differential diagnosis."

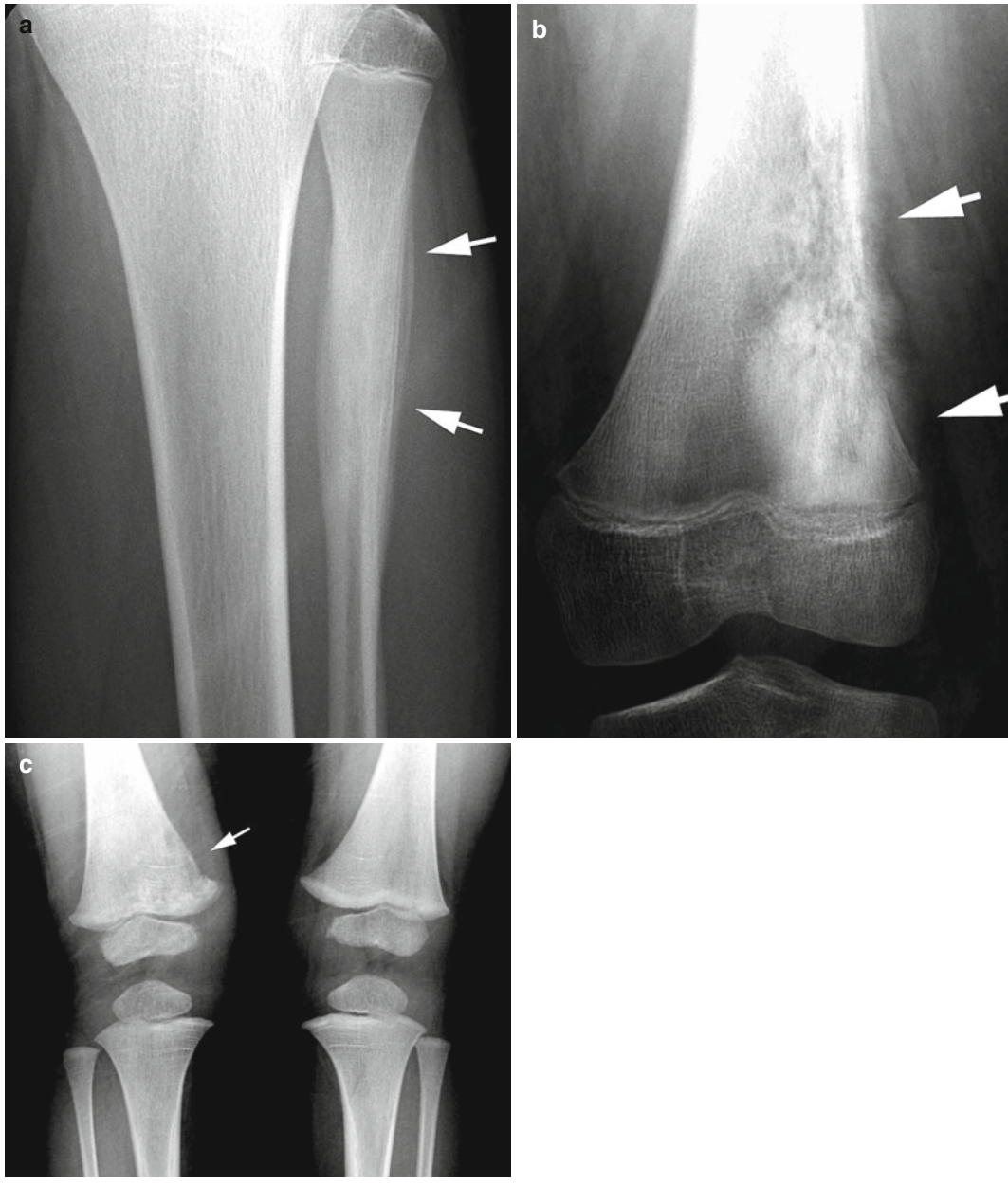


Fig. 3.2 Malignant tumors. (**a**) Ewing's sarcoma. Note periosteal new bone deposition (*arrows*) around a destructive lesion of the proximal fibula. (**b**) Osteosarcoma. Note moth-eaten destruction of the distal femur along with reactive sclerosis and cortical destruction (*arrows*). A Codman triangle also is present. (**c**) Neuroblastoma metastases. Note the permeated pattern of bony destruction (*arrows*) in the lower metaphysis of the right femur

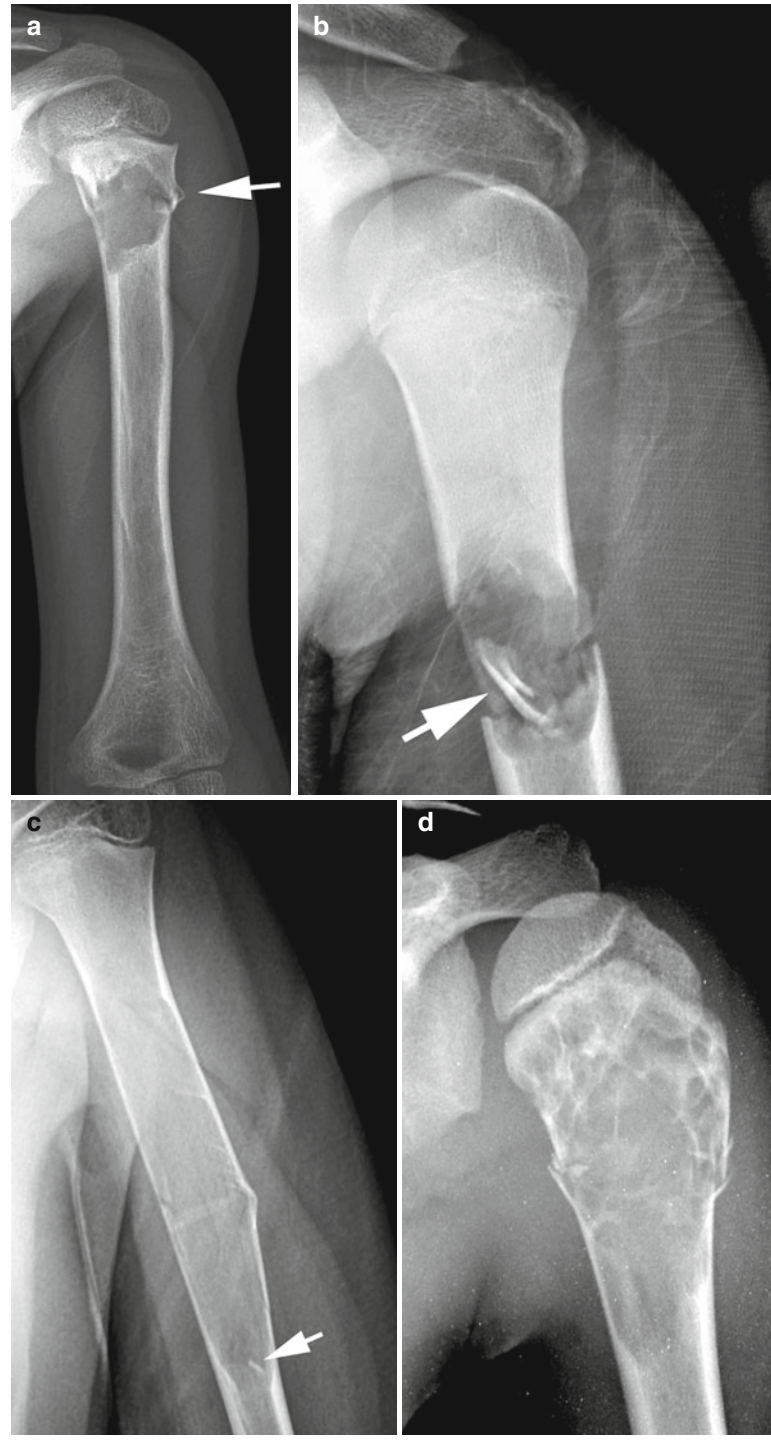


Fig. 3.3 Bone cyst. (**a**) Note a typical lucent bone cyst with a cortical fracture (*arrow*) in the proximal humerus. (**b**) Another patient with similar findings but, in addition, the demonstration of the "fallen fragment sign" (*arrow*). (**c**) Metaphyseal location. Note the large, lucent, and expanding lesion in the midshaft of the humerus. A fracture is present through the midportion, and in addition, there is a small fallen fragment (*arrow*). (**d**) Less common appearance. Note the typical location of this bone cyst which, however, is multiloculated. In addition, note the cortical buckle fractures

Fig. 3.5 Benign cortical defect and NOF. (**a**) Note the typical appearance of a benign cortical defect (*arrow*) in the distal femur. (**b**) Another patient with a more clearly defined defect (*arrow*) with a sclerotic periphery. (**c**) CT findings. Note the multilobulated cystic lesion within the cortex of the femur (*arrows*). (**d**) Nonossifying fibroma. Typical multiloculated eccentric cystic lesion typical of a nonossifying fibroma (*arrows*). (**e**) Partially healed nonossifying fibroma (*arrow*). (**f**) Healed nonossifying fibroma/benign cortical defect. Note the oval, dense/sclerotic area in the proximal tibia (*arrow*)

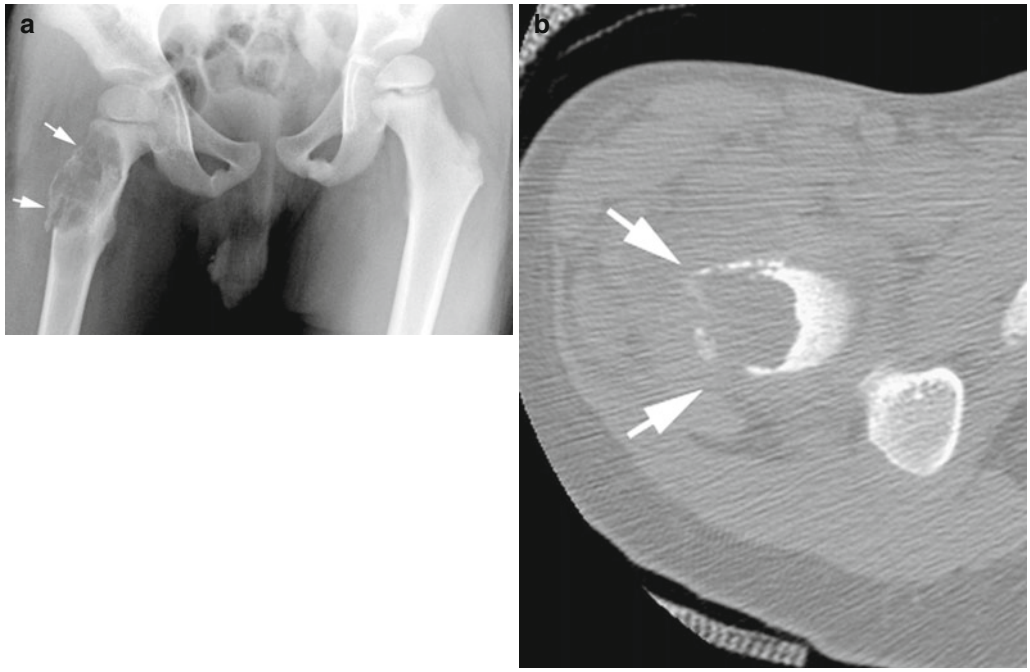
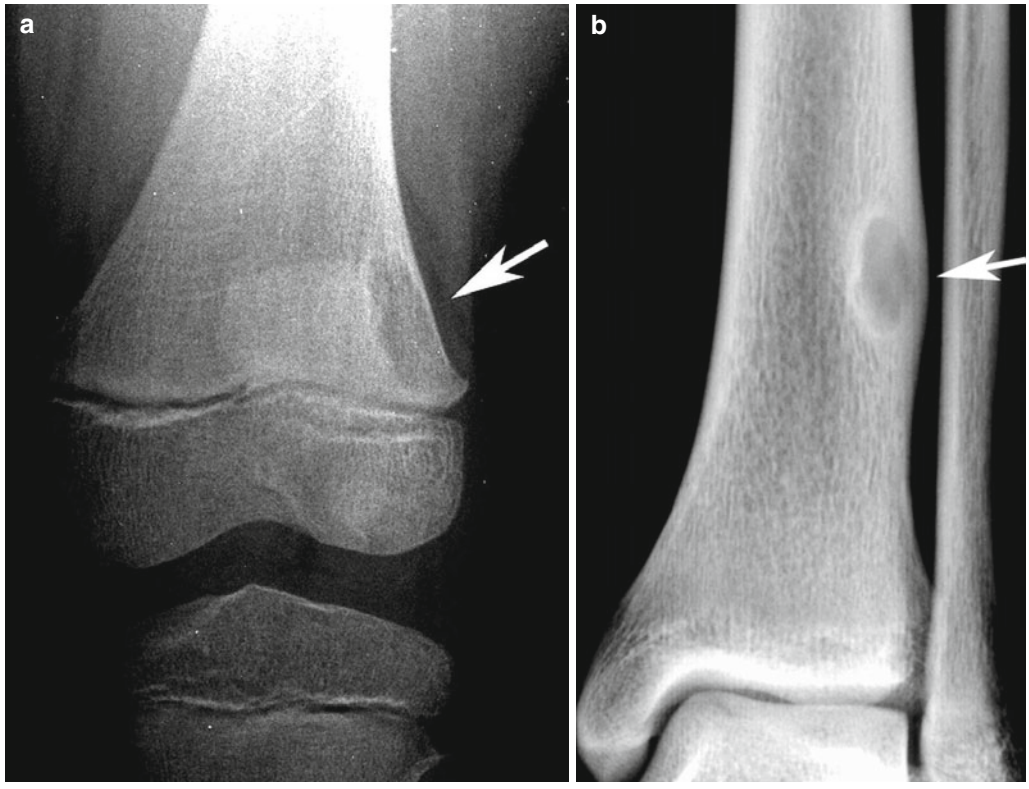


Fig. 3.4 Bone cyst: aggressive appearance. (**a**) Note the pathologic fracture (*arrows*) involving the cystic lesion in the proximal femur. The lesion appears somewhat aggressive. (**b**) CT study demonstrates a very thin irregular cortex (*arrows*) which would suggest an aggressive lesion. However, note that there is no associated soft tissue tumor/mass. This was simple bone cyst



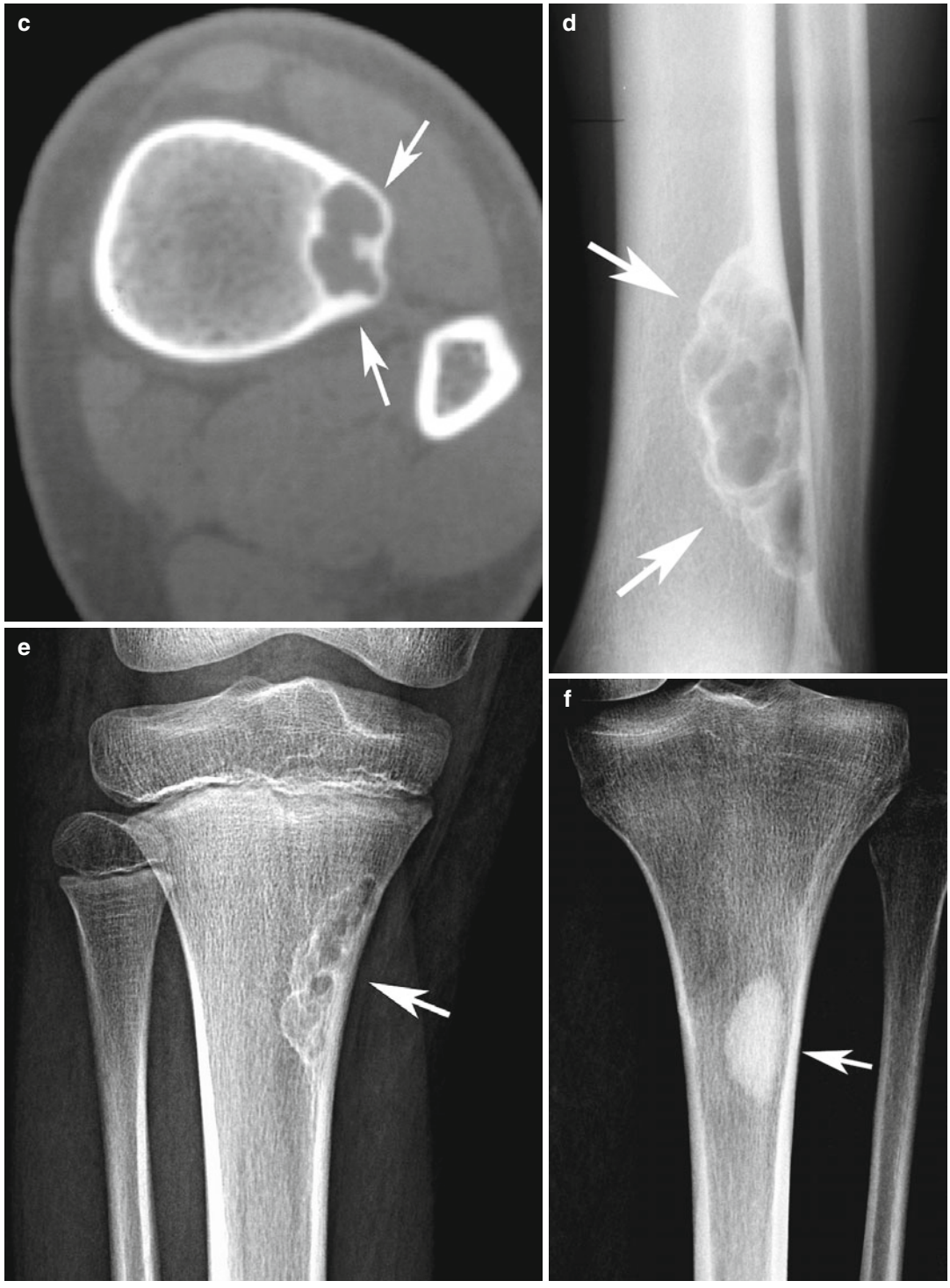


Fig. 3.5 (continued)

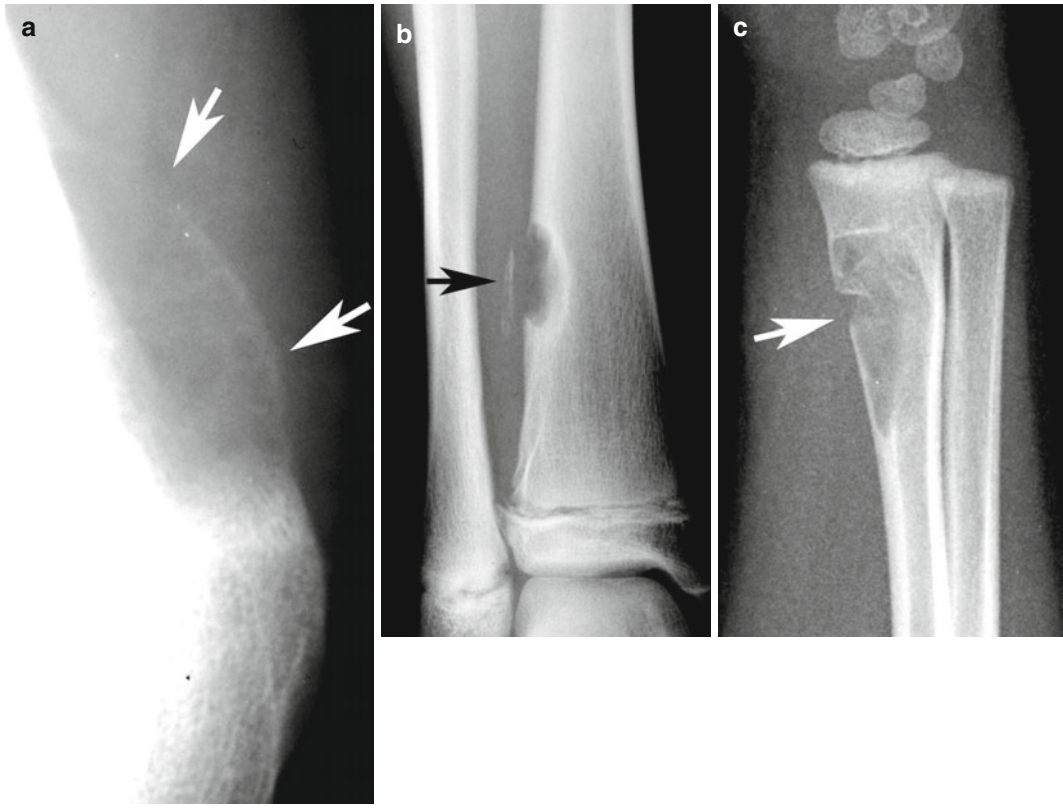


Fig. 3.6 Benign cortical defect/NOF with fracture. (**a**) Note the very thin cortical cover (*arrows*) of this benign cortical defect in the distal femur. The thin shell overlying the defect is very susceptible to avulsion fracturing. (**b**) In this patient, the thin roof over a benign cortical defect has been avulsed (*arrow*). (**c**) NOF with buckle fracture (*arrow*)

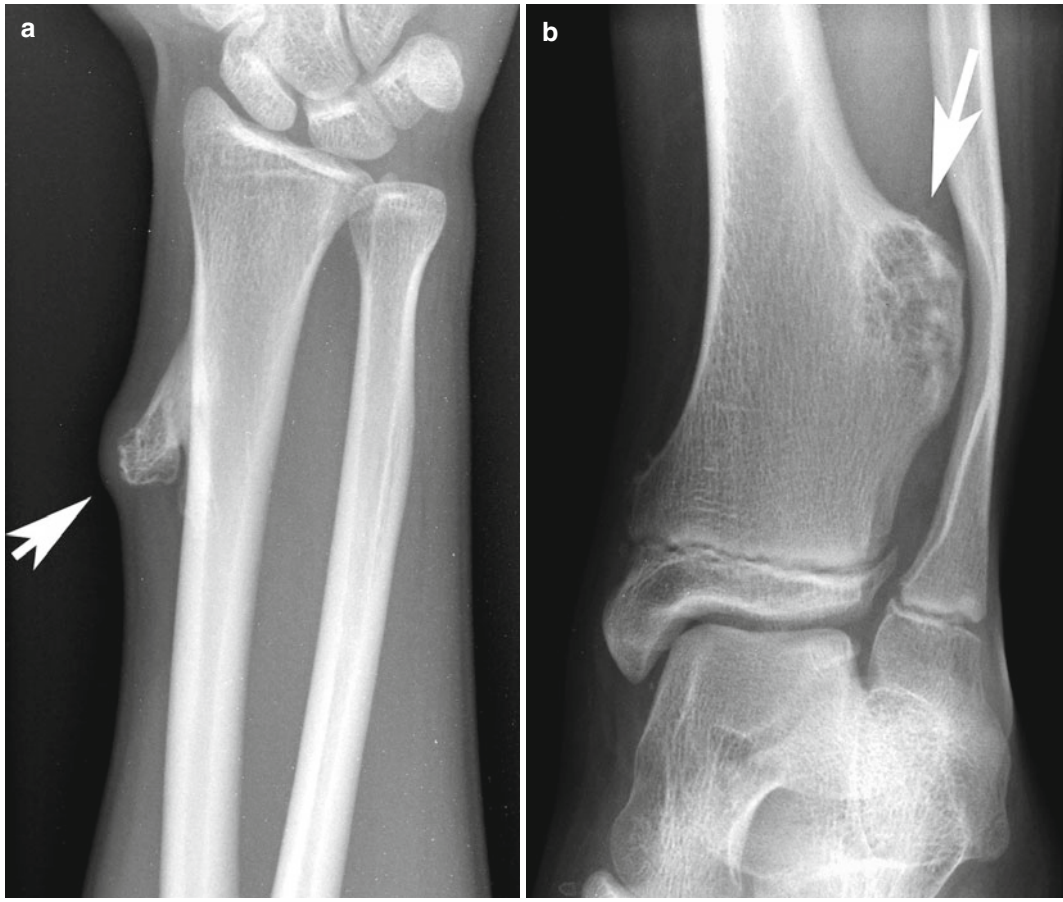


Fig. 3.7 Osteochondroma/exostoses. (**a**) Note the pedunculated osteochondroma (*arrow*) coming off the distal radius. Irregularity over the dome of the osteochondroma is common. (**b**) In this patient, the osteochondroma (*arrow*) is eroding and deforming the adjacent fibula. (**c**) Small sessile osteochondroma (*arrow*) with soft tissue swelling overlying the lesion. (**d**) Same patient. Coronal MR, STIR image demonstrates fluid and increased inflammatory signal over the osteochondroma (*arrows*) consistent with bursitis

Fig. 3.8 Osteoid osteoma. (**a**) Note the thickened cortex (*arrows*) over the midshaft of the tibia. A subtle central lucent nidus is suggested. (**b**) CT sagittal reconstruction more clearly demonstrates the nidus (*arrow*). (**c**) Axial CT study demonstrates the posteriorly thickened bone over the tibia and the central nidus (*arrow*)

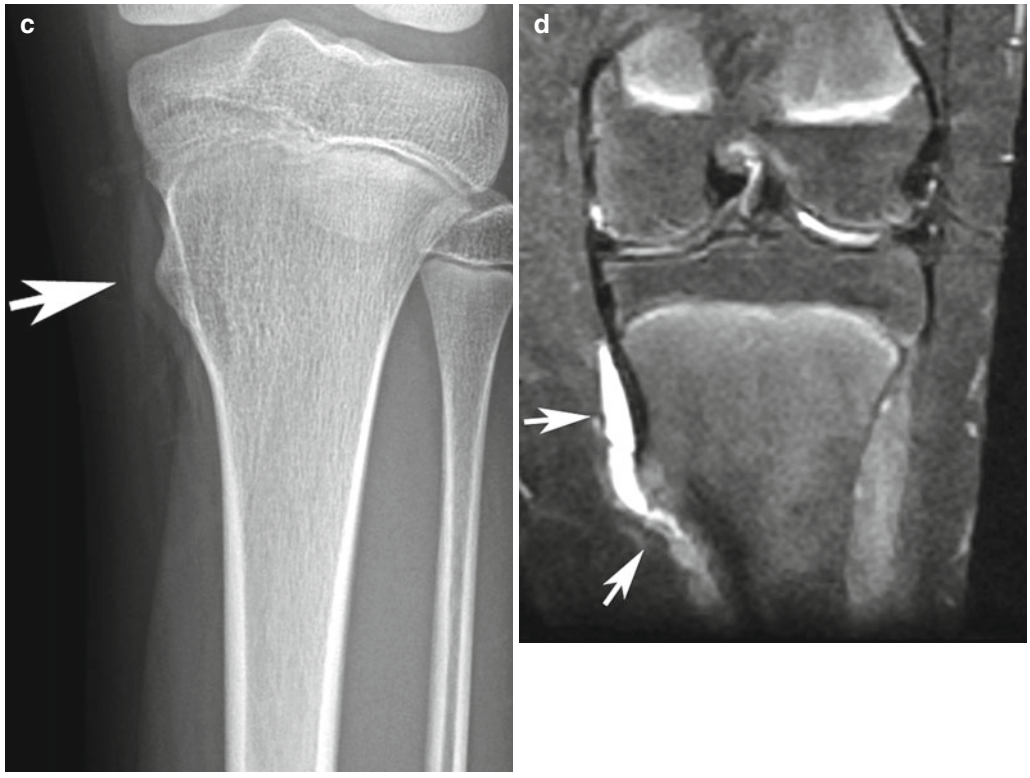
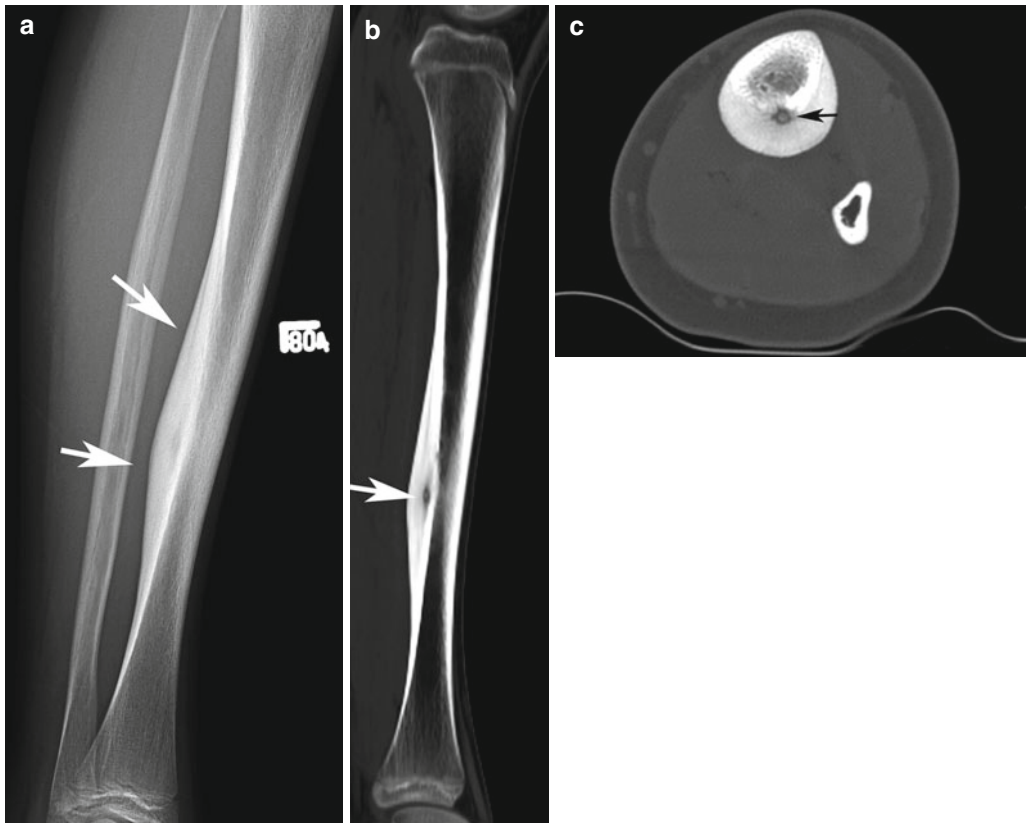


Fig. 3.7 (continued)



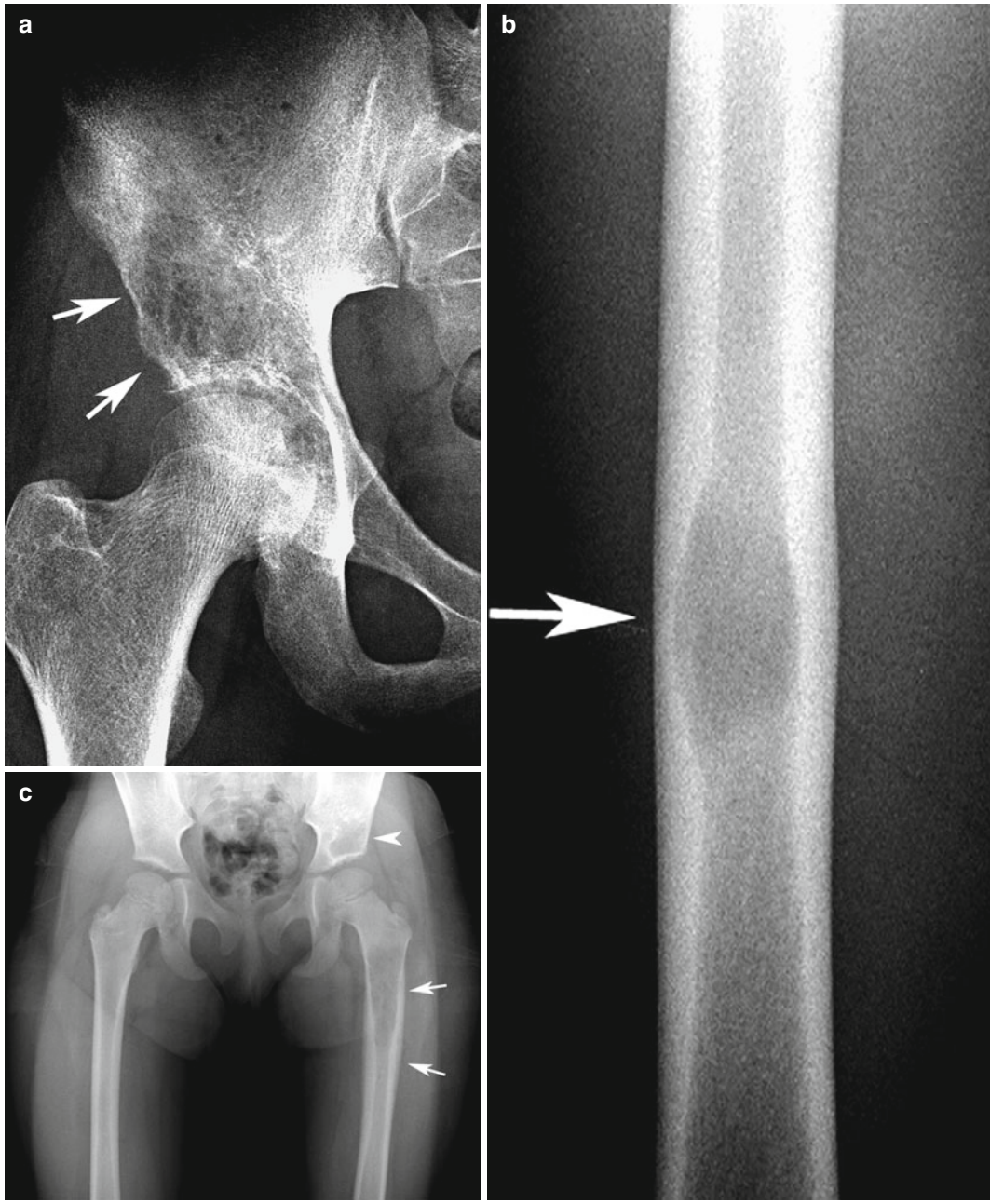


Fig. 3.9 Eosinophilic granuloma. (**a**) Note the multiloculated, lucent, slightly expanding lesion of the iliac wing (*arrows*). These findings also can be seen with fibrous dysplasia. (**b**) In this patient, with eosinophilic granuloma, there is a lucent area of medullary expansion (*arrow*) in the midshaft of this femur. Note that the edges of the lesion are not sclerotic. (**c**) In this patient, there is a lytic expanding lesion in the proximal femur with reactive periosteal new bone. This easily could be interpreted for a Ewing's sarcoma. However, note that there is no associated mass. There also is another lytic, well-defined lesion in the left iliac wing (*arrowhead*). This lesion would be less likely to be interpreted for a malignant bone tumor

References

1. Abiezza SS, Miller LS. The use of ultrasound for the diagnosis of soft-tissue masses in children. J Pediatr Orthop. 1995;15:566–73.
2. Glasier CM, Seibert JJ, Williamson SL, et al. High-resolution ultrasound characterization of soft tissue masses in children. Pediatr Radiol. 1987;17:233–7.
3. Karanick D, Schweitzer ME, Eschelman J, et al. Pictorial essay, symptomatic osteochondromas: imaging features. AJR. 1997;168:1507–12.

Types of Fractures in Children

4

Types of Fractures Seen in Children

The types of fractures most peculiar to childhood are (a) cortical/buckle or torus fractures, (b) greenstick fractures, (c) plastic bending or bowing fractures, and (d) epiphyseal–metaphyseal (Salter–Harris) fractures (Fig. 4.1). Of course, typical midshaft, transverse, spiral, oblique, and comminuted fractures also occur, but none are specifically peculiar to childhood, and most are not difficult to detect unless they are hairline fractures which occur most commonly in the tibia and small bones of the hands and feet. In the tibia, the original diaphyseal spiral toddler fracture described by Dunbar et al. [1] and the more recently described upper tibial hyperextension-induced fracture of the tibia [2] are the most common hairline fractures seen in the lower extremity. We have over the years referred to these fractures, respectively, as the *toddler fracture type I and toddler fracture type II*.

Buckle or torus fractures are simple axial load induced compression fractures which manifest as buckling, kinking, or notching of the cortex. They occur most frequently in the metaphyseal regions of long bones, for this is where the cortex is weakest. Some of these fractures are quite subtle, but *if one follows the rule that the distal ends of the long bones should have smooth, continuous curves, then one will not accept even the slightest bump, dent, buckle, or angled cortex as normal*. In this regard, there are two types of buckle/torus fractures [3].

The first type of buckle fracture is the typical buckle fracture which results in outward buckling/bulging of the cortex (Fig. 4.2), but equally common is the second type of buckle fracture which presents as unilateral angled buckling of the subepiphyseal metaphyseal cortex (Fig. 4.3). In the first case, the buckling results from a direct axial load transmitted down the length of the bone with an abrupt deceleration (i.e., the

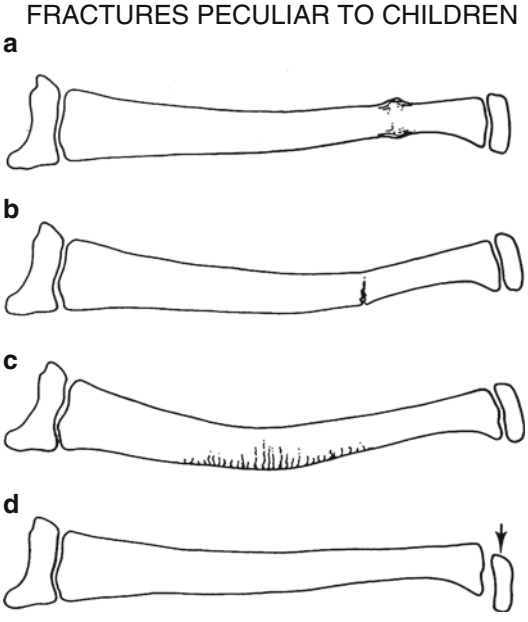


Fig. 4.1 Fractures peculiar to children. (**a**) Typical buckle fracture. (**b**) Greenstick fracture. (**c**) Plastic bowing fracture. (**d**) Salter–Harris epiphyseal metaphyseal fracture with a displaced epiphysis (*arrow*)

L.E. Swischuk, S.P. Jadhav (eds.), *Emergency Musculoskeletal Imaging in Children*,
DOI 10.1007/978-1-4614-7747-1_4, © Springer Science+Business Media New York 2014

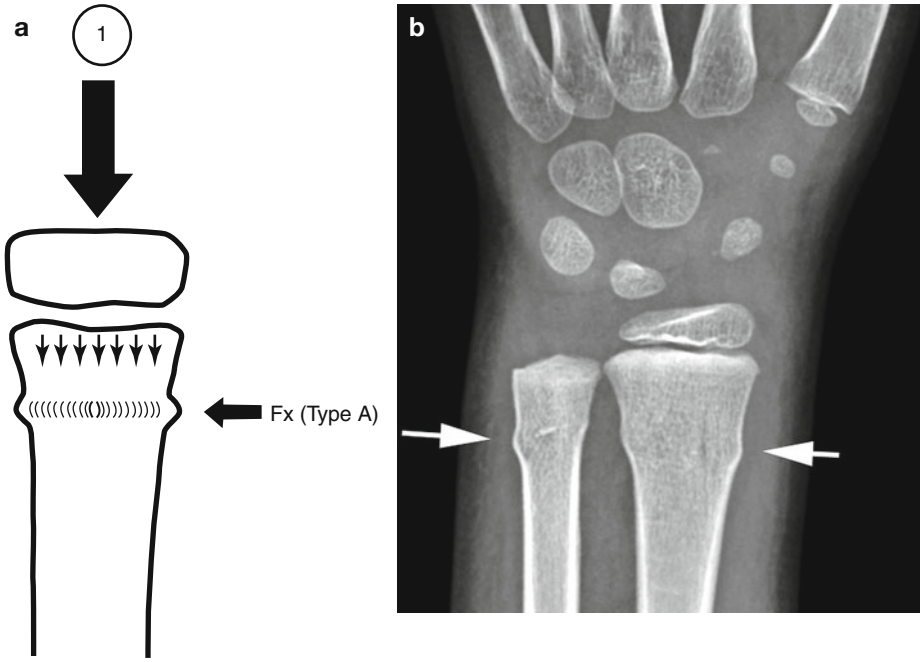


Fig. 4.2 Buckle fracture type (**a**) Axial loading forces (*1*) are exerted down the length of any given bone. The result is a cortical buckle fracture (*fx*). (**b**) Typical type A buckle fractures of the radius and ulna (*arrows*)

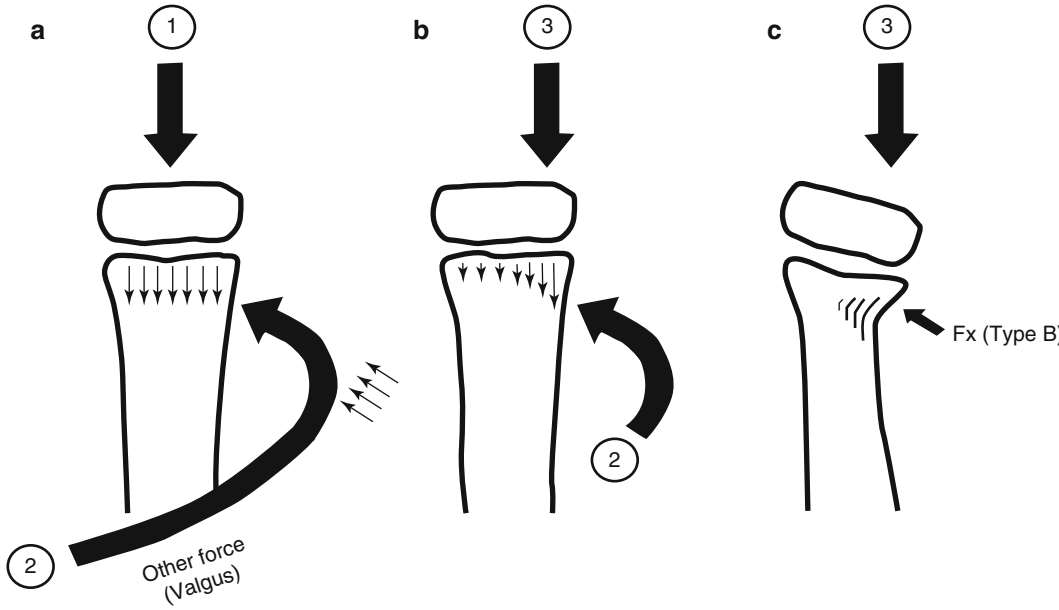


Fig. 4.3 Buckle fracture type B. (**a**) Axial loading forces (*1*) are exerted down the length of the bone. However, other forces such as valgus also are at play. (**b**) This results in shifting of the axial load axis (*3*) and compression of the underlying metaphysis (*2*). (**c**) The same laterally placed axial loading forces (*3*) eventually result in an angled buckle fracture (*fx*). (**d**) Typical angled buckle fracture of the distal radius (*arrow*). Compare with the smooth cortex over the anterior aspect of the radius

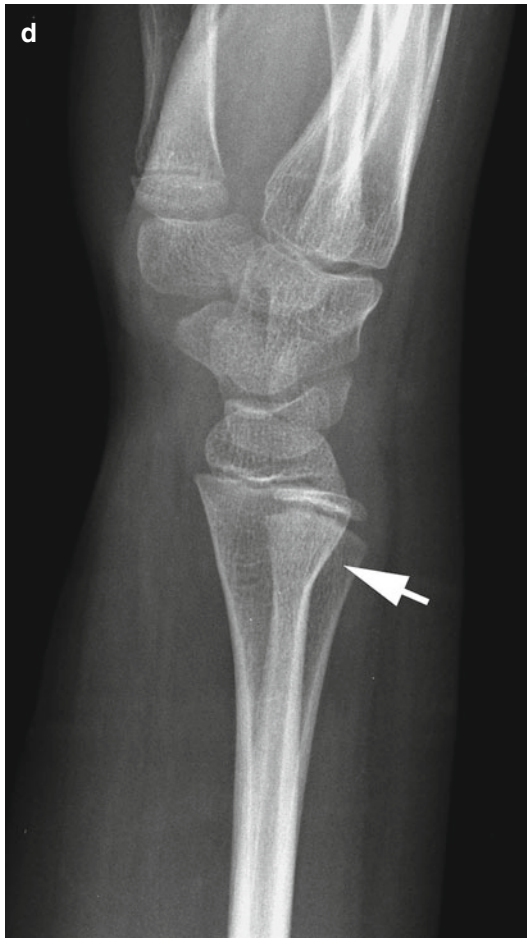


Fig. 4.3 (continued)

outstretched upper or lower extremity). With such abrupt deceleration the bone of the metaphysis impacts and crumbles/buckles. The trabeculae are compressed and outward bulging of the cortex through the metaphysis occurs (Fig. 4.2b). With the angled buckle fracture, the axial load is shifted off center, and as a result, the cortex buckles, in an angled configuration, to one side or another (Fig. 4.3d). In actual fact this fracture is the precursor of a frank Salter–Harris II fracture.

Greenstick and plastic bending/bowing fractures are related, both resulting from axial loading forces exerted along the long axis of a long bone. In infants and young children, because the bones are soft, before actually fracturing, plastic bending (bowing) occurs. Thereafter, if the forces are stronger, the plastic bending fracture becomes a "greenstick" fracture (Fig. 4.4). The term "greenstick" comes from the comparison of this type of fracture to the manner in which a "green," supple tree branch breaks if it is bent. It can be bent only so far, and then it snaps and breaks. Most often plastic/bending fractures occur in the forearm [4–6]. However, they are also very common in the clavicle. They are less common in the fibula [7]. These fractures are discussed in more detail in later sections, but it might be noted at this point that seldom, if ever, do these fractures show classic signs of healing. In other words, whereas with a greenstick fracture, one sees healing sclerosis and periosteal new bone formation, with the usual bending fracture, nothing but the persisting deformity is seen.

Epiphyseal–metaphyseal fractures are very common in childhood and, of course, occur exclusively in the child. Because the junction between the epiphysis and metaphysis is a weak area, if a shearing/twisting force is applied to the end of a long bone, it is quite natural that epiphyseal–metaphyseal slippage or separation would occur. A variety of injuries can be sustained at this junction, and to facilitate their understanding and categorization, the Salter–Harris classification of five types [8] usually still is employed (Fig. 4.5). Even though other more complicated classifications have been suggested, this basic classification still is most useful.

As far as the radiologist is concerned, the greatest challenge comes from Salter–Harris type I and II injuries. The reason for this is that if in these cases, the epiphysis is not displaced, bony changes are subtle, and one must rely more on soft tissue changes and widening of the epiphyseal line (Fig. 4.6). Salter–Harris type III and IV fractures usually are relatively easy to detect, for most often some degree of epiphyseal displacement exists and, in any case, the fracture lines are more readily visible. Type III fractures occur most commonly in the distal tibia, followed by the small bones of the hands and feet.

The type V Salter–Harris injury, that is, the one in which only epiphyseal-plate compression occurs [9], is the least common of all. Indeed, in the past, a question has been raised as to whether the type V fracture occurs at all [10]. However, it

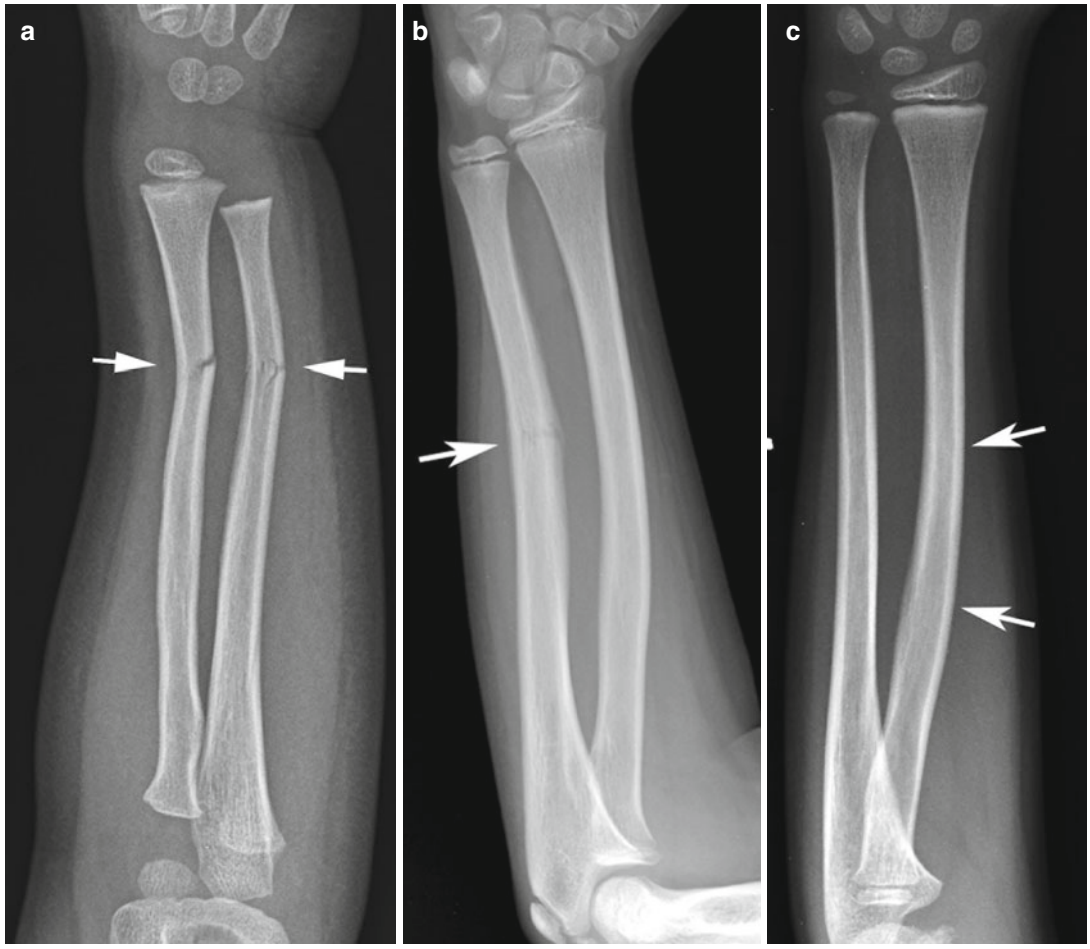


Fig. 4.4 Plastic/greenstick fractures. (**a**) Note typical greenstick fractures through the distal radius and ulna (*arrows*). (**b**) In this patient, a greenstick fracture is present through the midshaft of the ulna (*arrow*). A plastic bending fracture is present in the radius. (**c**) This patient demonstrates only a plastic bending fracture of the radius (*arrows*)

is considered one of the more serious injuries a child can sustain, for epiphyseal-plate damage and subsequent impaired epiphyseal growth are common [9–11]. Experimentally it has been shown that compression of the cancellous bone in the metaphysis occurs in these patients [11]. Growth abnormalities also are a significant complication of the type IV fracture but are a lesser problem with the other Salter–Harris epiphyseal–metaphyseal injuries. Roentgenographically, in the type V fracture, the film images usually are void of any bony abnormality but changes now are being seen on MR imaging. Indeed, occult Salter–Harris fractures in general now are readily demonstrable with MR. MR also is excellent for demonstration of premature growth plate fusion [12], as is CT.

Although the fractures outlined here constitute the majority of childhood fractures, one also can see acute compression, stress, and pathologic fractures. Stress fractures usually occur in perfectly normal but very active individuals. The most common site for such a fracture in a child is the upper tibia [13]. They also can occur in the femoral neck [14] and, rarely, even in the sacrum [15]. Stress fractures of the second metatarsal usually are referred to as "March fractures." Stress fractures also are common through the anterior diaphyseal tibial cortex, both in older children and adults. In young children, this

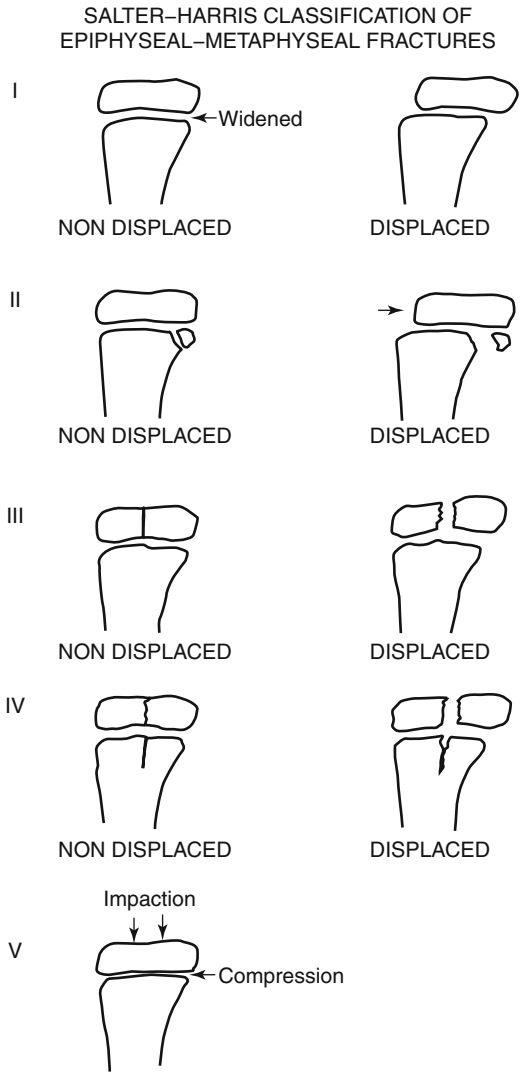


Fig. 4.5 Salter–Harris injuries. Note typical displaced and non-displaced Salter–Harris I through V fractures

fracture is probably responsible for "shin splints" [16]. Currently the problem of stress fractures in the upper anterior tibia is referred to as the medial or anteromedial tibial syndrome [17].

It is not unusual not to detect stress fractures in their initial stages, for unless a fracture line is seen, one will not even suspect that such an injury is present. Nuclear scintigraphy can be employed for the detection of stress fractures, and although the findings are nonspecific, they do localize the site of injury. However, currently, stress fractures are most definitively confirmed or discovered with magnetic resonance (MR) imaging [18, 19], but it has been noted that in chronic cases, the MR study may be negative [19]. This probably occurs because the stress phenomena are low grade.

Acute compression fractures [20] are more common than generally believed and primarily occur in hand and foot involving the carpals and tarsals. In any case what one sees is increased density of the bone, either generalized or focal, and in many cases decreased volume of the bone (Fig. 4.7). The findings often are subtle and are more readily detected with comparative views.

Role of MRI

Epiphyseal–Metaphyseal (Salter–Harris) Fractures

Indications for MRI in the setting of acute trauma with negative radiographs include persistent pain, refusal to bear weight or use of the affected extremity, or a high clinical suspicion for a fracture. With epiphyseal–metaphyseal fractures, MRI is useful in detecting occult Salter–Harris I fractures. MRI has also been shown to upgrade Salter–Harris fractures detected radiographically, which affects management [21]. MRI is also important in cases where satisfactory reduction of displaced Salter–Harris I fracture cannot be obtained. In these cases MRI may alter management by detecting mechanical causes of nonreduction like trapped periosteum or soft tissue in the physis [22]. In these cases, open reduction is warranted to ensure proper healing.

Stress Injuries and Fractures

Magnetic resonance imaging is preferred over bone scintigraphy for the diagnosis of stress fractures because of greater specificity [23]. Findings on MRI range from periosteal edema alone to presence of endosteal and marrow edema. When marrow edema is seen without a discrete fracture line through the cortex and marrow, the term stress reaction should be used (Fig. 4.8) [24]. In this regard Fredericson et al. [24] have proposed

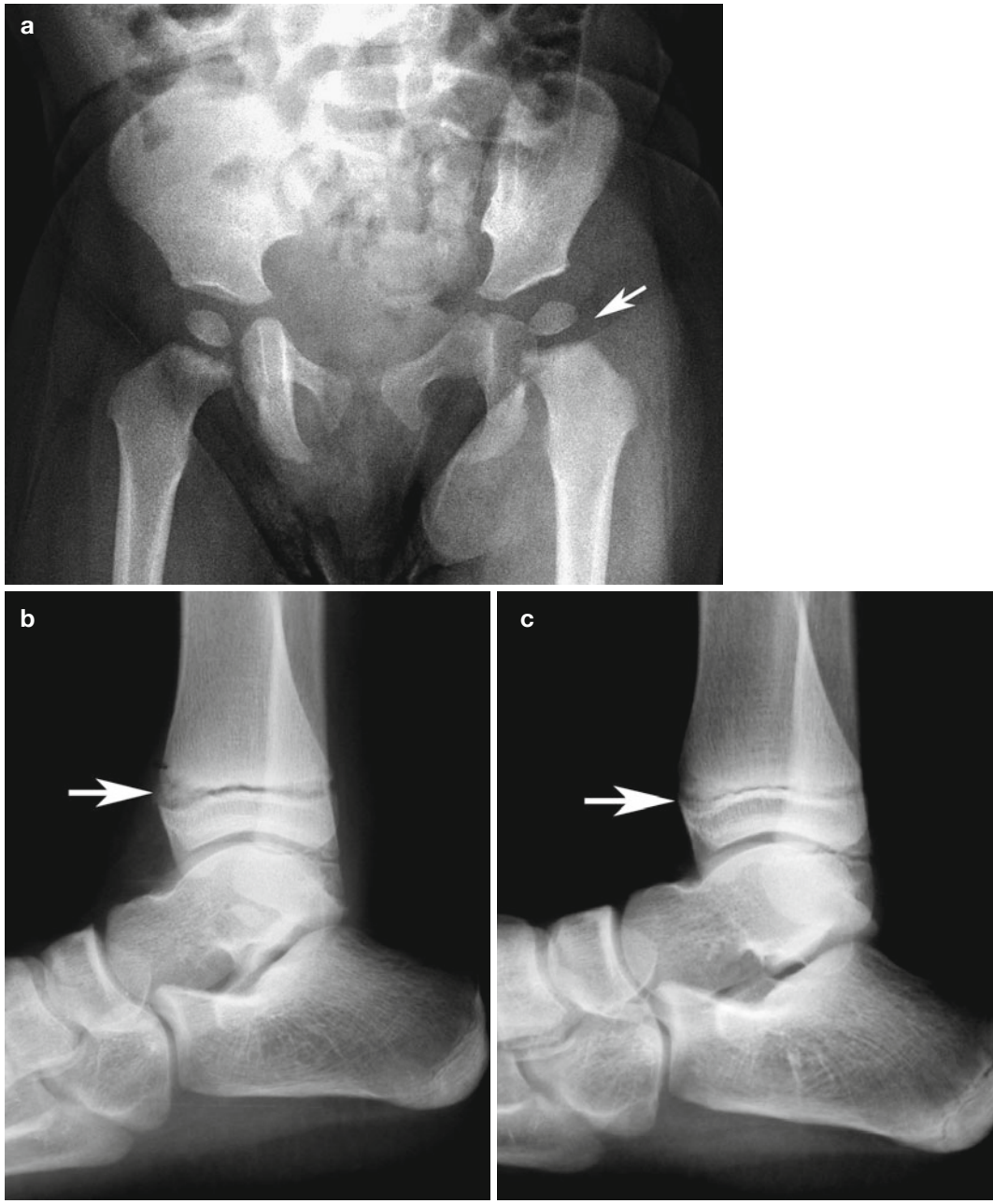


Fig. 4.6 Salter–Harris fractures. (**a**) Note the widened epiphyseal plate (*arrow*) in the upper femur, constituting a Salter–Harris I fracture. (**b**) In this older child, the epiphyseal plate (*arrow*) through the distal tibia is widened. However, it could be interpreted as normal. (**c**) With a comparative view of the other side, the normal epiphyseal plate now is demonstrated (*arrow*). Compare this plate with the now more obviously widened plate in (b)

an MRI grading system for tibial stress reaction. The most important finding on MRI is the presence of a linear fracture line which is perpendicular to the diaphysis and hypointense on T1W images and hypo- or hyperintense on STIR sequence. This should be reported as a stress fracture rather than stress reaction. Stress fracture will need longer activity modification and rest.

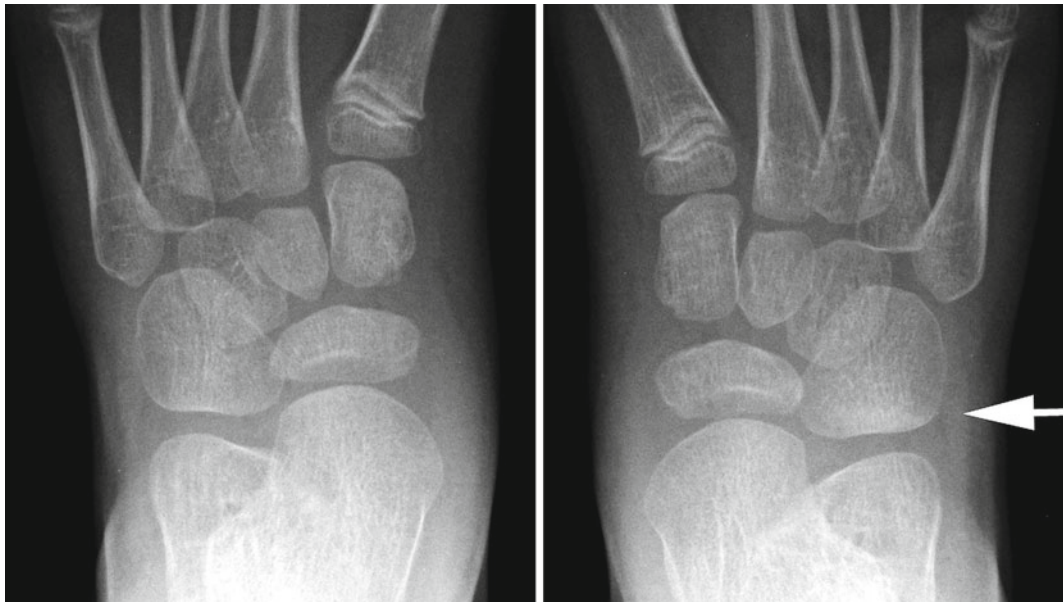


Fig. 4.7 Compression fracture. Note increased density through the base of the cuboid bone (*arrow*) on the left. This indicates the presence of a compression fracture

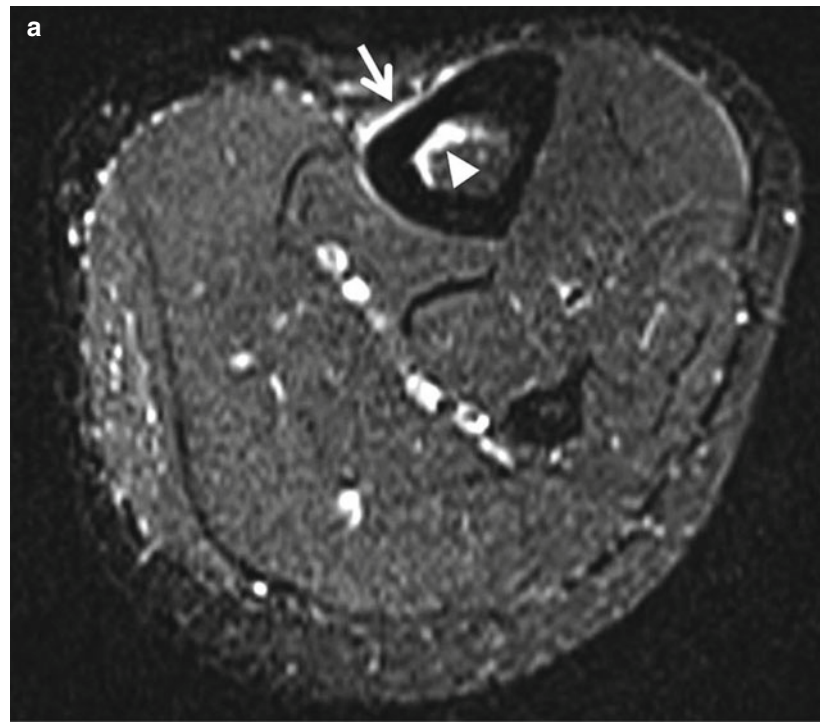


Fig. 4.8 Stress injury. Axial (**a**), sagittal (**b**), and coronal (**c**) STIR images in a 17-year-old with shin pain show periosteal (*arrows* in **a**, **b**) and endosteal edema (*arrowhead* in **a**) over the anteromedial cortex of the midtibia. Marrow edema is also noted in the sagittal (**b**) and coronal (**c**) images; however, no fracture line was seen. This represents stress injury rather than a stress fracture and requires shorter duration of activity restriction

Fig. 4.8 (continued)



References

1. Dunbar JS, Owen HF, Nogrady MB, McLeese R. Obscure tibial fracture of infants: the toddler's fracture. Can Assoc Radiol J. 1964;15:136–44.
2. Swischuk LE, John SD, Tschoepe EJ. Upper tibial hyperextension fractures in infants: another occult toddler's fracture. Pediatr Radiol. 1999;29:6–9.
3. Hernandez JA, Swischuk LE, Yngve DA, Carmichael KD. The angled buckle fracture in pediatrics: a frequently missed fracture. Emerg Radiol. 2003;10:71–5.
4. Borden IV S. Roentgen recognition of acute plastic bowing of the forearm in children. AJR. 1975;125:524–30.
5. Crowe JE, Swischuk LE. Acute bowing fractures of the forearm in children: a frequently missed injury. AJR. 1977;128:981–4.
6. Mabry JD, Fitch RD. Plastic deformation in pediatric fractures: mechanism and treatment. J Pediatr Orthop. 1989;9:310–4.
7. Strenstrom R, Gripenberg L, Bergius AR. Traumatic bowing of forearm and lower leg in children. Acta Radiol. 1978;19:243–9.
8. Salter RB, Harris WR. Injuries involving the epiphyseal plate. J Bone Joint Surg Am. 1963;45A:587–622.
9. Keret D, Mendez AA, Harcke HT, MacEwen GD. Type V physeal injury: a case report. J Pediatr Orthop. 1990;10:545–8.
10. Peterson HA, Burkhart SS. Compression injury of the epiphyseal growth plate: fact or fiction? J Pediatr Orthop. 1981;1:377–84.
11. Mendez AA, Bartal E, Grillot MB, Lin JJ. Compression (Salter-Harris type V) physeal fracture: an experimental model in the rat. J Pediatr Orthop. 1992;12:29–37.
12. Jaramillo D, Hoffer FA, Shapiro F, Rand F. MR imaging of fractures of the growth plate. AJR. 1990;155:1261–5.
13. Walker RN, Green NE, Spindler KP. Stress fractures in skeletally immature patients. J Pediatr Orthop. 1996; 16:578–84.

14. St. Pierre P, Staheli LT, Smith JB, Green NE. Femoral neck stress fractures in children and adolescents. J Pediatr Orthop. 1995;15:470–3.
15. Haasbeek JF, Green NE. Adolescent stress fractures of the sacrum: two case reports. J Pediatr Orthop. 1994;14:336–8.
16. Anderson MW, Ugalde V, Batt M, et al. Shin splints: MR appearance in a preliminary study. Radiology. 1997;204:177–80.
17. Tweed J, Avil S, Campbell J, Barnes M. Etiologic factors in the development of medial tibial stress syndrome: a review of the literature. J Am Podiatr Med Assoc. 2008;98(2):107–11.
18. Horev G, Korenreich L, Ziv N, Grunebaum M. The enigma of stress fractures in the pediatric age: clarification or confusion through the new imaging modalities. Pediatr Radiol. 1990;20:469–71.
19. Lee JK, Yao L. Stress fractures: MR imaging. Radiology. 1988;169:2217–20.
20. Gaeta M, Minutoli F, Scribano E, Ascenti G, Vinci S, Bruschetta D, Magaudda L, Blandino A. CT and MR imaging findings in athletes with early tibial stress injuries: comparison with bone scintigraphy findings and emphasis on cortical abnormalities. Radiology. 2005;235:553–61.
21. Close BJ, Strouse PJ. MR of physeal fractures of the adolescent knee. Pediatr Radiol. 2000;30:756–62.
22. Whan A, Breidahl W, Janes G. MRI of trapped periosteum in a proximal tibial physeal injury of a pediatric patient. AJR. 2003;181:1397–9.
23. Daffner RH, Weissman BN, Bennett DL. Expert panel on musculoskeletal imaging. ACR appropriateness criteria stress/insufficiency fracture, including sacrum, excluding other vertebrae. Reston: American College of Radiology; 2008.
24. Fredericson M, Bergman AG, Hoffman KL, Dillingham MS. Tibial stress reaction in runners: correlation of clinical symptoms and scintigraphy with a new magnetic resonance imaging grading system. Am J Sports Med. 1995;23:472–81.

Shoulder and Upper Arm

5

Normal Soft Tissues

There are no specific fat pads or soft tissues to evaluate around the shoulder or over the humerus. However, over the clavicle, the companion shadow is useful. This shadow represents the air-covered edge of the skin over the underlying soft tissues as they pass over the clavicle. Depending on positioning, this shadow is visible in most patients. However, it can become obliterated if there is swelling over the clavicle due to any inflammatory or traumatic cause of edema. This finding is readily evaluated and visualized when both shoulders are obtained on the same image (Fig. 5.1).

Joint Fluid

Fluid in the shoulder joint, be it pus, serous effusion, or blood, causes lateral displacement of humeral head and widening of the joint space, but this generally occurs only in very young children and infants. In older children, the joint capsule is too tight to allow this to happen. Associated swelling and edema of the soft tissues around the shoulder may or may not be present.

Clavicular Injuries

Overall, the clavicle is the most commonly injured bone of the shoulder in infants and young children. Injury usually results from falling on an outstretched extremity, falling directly on the shoulder, or from a direct blow to the clavicle. By far the most common location for a clavicular fracture is the midshaft, and while many such fractures are easy to identify, others are more elusive and can be hidden on one view (Fig. 5.2). In addition many clavicular fractures are not overt but rather greenstick or plastic bending fractures. Detecting these fractures is best accomplished by comparing one clavicle with the other, and any discrepancy should be treated with suspicion. In addition, one also should assess the soft tissues for a general increase in supraclavicular density resulting from edema and bleeding, and obliteration of the companion shadow of the clavicle (Fig. 5.3).

Acromioclavicular separations are not particularly common in infants and young children but are more common in the older child and adolescent. In such cases, one should first look for soft tissue prominence (bump) over the acromioclavicular joint (Fig. 5.4a) and then for separation of the joint itself. In addition, although the acromioclavicular joint is widened, one often also can see widening between the clavicle and the coracoid process of the scapula. Indeed, separation at this site caused by ligamentous sprain often is easier to detect than is acromioclavicular separation (Fig. 5.4b). In some cases, an associated coracoid process avulsion fracture can occur. In the infant and young child, rather than pure acromioclavicular separation, a fracture through the lateral end of the clavicle usually is sustained (Fig. 5.4c–e).

L.E. Swischuk, S.P. Jadhav (eds.), *Emergency Musculoskeletal Imaging in Children*,
DOI 10.1007/978-1-4614-7747-1_5, © Springer Science+Business Media New York 2014

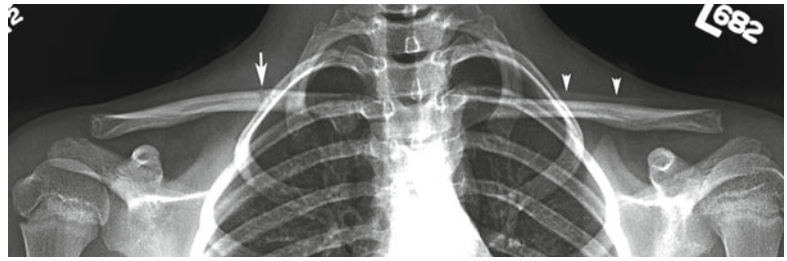


Fig. 5.1 Value of companion shadow. Note the companion shadow (*arrowheads*) over the left clavicle. On the right, there is no companion shadow because there is edema from an upward bending greenstick fracture (*arrow*)

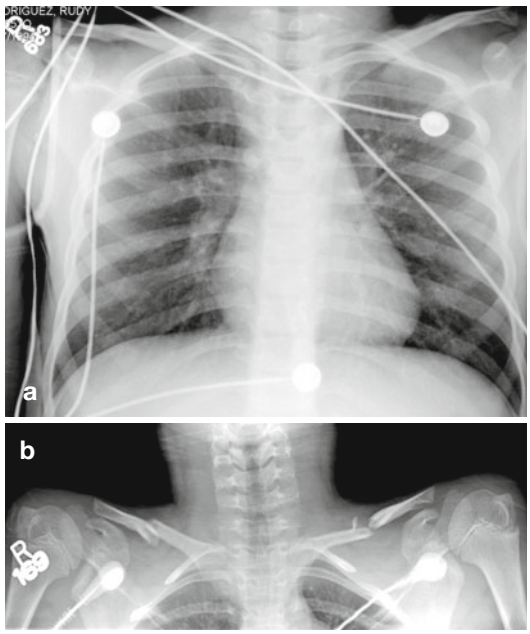


Fig. 5.2 Clavicle fracture, occult. (**a**) In this trauma patient, the clavicles appear normal. (**b**) A more dedicated view demonstrates bilateral displaced midshaft fractures. Fractures through the clavicle often are hidden on any given view

Medial clavicular injuries usually consist of anterior or posterior dislocations. In actual fact, these injuries are not dislocations but displaced Salter–Harris I or II fractures [1, 2]. The medial clavicular epiphysis is one of the last to fuse and it remains a weak point throughout adolescence and early adulthood. Because of this, any stresses applied to this area can result in a fracture dislocation. With anterior displacement, a clinically visible and palpable bulge is present over the involved sternoclavicular joint. With posterior displacement, such a clinical bulge is not present, but it is a more serious problem in terms of compression of neck vessels or the trachea [1, 2].

On frontal view, dislocation of the medial end of the clavicle, either anterior or posterior, should be suspected if the medial end of the involved clavicle is lower or higher than the medial end of the normal clavicle (Fig. 5.5). However, in some cases of anterior or posterior dislocation, the clavicles align normally on the AP view. In such cases, if there is any clinical suspicion of dislocation, one should proceed to CT with IV contrast for it will clearly define dislocation along with any associated vascular or visceral injury (Fig. 5.6).

Upper Humerus Injuries

In childhood, one of the more common injuries of the upper humerus is the Salter–Harris I or II epiphyseal–metaphyseal fracture. Salter–Harris type III injuries are less common and type IV and V injuries are very rare. In type I and II injuries where the epiphysis is completely separated, the diagnosis never is in doubt, but in more subtle cases, one should look for widening of the epiphyseal plate and/or a metaphyseal corner fracture (Fig. 5.7). In terms of the widened epiphyseal plate, one should be careful not to misinterpret the normal wide appearing epiphyseal plate for one which represents a fracture (Fig. 5.8).

Salter–Harris injuries to the proximal humerus, either acute or chronic, are seen in

young children playing baseball/softball and partaking in overexuberant, stressful pitching (Fig. 5.9a, b). In many cases, one will see evidence of a healing Salter–Harris I fracture and rarely posttraumatic osteophyte formation (Fig. 5.9c). This injury is termed "*Little Leaguer's shoulder*" [3]. The findings may be subtle on radiographs. MRI is a valuable tool in these situations to

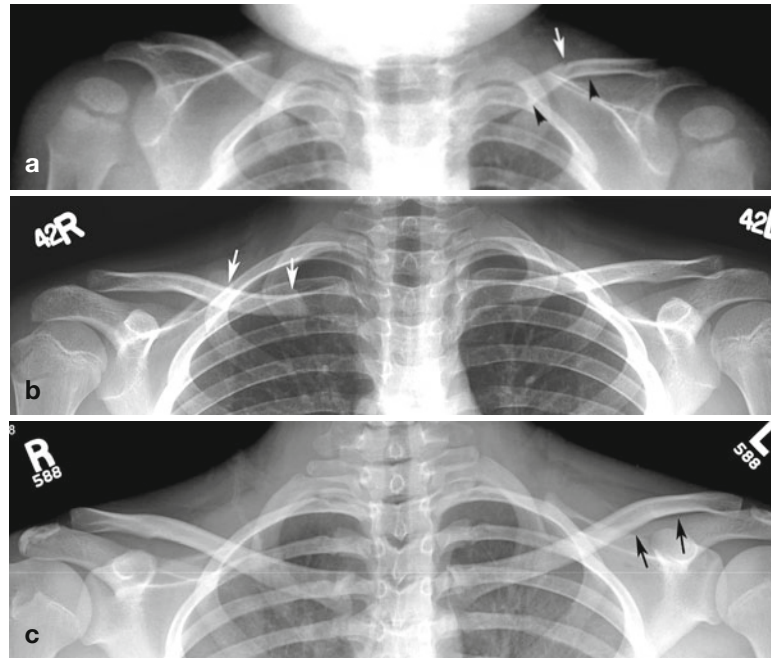


Fig. 5.3 Plastic bending–greenstick fractures: spectrum. (**a**) In this patient, there is an upward plastic bending fracture (*black arrowheads*) of the left clavicle. There also is a very subtle greenstick fracture visible over the superior surface (*arrow*) of the upwardly bent clavicle. (**b**) In this patient, there is a downwardly bent plastic bending fracture (*arrows*) through the medial half of the clavicle on the right. Compare with the normal clavicle on the left. (**c**) In this patient, a subtle upward plastic bending fracture (*arrows*) is seen through the lateral third of the left clavicle. Compare with the normal appearance of the right clavicle

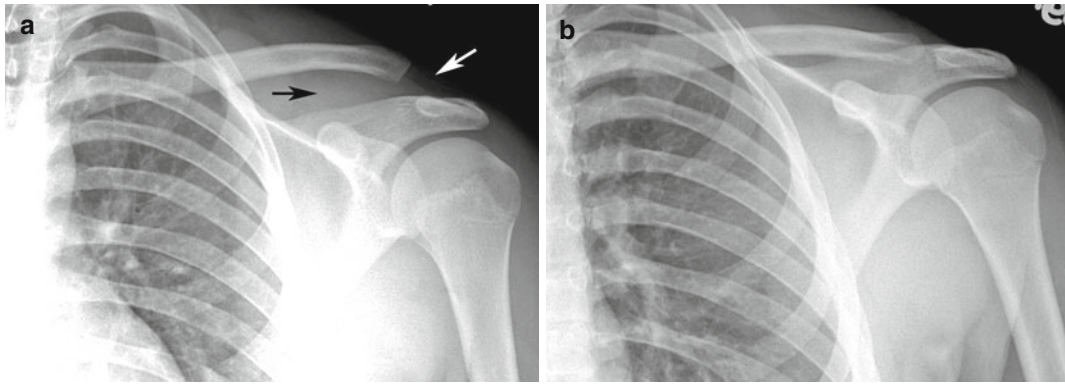


Fig. 5.4 Distal clavicular injuries. (**a**) Acromioclavicular and coracoclavicular separation. Note increased space between the distal clavicle and acromion (*white arrow*) and increased distance between the coracoid process and clavicle (*black arrow*). (**b**) Normal side for comparison. (**c**) Clavicle fracture and coracoclavicular ligament tear. Note the overt fracture through the distal clavicle (*white arrow*) and the increased coracoclavicular distance (*black arrows*). (**d**) Typical distal clavicular fracture. Note the typical buckle fracture (*arrow*) through the distal clavicle. This is the most common injury seen in this area in children. (**e**) Sleeve fracture of clavicle. Note the avulsed sleeve fracture (*arrow*) of the distal clavicle

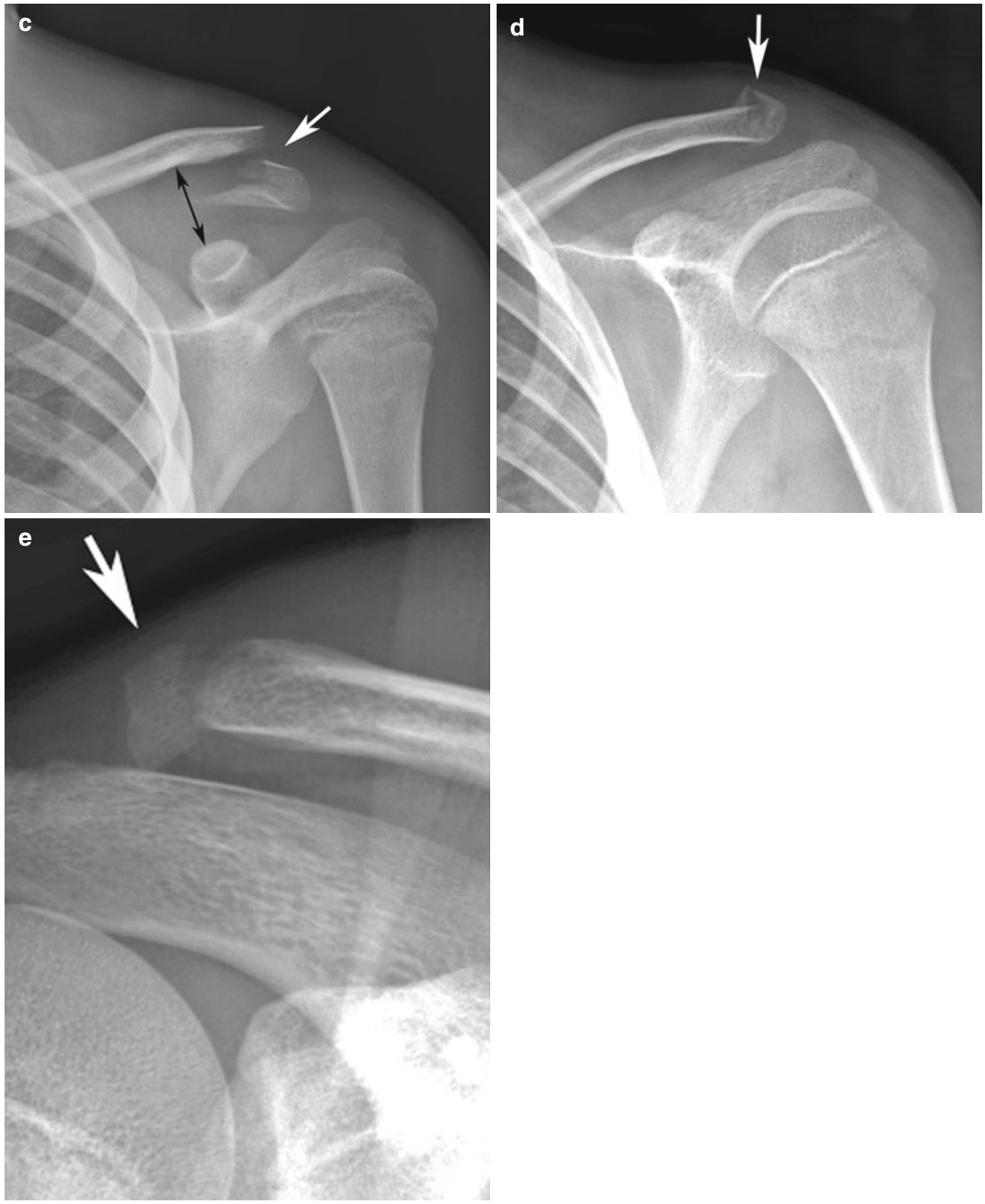


Fig. 5.4 (continued)

evaluate the extent of physeal injury and guide management.

Another variation of Salter–Harris fractures of the proximal humerus is that which occurs in older children where the epiphyseal plate has basically closed. However, with acute injuries one still can see a Salter–Harris fracture. The findings, however, are subtle and somewhat

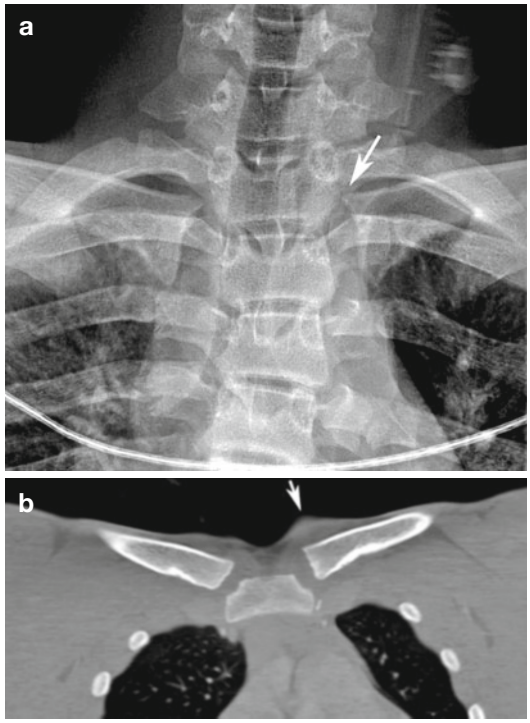


Fig. 5.5 Medial clavicular dislocation. (**a**) Note the slightly elevated medial left clavicle (*arrow*). (**b**) CT, coronal reconstructed view, demonstrates the slightly elevated medial left clavicle and the soft tissue bump (*arrow*) above it

different from the usual fracture. They consist of nothing more than a thin line of increased density (impaction with slipping and rubbing) along the epiphyseal plate (Fig. 5.10). These fractures probably are Salter–Harris I, but possibly Salter–Harris V fractures and now are more readily detected with MR imaging.

Other fractures occurring through the humerus include the impacted surgical neck fracture (Fig. 5.11a) and transverse or oblique humeral shaft fractures (Fig. 5.11b, c). *An important point to remember about surgical neck impacted fractures* is that they usually are the result of legitimate trauma. This is important because as isolated injuries, they frequently are suspected for non-accidental trauma. In our ongoing study of single bone fracture in infants and young children [4], it is becoming very apparent that these fractures are legitimate. Even if the patient is not ambulant but falls off of a bed, couch, etc., there is a natural instinct to extend the upper or lower extremity to break the fall and that is how we believe the fracture occurs. It would be very difficult to intentionally produce such a fracture. Contrarily, the outwardly angled midshaft humeral fracture (Fig. 5.11c, d) is highly suspect for non-accidental trauma [4].

Dislocations of the shoulder are not common in the young infant and child, for it is only after the epiphysis closes that it becomes a problem. The dislocation can be either anterior (i.e., subglenoid or subcoracoid) or posterior. Anterior dislocations usually have a rather characteristic appearance, with the humeral head being displaced downward and resting under the coracoid process or glenoid fossa (Fig. 5.12a). With chronic recurrent dislocations the rim of the glenoid fossa rubs and presses on to the humeral head to result in the Hill–Sachs notch (Fig. 5.12b, c).

Posterior dislocations are more difficult to detect, for overlapping of the humeral head and the glenoid fossa can be subtle (see Fig. 5.14a). Over the years, a number of signs have been suggested for assisting one in identifying posterior dislocations, and recently, a new sign, the "*Mouzopoulos*" sign has been described [5]. The reason the "*Mouzopoulos*" sign works is that with posterior dislocation the humerus comes to lie in a fixed internally rotated position. This being the case, both the greater and lesser tuberosities are seen en face and the tops of them outline the letter "M" or if you like, two mountains (Fig. 5.13). However, a word of caution is in order as the same finding can be seen with normal internal rotation of the shoulder, and so the sign is valid only with fixed shoulder dislocation. In any case however, and especially with posterior dislocations, a transaxillary view of the shoulder should be obtained for clearer definition. Of course, CT studies are especially useful for locating the humeral head and any associated glenoid avulsions in any of these cases. Similarly MR is the imaging of choice for identifying soft tissue

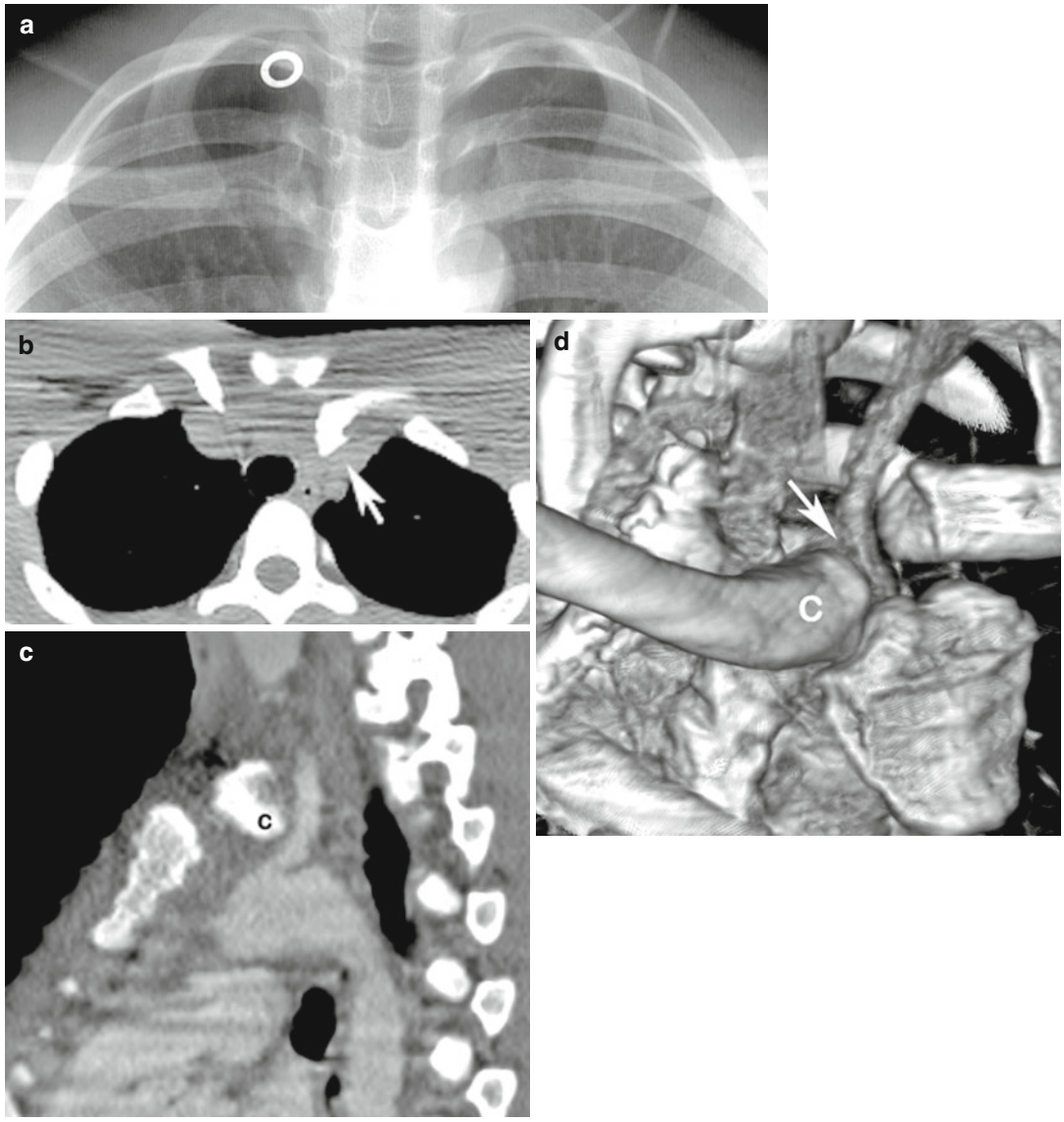


Fig. 5.6 Medial clavicular dislocation: various imaging. (**a**) AP view of the clavicles is normal. White circle is an artifact. (**b**) CT demonstrates marked posterior displacement of the left medial clavicle (*arrow*). (**c**) Sagittal reconstructed CT image demonstrates the medial end of the clavicle (*C*) impinging on the carotid artery. (**d**) 3D reconstruction demonstrates the site of impingement of the carotid artery (*arrow*) by the medial clavicle (*C*). (**e**) 3D reconstruction. Note the posterior position of the dislocated medial left clavicle (*arrow*). (**f**) Another view demonstrates the medial end of the clavicle (*C*) displaced posteriorly

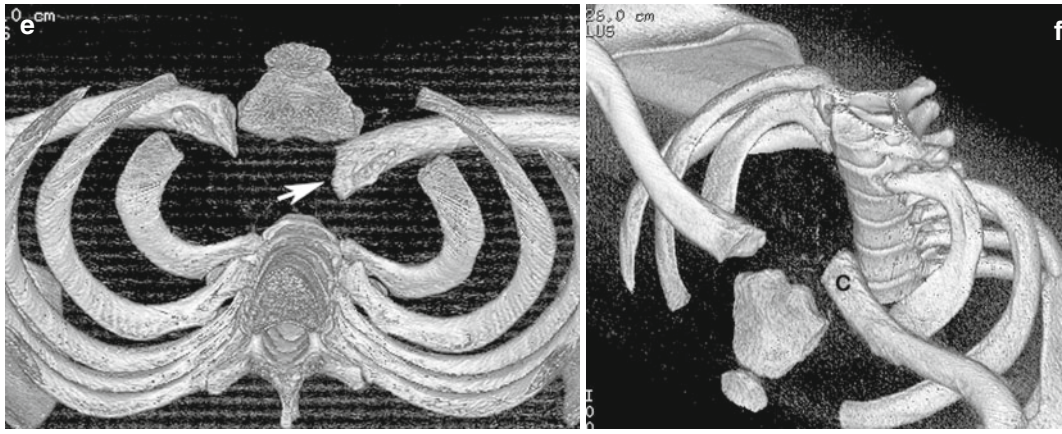


Fig. 5.6 (continued)

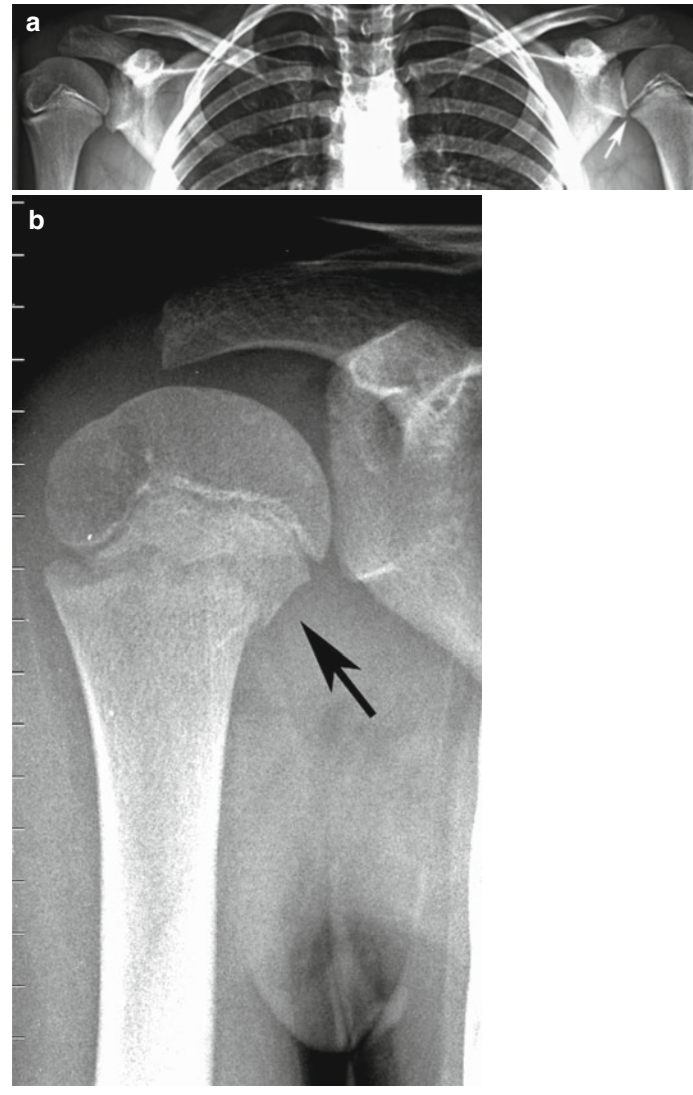


Fig. 5.7 Proximal humeral fractures. (**a**) Note widening of the left epiphyseal plate (*arrow*), consistent with a Salter–Harris I fracture. (**b**) In this patient, a small metaphyseal fragment (*arrow*) is seen consistent with a Salter–Harris II fracture

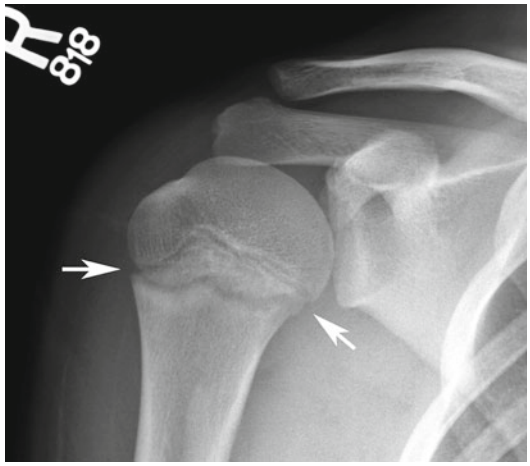


Fig. 5.8 Pseudo-epiphyseal fracture: normal epiphyseal plate. Normally with some angulation, the epiphyseal plate through the proximal humerus may appear normal anteriorly and widened (*arrows*) to suggest a pseudofracture posteriorly

articular and ligamentous and labral injuries and the subject is discussed later.

As mentioned earlier, in young children, dislocations of the shoulder are less common because fractures through the epiphyseal plate tend to occur. However, both can be seen together in some patients (Fig. 5.14a). In addition, especially with posterior dislocations, avulsion fracture of the glenoid rim can be seen (Fig. 5.14b, c).

Scapular Fractures

These fractures can occur through the body of the scapula or the acromial or coracoid processes of the scapula. Fractures through the body of the scapula usually result from direct blows and can be

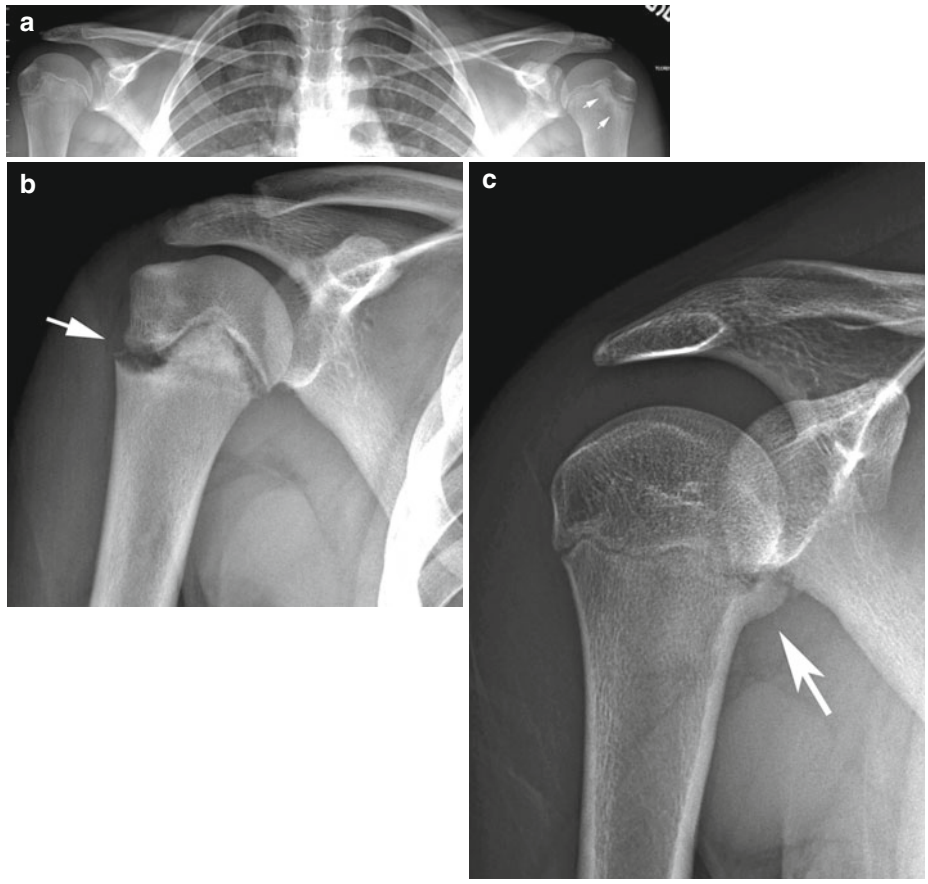


Fig. 5.9 Little Leaguer's shoulder. (**a**) Note slight widening of the lateral epiphyseal plate and adjacent metaphyseal sclerosis (*arrow*) in this subacute left Little Leaguer's elbow. (**b**) Another patient. Note the widened epiphyseal plate through the proximal humerus. In addition note the small fleck of avulsed bone (*arrow*). This was an acute injury. (**c**) Chronic Little Leaguer's shoulder. The epiphyseal plate appears relatively normal, but there is an acquired osteophyte (*arrow*) present

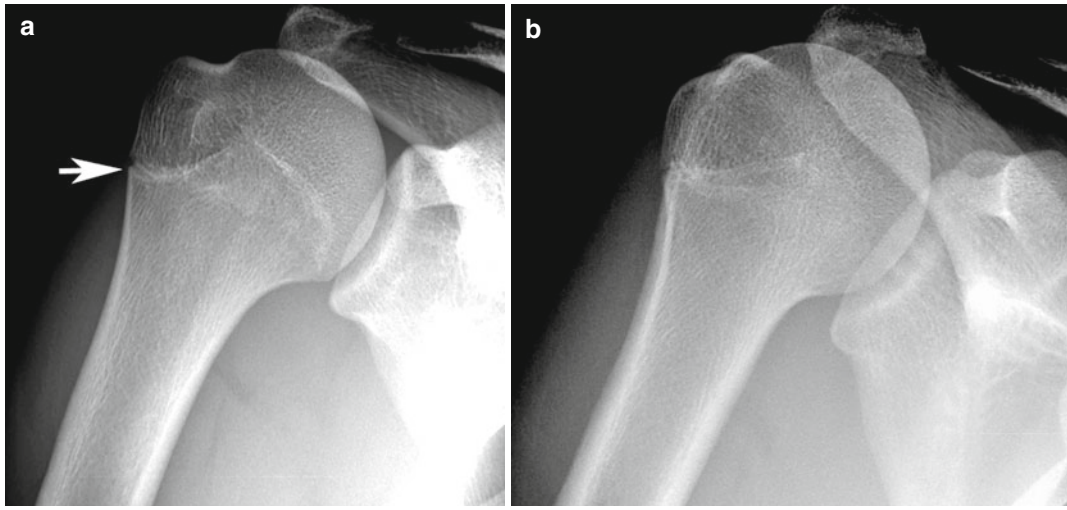


Fig. 5.10 Salter–Harris fracture: older child/adolescent. (**a**) In this adolescent with the epiphyses basically closed, the epiphyseal plate appears thin and sclerotic (*arrow*). (**b**) On the normal side, there is very little evidence of a residual epiphyseal plate

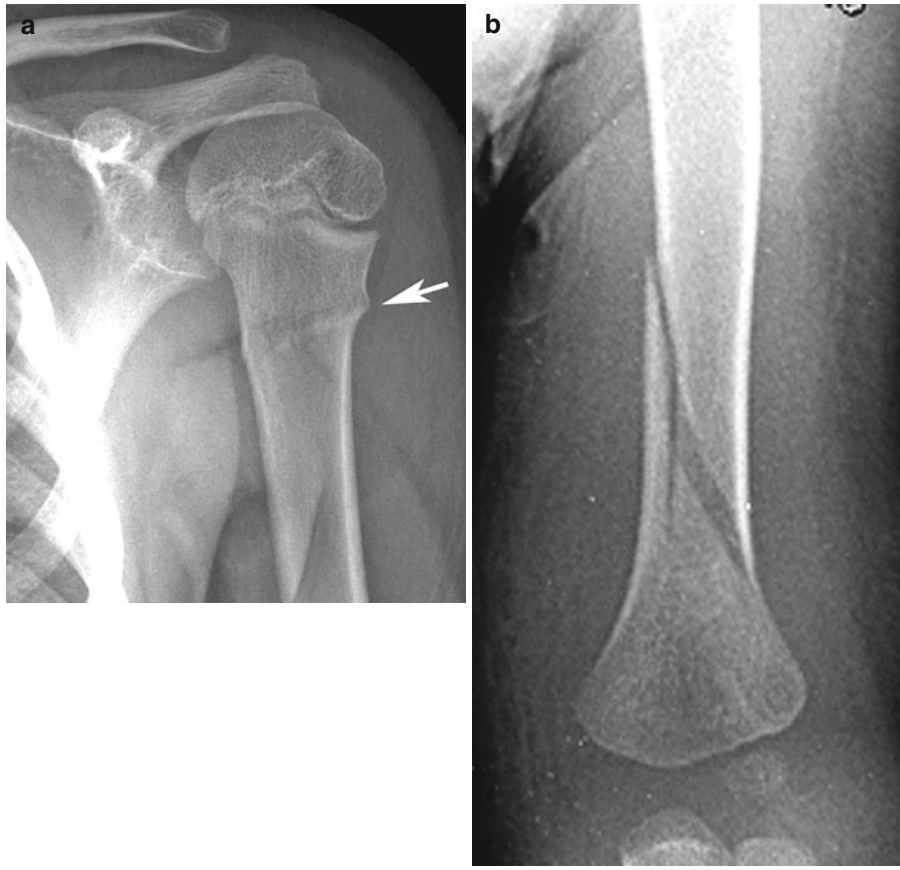
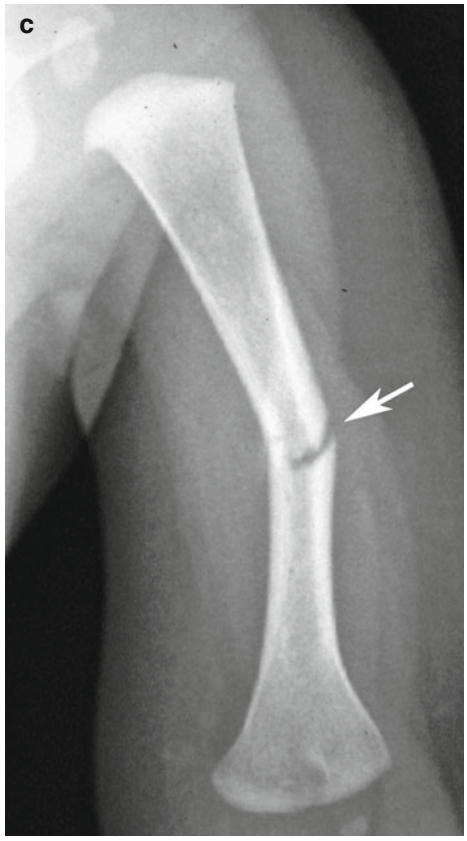


Fig. 5.11 Humeral fractures. (**a**) Note the typical buckle, impacted fracture (*arrow*) through the proximal humerus. (**b**) Typical spiral fracture through the distal humerus. (**c**) Transverse fracture (*arrow*) with outward angulation of the humerus. This becomes suspicious for non-accidental trauma. (**d**) Mechanism of injury in such cases. The lower arm is grabbed by the fingers and the thumb exerts pressure on the midshaft of the long bone. There also is a rotation component (*arrow*)



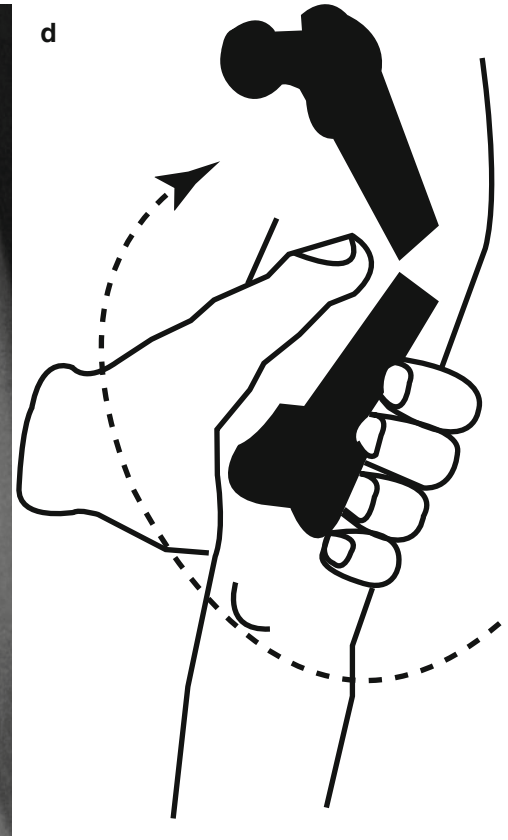


Fig. 5.11 (continued)

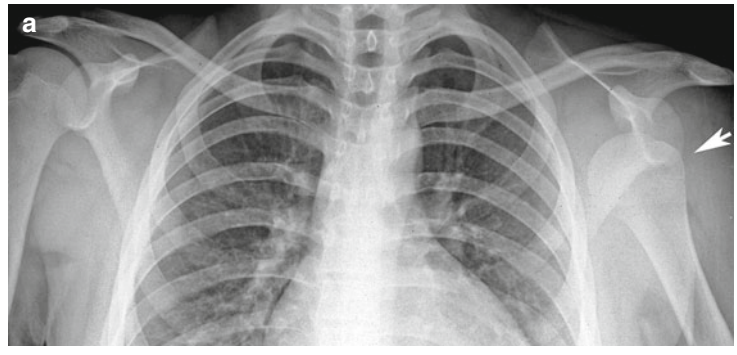


Fig. 5.12 Shoulder dislocation: anterior. (**a**) Note the typical inferior displacement of the humeral head (*arrow*). (**b**) Axial view demonstrates the location of the anterior glenoid rim (*arrow*). With chronic dislocations, constant impaction and erosion here result in a Hill–Sachs notch. (**c**) CT study in another patient demonstrates the characteristic appearance of the Hill–Sachs notch (*arrow*) with the glenoid rim in the notch

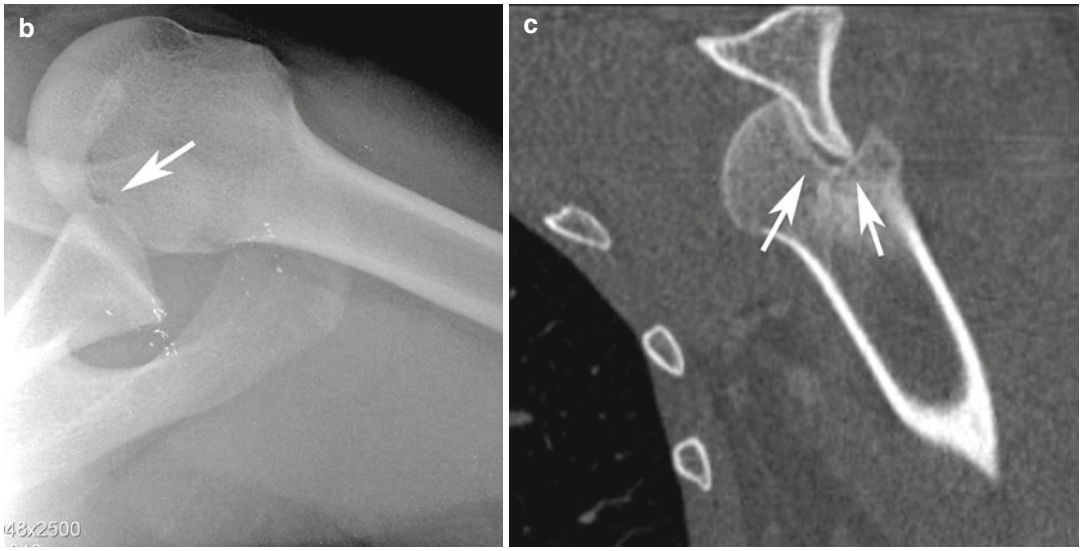


Fig. 5.12 (continued)

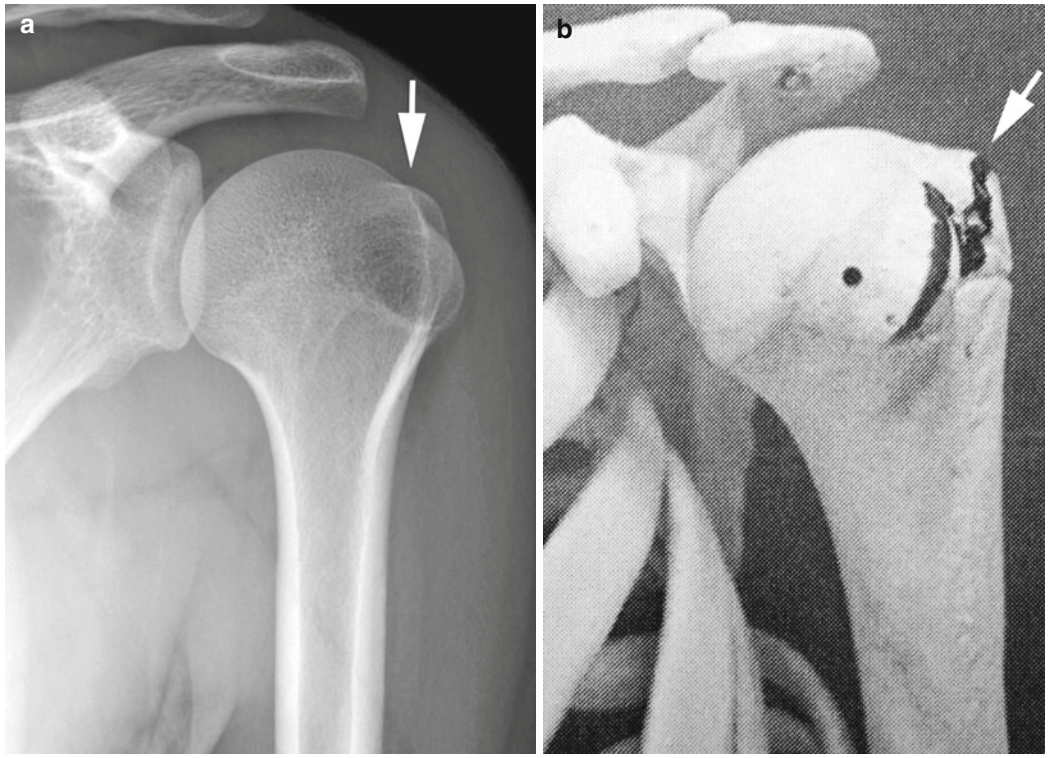


Fig. 5.13 Mouzopoulos sign. (**a**) Neutral position of shoulder. Note that the anterior borders of the lesser and greater tuberosities are seen on top of one another (*arrow*). (**b**) Diagrammatic representation of the same findings (*arrow*). (**c**) With internal rotation, the lesser and greater tuberosities are now seen partially en face. The "M" sign is now coming into view (*arrow*). (**d**) With marked internal rotation as occurs with posterior dislocation, the lesser and greater tuberosities now are seen fully en face and the letter "M" becomes apparent (*arrow*). (**e**) Radiographic findings of the Mouzopoulos sign. Note that the humerus appears normal as it articulates with the glenoid fossa but the Mouzopoulos sign (*arrows*) is positive for a dislocation. (**f**) Axial view confirms posterior dislocation of the humeral head (*arrows*) from the glenoid fossa (Reprinted with permission from Mouzopoulos [5]. With permission from Springer Science + Business Media)

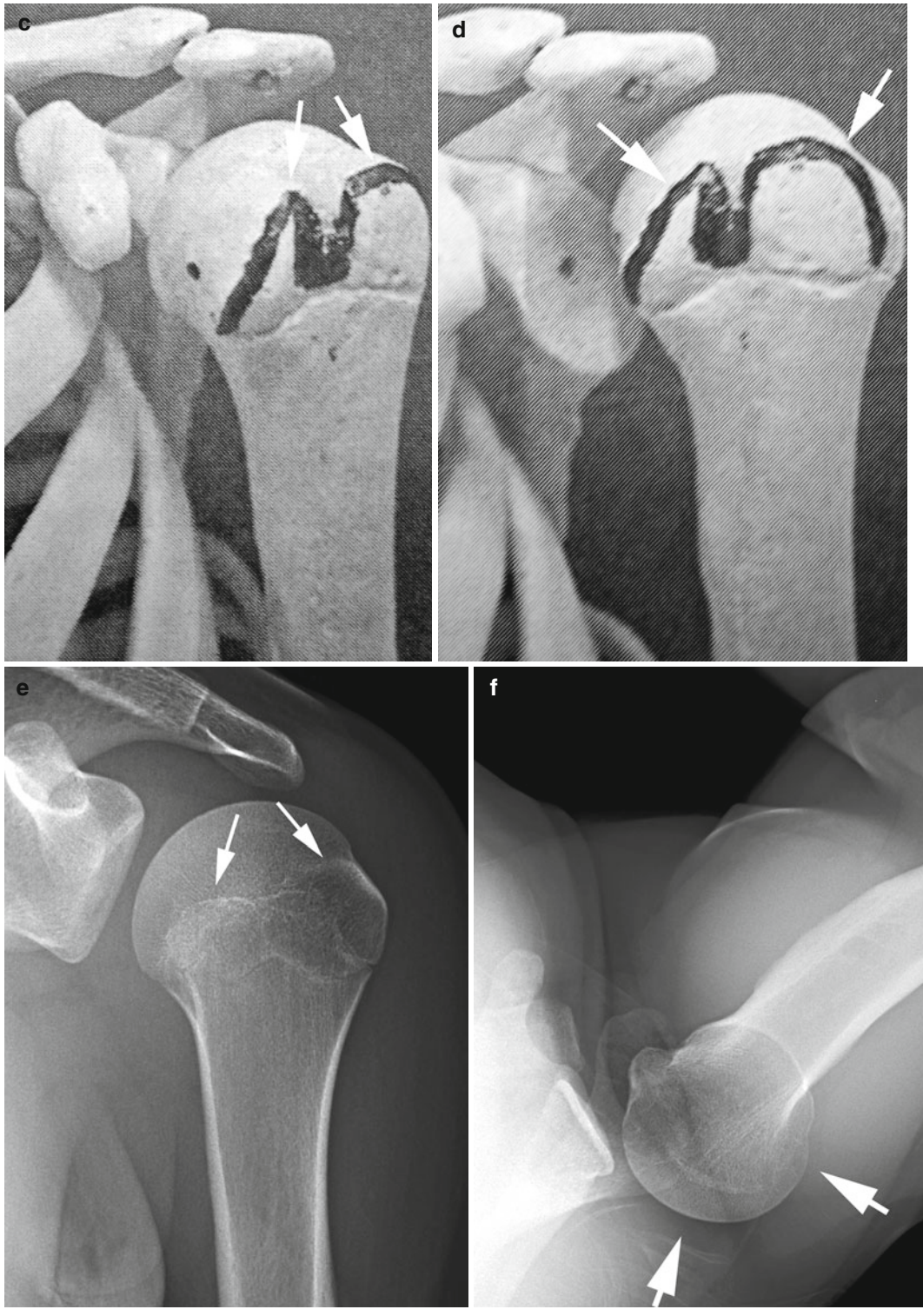


Fig. 5.13 (continued)

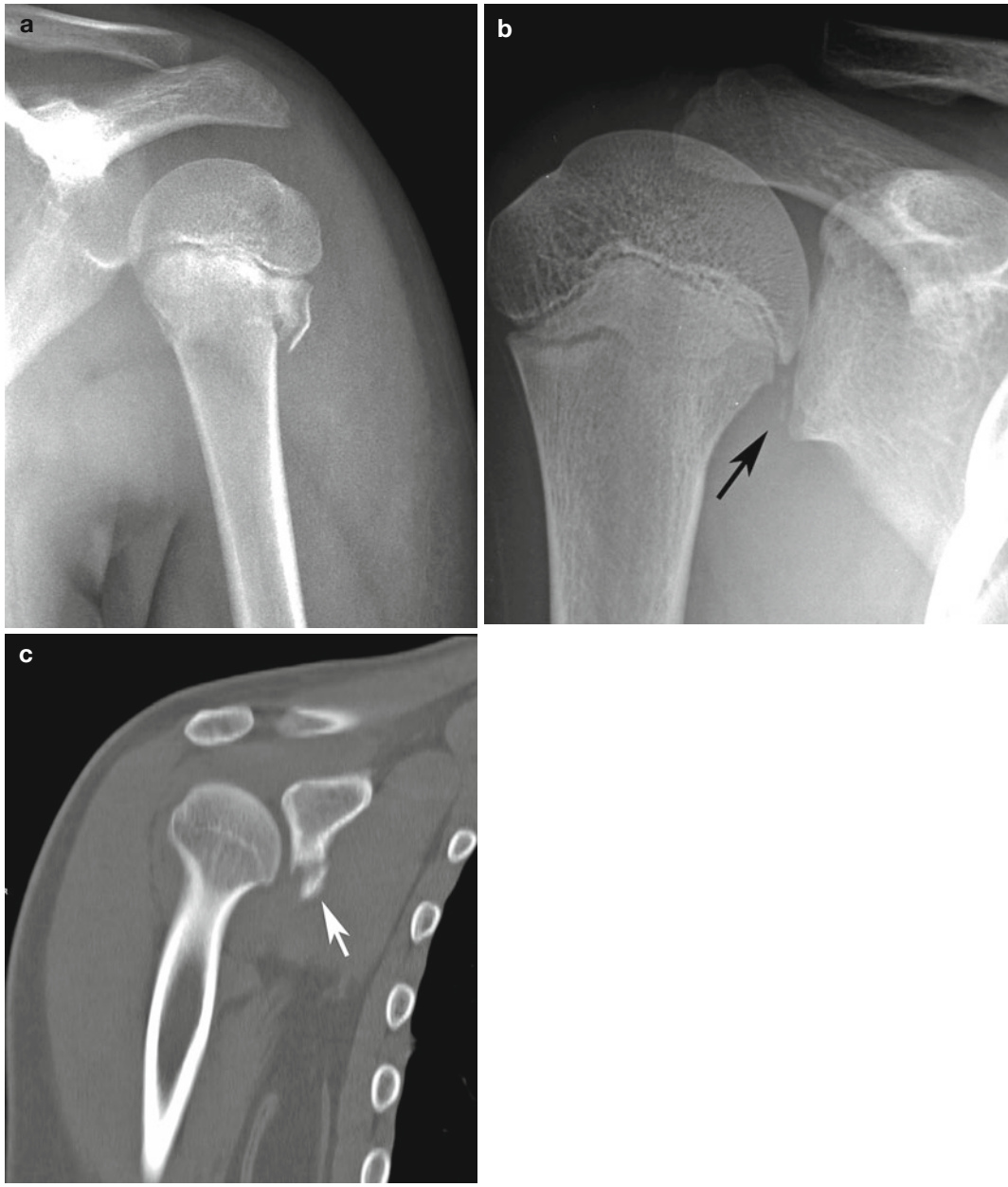


Fig. 5.14 Shoulder fracture–dislocation. (**a**) In this patient, a posterior dislocation is present (note overlap of the humeral head and the glenoid fossa). In addition, an impacted humeral metaphyseal fracture was present. (**b**) In this patient, after a posterior dislocation, a small bony fragment (*arrow*) was seen adjacent to the inferior glenoid rim. (**c**) CT study, coronal presentation, demonstrates the avulsion fracture (*arrow*) off of the glenoid rim

linear, curvilinear, or stellate (Fig. 5.15a). However, in some cases, only compression of the scapular trabeculae occurs and one will only see increased focal density just below the glenoid fossa (Fig. 5.15b). With healing, the findings can mimic a tumor such as Ewing's sarcoma (Fig. 5.15c).

Fractures through the acromial and coracoid processes of the scapula can result from direct

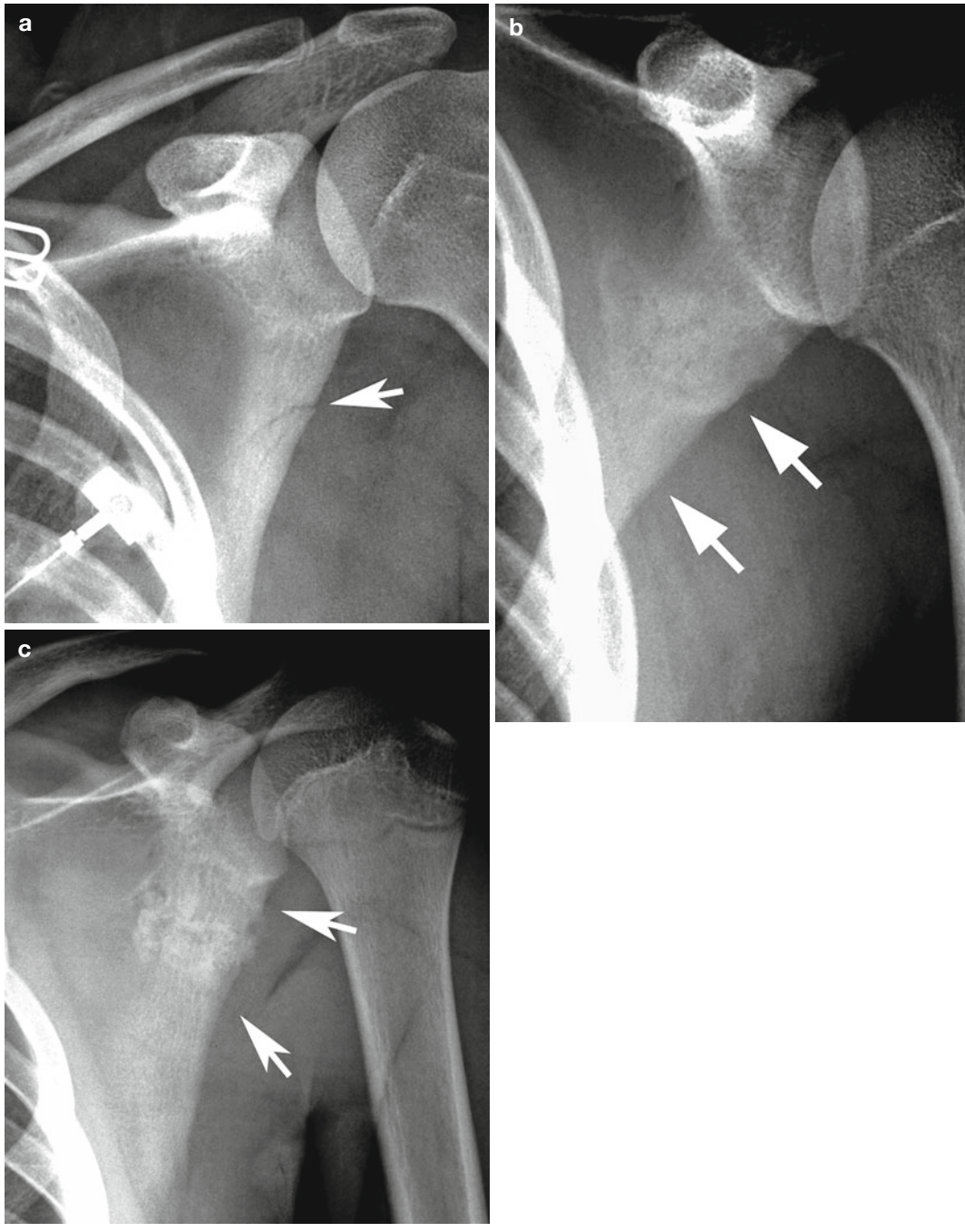


Fig. 5.15 Scapular fractures. (**a**) Note the linear-stellate fracture (*arrow*) through the scapula. (**b**) In this patient, only vague sclerosis is seen in the scapula (*arrows*). This represents an impaction fracture. (**c**) Healing impaction fracture note the mixed sclerotic-lytic appearance (*arrows*) of a healing impaction fracture. The findings often are mistaken for a tumor such as a Ewing's sarcoma

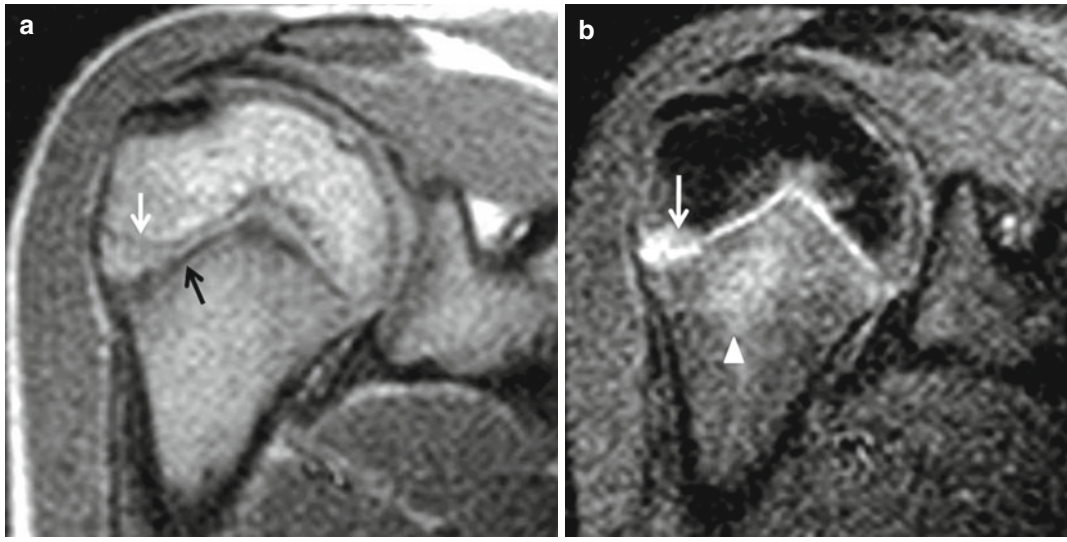
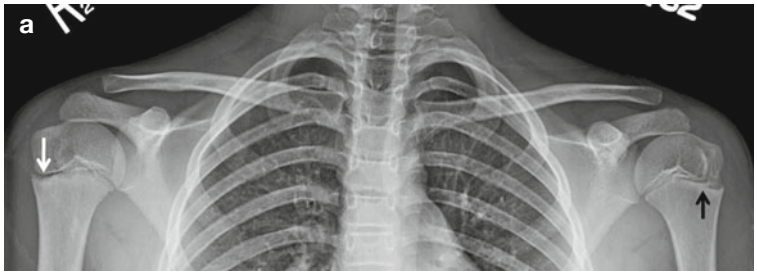


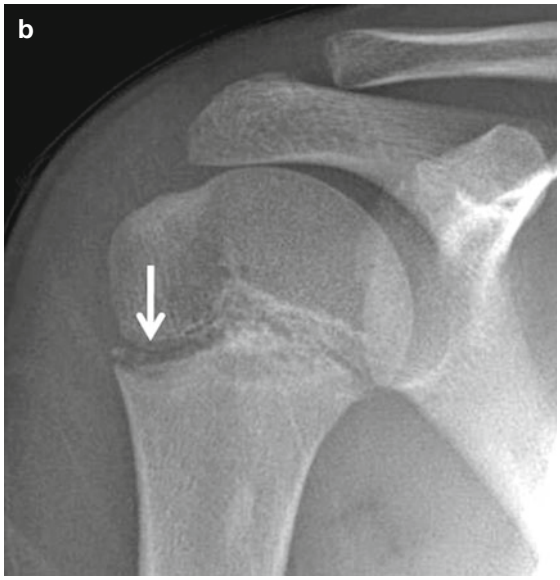
Fig. 5.16 Partial Salter–Harris I fracture. (**a**) T1-weighted coronal oblique image shows widening of the growth plate laterally (*white arrow*). The hypointense zone of provisional calcification (*black arrow*) seen along the margin of the growth plate is preserved. (**b**) Coronal oblique STIR image shows widening of the growth plate laterally (*arrow*) with edema extending into the metaphysis (*arrowhead*) confirming the presence of the partial Salter–Harris type I fracture

blows or falls on the outstretched extremity and may be difficult to detect. Comparative views are of the utmost importance here, especially with the more peculiar fractures, and of course CT studies are invaluable in detecting fractures of the scapula, especially those of the glenoid fossa (see Fig. 5.14c).

Finally, there are instances where plain films fail to, or are unable to show underling pathology. For the most part, these include physeal and chondrolabral injuries. Physeal injuries may present in the ER setting either as acute Salter–Harris I injury or due to pain secondary to chronic insult, namely, Little Leaguer's shoulder. These injuries may be subtle on radiographs and often are best evaluated with MRI. Salter–Harris I fracture of the proximal humerus presents after an acute event. In cases of non-displaced Salter–Harris I injury, radiographs are often inconclusive, sometimes even with comparative views. MRI will show widening of the physis, but more importantly, edema will be noted extending into the metaphysis (Fig. 5.16). Displaced Salter– Harris I and II fractures are readily diagnosed on radiographs and usually do not warrant MR imaging.

Little Leaguer's shoulder is seen in children involved in overhead throwing activity. The chronic, repetitive indirect trauma to the physis and metaphysis may result in ischemia to the zone of hypertrophy, disruption of the zone of provisional calcification, and arrest of metaphyseal endochondral ossification [6]. This leads to widening of the growth plate and an indistinct zone of provisional calcification on radiographs and MRI which helps to differentiate this injury from an acute non-displaced Salter–Harris I injury where the zone of provisional calcification is preserved (Fig. 5.17). Also on cartilage sensitive sequences, metaphyseal cartilaginous extensions may be noted in advanced cases. However, advanced cases are usually readily diagnosed radiographically. MRI is warranted only when there is diagnostic uncertainty, atypical response to treatment or atypical clinical presentation (Fig. 5.18).


a


b


c


d

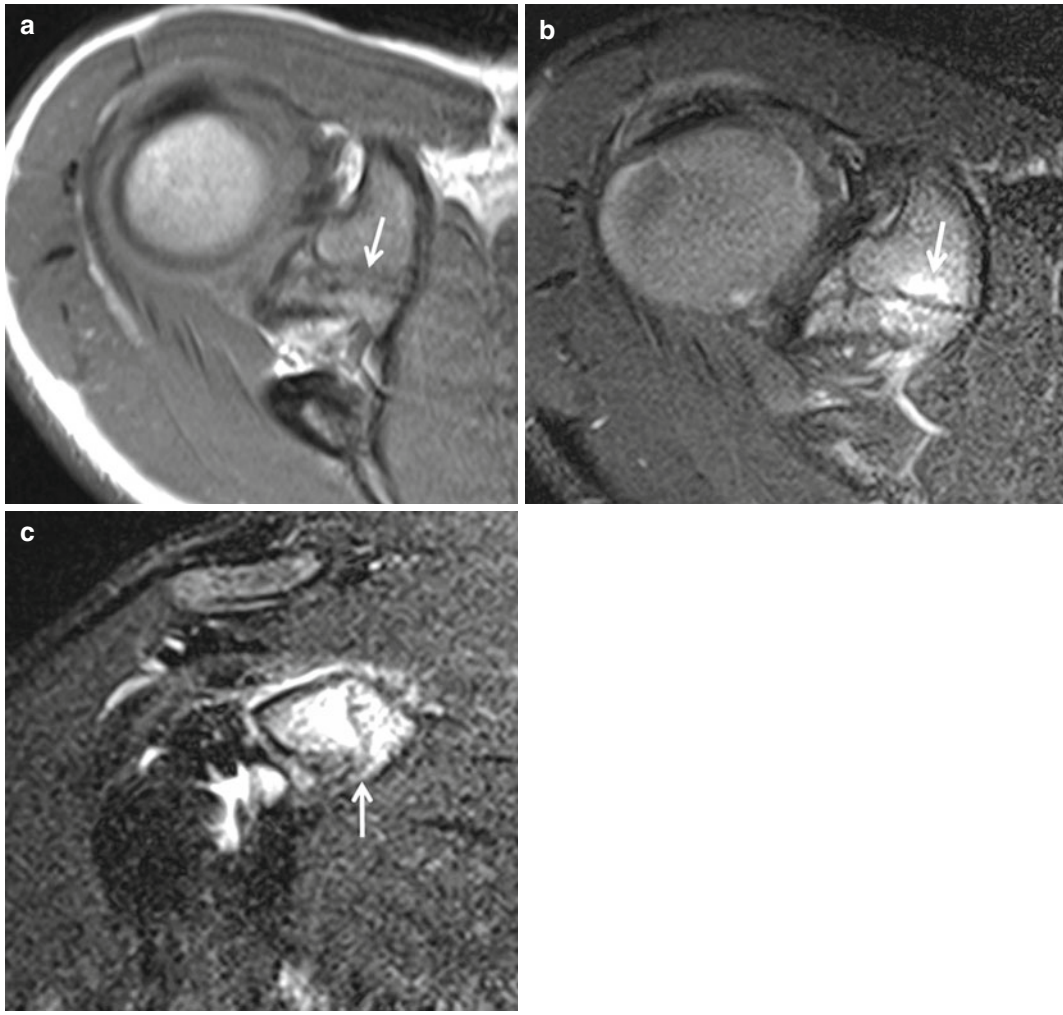


Fig. 5.18 Little Leaguer's shoulder variant: coracoid process avulsion. (**a**) Axial T1-weighted image shows widening of the coracoid physis (*arrow*). (**b**) Axial T2-weighted image with fat saturation shows bone edema on both sides of the coracoid physis (*arrow*). (**c**) Coronal oblique STIR image confirms significant bone edema on both sides of the coracoid physis (*arrow*). These findings are in keeping with an avulsion-type injury of the coracoid process due to excessive stress from muscles attached to it

Fig. 5.17 Little Leaguer's shoulder: early changes. (**a**) Frontal radiograph of the shoulders shows mild widening of the right proximal humeral growth plate laterally (*white arrow*) in this pitcher with acute on chronic pain. The dense zone of provisional calcification seen at the metaphyseal margin on the normal left side (*black arrow*) is indistinct on the right, suggesting a chronic process. (**b**) Magnified view of the right shoulder shows the widening of the growth plate (*arrow*) and the adjacent irregular/fragmented metaphyseal margin more clearly. (**c**) Sagittal T2-weighted image shows diffuse widening of the growth plate due to arrest of metaphyseal endochondral ossification, and in addition, loss of the normal hypointense zone of provisional calcification (*arrows*). (**d**) Coronal oblique STIR image shows diffuse widening of the high-signal epiphyseal plate (*white arrow*) and high-signal edema in the metaphysis (*black arrow*) confirming an acute on chronic epiphyseal/metaphyseal process. In cases of chronic insult alone, metaphyseal edema will be absent

Chondrolabral injuries usually are imaged with MRI in the non-emergent setting. An MR arthrogram is warranted in most cases for optimal evaluation (Fig. 5.19). Uncommonly a child may present to the ER with acute traumatic shoulder dislocation, and postreduction MRI may be obtained emergently to evaluate for Bankart fracture/lesion. With higher strength magnets and presence of joint effusion/hemarthrosis in the acute setting, chondrolabral injuries may be detected without need for an intra-articular injection. Suspected muscular injury is also a valid indication for an MRI.

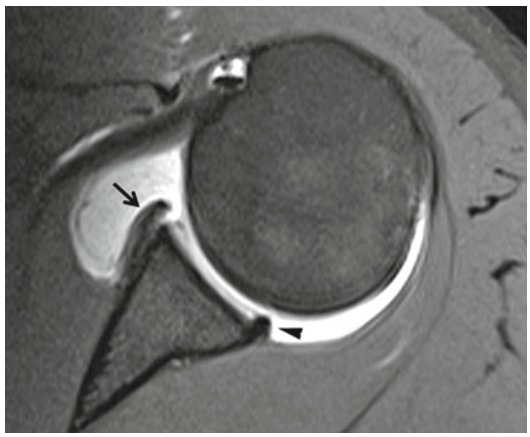


Fig. 5.19 Anterior labral periosteal sleeve avulsion (ALPSA) lesion: Bankart variant. Sixteen-year-old male who had an anterior shoulder dislocation. Postreduction axial T1-weighted fat saturation MRI with intra-articular contrast shows anterior periosteal avulsion along with displacement of the antero-inferior labrum (*arrow*) secondary to a labral fracture. Note the normal labrum posteriorly (*arrowhead*). The avulsed periosteum and medial displacement of the anterior labrum constitute the ALPSA lesion. With a true Bankart lesion, the labrum is fractured and the periosteum is torn and not avulsed

Normal Findings Causing Problems

There are a number of secondary ossification centers around the scapula which can cause difficulty in interpretation. However, the two most common secondary centers are the coracoid process which can be very large and suggest a fracture and the more common os acromiale (Fig. 5.20a) which also can be very large and suggest a fracture. Finally, the ring apophysis of the glenoid fossa, if caught tangentially, can erroneously suggest a glenoid rim fracture (Fig. 5.20b).

Humeral Shaft Injuries

Fractures through the humeral shaft usually are straightforward consisting of transverse and oblique/spiral fractures. When any of these fractures are outwardly angled, they become suspicious for non-accidental trauma (see Fig. 5.11c, d).

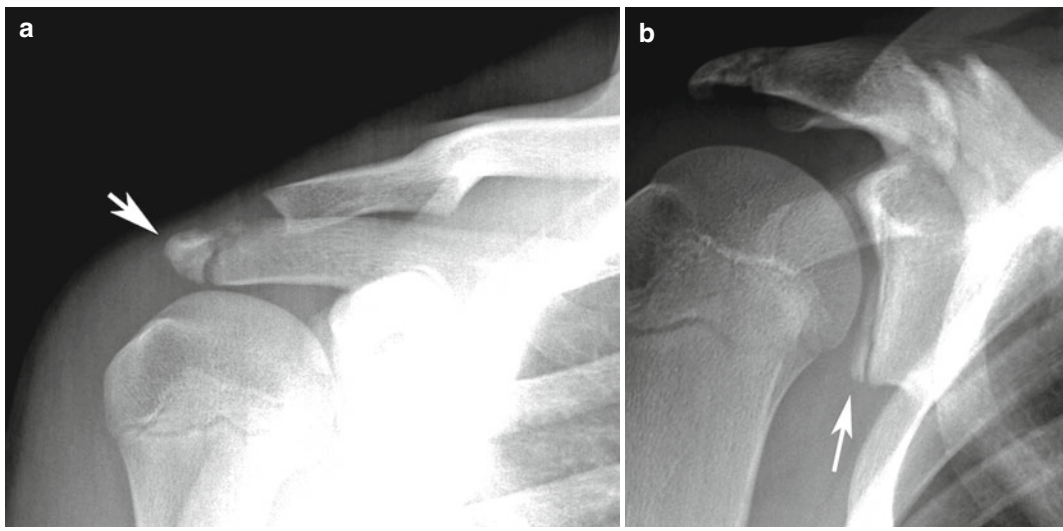


Fig. 5.20 Normal findings: pseudofractures. (**a**) Normal os acromiale (*arrow*). (**b**) Normal epiphysis (*arrow*) of the glenoid fossa

References

1. Carmichael KD, Longo A, Lick S, Swischuk L. Posterior sternoclavicular epiphyseal fracture-dislocation with delayed diagnosis. Skeletal Radiol. 2006;35:608–12.
2. Sykes JA, Ezetendu C, Sivitz A, Lee JRJ, Desai H, Norton K, Daly RA, Kalyanaraman M. Posterior dislocation of sternoclavicular joint encroaching on ipsilateral vessels in 2 pediatric patients. Pediatr Emerg Care. 2011;27(3):327–30.
3. Torg JS, Plllack H, Sweterlitsch P. The effect of competitive pitching on the shoulders and elbows of preadolescent baseball players. Pediatrics. 1972;49: 267–72.
4. Swischuk LE. Single bone fractures in infants and young children; Accidental or non-accidental trauma, In preparation.
5. Mouzopoulos G. The "Mouzopoulos" sign: a radiographic sign of posterior shoulder dislocation. Emerg Radiol. 2010;17:317–20.
6. Jaramillo D, Laor T, Zaleske DJ. Indirect trauma to the growth plate: results of MR imaging after epiphyseal and metaphyseal injury in rabbits. Radiology. 1993; 187:171–8.

Elbow and Forearm

6

Normal Soft Tissues and Fat Pads

In the elbow, the most important fat pads to assess are the anterior and posterior fat pads over the distal humerus [1]. The anterior fat pad is located in the coronoid fossa while the posterior fat pad is located in the olecranon fossa. These fat pads must be evaluated on true lateral, flexed views of the elbow, for with any degree of rotation or extension, their usefulness diminishes or becomes totally invalid. Normally, on the true lateral flexed view of the elbow, the anterior fat pad is visible, but the posterior fat pad is not (Fig. 6.1a). The reason for the lack of visualization of the posterior fat pad is that it lies deep in the olecranon fossa. It becomes visible only if fluid in the joint displaces it posteriorly. On extension it may be visible in normal individuals, but never on a flexed view. These fat pad configurations are very consistent, and any deviation from the normal pattern should be considered abnormal and suspicious. On the other hand, if the fat pads are normal, underlying abnormality is basically nonexistent [2].

Fluid in the elbow joint usually produces upward and outward displacement of the anterior and posterior fat pads, often referred to as the "sail sign" or the "fat pad sign" (Fig. 6.1b). These fat pads are intracapsular but extrasynovial [3] and their displacement is very accurate in reflecting the presence of intra-articular fluid. Ultrasonography also can be used to detect fluid in the elbow joint [4] but seldom is needed because the findings on true lateral elbow images are very sensitive.

The supinator fat pad [5] is another normal fat pad around the elbow. It also is seen on true lateral views and overlies the anterior aspect of the supinator muscle (Fig.6.1c). This fat pad is less consistently visualized in infants and young children, but in older children when it is obliterated/displaced, fractures of the proximal radius should be suspected. It also can be obliterated with generalized, nonspecific edema around the elbow.

Finally, in the elbow it is important to appreciate whether soft tissue swelling is present and whether it predominates medially or laterally. The reason for this is that *with lateral swelling a fracture of the lateral condyle and capitellum should be suspected, while with medial swelling fractures of the medial epicondyle should be sought for*. These findings are more specifically addressed in future sections of this chapter.

Elbow Fractures and Injuries

Injuries of the three bones around the elbow are perhaps one of the most commonly encountered injury groups in infants and children. Each of these bones, because of their configuration and articulations tend to fracture in different ways. It is most important to appreciate these mechanisms of injury because this enables one to detect the more subtle injuries [6]. For the most part, elbow injuries are sustained by falling on the hyperextended upper extremity ("FOOSH" injury). In this injury axial loading forces act on all three bones,

L.E. Swischuk, S.P. Jadhav (eds.), *Emergency Musculoskeletal Imaging in Children*,
DOI 10.1007/978-1-4614-7747-1_6, © Springer Science+Business Media New York 2014

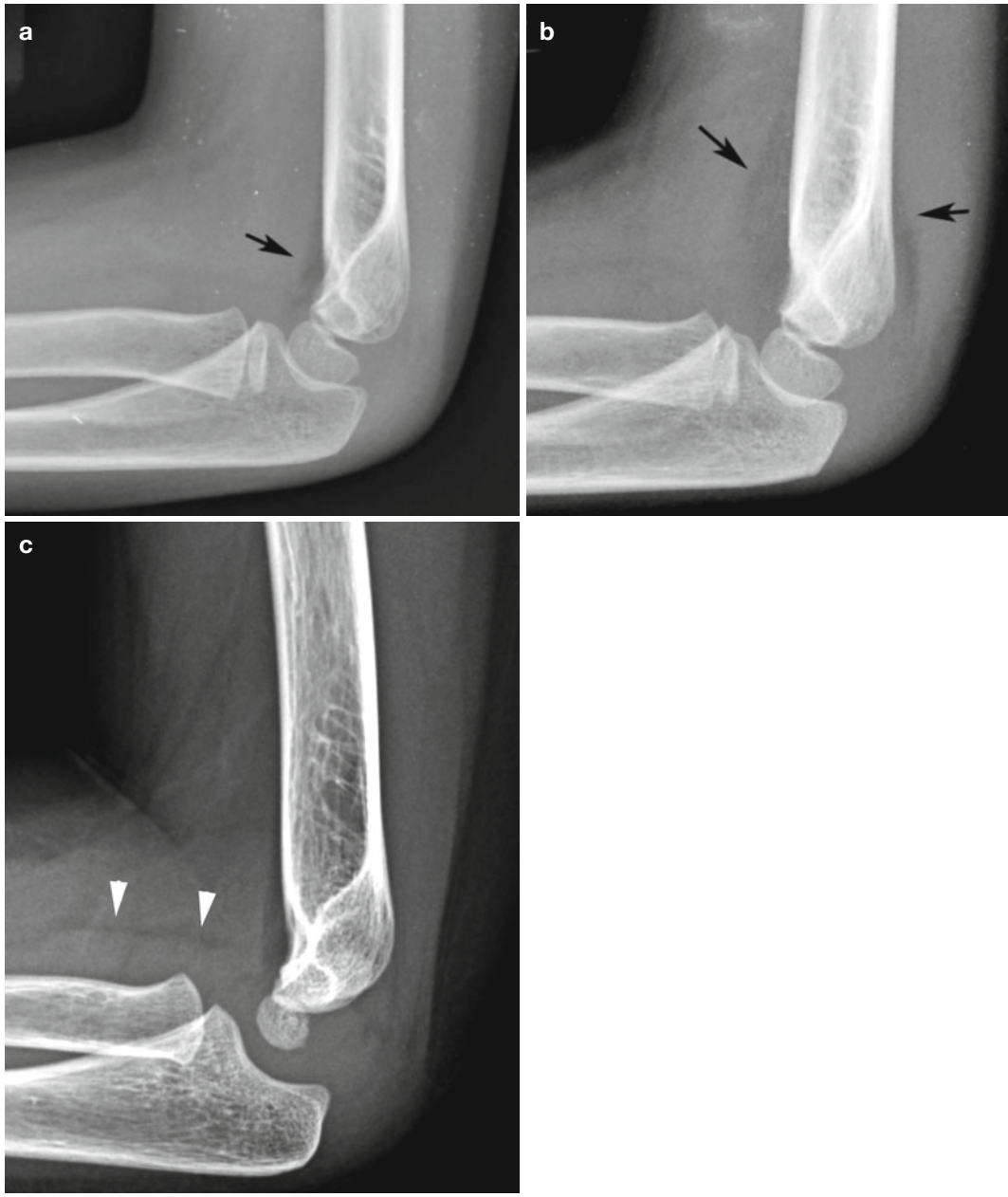


Fig. 6.1 Elbow fat pads. (**a**) Note the position of the normal anterior fat pad (*arrow*). The posterior fat pad is not visible on normal 90° flexed elbows. (**b**) In this patient with fluid in the joint from an injury, both the anterior and posterior fat pads (*arrows*) are elevated. (**c**) Normal supinator fat pad. Note the appearance and position of the normal supinator fat pad (*arrow*)

while hyperextension forces act on the distal humerus. Rotatory forces along with varus and valgus forces act on the radius and ulna. These force patterns are reviewed more specifically as the individual fractures are dealt with in this chapter. In children with elbow trauma, MR imaging reveals a broad spectrum of bone and soft tissue injury beyond that recognizable radiographically. However, the additional information afforded by MR imaging has little

bearing on treatment or clinical outcome [7]. As a result, MR of the elbow is rarely indicated in the ER setting.

Injuries of the Distal Humerus

The most common fracture sustained in the elbow is the supracondylar fracture through the distal humerus, and in our study of over 400 infants and children with elbow injuries [5], supracondylar fracture occurred in 68 % of the patients, lateral condylar fractures in 23 %, and medial epicondylar fractures in 9 % of patients.

The supracondylar fracture results from a fall on the outstretched upper extremity where the olecranon locks into the olecranon fossa producing a "can-opener" effect on the distal humerus resulting in a supracondylar fracture with the distal fracture fragment being posteriorly tilted (Fig. 6.2a). In the classic case the findings are not difficult to identify (Fig. 6.2b, c). However, in some cases while the fracture is obvious on lateral view, it is difficult to visualize on the frontal view. In addition, if the fracture is a plastic/bending fracture, less posterior angulation occurs, a fracture line is not visualized, and it may be difficult to confidently identify the fracture without comparative views. In this situation the anterior humeral line of Rogers et al. [8] becomes very useful.

The anterior humeral line is a line drawn along the anterior aspect of the distal humerus and should be applied on true lateral views. Under normal circumstances, it intersects the ossified capitellum somewhere through its middle or posterior third. If it intersects the capitellum through the anterior third or if it misses it entirely, a supracondylar fracture is present (Fig. 6.3). The anterior humeral line is a little more difficult to apply in the young infant where the capitellum is incompletely ossified, but even in these cases, if the findings are compared with those on the normal side, posterior displacement can be detected. In addition to the foregoing, I have found it useful to compare the classic supracondylar fracture to a hockey stick and the plastic bending supracondylar fracture to a polo stick [9] (Fig. 6.4). A spectrum of supracondylar fractures is presented in Fig. 6.5.

Another fracture occurring through the distal humerus in conjunction with the supracondylar hyperextension fracture is the "T" fracture. In these cases not only are hyperextension forces applied to the distal humerus, but axial loading on both the lateral and medial condyles results in splitting of the distal humerus and the resultant "T" fracture. This fracture is not difficult to detect. Finally, it should be noted that in some cases a supracondylar fracture with faulty alignment and subsequent healing can result in a cubitus varus (gunstock) deformity of the elbow [10].

A reverse supracondylar fracture results when forces are applied to the posterior aspect of the distal humerus, for example, with falling backwards and landing on the elbow. These fractures are not difficult to detect as they usually are overt.

With condylar and epicondylar injuries of the distal humerus, it is the lateral condyle and medial epicondyle which most commonly are injured. Medial condylar [11] and lateral epicondylar fractures are rare. Lateral condylar fractures tend to occur in young infants and children, while medial epicondylar fractures more often, but not exclusively, occur in older children. Many of these fractures are subtle and examination of the soft tissues becomes important. In this regard abnormality of the elbow fat pads usually is present, but more important is that there usually is telltale unilateral swelling and edema of the soft tissues over the involved area [12]. With lateral condylar fractures, such swelling occurs laterally, while with medial epicondylar fractures, it occurs medially. The presence of such unilateral soft tissue edema is especially important in the assessment of medial epicondylar injuries with minimal or no displacement of the epicondyle or in children younger than 7 years of age in whom the epicondyle often is not yet ossified.

Lateral condylar fractures [13] result when varus forces are applied to the elbow (Fig. 6.6), and in such cases it is most important to determine whether the fracture is undisplaced or displaced and rotated. If the fracture extends through the cartilage between the capitellum and the trochlea, the hinge-like stabilizing function of a nondisplaced fracture fragment is lost, and the injury becomes unstable (Fig. 6.7). At the other

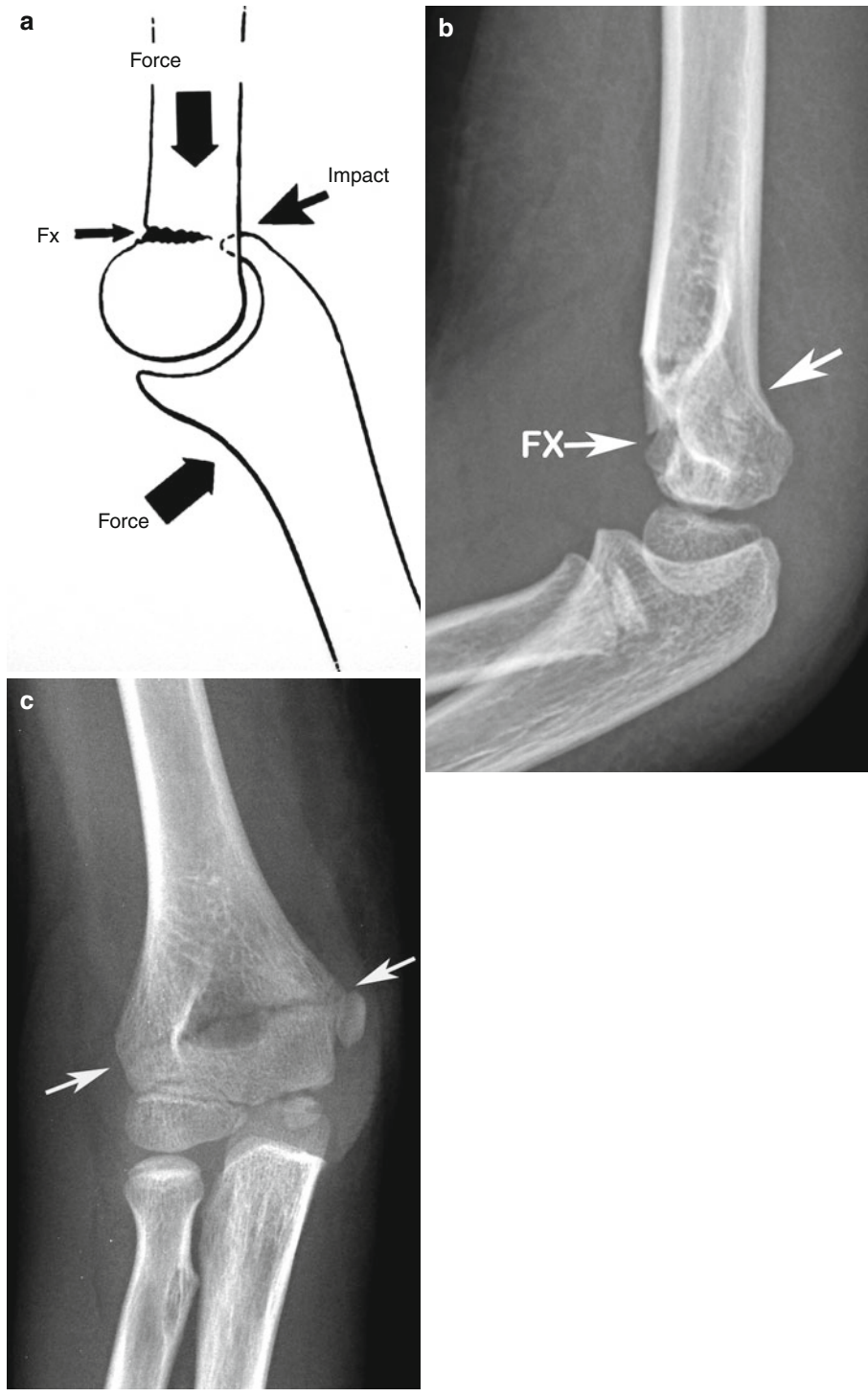


Fig. 6.2 Supercondylar fracture: injury mechanics. (**a**) Axial loading forces are applied down the humerus (*upper arrow*), while "can-opener"-like forces are applied to the distal humerus by the hyperextended ulna (*lower arrow*). The ulna becomes locked in the trochlear notch, leading to impaction forces (*Impact*) applied to the posterior aspect of the distal humerus and a fracture (*fx*) results. (**b**) Typical imaging findings: lateral view. The point of impact occurs posteriorly (*arrow*) with a resultant fracture (*fx*) anteriorly. The entire distal humeral fragment is posteriorly tilted. (**c**) Anteroposterior view demonstrates the transverse fracture (*arrows*)

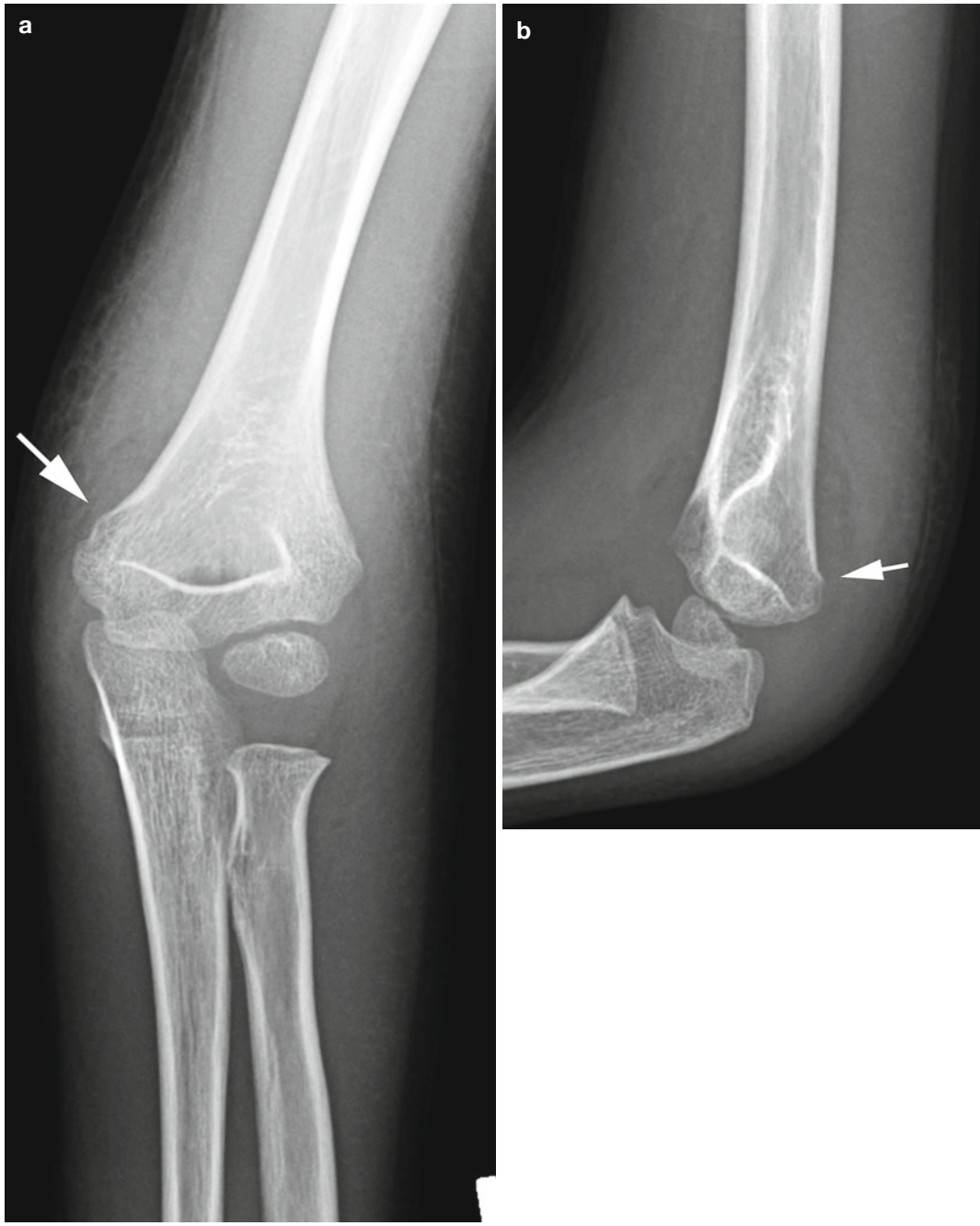


Fig. 6.3 Subtle supracondylar fracture: anterior humeral line. (**a**) Anteroposterior (AP) view. Note the very subtle buckle fracture (*arrow*) in the distal humerus. Swelling around the area is present. (**b**) Lateral view demonstrates a minimal posterior buckle fracture (*arrow*). Both fat pads are elevated. Note the position of the capitellum. (**c**) Normal side for comparison. First note the position of the capitellum and compare it to the posteriorly displaced capitellum in (b). (**d**) Anterior humeral line: fracture side. The anterior humeral line intersects the capitellum through the anterior third. (**e**) Anterior humeral line: normal side. The anterior humeral line intersects the normal capitellum through its posterior third



Fig. 6.3 (continued)

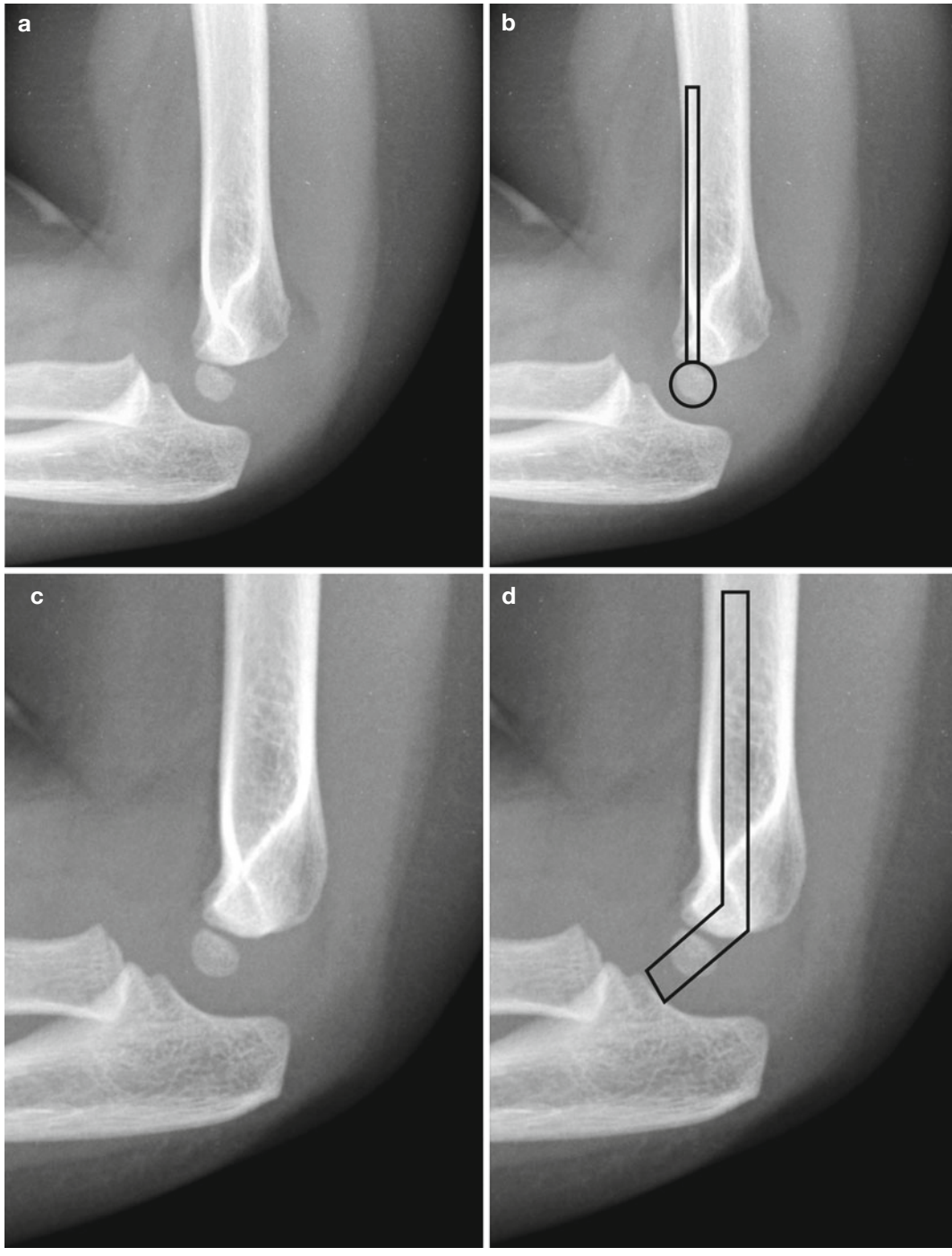


Fig. 6.4 Supracondylar fracture: polo versus hockey stick. (**a**) Note elevated fat pads. An overt fracture is not seen but the distal humerus and capitellum are slightly posteriorly tilted (plastic fracture). The capitellum lies directly below the humerus. (**b**) The configuration resembles a "polo stick" en face. (**c**) Normal side for comparison. Note the position of the capitellum. It is more anterior in location than in (a). (**d**) The overall configuration resembles a "hockey stick" (Reprinted from Swischuk [9]. With permission from Springer Science + Business Media)

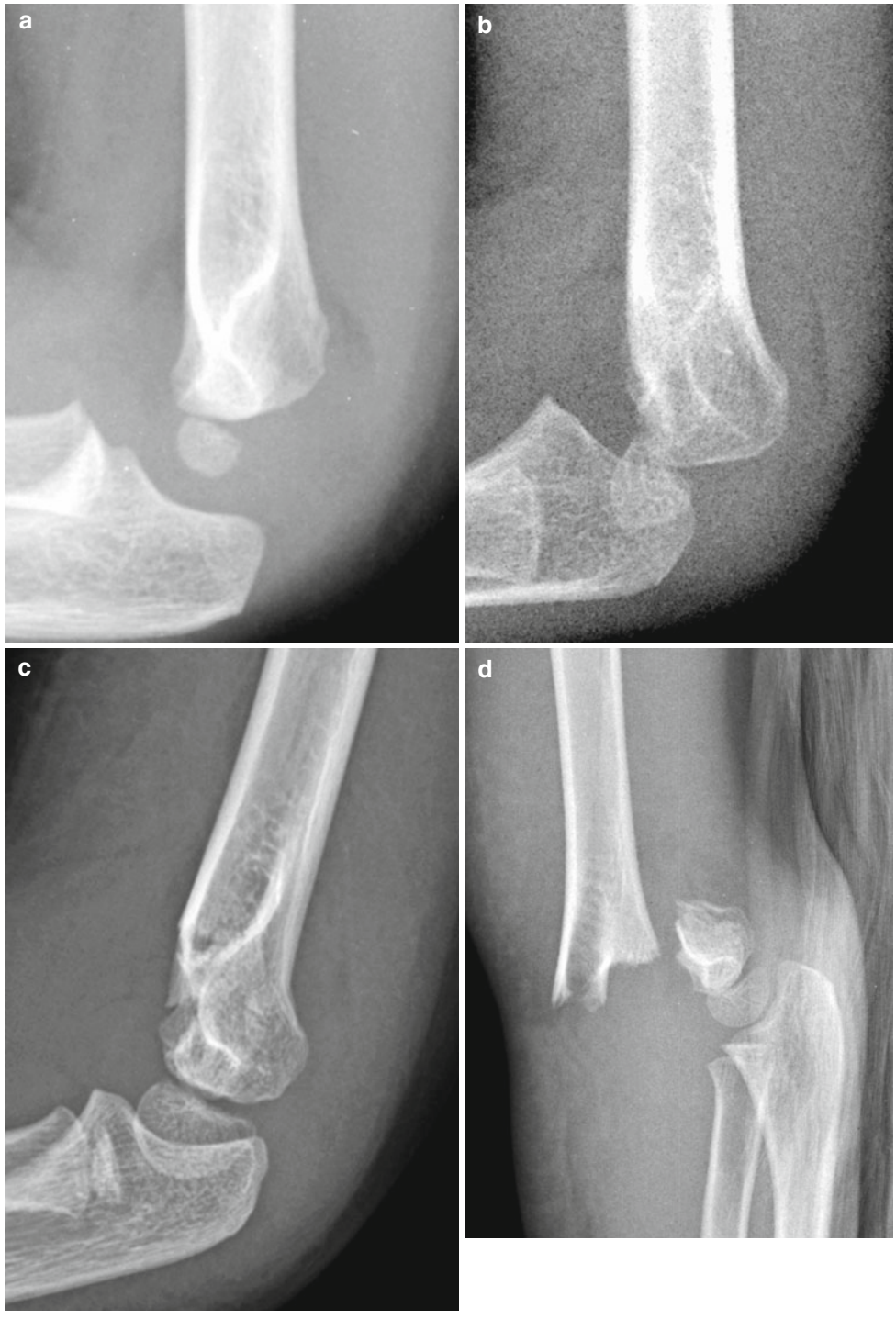


Fig. 6.5 Spectrum of supracondylar fractures. (**a**) Minimal plastic bending fracture with a subtle posterior buckle. Note position of the capitellum. (**b**) Plastic bending fracture of the distal humerus with smooth posterior angulation of the distal humerus. (**c**) Overt supracondylar fracture with posterior cortical angulation and an anterior fracture line. (**d**) Completely displaced supracondylar fracture

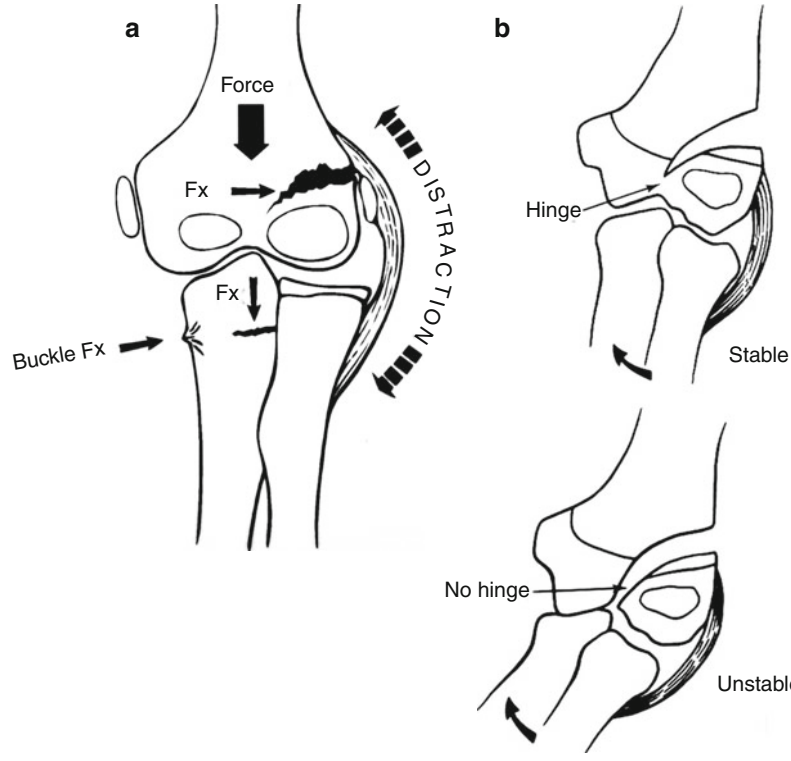


Fig. 6.6 Lateral condyle fracture. (**a**) Diagrammatic representation. Axial loading forces are present (*force*). In addition there are distraction forces applied to the lateral elbow resulting in a lateral condylar avulsion fracture (*fx*). Fractures of the proximal ulna can coexist. (**b**) Diagrammatic representation of instability. *Stable* the fracture does not traverse the cartilage plate. A hinge remains and the fracture is stable, *Unstable* with a complete fracture no hinge is present and the fracture is unstable

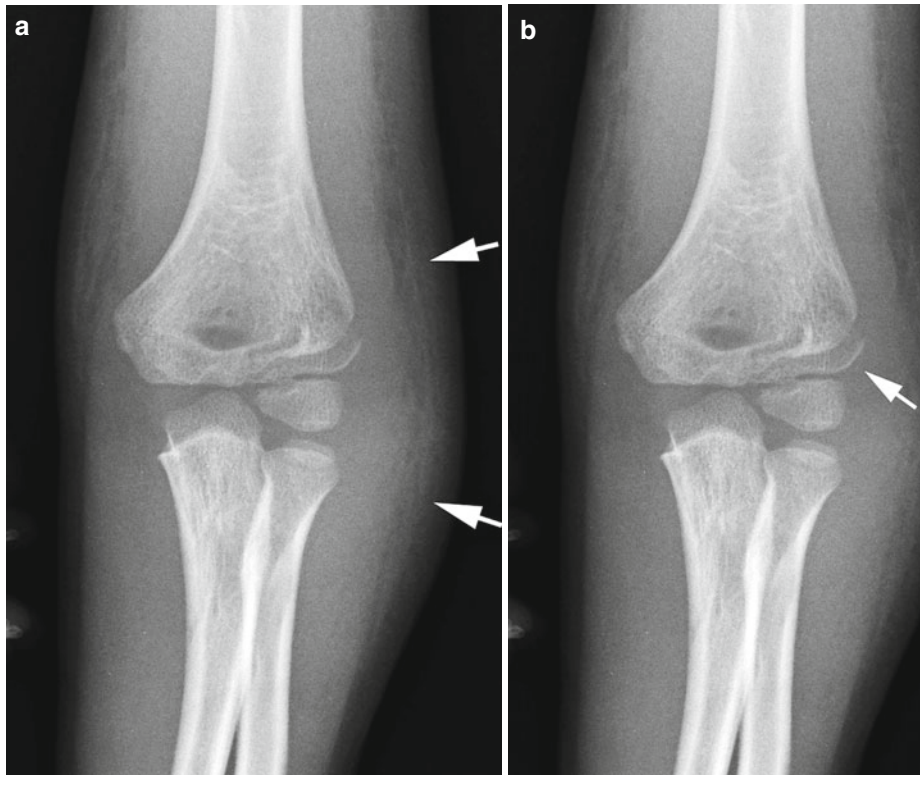


Fig. 6.7 Typical lateral condylar avulsion fracture. (**a**) First note the swelling (*arrows*) over the lateral aspect of the elbow. (**b**) Now note the avulsed fracture fragment (*arrow*)

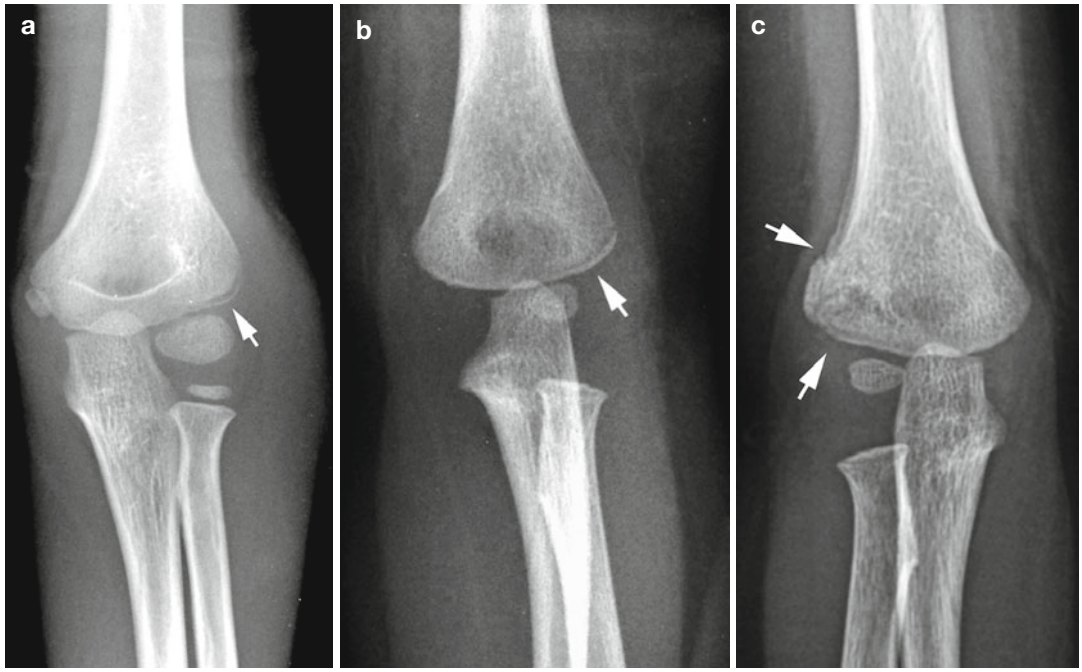


Fig. 6.8 Subtle, sliver-like avulsion fractures. (**a**) Note the subtle thin avulsed fracture fragment (*arrow*). (**b**) Another patient demonstrating similar, but less pronounced findings of an avulsion fracture (*arrow*). There is suggestion of a minimal buckle fracture of the distal humerus on the medial side. (**c**) Another patient. Healing phase. Note periosteal new bone and callus (*arrow*) at the fracture site

end of the spectrum of lateral condylar fractures, only a crescent-/sliver-shaped fragment of bone is avulsed (Fig. 6.8). This fragment can be clearly apparent or very difficult to identify because of its thin sliver-like configuration. In these latter cases it is important to appreciate that the sliver of bone curves downwardly with the apex of the curve pointing downward (Fig. 6.8). The reason this is important is because a psuedofracture configuration can be seen in normal elbows with superimposition of the capitellum on the metaphysis of the humerus. In these cases the apparent "pseudofracture" is convex in the opposite direction with the curve pointing upward (Fig. 6.9).

Finally, it might be appreciated that in some cases of lateral condylar avulsion fracture, the fracture is not seen on AP views but can be seen on lateral or oblique views (Fig. 6.10). Oblique views are not standard views for elbow injuries, but very often because a proper lateral view cannot be obtained, the one submitted is slightly obliqued and the fracture becomes visible. A spectrum of lateral condylar avulsion fractures is presented in Fig. 6.11.

With medial epicondylar injuries [14], a wide range of abnormality also occurs raging from simple separation of the epicondyle to complete dislocation, with or without intra-articular entrapment (with elbow dislocations) of the epicondyle. Medial epicondylar injuries result from rotatory forces applied to the bones distal to the elbow (Fig. 6.12). When this occurs there is excessive pull on the medial epicondyle by the flexor pronator muscle/tendon (Fig. 6.12). In some cases minimal or no displacement of the medial epicondyle is seen, but soft tissue changes are present (Fig. 6.13a). In addition the medial epicondyle often also can be avulsed after the epiphyses have fused (Fig. 6.13b).

The medial epicondyle also can be avulsed with dislocation of the elbow. In such cases the medial epicondyle is not visible in its normal position on any of the views of the elbow (Fig. 6.14a, b). Indeed, if one is not looking for it,



Fig. 6.9 Pseudofracture; lateral condyle. With certain positioning the cartilaginous plate between the capitellum and lateral condyle is visualized through the distal humeral metaphysis and may erroneously suggest a fracture (*arrowheads*). Compare with a true fracture in Fig. 6.8

it can be missed entirely. However, it usually becomes visible after the dislocation has been reduced (Fig. 6.14c). In these cases it is worthwhile to note that the medial epicondyle ossifies prior to the trochlea. So if the trochlear ossification center is visible but not the medial epicondyle, avulsion and intra-articular entrapment of the medial epicondyle should be suspected.

Little Leaguer's elbow is a traumatic lesion of the medial epicondyle resulting from too much pitching at too young an age, and when long-term chronic bony changes occur, they consist of fragmentation and enlargement of the medial epicondyle, representing a chronic avulsion fracture (Fig. 6.15). With chronic overuse of the elbow, other changes can occur including fragmentation and overgrowth of other secondary centers around the elbow [14], chronic anterior angulation of the radial head [15, 16], and nonunion of the olecranon apophysis [17]. A spectrum of medial epicondylar injuries is presented in Fig. 6.16. MRI is usually not indicated in these injuries since the diagnosis is usually readily evident or suspected on radiographs and the treatment is usually conservative. Medial epicondyle avulsions associated with elbow dislocations or with displacement greater than 5 mm are usually treated surgically with open reduction and internal fixation. Lateral epicondylar and medial condylar fractures, as noted previously, are much less common than the fractures just discussed.

Injuries of the Proximal Radius

For the most part, proximal radial fractures are radial head fractures. They result from axial loading causing impaction of the radial head [18] and often are accompanied by valgus forces (Fig. 6.17a). The end of this is that they result in an impacted Salter–Harris type II fracture with variable displacement of the proximal fracture fragment and radial head epiphysis. Gross, fragmented, or displaced fractures of the radial head are not difficult to detect (Fig. 6.17b). However, the more subtle, angled corner buckle fracture [19] frequently is missed (Fig. 6.17c, d). Of course, in most cases, abnormalities of the soft tissues and fat pads around the elbow can alert one to the presence of this fracture but still the fracture often remains elusive. In such cases comparative views are very helpful. Examples of radial head buckle fractures are presented in Fig. 6.18.

Radial head dislocation is not an uncommon problem. However, it is just rare enough that it can be missed. In this regard, it is important to realize that radial head dislocations usually occur in conjunction with ulnar fractures as the Monteggia fracture complex (see Fig. 6.25). Dislocation of the radial head from the annular



Fig. 6.10 Subtle fractures: value of lateral and oblique images. (**a**) In this patient a very subtle thin sliver-like avulsed fracture fragment (*arrow*) is seen. (**b**) On the oblique film the fracture fragment (*arrow*) is more clearly identified. (**c**) Another patient. Again note a subtle thin avulsed fracture fragment (*arrow*). (**d**) Lateral view more clearly demonstrates the fracture (*arrow*)

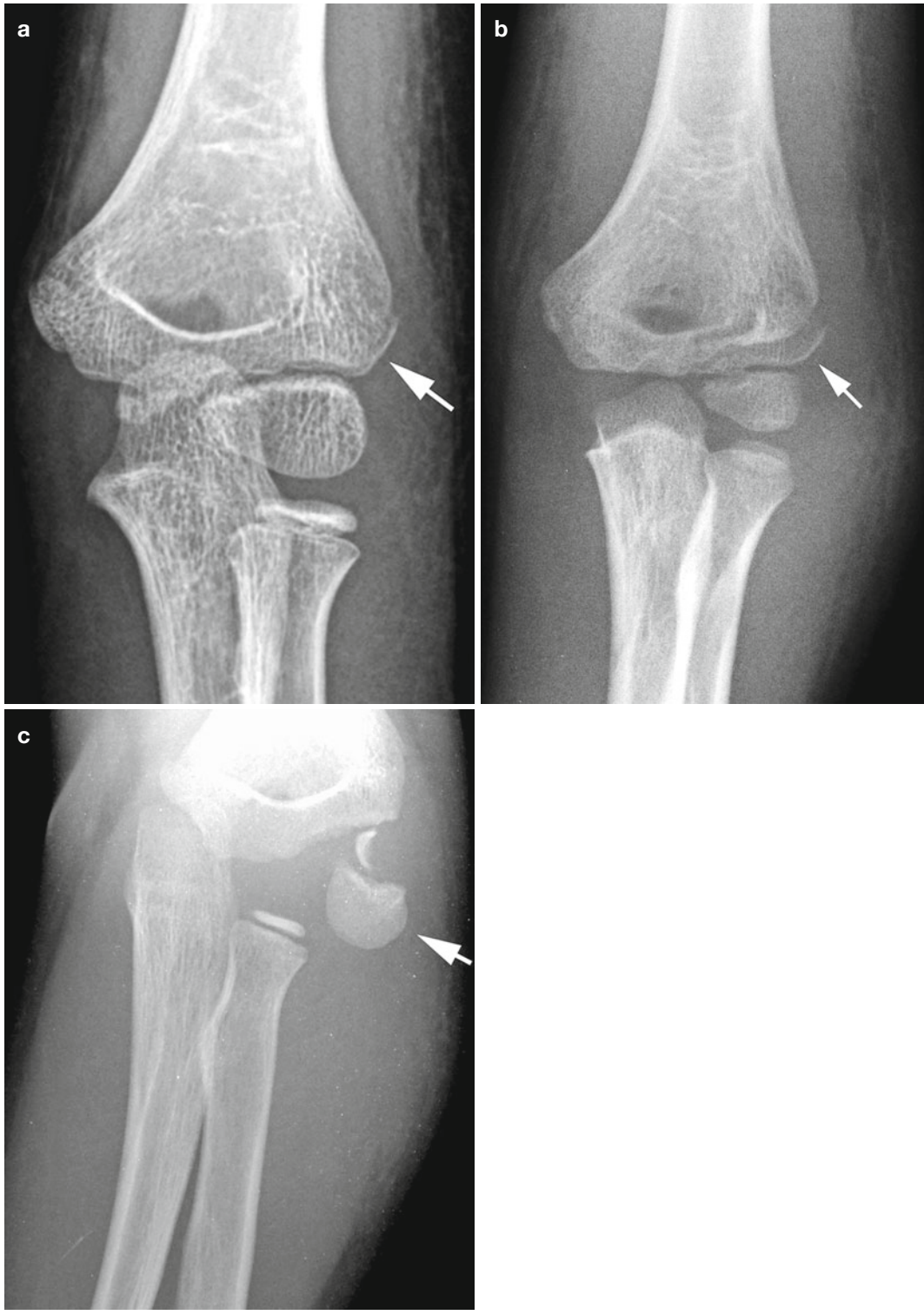


Fig. 6.11 Spectrum of lateral condylar fractures. (**a**) In this patient a minimal nondisplaced sliver-like avulsed fracture fragment (*arrow*) is seen. (**b**) A more classic fracture (*arrow*) is present. (**c**) Total avulsion of the capitellum and underlying condylar cortex along with rotation of the fracture fragment (*arrow*)

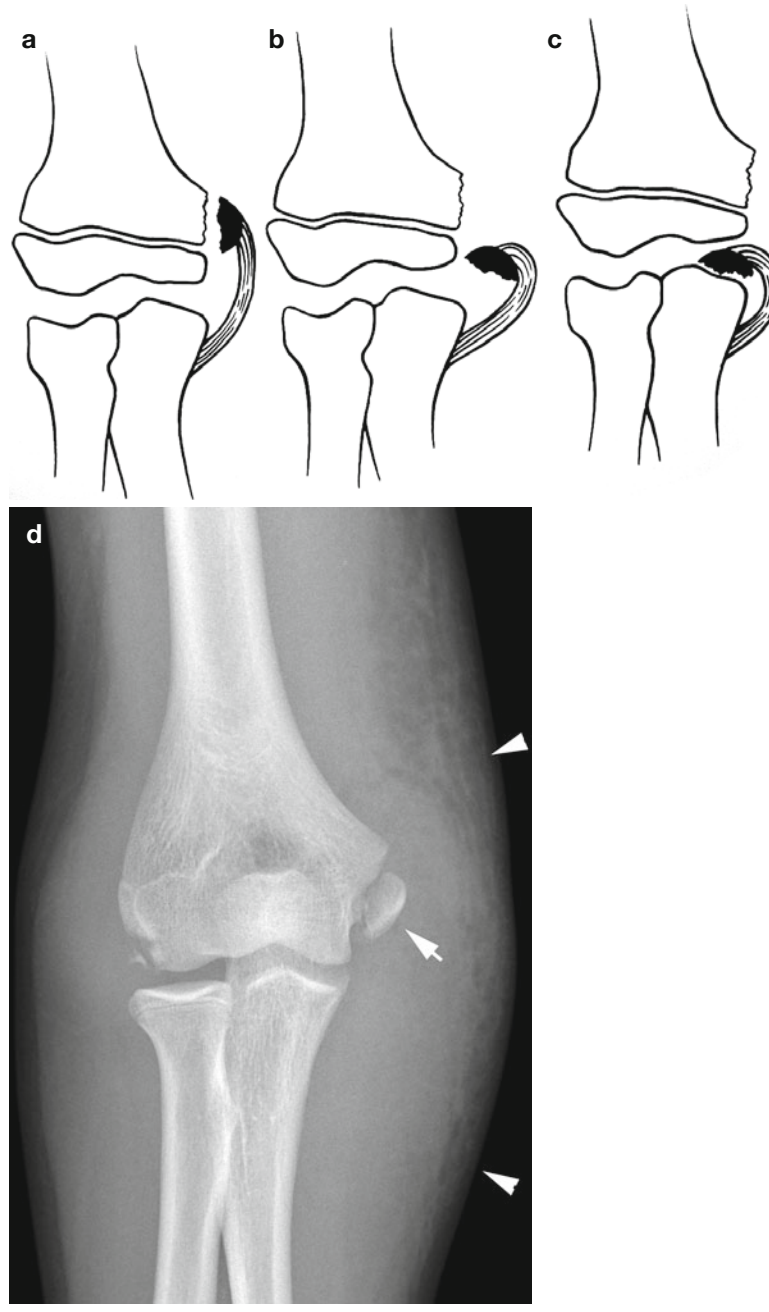


Fig. 6.12 Medial epicondyle avulsion: injury mechanics. (**a**) Simple avulsion of the medial epicondyle. (**b**) Complete avulsion of the medial epicondyle. (**c**) Complete avulsion and entrapment in the elbow joint. (**d**) Typical avulsed medial epicondyle (*arrow*). Note extensive swelling over the medial aspect of the elbow (*arrowheads*)

ligament without a fracture, or the so-called pulled, curbstone, or nursemaid's elbow, is not a true dislocation [20]. Rather, there is subluxation of the radial head from the annular ligament, incomplete tearing of the ligament, and subsequent entrapment of a portion of the ligament in the joint space. This is a very common elbow injury in infancy and early childhood and results from a brisk pull on the elbow such as in lifting or pulling the child/infant by one arm. The condition produces exquisite pain and a most unhappy child. The clinical picture is absolutely characteristic: A previously well child suddenly refuses to move the involved extremity. Clinical examination

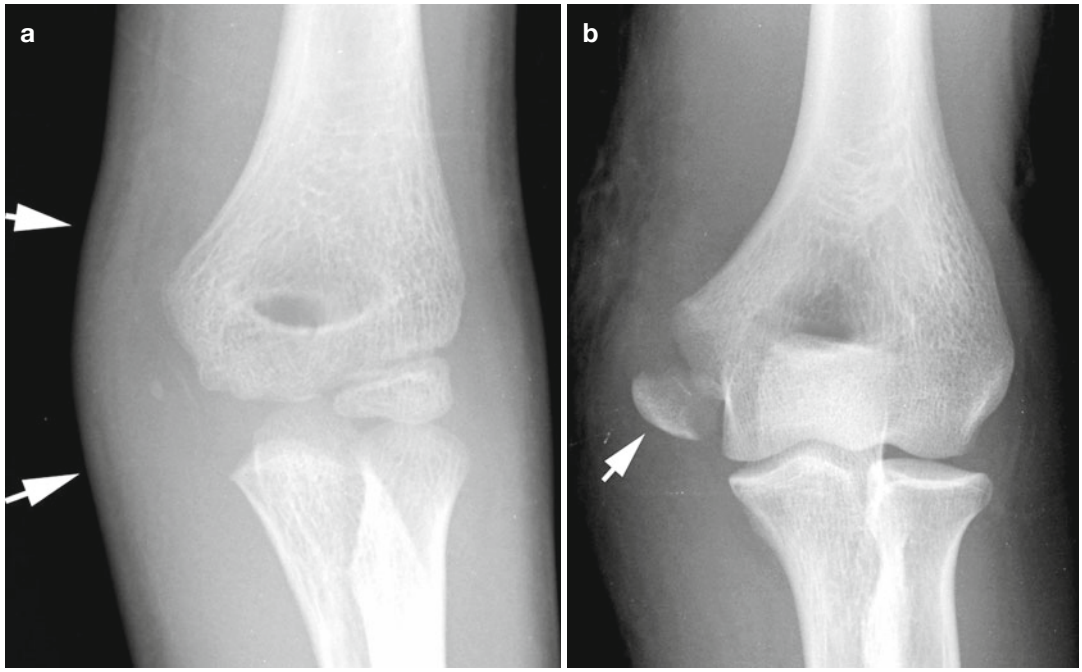


Fig. 6.13 Medial epicondyle fracture: subtle findings. (**a**) Note soft tissue swelling (*arrowheads*). This signifies the presence of an avulsion injury. The small epicondyle is barely visible but is displaced. (**b**) Older child with fused epiphyses. Note the avulsed medial epicondyle (*arrow*)

is not productive, because no matter which way one moves, or indeed, even touches the arm, the child reacts with considerable pain. The arm is held in slight flexion and pronation, with supination being difficult to accomplish. Occasionally the problem can be bilateral [21].

The roentgenographic findings in "pulled" elbow usually are negative in terms of both bony and soft tissue abnormality, but occasionally fat pad changes are seen. In addition the views obtained often are suboptimal, for it is very difficult to position these patients for adequate roentgenograms. On the other hand however, many times the technician, trying to position the arm properly, reduces the dislocation. Indeed, almost as if by magic, there is an immediate full or near-full return to normal movement of the extremity, and a previously crying, tormented child is all smiles. In other cases, mild discomfort may persist for 30 min to 1 or 2 h. Actually, if one is cognizant of this injury, it can be reduced before roentgenograms are ever obtained, for with the thumb over the radial head, supination and slight flexion of the elbow result in a palpable click and reduction of the radial head.

Injuries of the Proximal Ulna

Fractures of the proximal ulna are varied. One of the reasons for this is that the ulna, more than the other two bones around the elbow, is subject to all of the forces applied to the elbow during "FOOSH" injuries. The ulna in the outstretched extremity injury is locked into the olecranon fossa and cannot move freely. The radius, of course, can rotate easily around the capitellum, but the ulna is rigidly fixed and prone to a number of leverage/twisting fractures.

Transverse fractures, through the proximal ulna, visualized on frontal view can occur both with varus and valgus forces applied to the elbow joint (Fig. 6.19a). They seldom occur alone and usually an associated radial fracture is present.



Fig. 6.14 Medial epicondyle avulsion fracture and elbow dislocation. (**a**) The elbow is dislocated. The medial epicondyle is displaced (*arrow*) into the elbow joint. (**b**) On AP view the dislocation of the elbow is seen, but the medial epicondyle (*arrow*) is just barely visible. It is in the elbow joint. (**c**) Post reduction. With reduction the medial epicondyle has returned to its normal location but clearly is avulsed (*arrow*)

Another fracture peculiar to the proximal ulna is the longitudinal linear, often hairline, fracture [22]. This fracture results from a shearing force being applied to the proximal ulna when the elbow rotates. Because the ulna is locked into the olecranon fossa, twisting forces result in longitudinal,

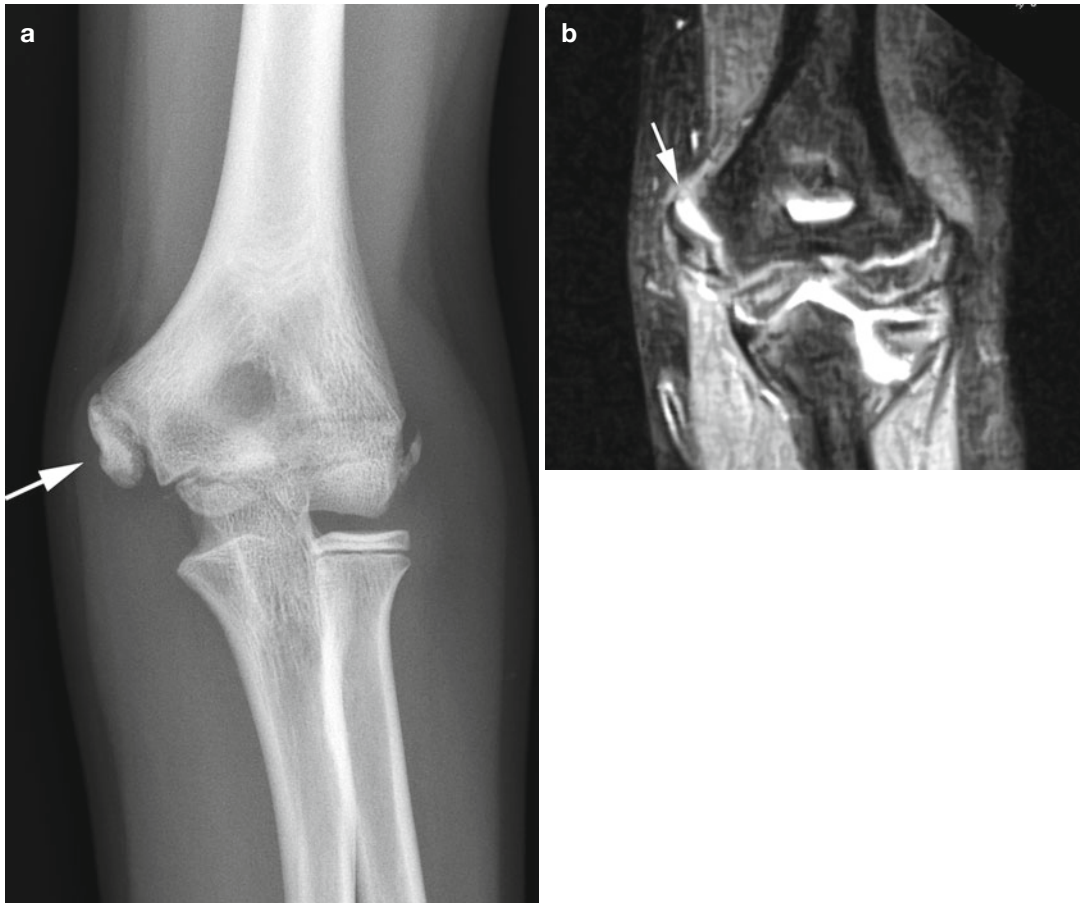


Fig. 6.15 Medial epicondyle avulsion, chronic Little Leaguer's elbow. (**a**) Note the sclerotic and deformed epicondyle (*arrow*). (**b**) MR coronal STIR image. Note the high signal (*arrow*) between the chronically avulsed medial epicondyle and the humeral metaphysis

often slightly spiral fractures as well as buckle fractures (Fig. 6.19b). It is like twisting a stalk of celery. A spectrum of proximal ulnar fractures is presented in Fig. 6.20, including the olecranon sleeve fracture [23].

Hairline fractures usually are visualized on lateral views of the elbow and are not uncommon in the proximal ulna. They occur from posteriorly applied broad surface forces. The resulting impact is associated with a pull by the brachialis and triceps muscles which causes a transverse fracture, with variable separation of the fracture fragments (Fig. 6.21a, b). If the fall is on a sharp or wedge-like object, a fulcrum results and the fracture is then V shaped, being diastatic at the articular surface (Fig. 6.21c, d).

Finally, one should be aware of the fact that avulsion fractures of the proximal ulna also occur. The most common is that which involves the coronoid process. This fracture occurs with elbow dislocations or hyperextension–rotation injuries in which forceful contraction of the brachialis muscle causes avulsion of the coronoid process (Fig. 6.22a). The avulsed fragment is usually relatively small and can be overlooked, but its characteristic location allows for its identification with confidence (Fig. 6.22b). Less commonly, avulsion of the olecranon apophysis, or portion thereof, occurs. This results from forceful contraction of the triceps muscle, but because the muscle tends to insert more distally on the ulna (Fig. 6.22c), the apophysis seldom is avulsed, but

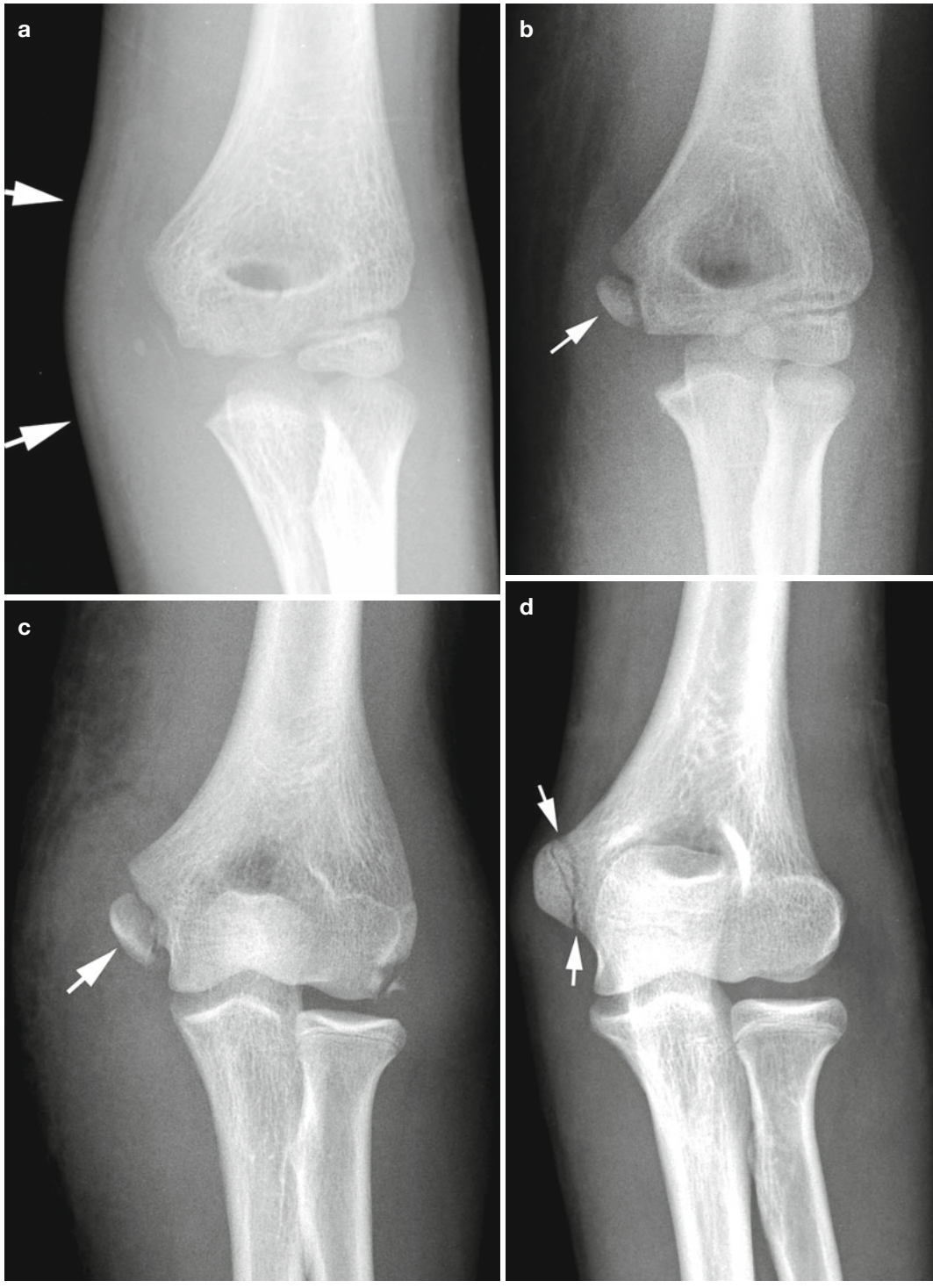


Fig. 6.16 Medial epicondyle avulsion fracture: spectrum. (**a**) Soft tissue changes primarily. Note swelling of the soft tissues over the medial aspect of the elbow (*arrows*). One or two very small bony fragments are seen. (**b**) Avulsion of the medial epicondyle (*arrow*) with widening of the lucent space between it and the humeral metaphysis. Note soft tissue swelling. (**c**) Complete avulsion of the medial epicondyle (*arrow*). (**d**) Fracture in older patient (*arrows*) after apophyses has closed

it does occur (Fig. 6.22d, e). Avulsion of the apophysis of the olecranon also can result from direct blows to the back of the elbow.

Dislocation of the Elbow

Total dislocation of the elbow is not particularly common in infancy but can occur in the older child. In these cases it frequently is associated with avulsion of the medial epicondyle and entrapment of the epicondyle in the joint. More often rather than a true dislocation, what occurs is that a complete supracondylar fracture is sustained and the entire fracture fragment is so displaced that, clinically, dislocation of the elbow is mimicked [6]. An uncommon dislocation of the elbow is the so-called split dislocation where the humerus fractures vertically and the radius and ulna point outwardly in opposite directions [24]. The fracture is not difficult to detect.

Osteochondritis Dissecans of the Elbow

Although not a common problem, osteochondritis dissecans of the elbow can involve the capitellum and results in a bony defect with subtle adjacent sclerosis [25] (Fig. 6.23a). CT imaging is very useful in determining the exact position of the fragment (Fig. 6.23b).

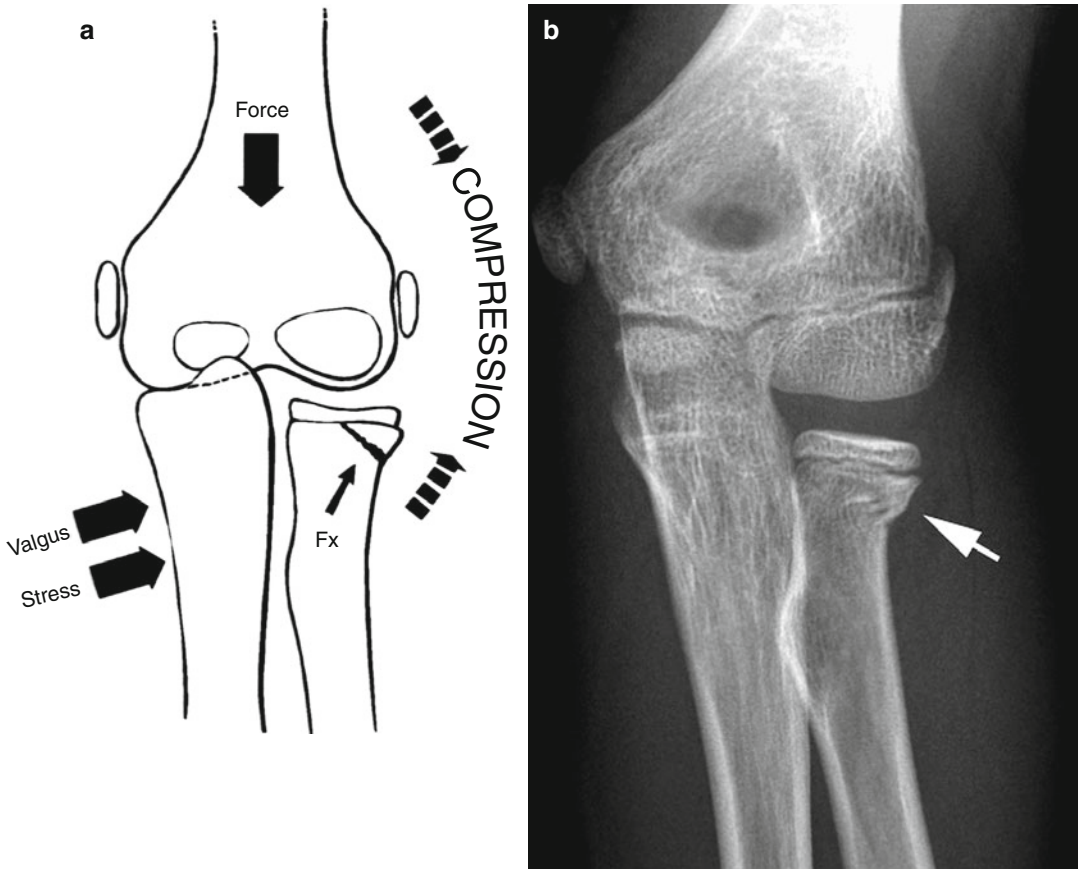
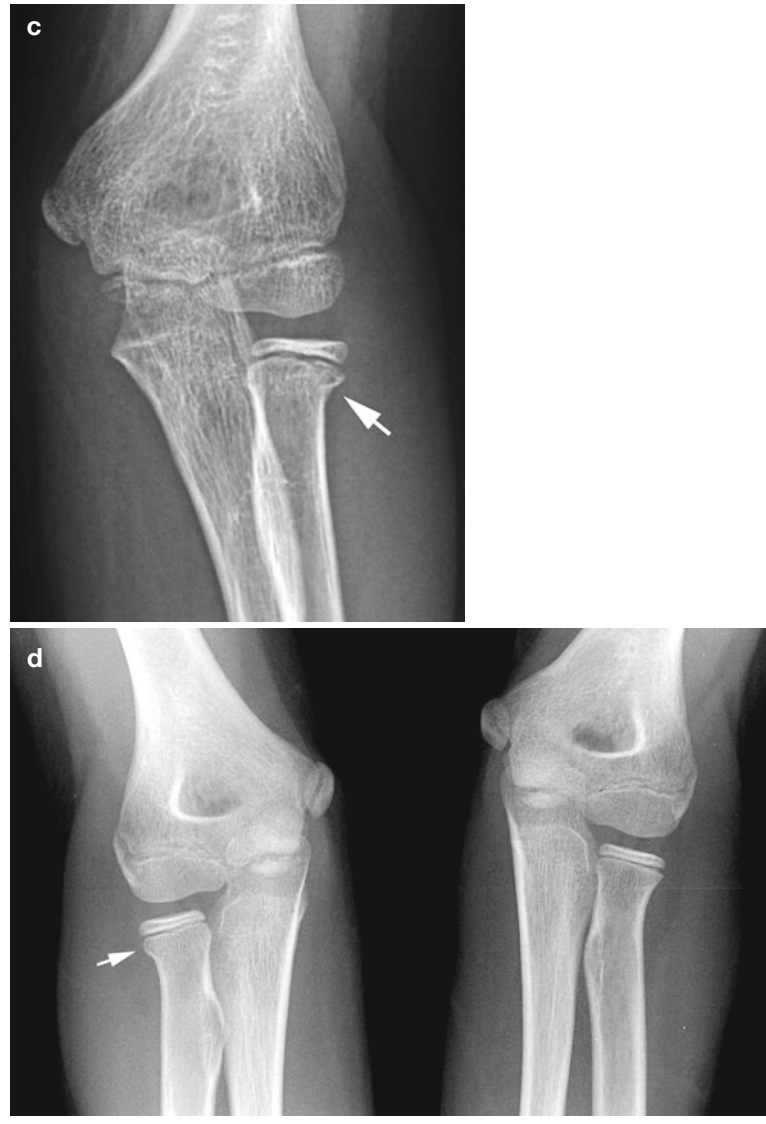


Fig. 6.17 Radial head impaction fractures: injury mechanism and spectrum. (**a**) Axial loading forces (*force*) along with valgus stress (*valgus stress*) produce compression (*compression*) of the elbow over its lateral aspect resulting in a compression fracture (*fx*) of the radial head. (**b**) Note typical compression fracture (*arrow*) of the radial head. (**c**) A more subtle buckle fracture (*arrow*). (**d**) Very subtle buckle fracture (*arrow*) of the radial head. Compare to the normal side

Fig. 6.17 (continued)



Normal Variations Causing Problems

The most common normal variations misinterpreted as fractures are the various secondary ossifications centers around the elbow. Of these, the sliver-like lateral epicondyle and the frequently irregularly ossified medial condyle are the two most problematic bones (Fig. 6.24a). They are followed, however, in short order by the accessory center of the olecranon (Fig. 6.24b).

Injuries of the Forearm

The types of fractures that can occur through the midshaft of the bones of the forearm include clearly visible transverse, spiral, and oblique fractures (Fig. 6.25) and the more subtle greenstick and plastic bending or bowing fractures. Buckle or torus fractures are uncommon in the midshaft of these bones, because compared with the metaphyseal regions, the cortex of the midshaft is rather sturdy and not prone to buckling.



Fig. 6.18 Radial head angled buckle fracture: various locations. (**a**) Typical, although subtle, angled buckle fracture (*arrow*) in the proximal radius. (**b**) An angled buckle fracture (*arrow*) involving the inferior aspect of the radial head. (**c**) Another angled buckle fracture (*arrow*) involving the superior aspect of the radial head. All of these locations are common

Greenstick and plastic bowing fractures of the forearm are common [26–33], and the latter commonly are missed. The two fractures are related with the greenstick fracture being one step further in the bending process than simple bending (Fig. 6.26). In this regard plastic bending fractures can be considered the greenest of "greenstick fractures." Comparative views are essential for detecting some of these fractures for they can be very subtle (Fig. 6.26a, b). In many of these cases is it very helpful to examine the image vertically because the curvature is exaggerated (Fig. 6.26c, d). This is of further importance because normal bowing is common and can be misinterpreted for a plastic bending fracture (Fig. 6.27).

Finally, in terms of ulnar fractures it should be remembered that if the ulnar fracture is isolated, no matter what type, one should look at the head of the radius to determine a whether Monteggia fracture complex is present (see Fig. 6.28). The "radiocapitellar line" is often useful in these cases. Normally this line, drawn lengthwise through the radial shaft, always passes through the capitellum on the frontal as well as the lateral view. If it misses the capitellum, dislocation is present.

Normal Variations Causing Problems

The only normal finding in the midshaft of the radius and ulna that can be misinterpreted as a fracture is a vascular groove in either bone. These

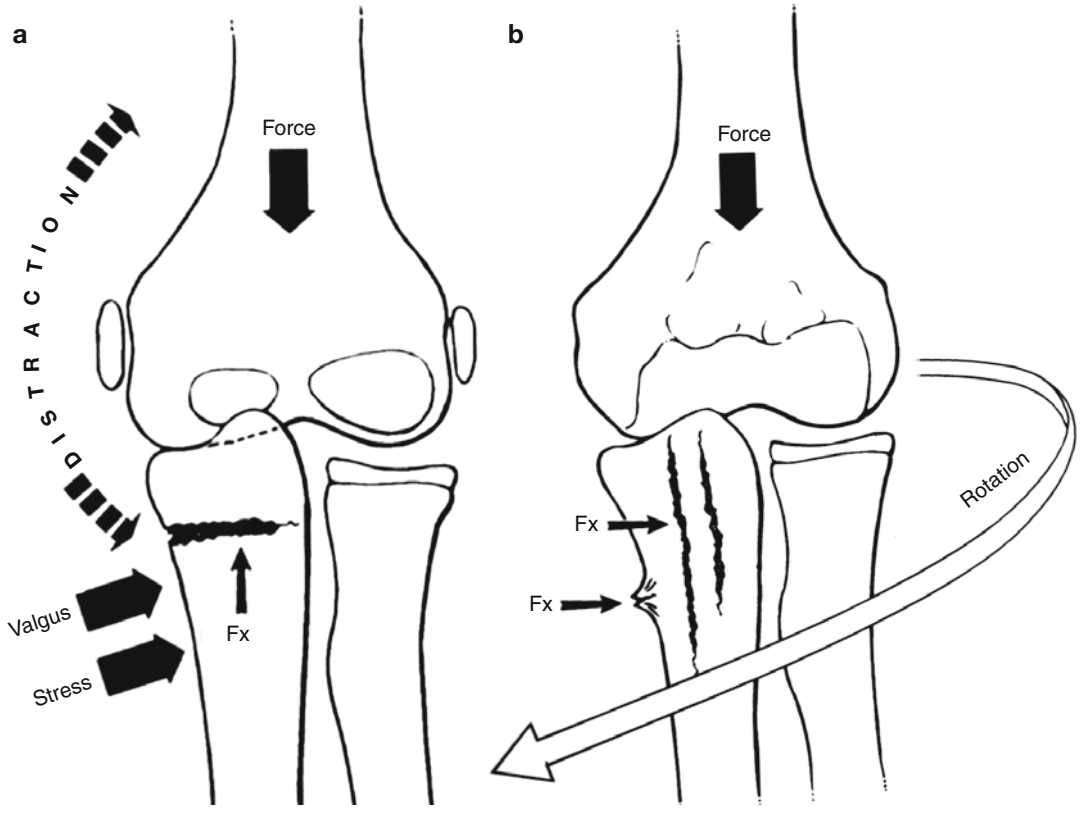


Fig. 6.19 Proximal ulnar fractures: injury mechanics. (**a**) Axial loading forces (*force*) plus valgus distraction forces over the medial elbow result in a transverse fractures (*fx*) of the ulna. (**b**) With axial loading forces (*force*) plus rotation, vertical linear and buckle fractures (*fx*) occur. Also see Fig. 6.6a.

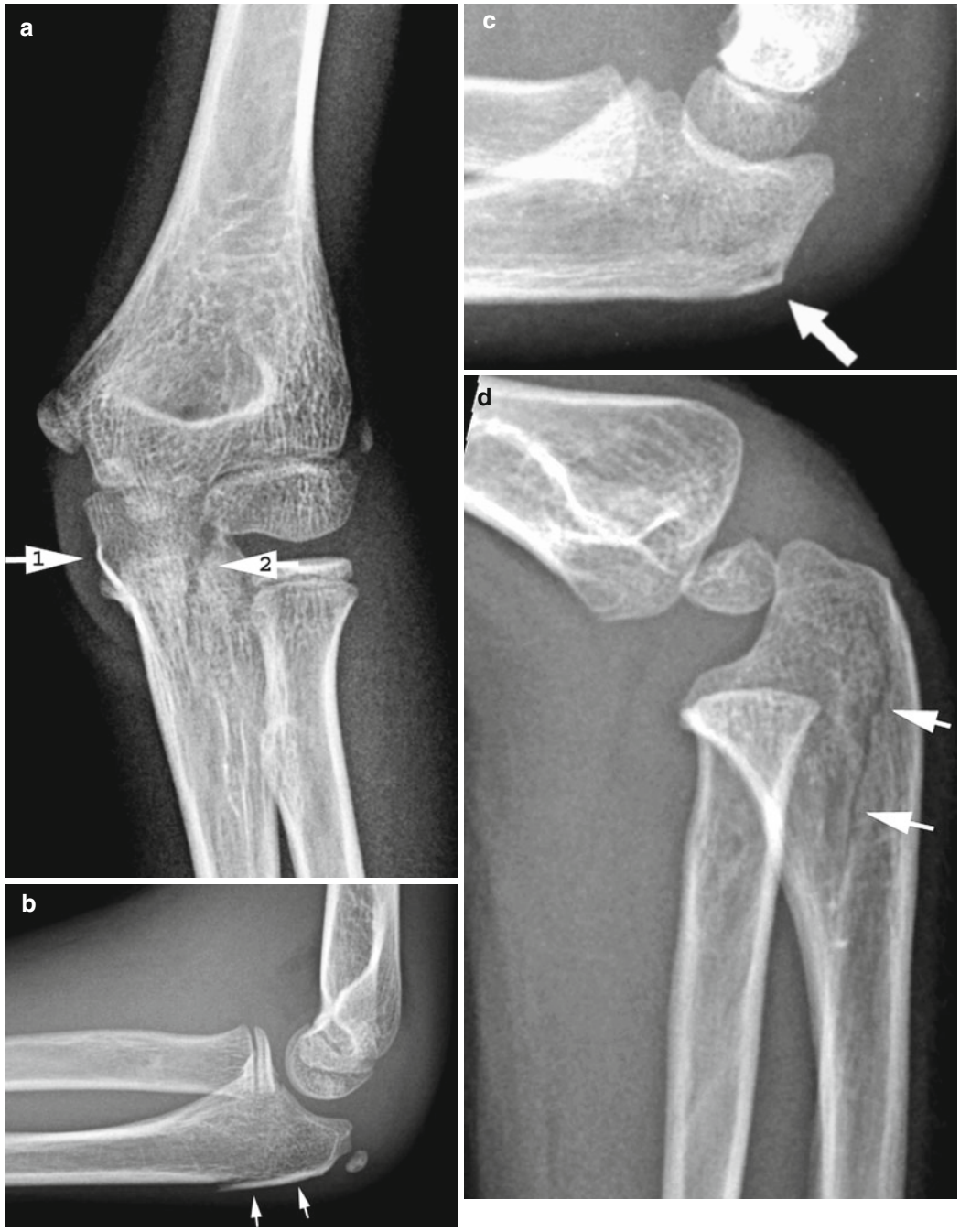


Fig. 6.20 Proximal ulnar fractures: various. (**a**) In this patient a subtle buckle fracture (*1*) is present along with a vertical linear fracture (*2*). (**b**) This patient demonstrates a longitudinal avulsion fracture (*arrows*). (**c**) Minimal buckle fracture (*arrow*). (**d**) Typical vertical linear hairline fracture (*arrows*)

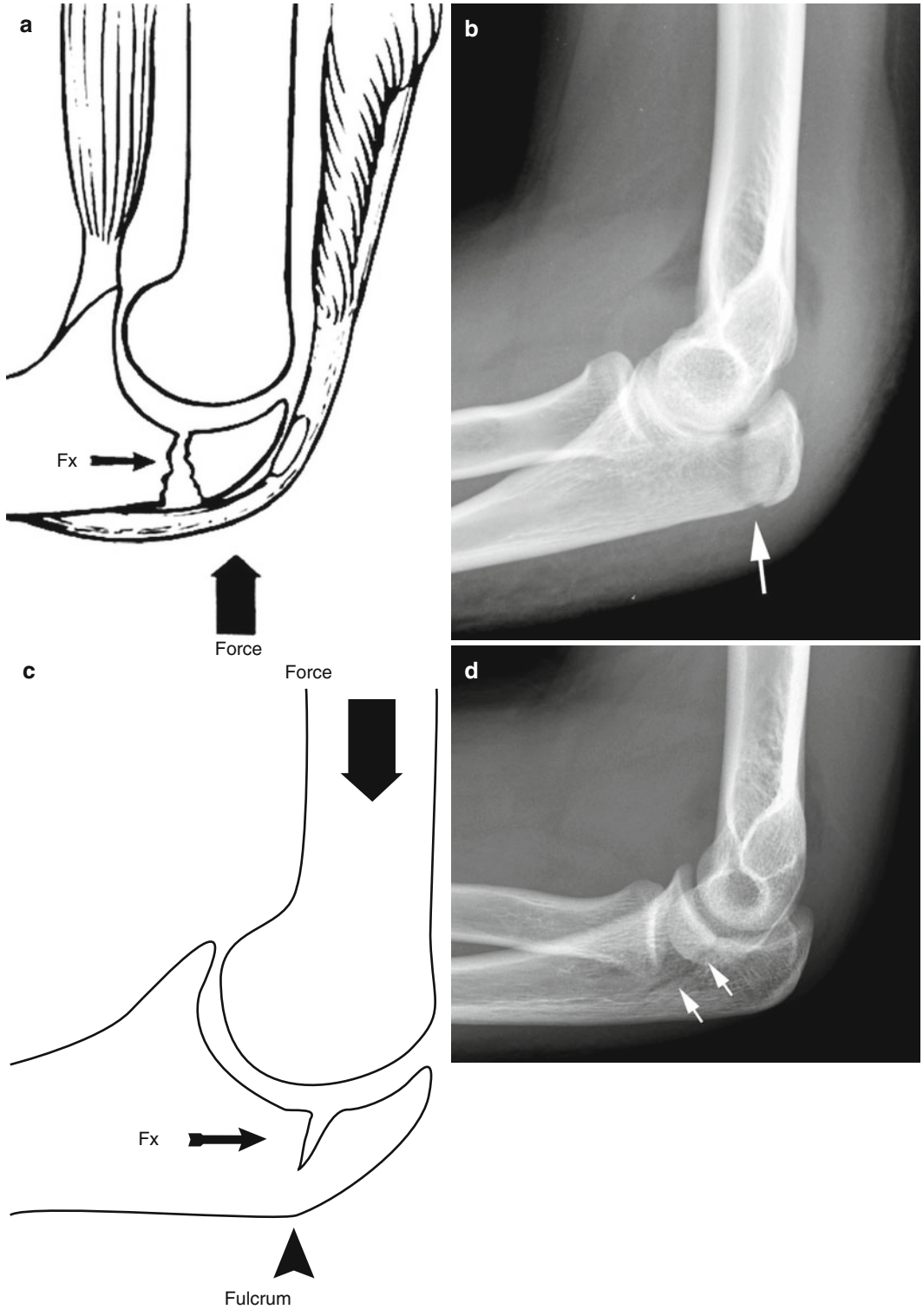


Fig. 6.21 Broad surface injuries of the proximal ulna: injury mechanics. (**a**) With broad surface forces applied to the posterior elbow, a fracture of the olecranon results. Because of pull by the biceps and triceps muscles, the fracture often is diastatic. (**b**) Typical fracture through the olecranon (*arrow*). (**c**) With forces (*force*) of the downward heading humerus, a fulcrum develops over the posterior surface of the ulna and a diastatic hairline fracture (*fx*) results. (**d**) Typical hairline fracture (*arrows*)

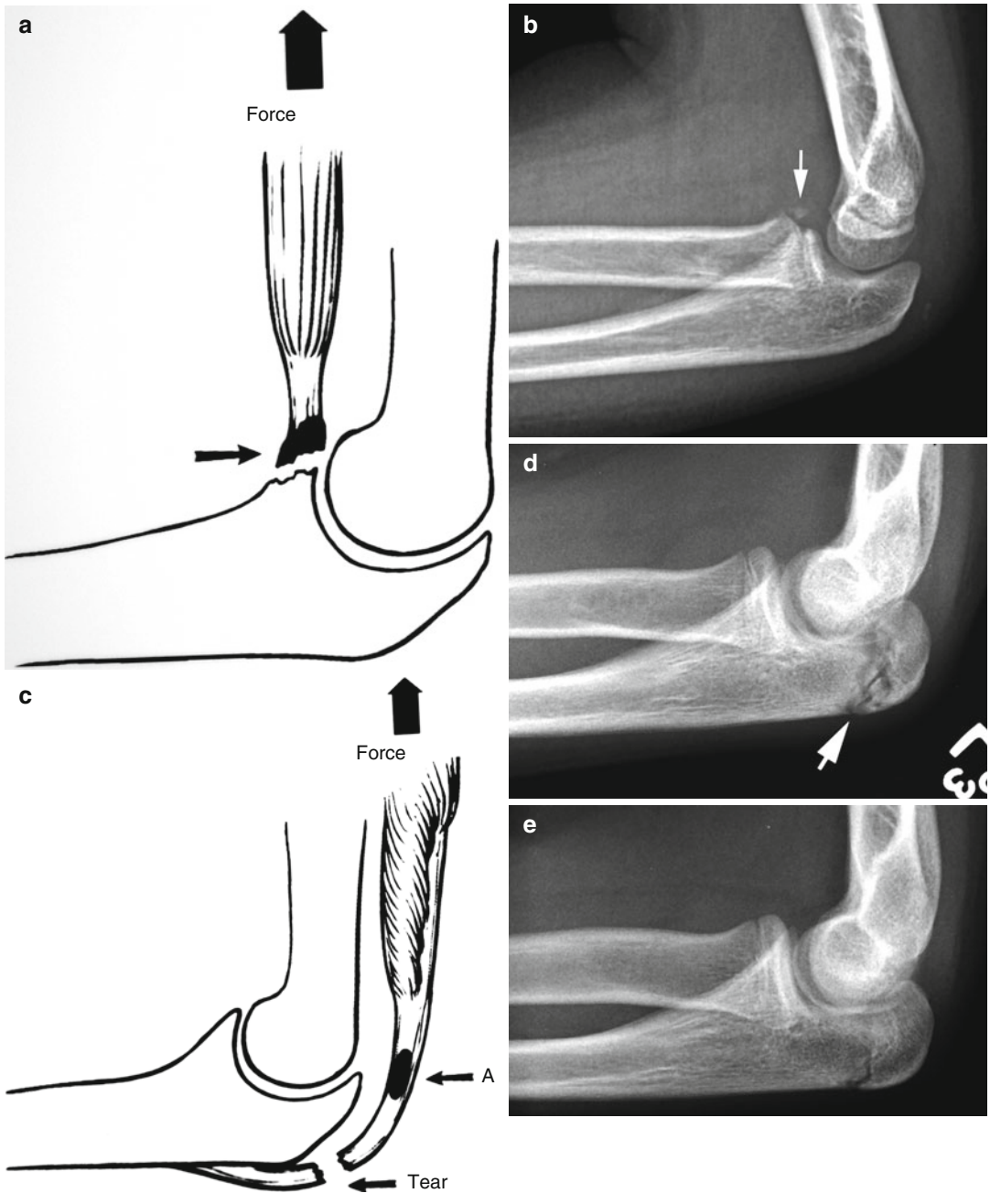


Fig. 6.22 Proximal ulnar avulsion fractures: injury mechanism. (**a**) With avulsion force (*force*) of the brachialis muscle, an avulsion fracture (*arrow*) of the coronoid process can occur. (**b**) Typical appearance of such a fracture (*arrow*). (**c**) With distraction forces by the triceps muscle, the apophysis of the olecranon (*A*) can be avulsed. There also usually is a tear of the tendon (*tear*). (**d**) Note subtle avulsion of the apophysis (*arrow*). (**e**) Normal side for comparison

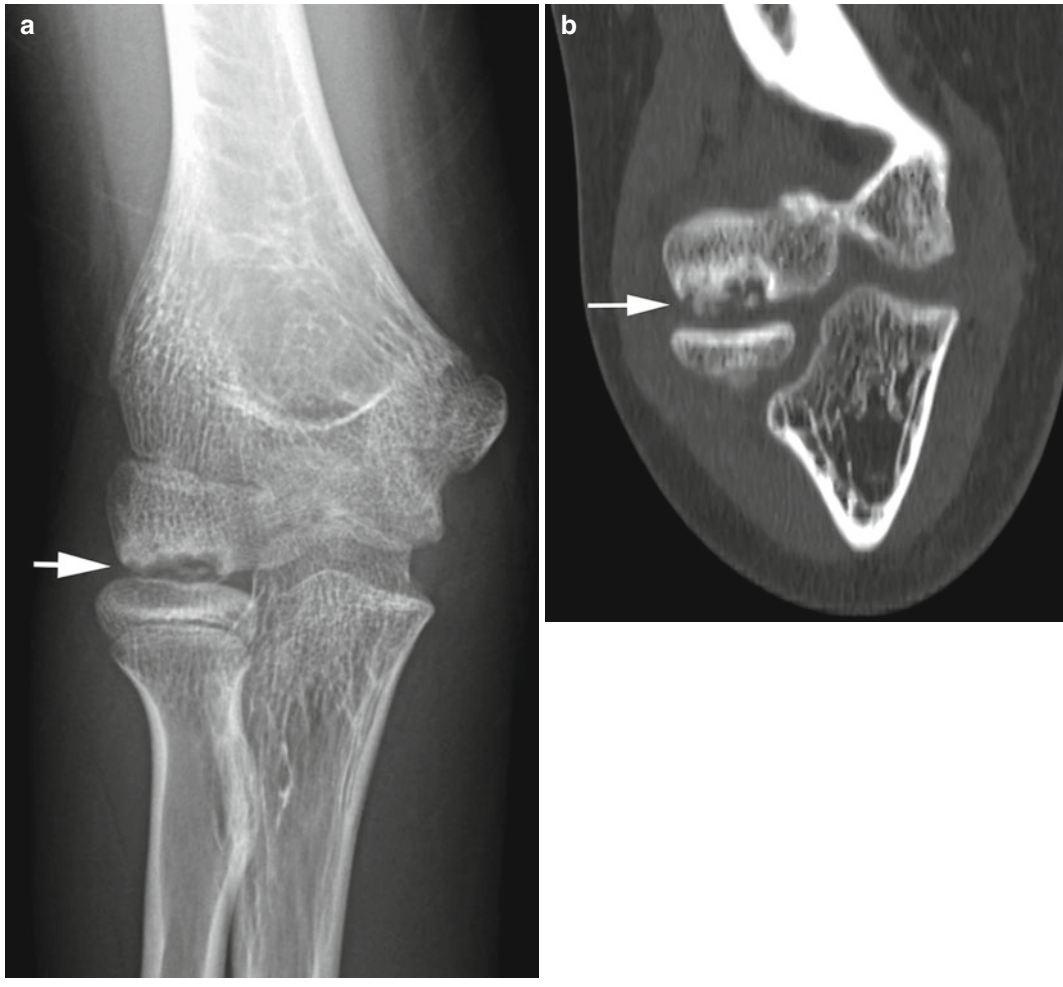


Fig. 6.23 Osteochondritis dissecans: capitellum. (**a**) Note typical defect with some adjacent sclerosis (*arrow*) in the capitellum. (**b**) CT study demonstrates the same defect (*arrow*)

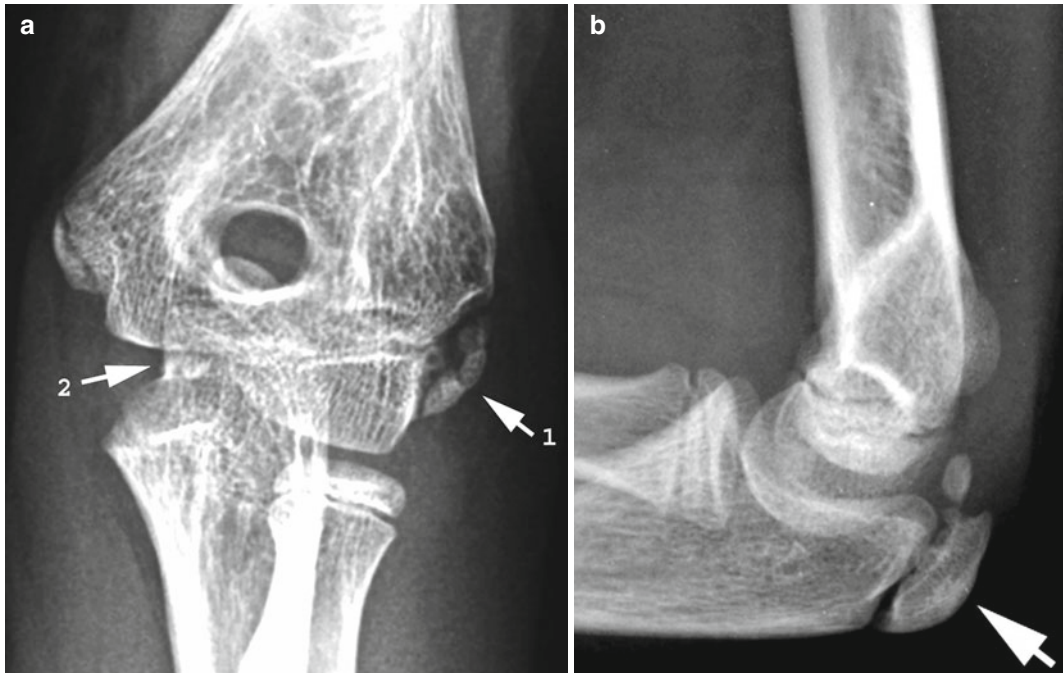


Fig. 6.24 Normal ossification centers: elbow. (**a**) Note the irregular-appearing lateral epicondyle (*1*) and the medial condyle (*2*). These centers characteristically are irregular but normal. (**b**) Normal apophysis of the olecranon (*arrow*). A secondary center is seen above it



Fig. 6.25 Plastic and greenstick fractures of the forearm. (**a**) Note a typical greenstick fracture (*arrow*) of the midshaft of the radius. (**b**) In this patient a greenstick fracture is present in the radius (*arrow*), while a plastic bending fracture (*arrowheads*) is present in the ulna

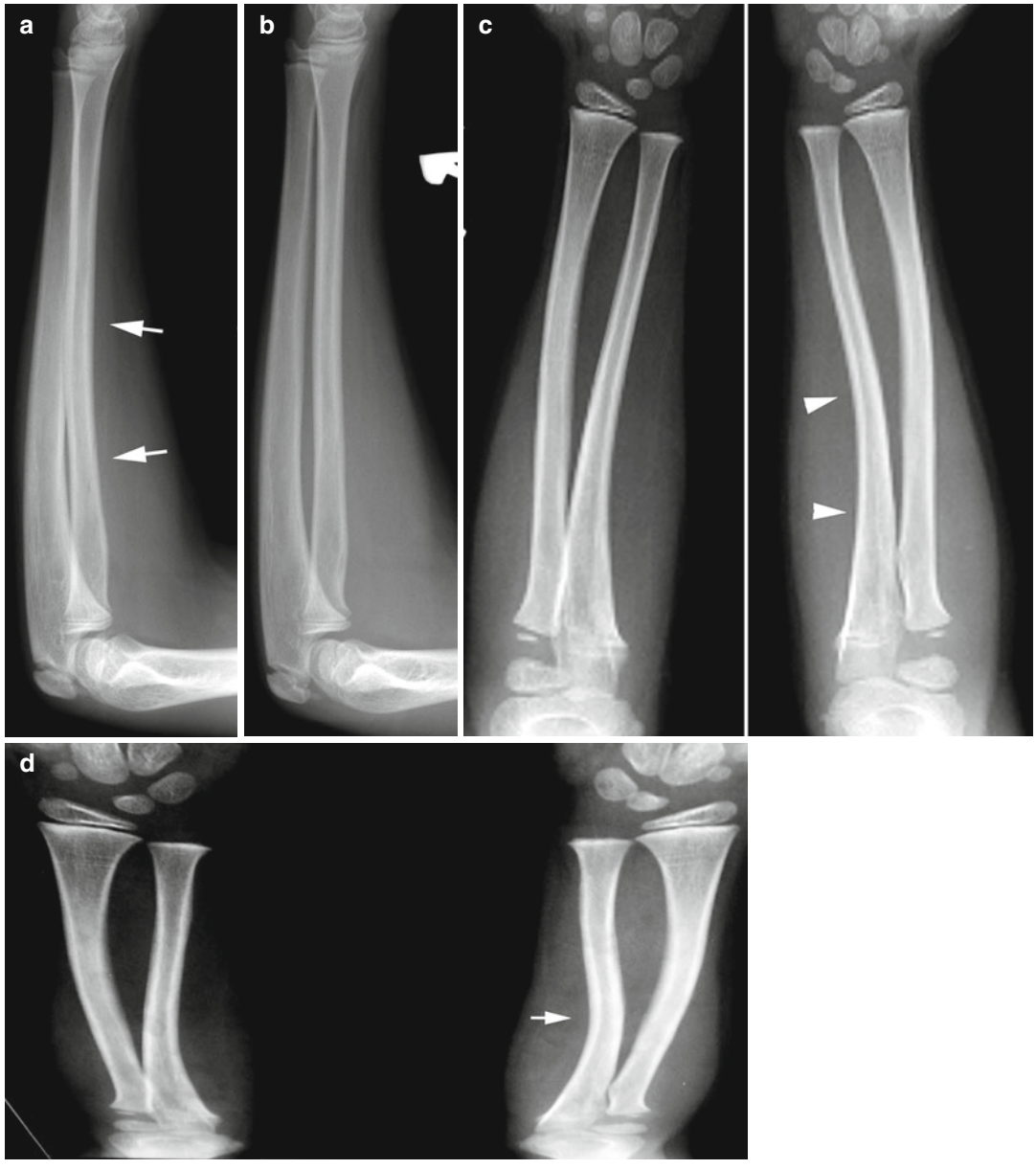


Fig. 6.26 Plastic bending fractures: subtle findings. (**a**) Note subtle bending of the radius (*arrows*) and ulna. (**b**) Normal side for comparison. Both bones are straighter. (**c**) Note bowing of the right ulna (*arrowheads*). Compare to the opposite normal side. (**d**) With looking at the image vertically, the bowing of the ulna (*arrow*) is exaggerated and easier to see



Fig. 6.27 Normal bowing forearm bones. Note that the radius and ulna are bowed to the same degree in both forearms. Such normal bowing is common and thus comparative views become very important

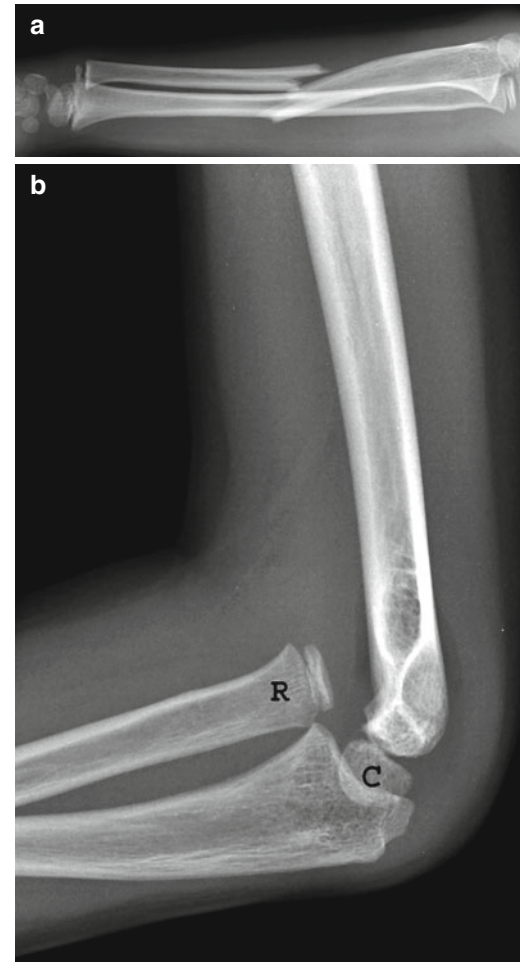


Fig. 6.28 Long bone fractures. (**a**) Note the transverse displaced and slightly overriding fracture of the ulna. The radius appears normal. (**b**) Lateral view of the elbow demonstrates that the fracture is a Monteggia fracture with dislocation of the radial head (*R*) anteriorly. Capitellum (*C*)

vascular grooves are diaphyseal and appear no different from those in other long bones.

References

1. Bohrer SP. The fat pad sign following elbow trauma. Its usefulness and reliability in suspecting "invisible" fractures. Clin Radiol. 1970;21:90–4.
2. Blumberg SM, Kunkov S, Crain EF, Goldman HS. The predictive value of a normal radiographic fat pad sign following elbow trauma in children. Pediatr Emerg Care. 2011;27(7):596–600.
3. Bledsoe RC, Izenstark L. Displacement of fat pads in disease injury of the elbow: a new radiographic sign. Radiology. 1959;73:717–24.
4. Markowitz RI, Davidson RS, Harty MP, Bellah RD, Hubbard AM, Rosenberg HK. Pictorial essay. Sonography of the elbow in infants and children. AJR. 1992;159:829–33.
5. Rogers SL, MacEwan DW. Changes due to trauma in the fat plane overlying the supinator muscle: a radiologic sign. Radiology. 1969;92:954–8.
6. John SD, Wherry K, Swischuk LE, Phillips WA. Improving detection of elbow fractures by understanding their mechanics. Radiographics. 1996;16: 1443–60.
7. Griffith JF, Roebuck DJ, Cheng JCY, et al. Acute elbow trauma in children: spectrum of injury revealed by MR imaging not apparent on radiographs. AJR. 2001;176:53–60.
8. Rogers LF, Malave Jr S, White H, Tachdjian MO. Plastic bowing, torus and greenstick supracondylar fractures of the humerus: radiographic clues to obscure fractures of the elbow in children. Radiology. 1978;128:145–50.
9. Swischuk LE. Musculoskeletal: what's different in children? Playing on the couch, fell from couch, favoring left upper extremity. Emerg Radiol. 2010;17:203–4.
10. Labelle H, Bunnell WP, Duhaime M, Poitras B. Cubitus varus deformity following supracondylar fracture of the humerus in children. J Pediatr Orthop. 1982;2:539–46.
11. Papavasiliou V, Nenopoulos S, Venturis T. Fractures of the medial condyle of the humerus in childhood. J Pediatr Orthop. 1987;7:421–3.
12. Swischuk LE. Musculoskeletal: what's different in children? Jumping around and falls on floor: will not move right arm. Emerg Radiol. 2012;19(6):485–7.
13. Swischuk LE. Musculoskeletal: what's different in children? Three-year-old with sore elbow; unknown type of injury. Emerg Radiol. 2010;17:431–3.
14. Swischuk LE. Musculoskeletal: what's different in children? Jumping from pool to pool; fall and slips; elbow hurts. Emerg Radiol. 2011;18:513–4.
15. Gore RM, Rogers LF, Bowerman J, Suker J, Compere CL. Osseous manifestations of elbow stress associated with sports activities. AJR. 1980;134:971–7.
16. Ellman H. Anterior angulation deformity of the radial head: an unusual lesion occurring in juvenile baseball players. J Bone Joint Surg Am. 1976;11:281.
17. Pavlov H, Torg JS, Jacobs B, Vigorita V. Non-union of olecranon epiphysis: two cases in adolescent baseball pitchers. AJR. 1981;136:819–29.
18. Swischuk LE. Musculoskeletal: what's different in children? Fell on arm, favors arm; know what to look for. Emerg Radiol. 2010;17:95–6.
19. Swischuk LE. Musculoskeletal: what's different in children? Playing basketball and falling on outstretched upper extremity. Emerg Radiol. 2012;19(3):185–6.
20. Illingworth CM. Pulled elbow: study of 100 patients. Br Med J. 1975;2:672–4.
21. Michaels MG. A case of bilateral nursemaid's elbow. Pediatr Emerg Care. 1989;5:226–7.
22. Swischuk LE. Musculoskeletal: what's different in children? Running and fell on the outstretched upper extremity. Emerg Radiol. 2009;16:251–3.
23. Rath NK, Carpenter EC, Thomas DP. Traumatic pediatric olecranon injury: a report of suture fixation and review of the literature. Pediatr Emerg Care. 2011;27:1167–9.
24. George HL, Unnikrishnan PN, Bass A, Waseem M, Brownson P. Transverse divergent dislocation of elbow in a child: a case report and review of current literature. Pediatr Emerg Care. 2011;27(5):411–3.
25. Jawish R, Rigault P, Padovani JP. Osteochondritis dissecans of the humeral capitellum in children. Eur J Pediatr Surg. 1993;3:97–100.
26. Attia MW, Glasstetter DS. Plastic bowing type fracture of the forearm in two children. Pediatr Emerg Care. 1997;13:392–3.
27. Borden S. Roentgen recognition on acute plastic bowing of the forearm in children. AJR. 1975;125:524–30.
28. Crowe JE, Swischuk LE. Acute bowing fractures of the forearm in children: a frequently missed injury. AJR. 1977;128:981–4.
29. Stenstrom R, Gripenbert L, Bergius AR. Traumatic bowing of forearm and lower leg in children. Acta Radiol. 1978;19:243–9.
30. Swischuk LE. Musculoskeletal: what's different in children? Fell off of pogo stick; sore hand. Emerg Radiol. 2010;17(5):343–5.
31. Swischuk LE. Musculoskeletal: what's different in children? Pain in the forearm due to a fall. Emerg Radiol. 2011;18:187–8.
32. Swischuk LE. Musculoskeletal: what's different in children? Falling on outstretched upper extremity: diagnosis by serendipity. Emerg Radiol. 2010;17: 259–60.
33. Swischuk LE. Musculoskeletal: what's different in children? Pushed into ditch; left forearm pain. Emerg Radiol. 2009;16:423–4.

Wrist and Hand

7

Injuries of the Wrist

Evaluation of Fat Pads and Soft Tissues

There are two fat pads around the wrist that can be utilized in the assessment of wrist injuries. The first is the pronator quadratus fat pad [1], and the second is the navicular fat pad [2]. The pronator quadratus fat pad is seen on lateral views of the wrist and lies along the pronator quadratus muscle (Fig. 7.1a). The navicular fat pad lies just medial to the scaphoid bone and is seen on anteroposterior views of the wrist (Fig. 7.1b). In young infants, this latter fat pad is not visualized with as much consistency as it is in older children. However, this is not so unfortunate because obliteration of the navicular fat pad is utilized primarily for the detection of navicular fractures, and these fractures are not particularly common in infants and young children. Distal radial and ulnar fractures, on the other hand, are quite common, and it is in this regard that displacement and obliteration of the pronator quadratus fat pad becomes most useful.

Determining the Presence of Fluid in the Wrist Joint

Determining the presence of fluid in the wrist joint is not possible with plain films and thus one must rely on soft tissue edema to focus ones attention on any possible underlying bony abnormality. In terms of swelling, if the problem is in the wrist proper, swelling will be most pronounced distal to the radial epiphyseal plate (Fig. 7.2c, d), but if the problem is in the distal radius/ulna, swelling is most pronounced proximal to the radial epiphyseal plate (Fig. 7.2a, b).

Injuries of the Distal Radius and Ulna

Although a variety of overt transverse and oblique fractures commonly occur through the distal third of the radius and ulna, these fractures usually are not difficult to detect (Fig. 7.3). At the other end of the spectrum of distal radial and ulnar fractures are the cortical buckle or torus fractures [3]. Both standard buckle and angled buckle fracture are common, but these fractures often can be subtle on AP and oblique views. They are usually more clearly seen on lateral views of the wrist (Figs. 7.4 and 7.5). Indeed, *the lateral view is the money view* for wrist fractures of the distal radius and ulna, including the relatively uncommon childhood equivalent of the Smith's fracture (Fig. 7.6).

Epiphyseal/metaphyseal Salter–Harris fractures also are very common in the wrist, especially the distal radius. The most common of these are the Salter–Harris I and II fractures. Types III, IV, and V injuries are relatively uncommon. Salter–Harris type I injuries can be very subtle [4]. In most instances the injury results from falling on the outstretched extremity, and most often it is the distal radial epiphysis which is involved

L.E. Swischuk, S.P. Jadhav (eds.), *Emergency Musculoskeletal Imaging in Children*,
DOI 10.1007/978-1-4614-7747-1_7, © Springer Science+Business Media New York 2014

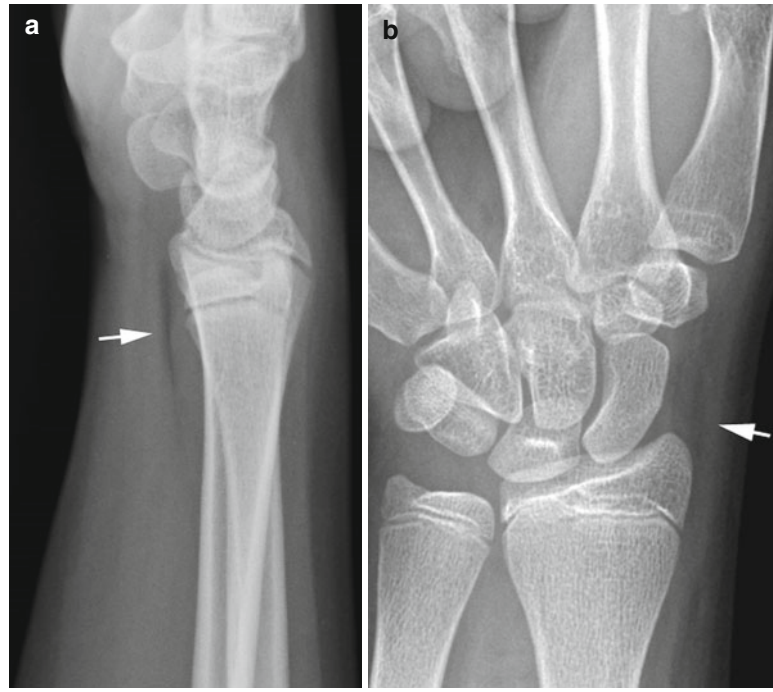


Fig. 7.1 Normal fat pads. (**a**) Note the position and configuration of the *quadratus fat pad* (*arrow*). (**b**) Navicular fat pad. This fat pad (*arrow*) lies adjacent to the scaphoid bone

and displaced posteriorly (Fig. 7.7). These Salter injuries can occur even in older children where the epiphysis is basically closed (Fig. 7.8).

Finally in terms of Salter–Harris fractures, it should be noted that chronic stress-induced epiphyseal/metaphyseal fractures of the distal radius and ulna can be seen in gymnasts and other young athletes who overuse the wrist [5–9]. These fractures appear as healing Salter–Harris I epiphyseal/metaphyseal fractures (Fig. 7.9). The problem is one of chronic, repetitive subclinical stress on the wrist and, hence, the gymnast wrist.

Ulnar styloid fractures although appearing innocuous are very important. The reason for this is that they usually herald the presence of an associated significant radial fracture [10]. This occurs because the wrist is encircled by strong ligaments and muscles, and when rotation/impaction injuries occur, the forces involve both the radius and ulna. In terms of the ulna, it is the ulna styloid tip which is fractured and avulsed. If the associated radial fracture is obvious, there is no problem (Fig. 7.10a). However, in lesser cases only the ulnar styloid fracture is apparent on AP views (Fig. 7.10b). In such cases one should look for an almost always present distal radial fracture, either a buckle fracture or a Salter–Harris fracture (Fig. 7.10c). Isolated ulnar styloid fractures can be seen if direct blows to the styloid process are sustained [10].

Old, ununited styloid avulsion fractures may erroneously suggest the presence of a secondary ossification center. I have seen only one such secondary center in my career. Otherwise, the finding should represent an old, ununited fracture of the tip of the ulnar styloid. However, the normal ulnar epiphysis can be bipartite through its midpoint (Fig. 7.10d). In these cases there should be no confusion with a fracture for such fractures basically do not occur.

Galeazzi's fracture (see Fig. 7.3c, d), which often is associated with radioulnar disassociation, is rare in childhood [11]. The radioulnar disassociation is best evaluated on lateral views and usually is finally delineated with CT scanning [12].

Injuries of the Carpal Bones

Fractures or dislocations of the carpal bones in infants and young children are uncommon. They

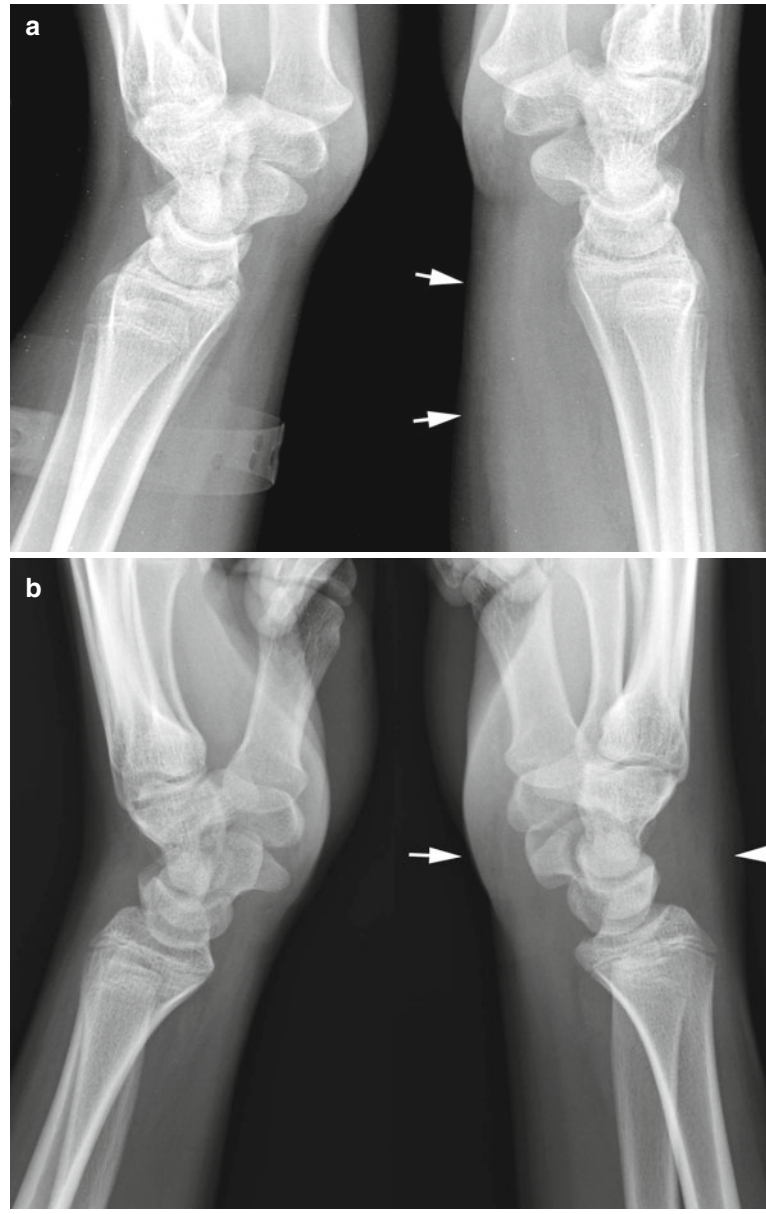


Fig. 7.2 Value of soft tissue swelling location. (**a**) In this patient most of the swelling is in the proximal wrist and distal forearm (*arrows*), proximal to the radial epiphyseal plate. With swelling in this area, one should look for fractures in the distal radius. In this regard there is a minimal angle buckle fracture over the dorsum of the distal wrist. (**b**) In this patient swelling is more distal, that is, in the wrist proper (*arrows*), and in such cases, one should look for fractures of the carpal bones, most often the scaphoid bone

are more common in the older child and adolescent, and of these, fractures of the scaphoid bone are most common [13]. The clinical findings in these fractures are similar to those seen in adults (i.e., acute tenderness in the anatomic snuff box), and the fractures result from falls on the outstretched extremity.

In terms of plain film imaging, this fracture can be suspected if there is juxta-navicular soft tissue swelling and/or obliteration of the adjacent navicular fat pad [1, 13]. If the fat pad is intact, it is highly unlikely that a scaphoid fracture is present. In the classic case of a transverse fracture, the findings are not difficult to detect (Fig. 7.11). However, in children an impacted buckle/stress fracture of the scaphoid bone is probably just as common or even more common than the transverse fracture [14–16]. The findings often are very subtle, and



Fig. 7.3 Distal radius and ulna fractures. (**a**) Typical transverse overriding fractures of both the radius and ulna. (**b**) In this patient a direct blow to the ulna resulted in a greenstick fracture (*arrow*). (**c**) Galeazzi's fracture. Note the fracture and angulation of the radius. The ulna is dislocated. (**d**) Lateral view demonstrating same findings

comparative views are critical (Fig. 7.12). In puzzling cases, if a question about a fracture is still present, one can resort to nuclear scintigraphy [17] or MR imaging [18–20].

Finally one must be careful of normal buckling of the scaphoid bone and not misinterpret the finding for a buckle fracture (Fig. 7.13). MR is very useful for the detection of occult carpal bone fractures (Fig. 7.14). A targeted MR with T1-weighted and STIR sequences can be obtained in most children within 10 min without the need for sedation to provide the diagnosis in the ER

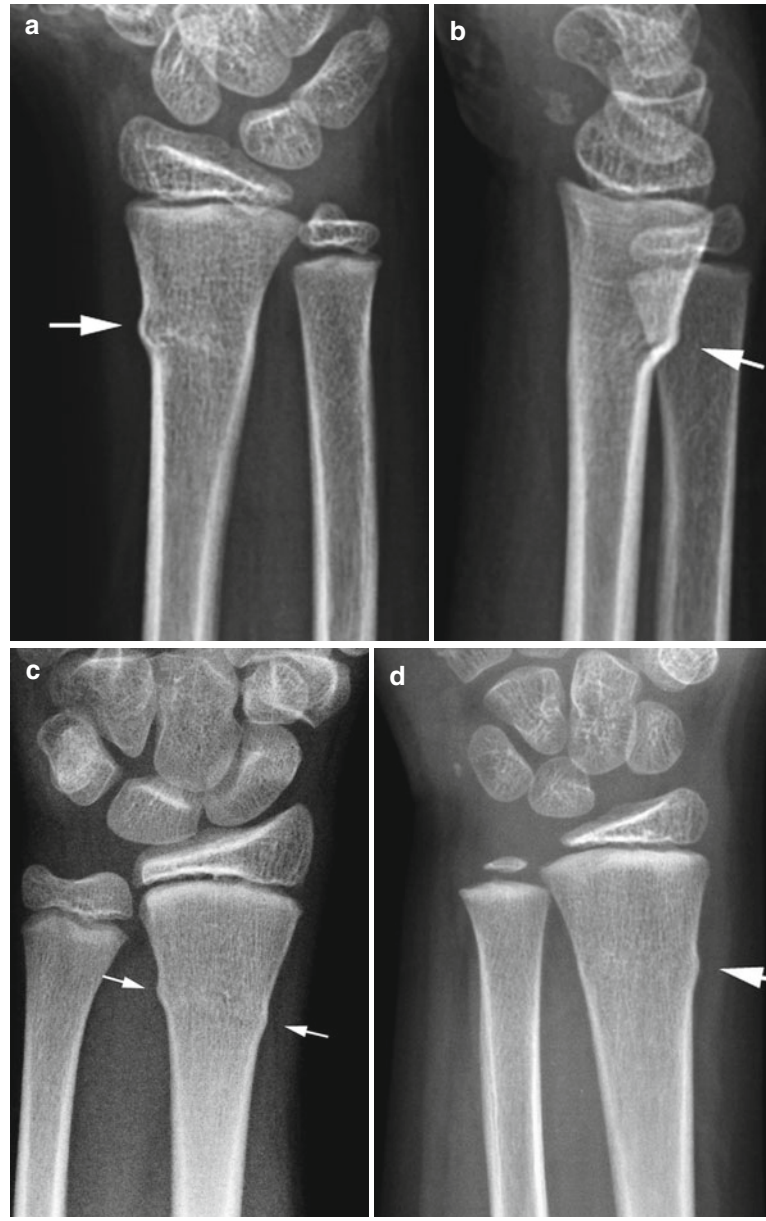


Fig. 7.4 Buckle (torus fractures): typical. (**a**) Note the typical impacted buckle fracture with outward bulging of the cortex (*arrow*). (**b**) Lateral view demonstrates similar findings (*arrow*). (**c**) In this patient cortical bulging is seen on both sides (*arrows*). (**d**) Very subtle buckle fracture (*arrow*)

setting. This also obviates the need for CT scan which involves radiation risks.

Aseptic necrosis as a complication of scaphoid fractures is not as common in children as in adults, but it does occur [21]. Usually it is the proximal fragment that becomes necrotic, and the radiographic findings consist of nonunion of the fracture and sclerosis of the necrotic fragment. MR imaging is useful in early detection of aseptic necrosis (Fig. 7.15). T1-weighted unenhanced MRI is an acceptable alternative to delayed-enhanced MRI for diagnosis of aseptic necrosis [22]. Indeed, this communication suggests that diffusely decreased T1 signal in the involved segment of the scaphoid bone is more reliable than decreased signal on STIR or T2-weighted fat saturation sequences. Aseptic necrosis of the other carpal bones is uncommon but occasionally is encountered.

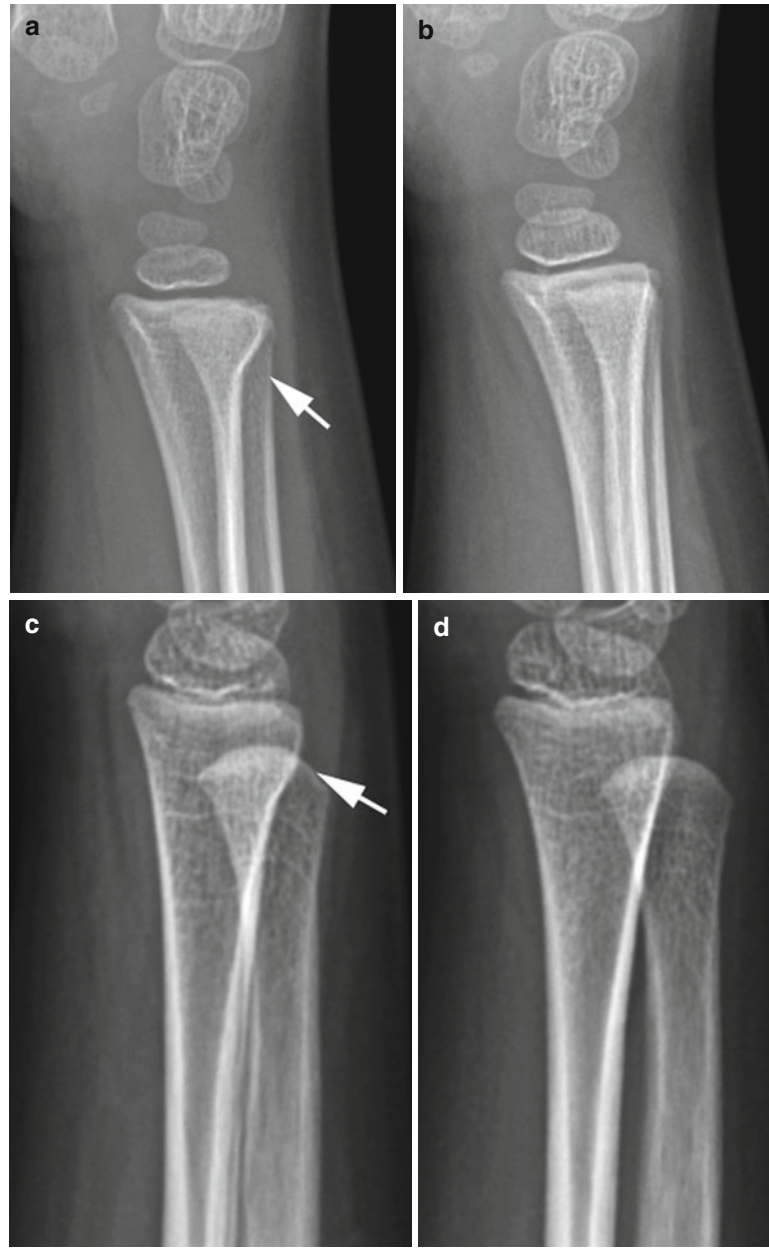


Fig. 7.5 Buckle (torus fractures): angled. (**a**) Note the angled buckle fracture (*arrow*) in the distal radius. (**b**) Normal side for comparison. Note the smooth configuration of the dorsal cortex of the radius. (**c**) Very minimal angled buckle fracture of the distal radius (*arrow*). (**d**) Normal side for comparison

The only other bones in the wrist to fracture with any frequency in childhood are the pisiform and triquetrum. The pisiform fracture can result from a direct blow, but the triquetral fracture usually results from falling on the outstretched extremity. These fractures often are subtle and can be demonstrated with MR imaging (Fig. 7.16).

Carpal Bone Dislocation

Carpal bone dislocations are uncommon in infants and young children [23]. In older children one can encounter scaphoid, perilunate, or lunate dislocations. These injuries present with malalignment of the proximal row of the carpal

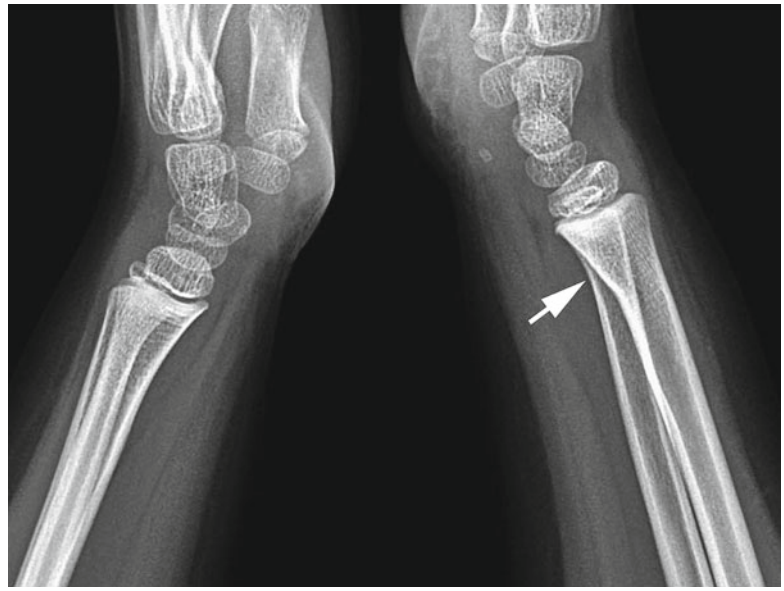


Fig. 7.6 Angled buckle fracture: Smith's fracture equivalent. Note the angled buckle fracture (*arrow*) through the distal ventral aspect of the radius. Compare with the normal other side

bones and associated discrepancy in the width (wider or narrower) of the involved joint spaces. With scaphoid dislocations the space between the scaphoid and lunate bones becomes wider (Fig. 7.17a). In addition the scaphoid bone rotates and as such can telescope and result in the ring sign (Fig. 7.17b).

With lunate and perilunate dislocations, the normal alignment of the carpal bones on lateral view is disrupted. In the normal patient, there is a vertical sequential arrangement of the capitate, lunate, and distal radial epiphysis. Any deviation from this arrangement of the carpal bones should indicate an underlying dislocation. In this regard with a perilunate dislocation, the lunate bone and distal radial epiphysis lie one on top of another, while the other carpal bones lie posterior to them (Fig. 7.17c, d). With lunate dislocations the carpal bones and distal radius including the epiphysis lie posterior to the anteriorly dislocated lunate bone. Other fractures and dislocations of the carpal bones in young children are uncommon. However, one occasionally can encounter fractures of the triquetral and trapezium bones. Pisiform fractures also occasionally can occur.

Normal Findings Causing Problems

For the most part, the carpal bones ossify as single smooth structures, and there is very little problem with psuedofractures resulting from aberrant, but normal ossification patterns. The distal ulnar epiphysis maybe bipartite on a normal basis (see Fig. 7.12c) and should not misinterpret this for a fracture. However, one often can encounter somewhat aberrant proximal apophyses of the metacarpals and these can be misinterpreted for Salter–Harris fractures, similar to what can occur in the foot (see Fig. 11.39).

Injuries of the Hand

Evaluation of the Fat Pads and Soft Tissues

There are no specific fat pads to evaluate in the hand, and evaluation of the soft tissues consists primarily of noting whether localized soft tissue edema and swelling are present. This latter finding however, as nonspecific as it is, is very helpful in localizing the site of injury in the fingers.

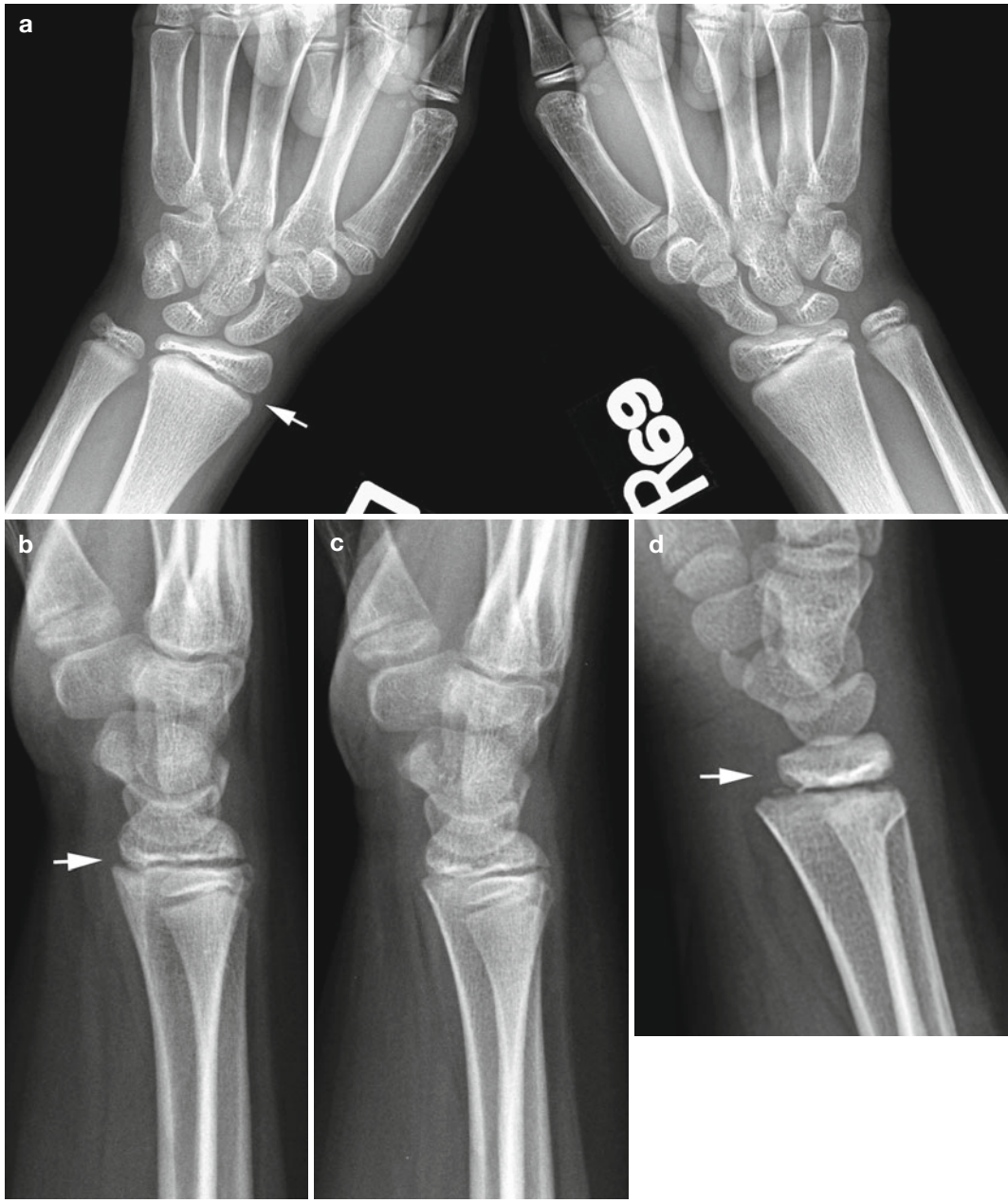


Fig. 7.7 Salter–Harris epiphyseal/metaphyseal fractures. (**a**) Salter–Harris I fracture. Note slight widening of the epiphyseal plate on the left (*arrow*). Compare with the normal right side. (**b**) On lateral view widening of the epiphyseal plate is again seen and there is slight posterior displacement of the distal radial epiphysis (*arrow*). (**c**) Normal side for comparison. Note the normal width of the epiphyseal plate and the position of the epiphysis. (**d**) Salter–Harris II equivalent fracture. The distal radial epiphysis is posteriorly displaced (*arrow*), and the epiphyseal plate is widened. The dorsal cortex of the radius is angled. With more force this fragment of bone would break off and become a classic Salter–Harris II fracture fragment

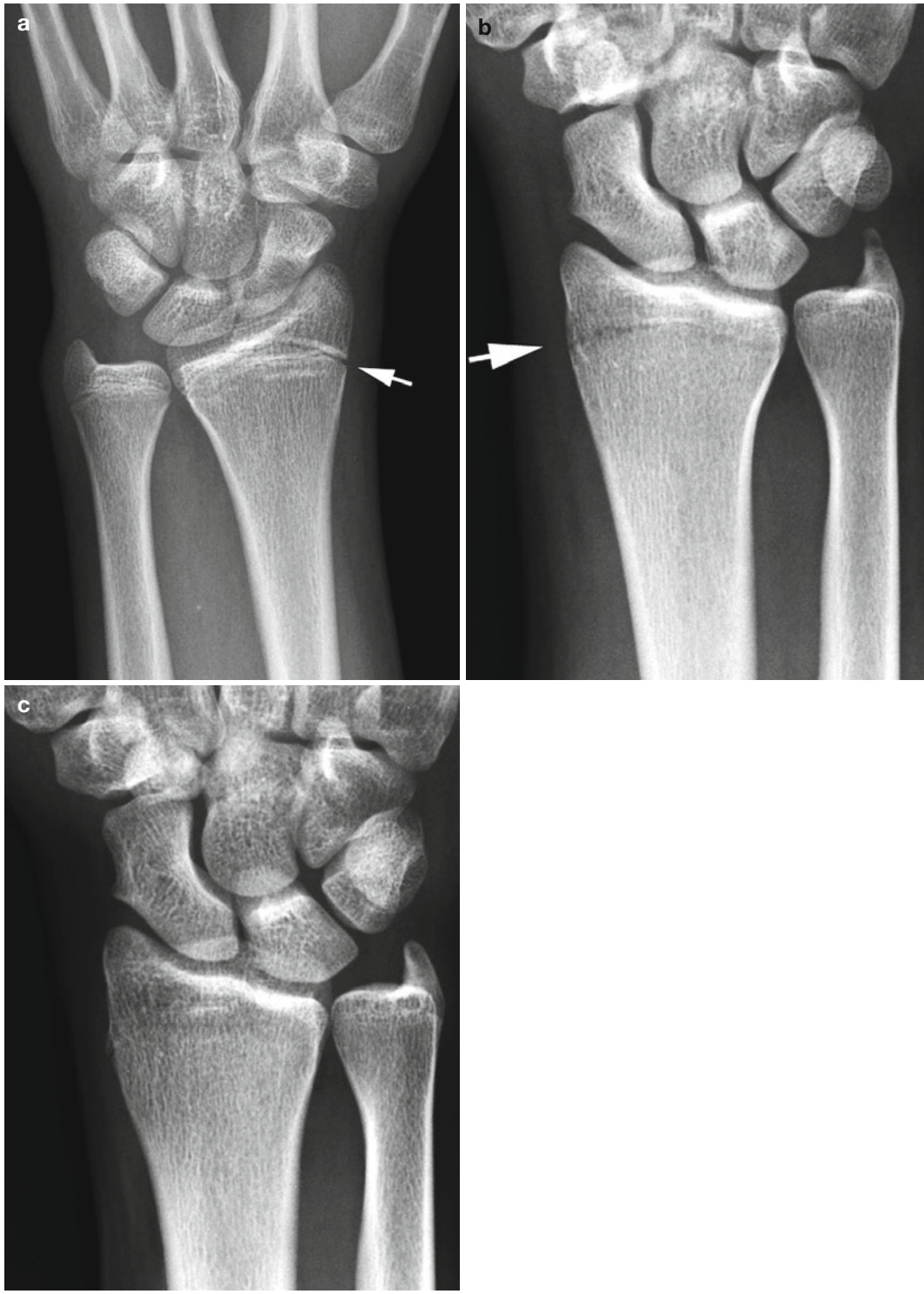


Fig. 7.8 Salter–Harris fracture: older children. (**a**) Note that the ulnar epiphysis is nearly closed. However, the distal radial epiphyseal plate is slightly open (*arrow*) and there is some adjacent sclerosis in the metaphysis. These findings are typical for a Salter–Harris I fracture in a patient where the epiphyses have basically closed. (**b**) Another patient with a very minimal Salter–Harris fracture (*arrow*) through the fused epiphyseal plate. Also note the fracture of the tip of the ulnar styloid process. Note that the ulnar epiphyseal plate is closed. (**c**) Normal side for comparison

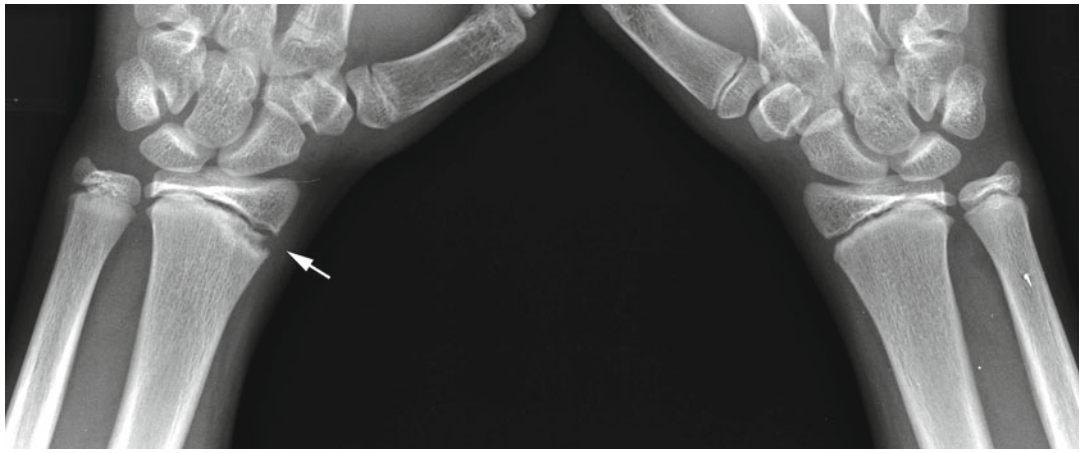


Fig. 7.9 Gymnast wrist. Note the widened epiphyseal line and sclerosis in the metaphysis (*arrow*). These findings are typical for a chronic Salter–Harris I fracture, that is, a gymnast wrist

Detecting Fluid in the Small Joints of the Hand

Detection of fluid in the small joints of the hand depends primarily on noting the presence of swelling around the joint. In some cases, the joint space may be widened, but this finding is rare and subtle and usually not present. There are no specific fat pads to evaluate, and thus, in most cases, one is left only with localized swelling.

Injuries of the Metacarpals and Phalanges

Injuries of the small bones of the hand consist of crush injuries, spiral/oblique fractures (often hairline), epiphyseal/metaphyseal Salter–Harris fractures (predominately types I and II), and a variety of buckle fractures all of which can be quite subtle. Crush injuries to the terminal phalanges are not difficult to detect. There usually is swelling over the tip of the finger and the crush fracture becomes evident on one or other of the views (Fig. 7.18a). Spiral, oblique, and transverse fractures also are not difficult to detect either in the phalanges or the metacarpals (Fig. 7.18b). Similarly buckle (torus) and epiphyseal and metaphyseal (Salter–Harris) fractures are not difficult to detect if there are gross (Fig. 7.18c, d). However, many of these fractures may be subtle, especially on AP views of the involved extremity (Fig. 7.18e). In these cases comparative and oblique views are very helpful. *Indeed, in the hand and foot, the oblique view is the money view*. Examples of these fractures and how they can be aided with comparative and oblique views are presented in Figs. 7.19–7.21.

In addition to the foregoing, it might be remembered that many times fractures of the small bones of the hands are multiple; they may be profound in one digit and yet less profound or, indeed, invisible in another digit. An example of this phenomenon is seen in Fig. 7.22.

Finally, in terms of fractures, one might address the boxer's fracture. This is a fracture of the head of the fifth metacarpal. In older children where the epiphyses have fused and in adults, a classic fracture results. However, in young children there is a spectrum from a classic fracture through a simple plastic bending fracture (Fig. 7.23).

Dislocations of the fingers and thumb are not particularly common in childhood, for rather than a dislocation an epiphyseal–metaphyseal separation (Salter–Harris fracture) occurs. Clinically, however, these fractures often appear as dislocations. The classic fracture dislocation of the base of the first metacarpal bone (Bennett's fracture) occurs only after the epiphysis of the thumb has

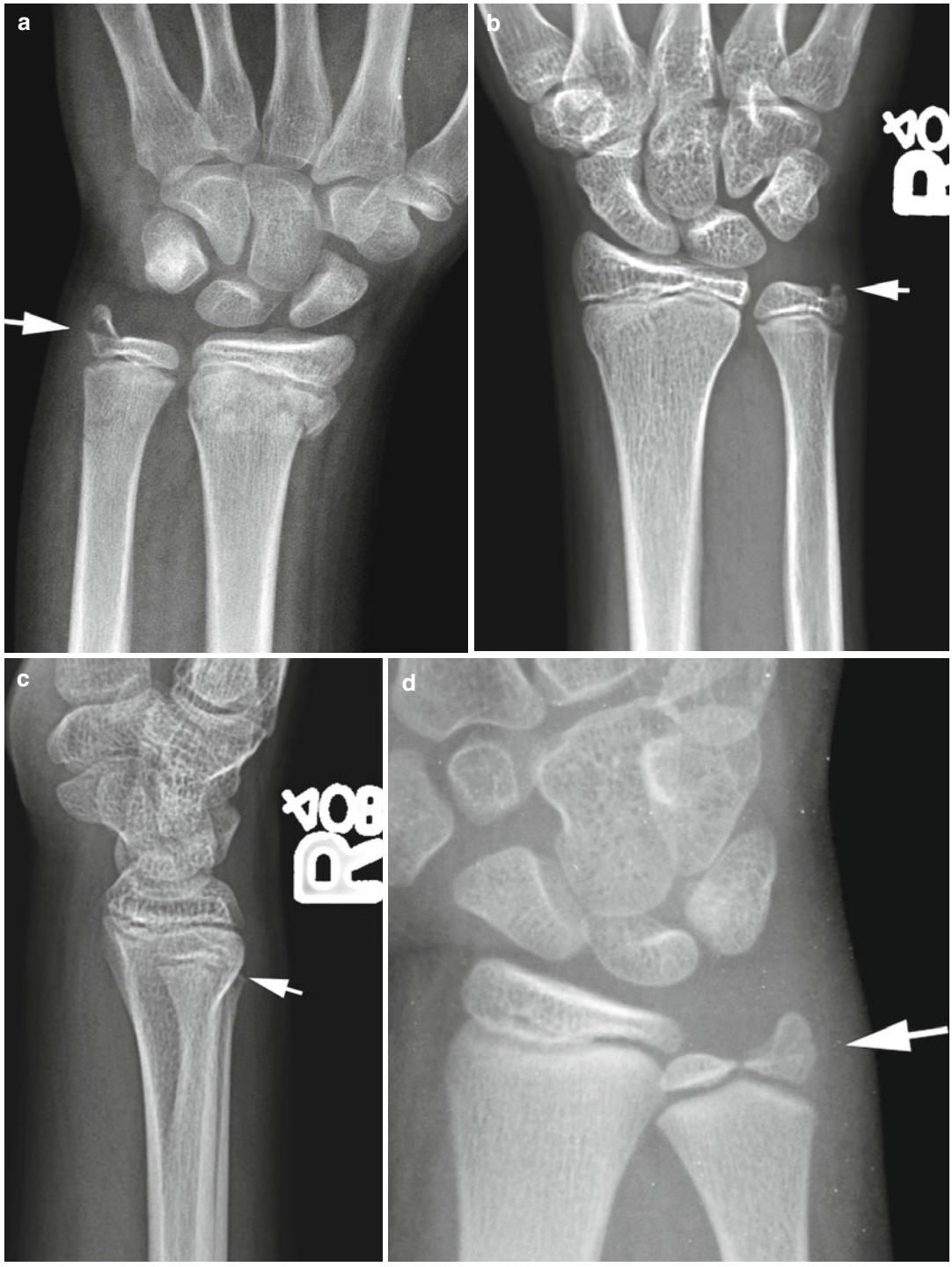


Fig. 7.10 Ulnar styloid tip fractures: significance. (**a**) Note the ulnar styloid tip fracture (*arrow*) and an associated impaction fracture of the distal radius. (**b**) In this patient the ulnar styloid fracture is very subtle (*arrow*). In addition there is subtle irregularity of the trabeculae and slight bulging of the cortex in the distal radius (*arrows*). (**c**) On lateral view, an angled buckle fracture (*arrow*) of the distal radius is seen. D. Normal bifid ulnar styloid epiphysis (*arrow*)



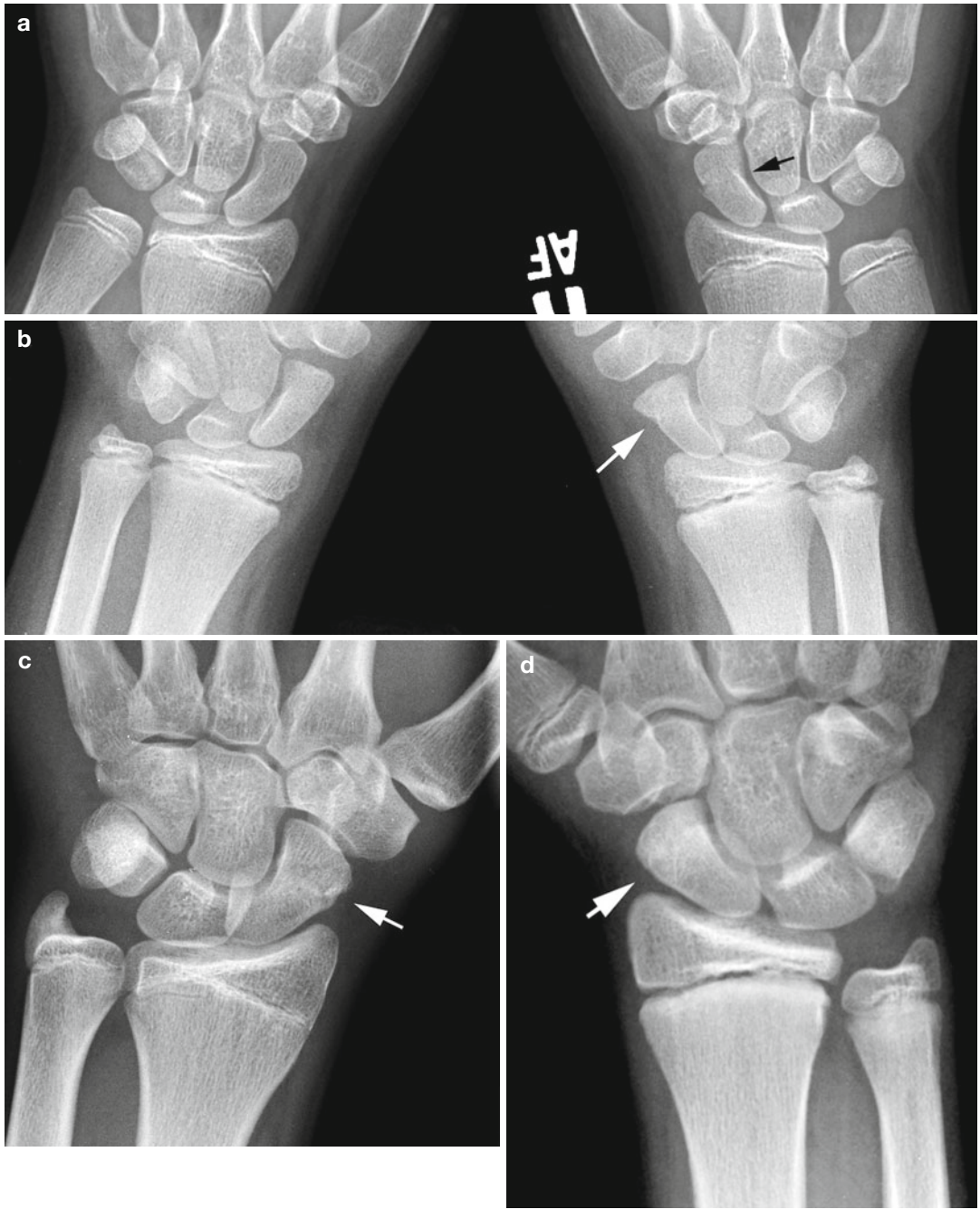
Fig. 7.11 Scaphoid fracture. Note a typical transverse fracture (*arrow*) through the scaphoid bone

fused. Until this time, the equivalent injury is a Salter–Harris type I or II fracture. In the older child in whom the epiphysis has fused or is near fusion, the same injury can result in the so-called gamekeeper's thumb. Aseptic necrosis of the metacarpal heads can occur [24] but is not common.

Normal Findings Causing Problems

Overall, normal findings in the hand causing problems with interpretation are few. Bipartite epiphyses are uncommon, but the numerous epiphyses and apophyses of the metacarpals can be misinterpreted for fractures by the uninitiated although not as common as in the foot they appear the same (see Fig. 11.39).

Fig. 7.12 Fractures of scaphoid bone: buckle (torus) type. (**a**) In this patient a very subtle buckle fracture is seen in the scaphoid bone (*arrow*). First note that the scaphoid bone is shorter than the normal one in the opposite extremity and then note that it also is slightly impacted (increase density). Finally, note a small buckle fracture over the outer surface of the scaphoid bone. Also note adjacent swelling. Compare with the normal side. (**b**) In this patient an angled impacted buckle fracture is seen (*arrow*) with impaction sclerosis at the fracture site. Also note adjacent swelling. (**c**) Another patient. Note a subtle cortical buckling irregularly (*arrow*) through the distal scaphoid bone. (**d**) In this patient one does not see a fracture line but rather impaction sclerosis (*arrow*). (**e**) Normal side for comparison


a
b
c
d

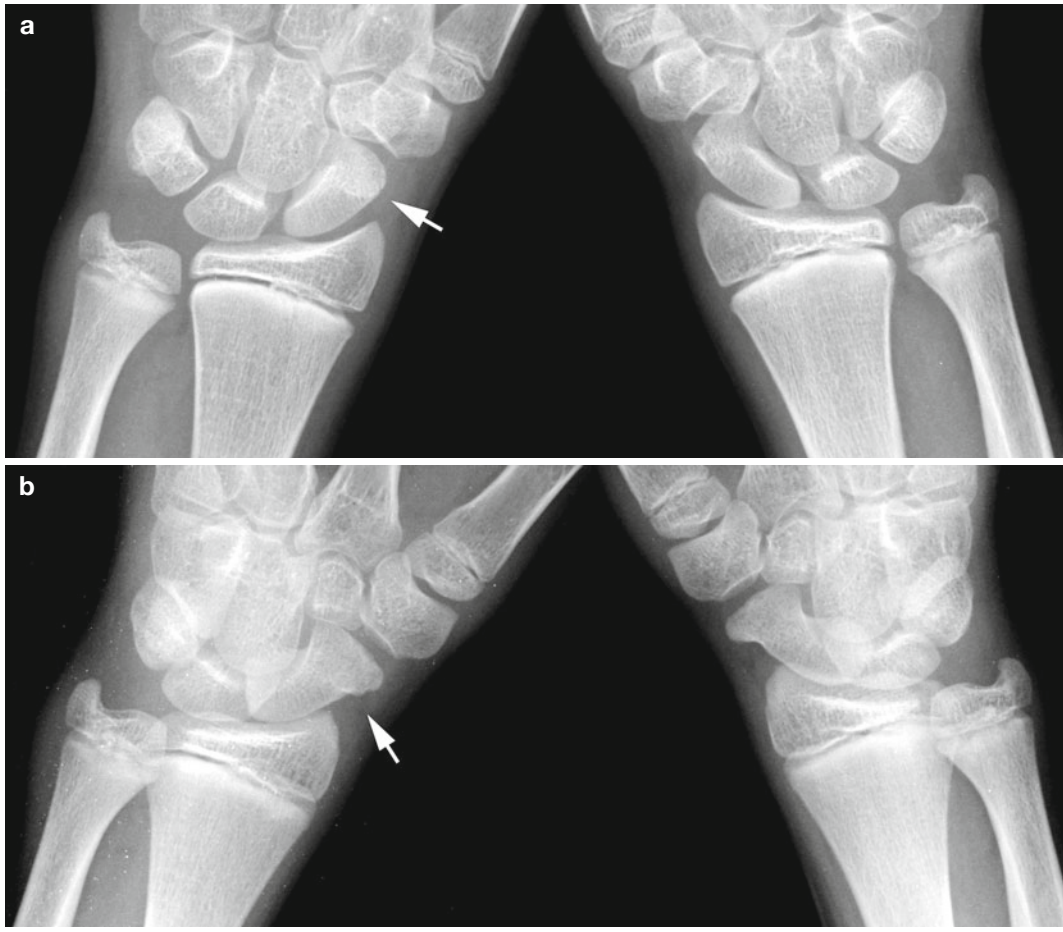


Fig. 7.13 Scaphoid buckle fracture versus normal cortical buckling. (**a**) Note the impacted scaphoid fracture (*arrow*) on the left. (**b**) Oblique view demonstrates the area of sclerosis (*arrow*). However, also note that on the normal side the scaphoid bone appears buckled. This was a normal scaphoid. One needs to be careful about normal buckling and therefore comparative views are very important

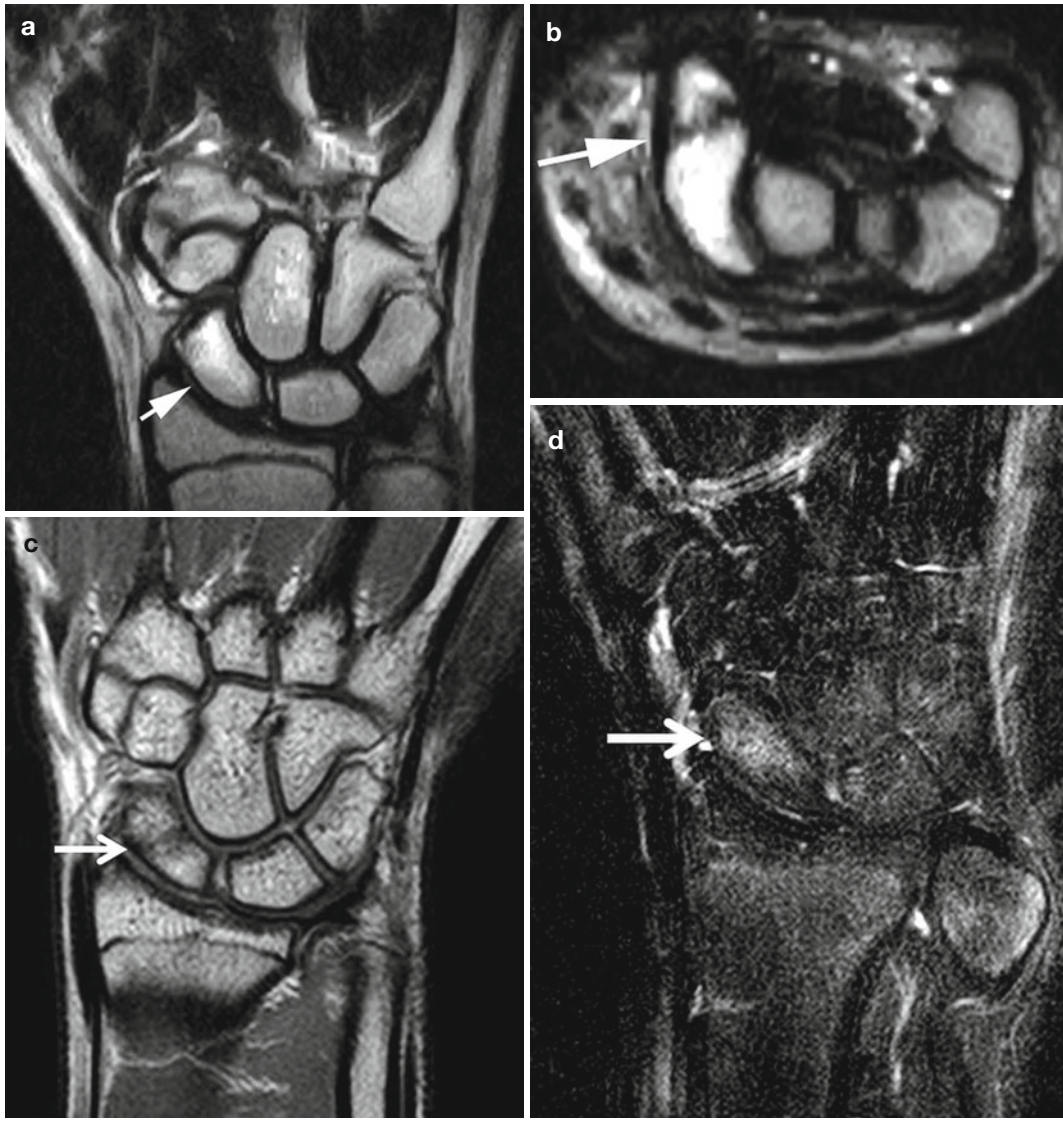


Fig. 7.14 Scaphoid fractures: MR imaging. (**a**) In this patient with a questionable fracture on plain films, this coronal T2-weighted study demonstrates increase signal (*arrow*) in the scaphoid bone. (**b**) Axial T2-weighted image again demonstrates increase signal in the scaphoid bone and a fracture (*arrow*). (**c**) Coronal PD-weighted image shows a nondisplaced fracture through the waist of the scaphoid (*arrow*). This was not evident on radiographs. (**d**) Coronal STIR image shows edema in the waist of the scaphoid surrounding the fracture (*arrow*). A bone contusion is also noted in the distal ulna. (**e**) Coronal T2-weighted image in this child with fall on outstretched hand shows a nondisplaced impaction fracture at the proximal pole of the scaphoid (*arrow*). The adjacent articular surface of the radius is also depressed. (**f**) Coronal STIR image shows edema in the proximal pole of the scaphoid (*arrow*) and the distal radius epiphysis

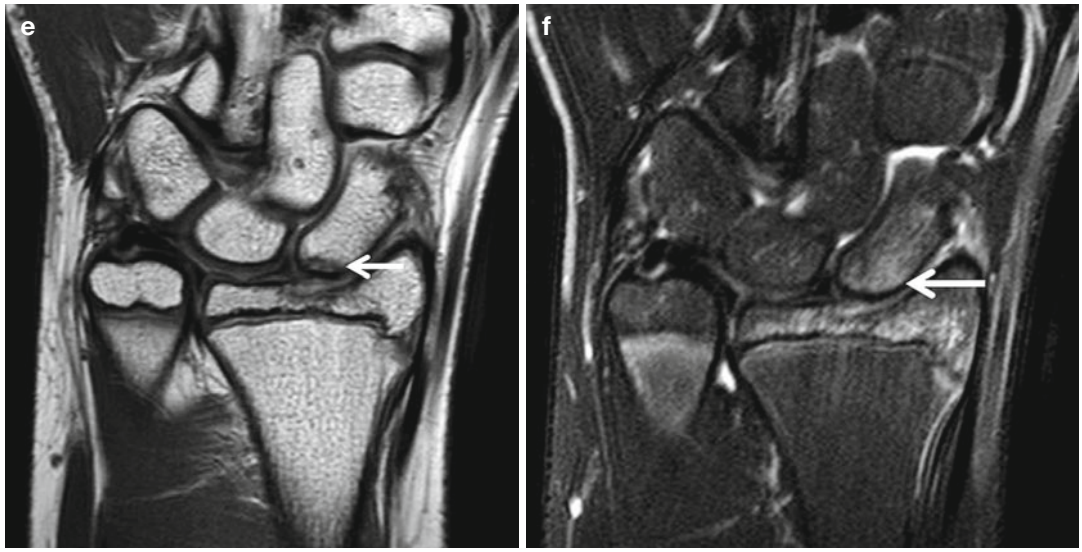


Fig. 7.14 (continued)

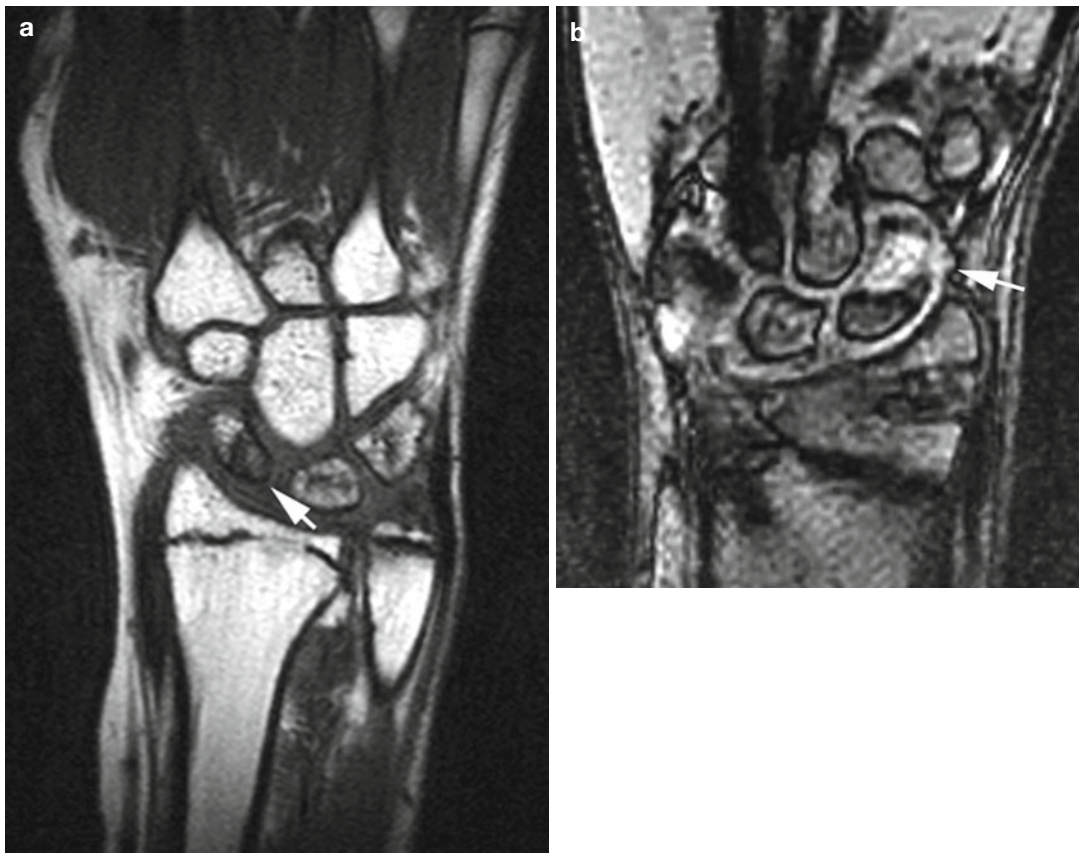


Fig. 7.15 Avascular necrosis: scaphoid. (**a**) Coronal T1-weighted image shows hypo-intense signal in the proximal pole of the scaphoid (*arrow*). Irregular loss of signal in the lunate and triquetrum suggests contusions. (**b**) Coronal T-2 weighted image with fat saturation shows corresponding hypointensity (*arrow*) in the scaphoid consistent with avascular necrosis. The hyperintense bone marrow edema in the lunate and triquetrum again are consistent with bone contusions

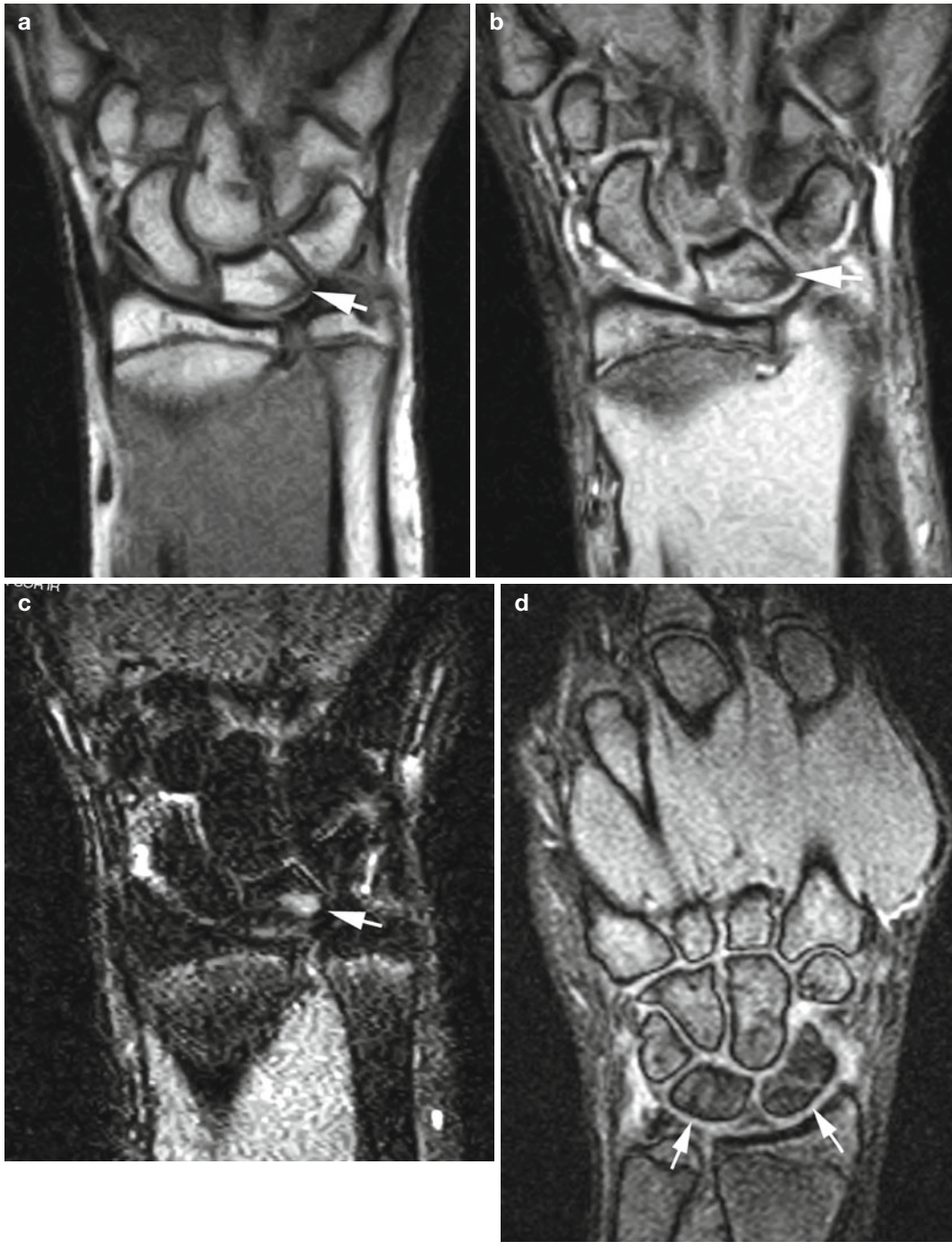


Fig. 7.16 Carpal bones, other fractures: value of MR. (**a**) T2 fat-suppressed image. (**b**) Coronal T1-weighted image. Note the linear low-signal, nondisplaced fracture (*arrow*) through the lunate bone. Again note the low-signal fracture line (*arrow*). (**c**) Coronal STIR image. The fracture line now shows high signal (*arrow*). (**d**) This patient had normal plain films. On this coronal T2* image, note low signal in both the lunate and scaphoid bones (*arrows*). (**e**) Coronal, STIR-weighted image demonstrates increase signal through the scaphoid (*arrows*) and lunate (*arrowhead*) bones consistent with compression fractures



Fig. 7.16 (continued)





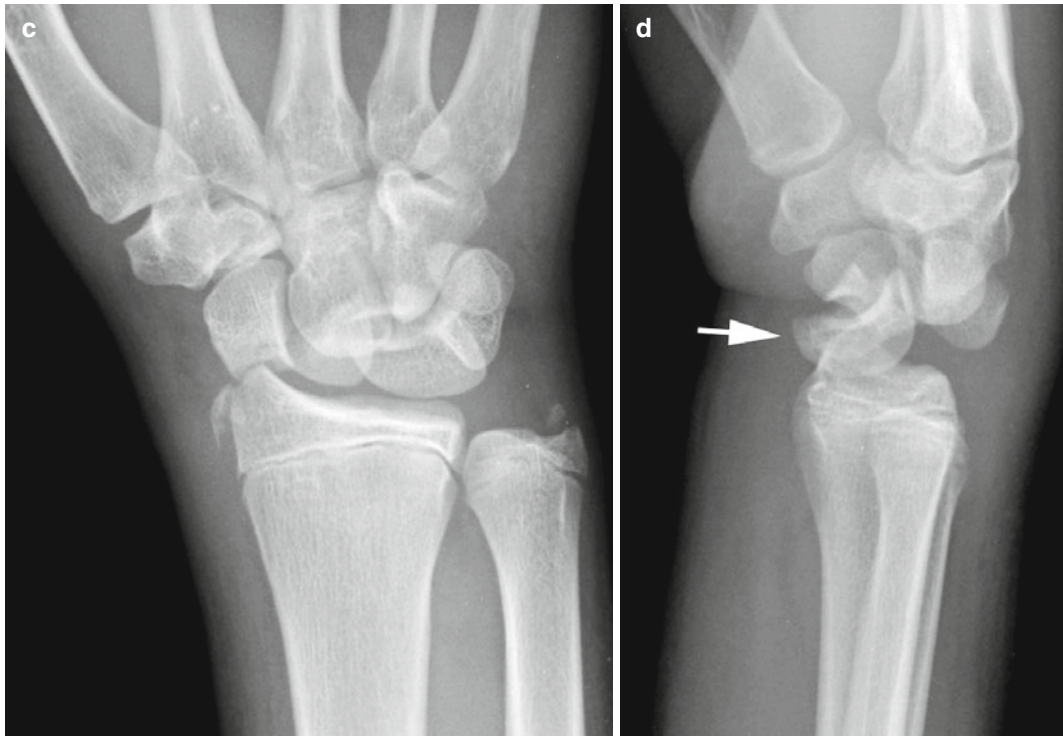


Fig. 7.17 (continued)

Fig. 7.17 Carpal bone dislocations. (**a**) Scaphoid dislocation. Note the increased distance between the scaphoid and capitate bones (*arrows*) consistent with scaphoid dislocation. (**b**) With more rotation of the scaphoid bone in another patient, the wide space between the lunate and scaphoid bone is again seen (*arrow*), but now the ring sign (*arrowhead*) also is seen. (**c**) Perilunate dislocation. Note malalignment of the carpal bones and a small fracture fragment just off of the distal radial epiphysis. This fragment came from the trapezium. Also note a styloid tip fracture. (**d**) Lateral view. The lunate bone (*arrow*) is slightly subluxed but generally in line with the distal radius and its epiphysis. All of the other carpal bones are posteriorly displaced. These findings are consistent with perilunate dislocation. The fracture fragment is again seen



Fig. 7.18 Fractures of the hand: typical findings. (**a**) Crush fracture terminal phalanx (*arrow*). (**b**) Spiral fracture of (*arrow*). (**c**) Buckle, torus fractures. Note buckle fractures (*arrows*) through the bases of the proximal phalanges of the third and fourth digits. (**d**) Typical epiphyseal–metaphyseal Salter–Harris fracture II. Note the widened epiphyseal plate, metaphyseal fracture fragment, and slight displacement of the fracture through the base of the proximal phalanx of the fifth digit (*arrow*). (**e**) Angled buckle fracture. Note the angled buckle fracture (*arrow*) through the base of the proximal phalanx of the index finger. The epiphyseal plate also is a little widened



Fig. 7.18 (continued)

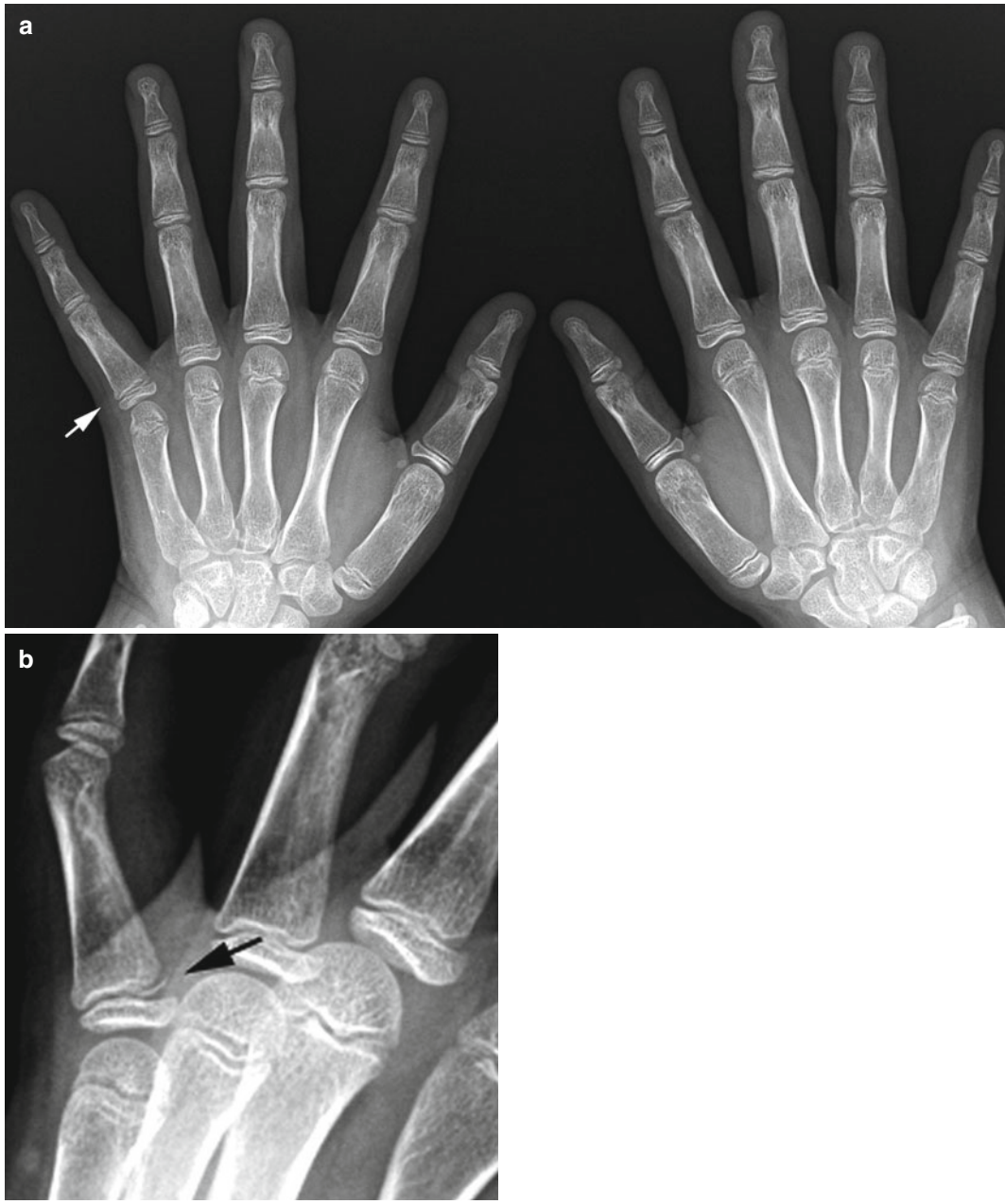


Fig. 7.19 Salter–Harris fractures: value of comparative and oblique views. (**a**) Note the subtle Salter–Harris II fracture (*arrow*) through the base of the proximal phalanx of the fifth digit on the left. The finger also is swollen and slightly abducted. Compare with the same finger on the normal other side. (**b**) Oblique view more clearly demonstrates the fracture fragment (*arrow*). (**c**) Note subtle widening of the epiphyseal plate (*arrow*) through the base of the proximal phalanx of the index finger. Compare it with the other epiphyseal plates and the corresponding epiphyseal plate on the normal right side. (**d**) Oblique view more clearly demonstrates a small avulsed bony fragment (*arrow*) and widening of the epiphyseal plate. These findings are consistent with a minimal Salter–Harris II fracture

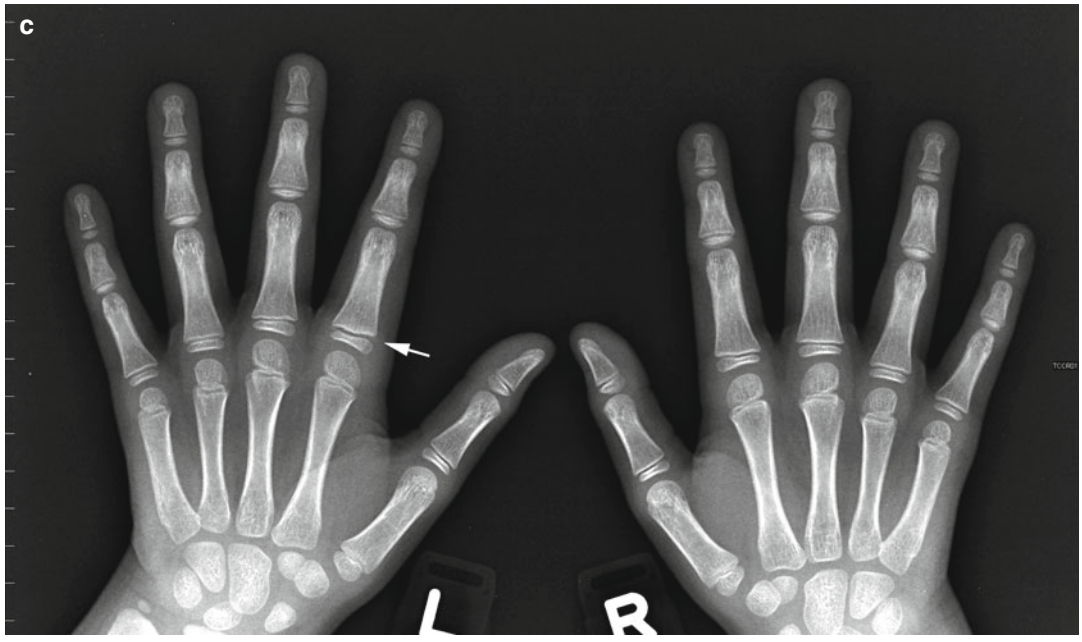




Fig. 7.19 (continued)

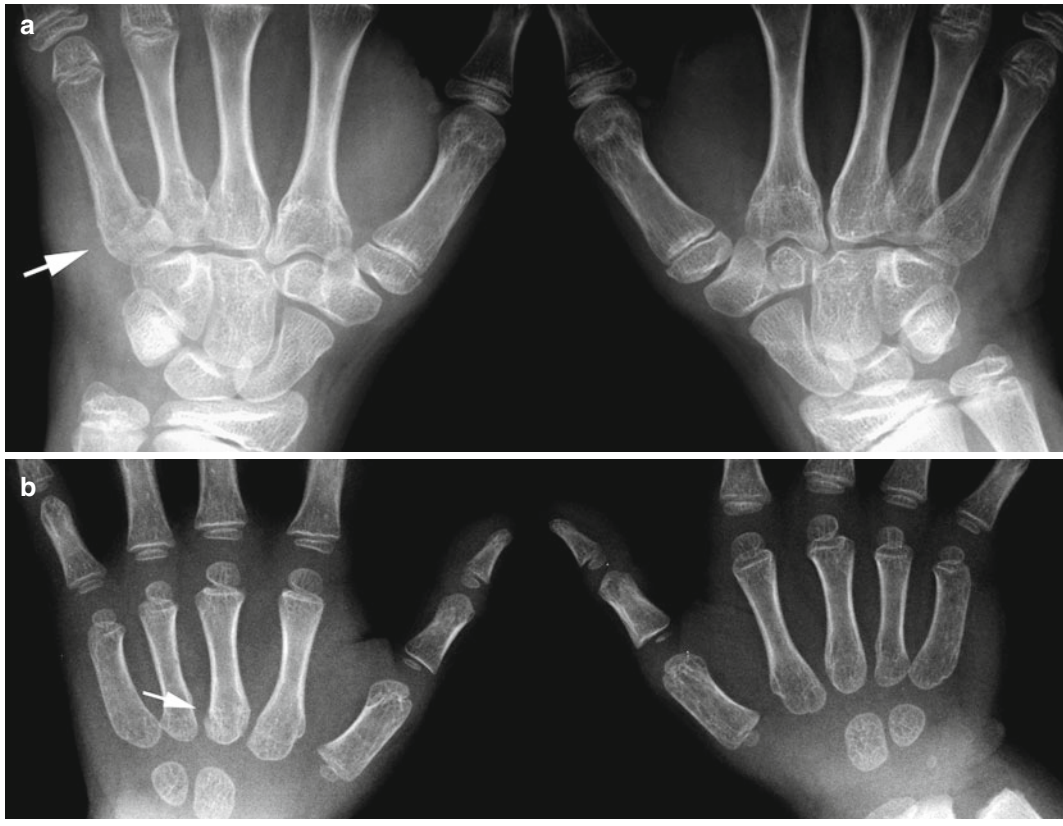


Fig. 7.20 Buckle (torus) fractures: value of comparative views. (**a**) Note the impacted buckle fracture through the base of the fifth metacarpal (*arrow*) on the left. Compare with the other metacarpals and the same metacarpal on the normal other side. (**b**) In this patient there is a subtle impaction fracture through the base of the third metacarpal (*arrow*). Compare with the configuration of this bone on the other normal side

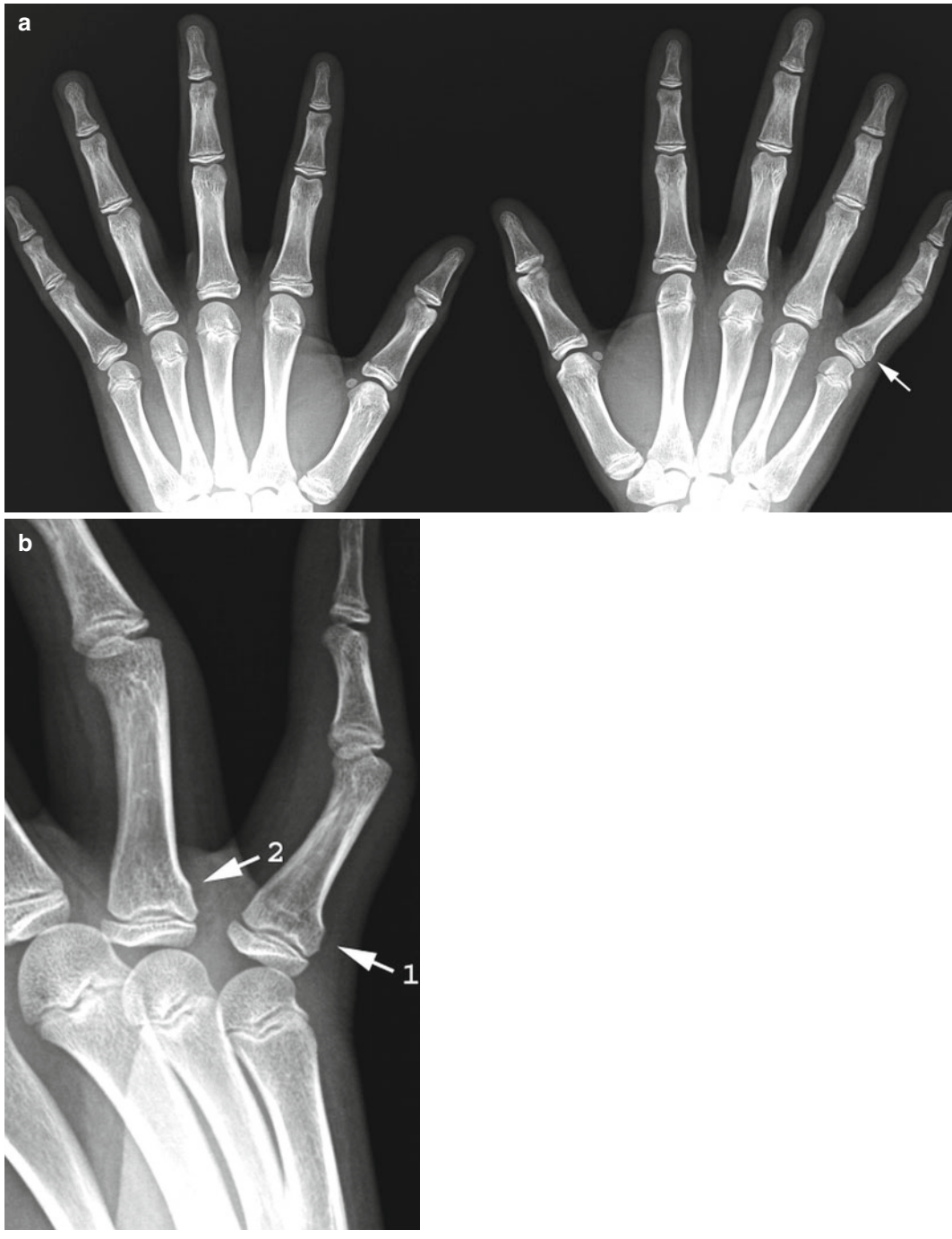


Fig. 7.21 Buckle (torus) fractures: value of comparative and oblique views. (**a**) Note the subtle buckle fracture (*arrow*) through the base of the fifth digit on the right. In addition note that the fifth digit is abducted. (**b**) Oblique view more clearly identifies the buckle fracture through the base of the proximal phalanx of the fifth digit (*1*) but also demonstrates a minimal buckle fracture through the base of the proximal phalanx of the fourth digit (*2*). (**c**) In this patient arrows point to questionable buckle fractures through the bases of the proximal phalanges of the fourth and fifth digits. (**d**) Oblique view demonstrates a typical angle buckle fracture through the base of the proximal phalanx of the fourth digit (*arrow*) and a very subtle buckle fracture through the base of the proximal phalanx of the fifth digit (*arrow*). Compare the contour of the cortices with the normal contours in the other phalanges



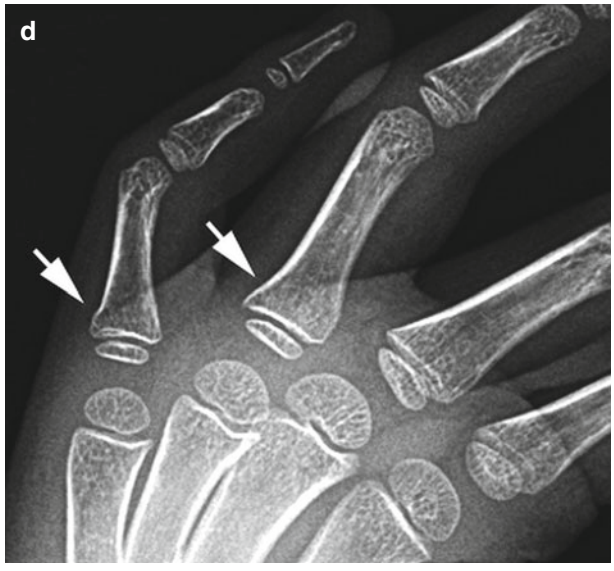


Fig. 7.21 (continued)

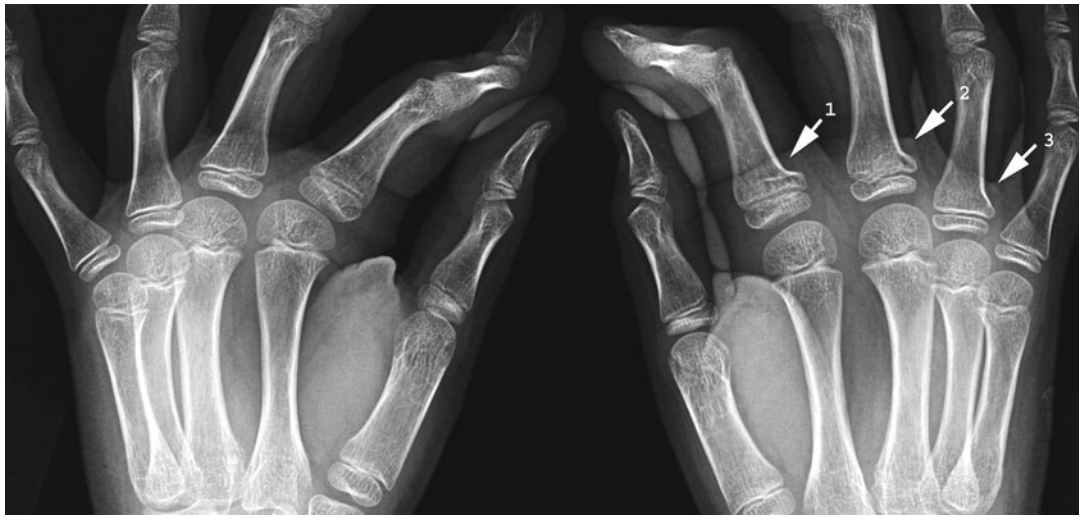


Fig. 7.22 Multiple fractures. Note the overt buckle fracture through the base of the proximal phalanx of the second digit (*1*). Lesser fractures are seen through the bases of the third (*2*) and fourth (*3*) proximal phalanges

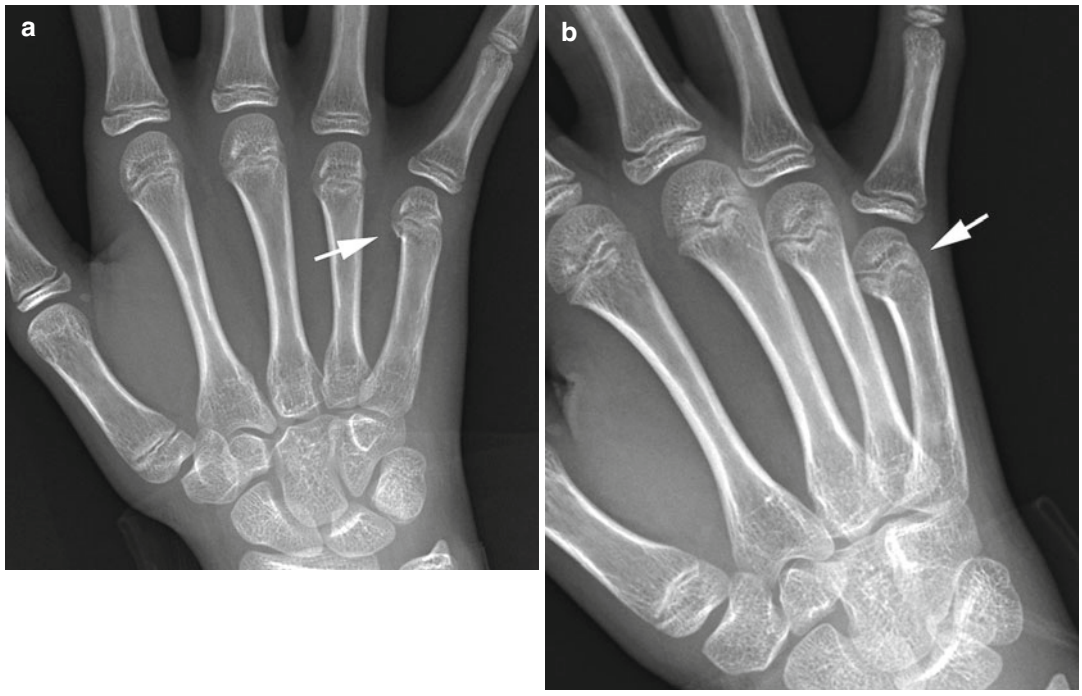


Fig. 7.23 Boxer's fracture. (**a**) Note the typical impacted boxer's fracture (*arrow*) through the head of the fifth metacarpal. (**b**) Oblique view more clearly demonstrates the fracture. (**c**) In this patient only an angled buckle fracture (*arrow*) is seen. (**d**) This patient demonstrates a simple plastic bending fracture (*arrow*) of the head of the fifth metacarpal

Fig. 7.23 (continued)



References

1. MacEwan DW. Changes due to trauma in the fat plane overlying the pronator quadratus muscle: a radiologic sign. Radiology. 1964;82:879–86.
2. Terry Jr DW, Ramin JE. The navicular fat stripe: a useful roentgen feature for evaluating wrist trauma. AJR. 1975;124:25–8.
3. Swischuk LE. Musculoskeletal: what's different in children? I fell on my wrist and now it hurts. Emerg Radiol. 2009;16:83–5.
4. Swischuk LE. Musculoskeletal: what's different in children? Dancing, fall: goes for a week but pain in the wrist persists. Emerg Radiol. 2013;20:309–10.
5. Caine D, Roy S, Singer KM, Broekhoff J. Stress changes of the distal radial growth plate. Am J Sports Med. 1992;20:290–8.
6. Carter SR, Aldridge MJ, Fitzgerald R, Davies AM. Stress changes of the wrist in adolescent gymnasts. Br J Radiol. 1988;61:109–12.
7. Liebling MS, Berdon WE, Ruzal-Shapiro C, Levin TL, Roye Jr D, Wilkinson R. Case report. Gymnast's wrist (pseudorickets growth plate abnormality) in adolescent athletes: findings on plain films and MR imaging. AJR. 1995;164:157–9.
8. Roy S, Caine D, Singer KM. Stress changes of the distal radial epiphysis in young gymnasts: a report of twenty-one cases and a review of the literature. Am J Sports Med. 1985;13:301–8.
9. Poletto ED, Pollock AN. Radial epiphysitis (aka gymnast wrist). Pediatr Emerg Care. 2012;28(5):484–5.
10. Stansberry SD, Swischuk LE, Swischuk JL, Midgett TA. Significance of ulnar styloid fractures in childhood. Pediatr Emerg Care. 1990;6:99–103.
11. Landfried MJ, Stenclik M, Susi JG. Variant of Galeazzi fracture-dislocation in children. J Pediatr Orthop. 1991;11:332–5.
12. Scheffler R, Armstrong D, Hutton L. Computed tomographic diagnosis of distal radio-ulnar joint disruption. J Can Assoc Radiol. 1984;35:212–3.
13. Wulff RN, Schmidt TL. Carpal fractures in children. J Pediatr Orthop. 1998;18:462–5.
14. Swischuk LE. Musculoskeletal: what's different in children? Injury to wrist in a ten-year-old boy. Emerg Radiol. 2008;15:343–4.
15. Swischuk LE. Musculoskeletal: what's different in children? Fall from bicycle; pain, and tenderness of right wrist. Emerg Radiol. 2013;20:87–8.
16. Oestreich AE, Bhojwani N. Stress fractures of ankle and wrist in childhood: nature and frequency. Pediatr Radiol. 2010;40:1387–9.

17. Rolfe EB, Garvie NW, Khan MA, Ackery DM. Isotope bone imaging in suspected scaphoid trauma. Br J Radiol. 1981;54:762–7.
18. Breitenseher MJ, Metz VM, Gilula LA, Gaebler C, Kukla C, Fleischmann D, Imhof H, Trattnig S. Radiographically occult scaphoid fractures: value of MR imaging in detection. Radiology. 1997;203: 245–50.
19. Hunter JD, Escobedo EM, Wilson AJ, Hanel DP, Zink-Brody GC, Mann FA. MR imaging of clinically suspected scaphoid fractures. AJR. 1997;168: 1287–93.
20. Obdeijin MC, Vliet CV, Rijin RRV. Capitate and hamate fracture in a child: the value of MRI imaging. Emerg Radiol. 2010;17:157–9.
21. Southcott R, Rosman MA. Nonunion of carpal scaphoid fractures in children. J Bone Joint Surg. 1977; 59B:20–3.
22. Fox MG, Gaskin CM, Chhabra AB, Anderson MW. Assessment of scaphoid viability with MRI: a reassessment of findings on unenhanced MR images. AJR. 2010;195(4):W281–6.
23. Kannineswaran N, Sethuraman U. Lunate and perilunate dislocations. Pediatr Emerg Care. 2010;26: 921–4.
24. Sagar P, Sailam R, Nimkin K. Avascular necrosis of the metacarpal head: a report of two cases and review of literature. Pediatr Radiol. 2010;40: 1895–901.

Pelvis and Sacrum

8

Fractures of the Sacrum

Sacral fractures usually are associated with pelvic injuries and overall may be difficult to detect. However, if one systematically compares the cortical margins of the sacral ala on one side to those on the other, disruption of their margins/accurate lines [1] provides a clue to the presence of a fracture (Fig. 8.1a). In addition to sacral fractures, many of these patients demonstrate associated sacroiliac joint separation and pelvic fractures. In this regard, CT scanning is more specific in confirming or initially detecting these injuries (Fig. 8.1b, c).

Fractures of the Pelvis

Pelvic fractures frequently are multiple and can range from simple buckle fractures to extensive fracture dislocations associated with internal organ or vascular injury. Most often these latter fractures are sustained in automobile accidents and of these fractures, fractures resulting in separation of the symphysis pubis, fractures through the acetabulum, and the so-called diametric (ring) fractures of the pelvis are considered unstable. These usually are finally imaged with CT and more often are seen in older children and adolescents.

Isolated pelvic fracture most commonly occur through the pubic bone or iliac wing. These can be overt or subtle and in infants and young children may manifest as simple buckle fractures (Fig. 8.2a). Multiple fractures are more common in older children (Fig. 8.2b–d). Acetabular [2] and acetabular rim fractures are not particularly common in childhood but can be seen in older children in association with posterior hip dislocations. They may be difficult to detect on plain films and in infants and young children, these fractures tend to occur through the triradiate cartilage.

Avulsion fractures of the pelvic bones commonly occur in children and the sites are shown in Fig. 8.3. In a study of 203 avulsion injuries in young athletes, the most common avulsion injury of the pelvic girdle involved the ischial tuberosity [3]. However, in our practice we have found that most often they are seen along the outer aspect of the iliac wing as anterior inferior or superior iliac spine fractures [4]. Thereafter, the next most common place is over the inferior aspect of the ischium. Less commonly they occur over the iliac crest and then off of the greater and lesser trochanters.

With most iliac wing avulsion fractures, actual fracture fragments are seen, and as noted earlier, these most commonly involve the anterior superior and anterior inferior iliac spines (Fig. 8.4). Next most common are avulsion injuries involving the inferior cortex of the ischium where the avulsed fracture fragment often is somewhat thin and curved as it conforms to the curve of the ischium (Fig. 8.5a, b). Next most common are avulsion fractures involving the iliac crest where most often a portion of the apophysis is avulsed (Fig. 8.5c). Finally, avulsion fractures of the greater and lesser trochanters occur but are rather

L.E. Swischuk, S.P. Jadhav (eds.), *Emergency Musculoskeletal Imaging in Children*,
DOI 10.1007/978-1-4614-7747-1_8, © Springer Science+Business Media New York 2014

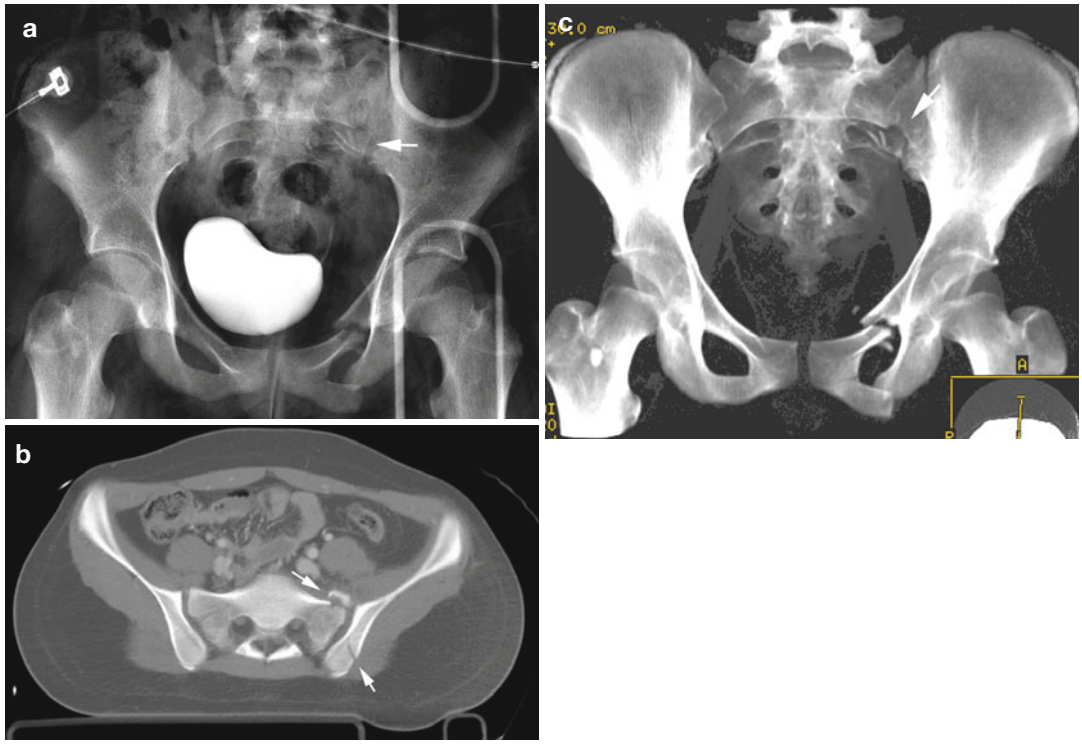


Fig. 8.1 Sacral fracture. (**a**) Note the distorted sacral ala on the left (*arrow*). Also note fractures through the pelvis on the same side. A minimal buckle fracture through the pubic bone is present on the right. (**b**) CT study demonstrates the sacral fracture (*upper arrow*) but also demonstrates an iliac wing fracture (*lower arrow*). In addition the sacroiliac joint on the left also is a little widened suggesting separation. (**c**) Reconstructed CT study more clearly demonstrates the sacral fractures (*arrow*)

uncommon. Lesser trochanter avulsion injuries, often chronic, most commonly occur with spastic cerebral palsy (Fig. 8.5d).

In some cases of pelvic avulsion fractures, initially there is no visible bony fragment, but later evidence that the injury has occurred is seen in the fact that bony resorption at the site occurs. This often is mixed with reparative bone and the findings first may suggest tumor or infection [5] (Fig. 8.6). In some cases an avulsion fracture may be occult on plain films but is demonstrable with MR imaging (Fig.8.7).

Stress fractures of the pelvic bones are quite uncommon in children and are more likely to occur in adolescents and adults. The key findings include an area of sclerosis which occasionally is associated with periosteal new bone formation. These fractures are positive on bone scans and also are readily detectable with MR imaging.

Normal Findings Causing Problems

There are a number of normal findings in the pelvis and sacrum which frequently are misinterpreted for pathology. First of all, the normally wide space between the pubic bones in infants frequently is mistaken for a pubic bone separation (Fig. 8.8a). Secondly, and more commonly, the exceedingly variable and pathology suggestive appearance of the normal ischiopubic synchondrosis can be misinterpreted for a tumor

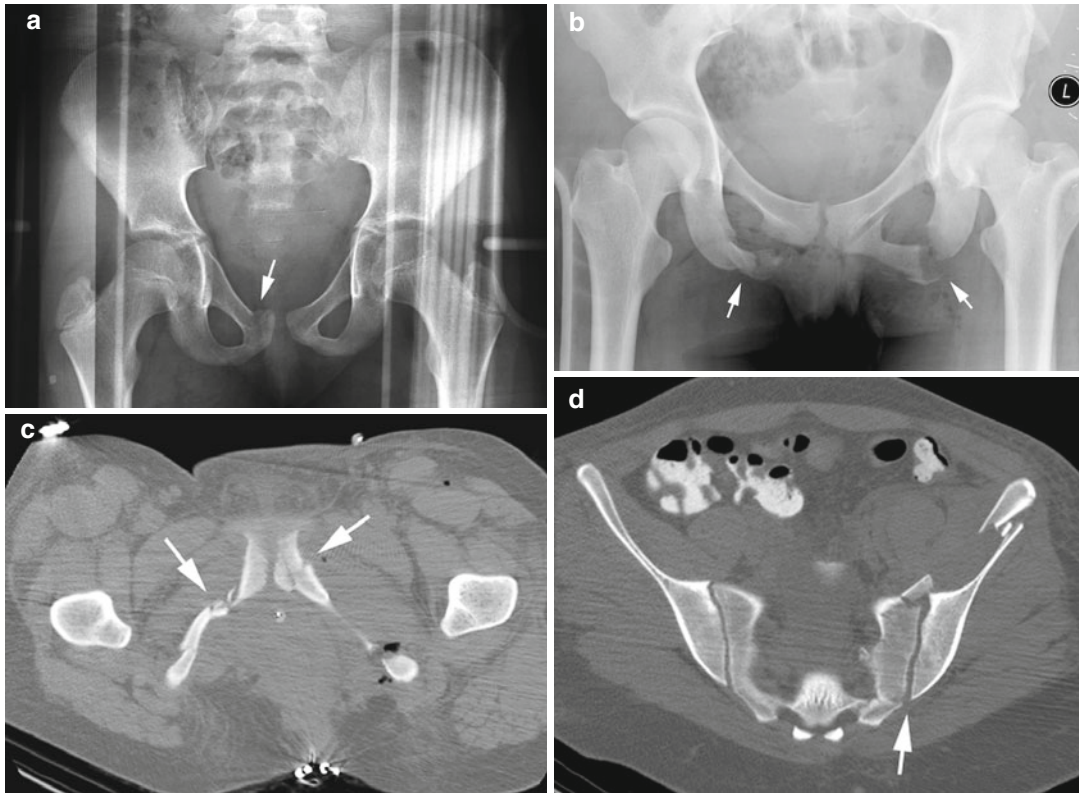


Fig. 8.2 Pelvic fractures. (**a**) In this young child a buckle fracture through the pubic bone (*arrow*) is seen. (**b**) In this adolescent bilateral pelvic fractures are obvious (*arrows*). (**c**) CT study demonstrates the same comminuted fractures (*arrows*). (**d**) CT study through the upper pelvis demonstrates fractures through the iliac bones and sacrum. In addition there is widening of the sacral iliac joint (*arrow*)

(Fig. 8.8b, c). Finally the os acetabulum may erroneously be misinterpreted for an avulsion fracture off of the acetabulum (Fig. 8.8d).

In the sacrum normal accessory ossification centers may at first suggest a fracture (Fig. 8.9a). However, when one notices that the cortex of these pieces of bone is smooth and fits precisely into the contour of the sacrum, the fact that they are normal becomes more apparent. Another phenomena which can occur on a normal basis in the sacrum is a vacuum joint phenomenon of the sacral iliac joint (Fig. 8.9b).

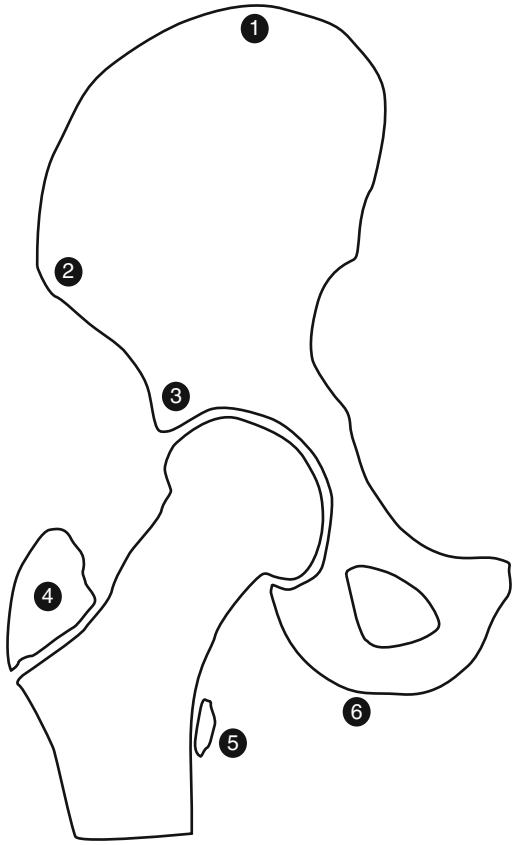


Fig. 8.3 Pelvis and upper femoral avulsion fracture sites. (*1*) Iliac crest, (*2*) anterior superior iliac spine, (*3*) anterior inferior iliac spine, (*4*) greater trochanter, (*5*) lesser trochanter, and (*6*) ischium. Most commonly these fractures occur at sites *2*, *3*, and *6*

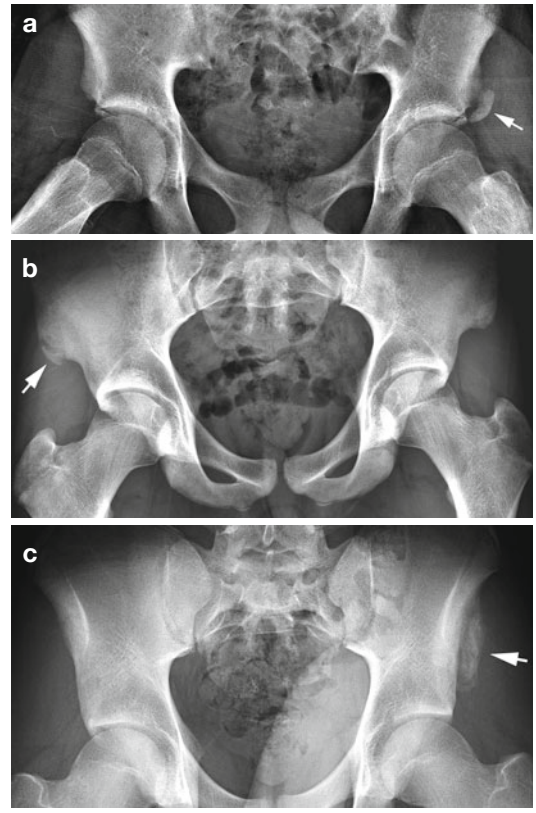


Fig. 8.4 Avulsion fractures: anterior superior and inferior iliac spines. (**a**) Note the avulsed fracture fragment (*arrow*) involving the anterior inferior iliac spine on the left. Also note the adjacent, subacetabular ossicle which also is seen on the other side, representing the normal os acetabulum. (**b**) In this patient an avulsion fracture (*arrow*) of the anterior superior iliac spine is seen. The small, sliver-like crescent-shaped bones over the inferior aspect of the ischia represent normal apophyses. (**c**) Anterior superior iliac spine avulsion fracture fragment (*arrow*). This is a flake/avulsion fracture and its appearance is not that of a typical fracture

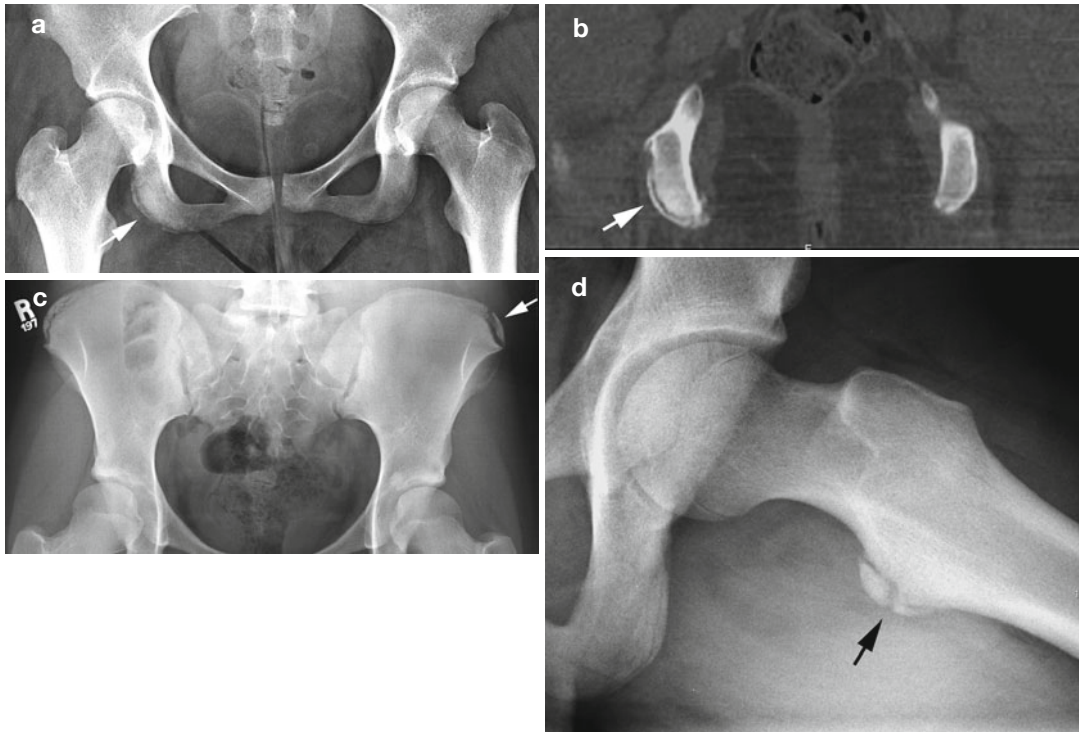


Fig. 8.5 Other pelvic avulsion fractures. (**a**) Note the thin crescentic avulsion fracture (*arrow*) off of the inferior aspect of the right ischium. (**b**) CT study demonstrates the same fracture (*arrow*). (**c**) Avulsion fracture of the iliac crest. Note the avulsed fragment of bone (*arrow*) from the iliac wing apophysis. Compare with the normal apophysis on the right. (**d**) Avulsion lesser trochanter. Note the slightly avulsed and fractured lesser trochanter (*arrow*). This patient had cerebral palsy

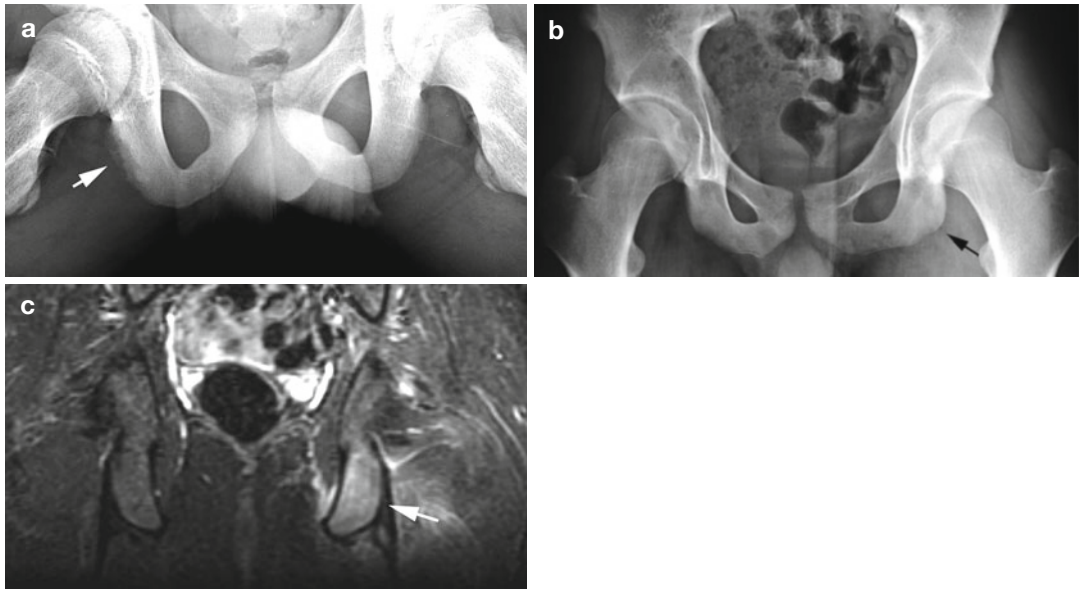


Fig. 8.6 Pelvic avulsion injuries: pseudotumoral appearance. (**a**) In this patient a mixture of bone resorption and early healing (*arrow*) might at first suggest a tumor or osteomyelitis. However, it is a subacute and early healing avulsion injury. (**b**) In this patient the ischium is hypertrophied (*arrow*) due to repetitive avulsion injuries with healing. (**c**) MR, coronal STIR study demonstrates increased signal in the ischium (*arrow*)

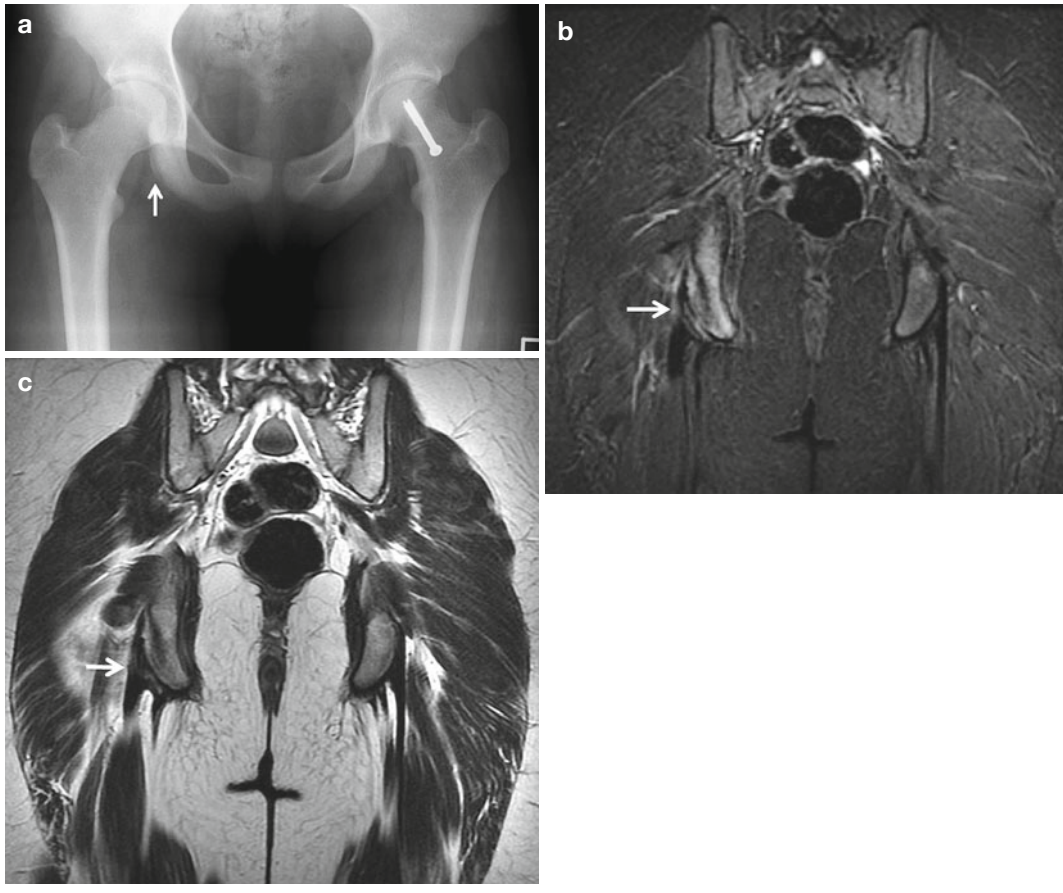


Fig. 8.7 Occult avulsion fracture: value of MR. (**a**) AP radiograph of the pelvis in a teenager complaining of right hip pain after splits. This was reported as normal, but retrospectively a sliver of bone is likely present at the ischial tuberosity (*arrow*). Left hip has a screw from prior SCFE surgery. (**b**) Coronal STIR and (**c**) T2-weighted images show avulsion of the common origin of the hamstring (biceps femoris and semimembranosus components) with extensive edema in the ischial tuberosity (*arrow*). Compare with the normal findings on the left side

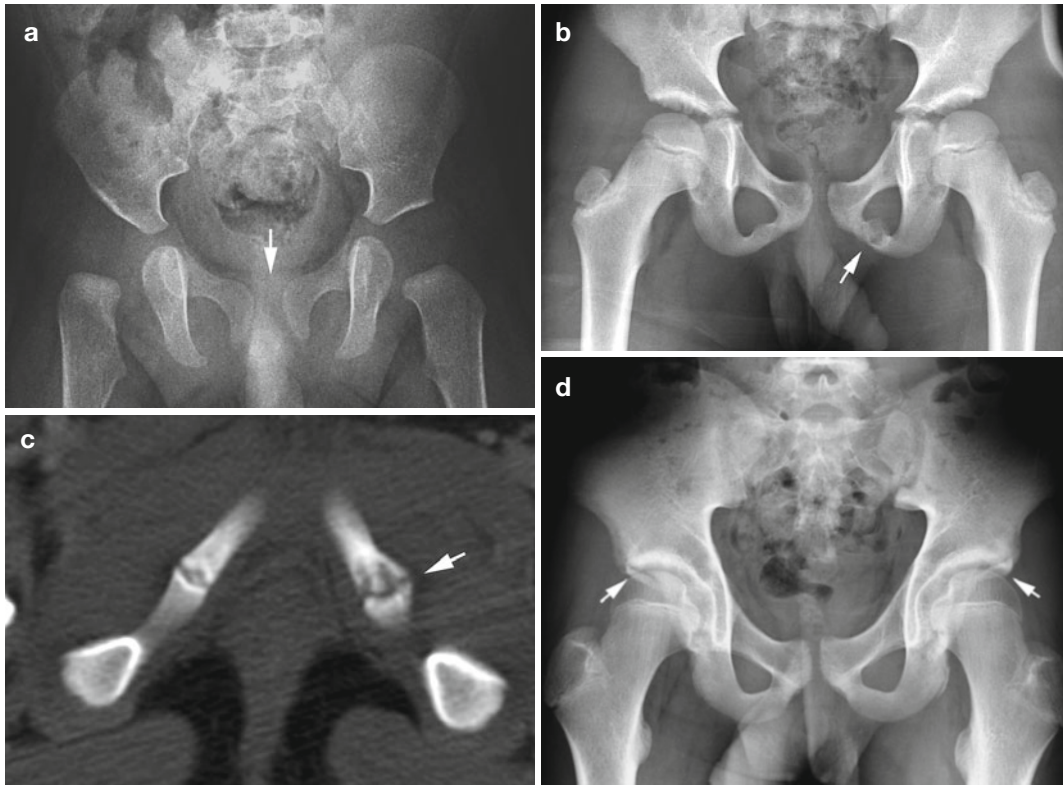


Fig. 8.8 Normal findings causing problems. (**a**) Wide pubic bone space. Note the wide space between the pubic bones (*arrow*) in this young infant who obtained the study for a congenital hip dislocation on the right. In this regard, note the slanted, shallow, and dysplastic right acetabular roof. (**b**) Normal bulky ischiopubic synchondrosis. Note the bulky ischiopubic synchondrosis (*arrow*) which often suggests a tumor. On the other side, it is not nearly as prominent. (**c**) CT study demonstrates the same bulky ischiopubic synchondrosis (*arrow*). (**d**) Normal os acetabulum. Note the typical appearance of the normal os acetabulum on both sides (*arrows*). These can be avulsed, but it is not common

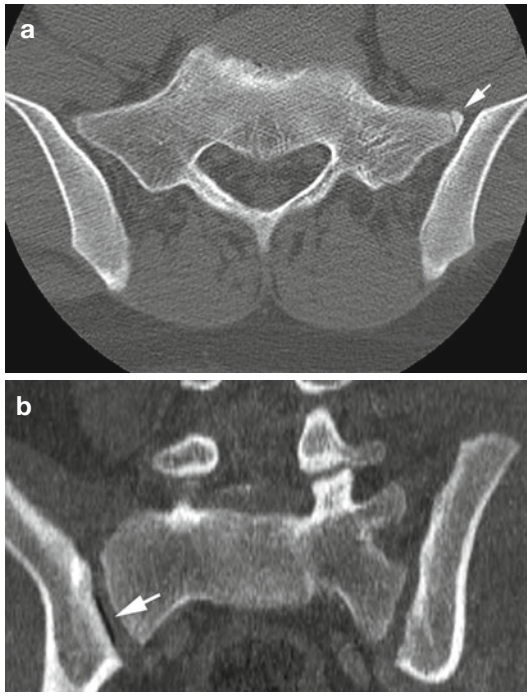


Fig. 8.9 Normal findings in the sacrum. (**a**) Note the accessory ossicle on the left (*arrow*), which can be misinterpreted for a fracture. (**b**) Vacuum joint. Note the vacuum joint phenomena (*arrow*) in the right sacral iliac joint

References

1. Jackson H, Kam J, Harris Jr JH, et al. The sacral arcuate lines in upper sacral fractures. Radiology. 1982;145:35–9.
2. Nodzo SR, Hohman DW, Galpin RD. Bilateral acetabular fractures in a adolescent after low-energy trauma. Pediatr Emerg Care. 2012;28:568–9.
3. Rossi F, Dragoni S. Acute avulsion fractures of the pelvis in adolescent competitive athletes: prevalence, location and sports distribution of 203 cases collected. Skeletal Radiol. 2001;30:127–31.
4. Swischuk LE. Musculoskeletal: what's different in children? Running for track: springtime, hip pain. Emerg Radiol. 2012;19(5):397–8.
5. Brandser EA, El-Khoury GY, Kathol MH. Adolescent hamstring avulsions that stimulate tumors. Emerg Radiol. 1995;2:273–8.

Hip and Femur/Femoral Shaft

9

Normal Fat Pads and Joint Space

The two views generally obtained for evaluating the hip are the anteroposterior and frog-leg views. The fat pads surrounding the hip and the joint space are best assessed on the straight anteroposterior view and include the iliopsoas, gluteus, and obturator internus fat pads (Fig. 9.1). These fat pads do not lie against the joint capsule directly and thus are not displaced outwardly if fluid accumulates within the joint but can be moved outwardly and obliterated secondary to edema around the hip joint (Fig. 9.2a).

Detecting Fluid in the Hip Joint

When fluid (blood, pus, serous fluid) accumulates in the hip joint, the femoral head is displaced laterally in infants and young children because this is the venue of least resistance. At the same time it causes the joint space to become widened (Fig. 9.2a), but this is less commonly seen in older children because the ligaments and muscles are stronger and resist displacement. Detecting fluid in the hip joint is now best accomplished with ultrasonography [1] where with imaging in the sagittal plane one easily can detect joint fluid, the commonest cause of which is *transient synovitis* (Fig. 9.2b, c). In some cases some degree of synovial thickening may be seen. In addition, in some cases a little joint fluid debris may be present (Fig. 9.2d), but usually it is clear. With pus, as part of septic arthritis, the joint fluid is dirty, the synovium thickened, and the overlaying iliopsoas muscle thick and edematous (Fig. 9.3).

Injuries of the Upper Femur

Fractures through the femoral neck and intertrochanteric region of the femur are distinctly less common in children than in adults, but they do occur (Fig. 9.4). These usually result from axial loading on the femur and hip. Very often

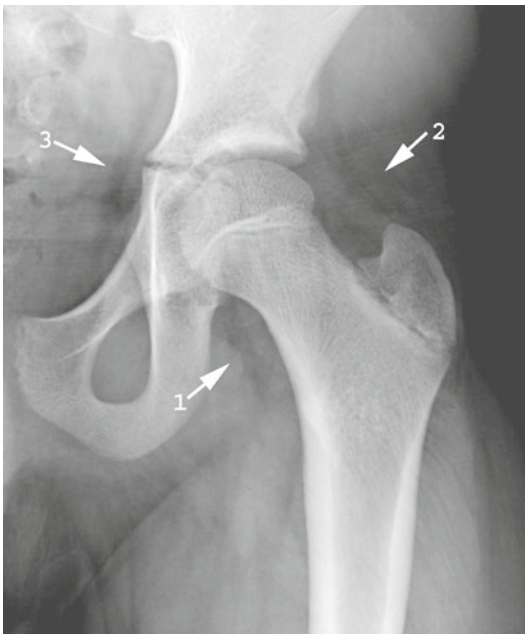


Fig. 9.1 Normal fat pads around the hip. Note the iliopsoas (*1*), gluteus (*2*), and obturator internus (*3*) fat pads

L.E. Swischuk, S.P. Jadhav (eds.), *Emergency Musculoskeletal Imaging in Children*,
DOI 10.1007/978-1-4614-7747-1_9, © Springer Science+Business Media New York 2014

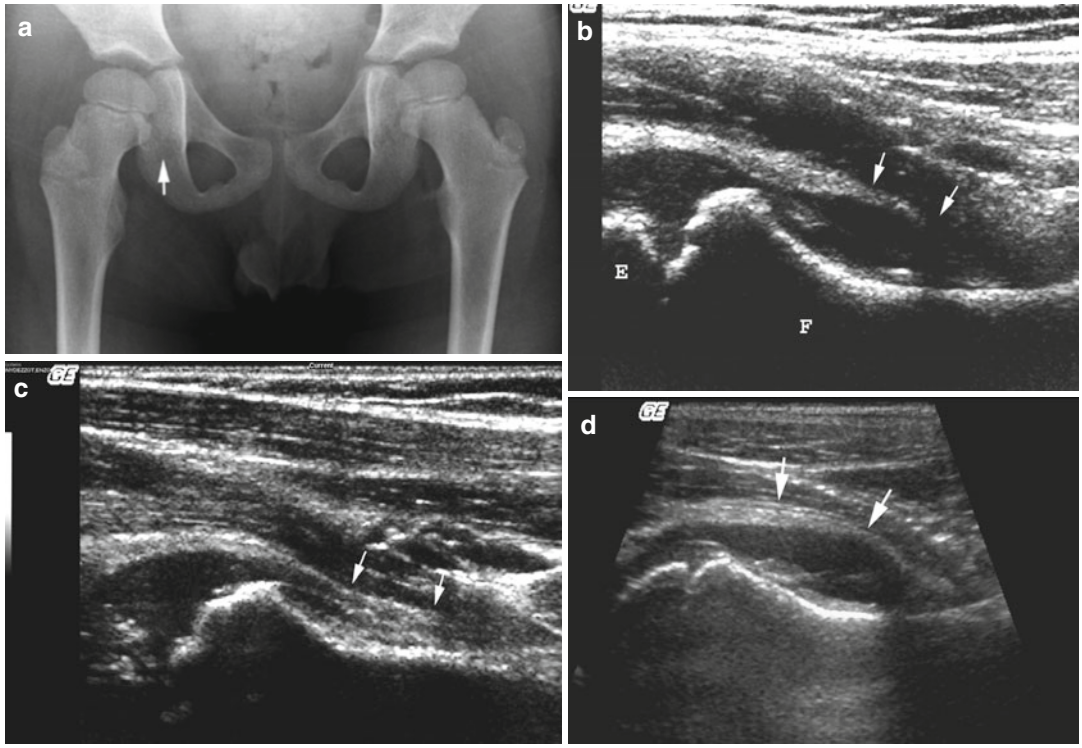


Fig. 9.2 Transient synovitis. (**a**) On this AP view of the pelvis, note joint space widening (*arrow*) involving the right hip. (**b**) Ultrasound demonstrates relatively clear fluid accumulating between the capsule (*arrows*) and the underlying echogenic cortex of the femoral neck (F). Epiphysis (E). (**c**) Normal side for comparison. Note the position of the joint capsule (*arrows*) and that there is no joint fluid present. (**d**) Transient synovitis with some debris. Note fluid under the slightly thickened joint capsule (*arrows*) which in this case is a little thickened. The fluid also contains a little debris

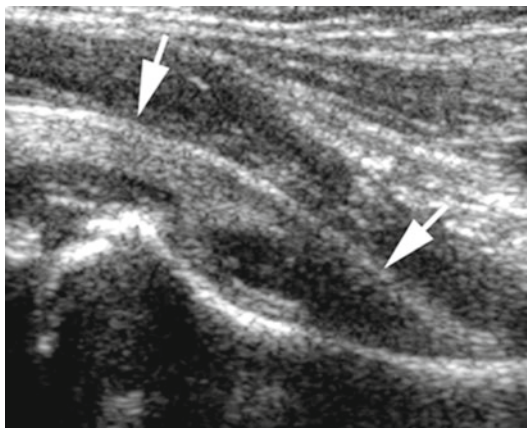


Fig. 9.3 Septic arthritis: ultrasound. Note thickening of the synovium and capsule (*arrows*), joint fluid with some speckled debris, and thickening of the overlying muscle

these fractures are first considered to be the result of child abuse, but this type of fracture is very uncommon with child abuse (see Chap. 12).

Salter–Harris epiphyseal–metaphyseal fractures on the other hand are more common and most often are Salter–Harris type I or II injuries [2]. In assessing the upper femur for the presence of these fractures, one first should look for an increase in the width and radiolucency of the involved epiphyseal plate and then for widening of the medial joint space (Fig. 9.5). The first finding indicates the presence of an epiphyseal–metaphyseal separation and the second the presence of associated joint fluid/blood. With Salter–Harris type II fractures, a metaphyseal corner fracture is seen.

Anterior or posterior dislocation of the hip is not particularly common in childhood [3]. The reason for this is that the epiphysis is still open and as such represents the weakest point of the femoral head/neck complex. Therefore, Salter–Harris type I and II injuries are more likely to occur. Of course, in the older child, with

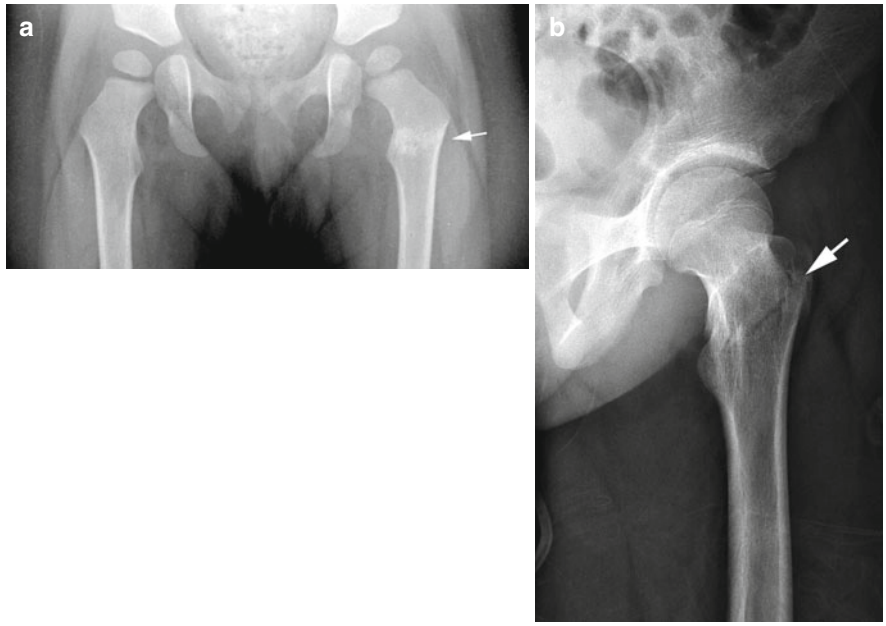


Fig. 9.4 Fractures; proximal femur. (**a**) Note the transverse impacted intertrochanteric fracture (*arrow*). (**b**) Older child with an intertrochanteric fracture (*arrow*)

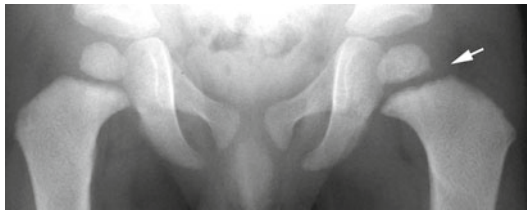


Fig. 9.5 Salter–Harris I fracture. Note widening of the epiphyseal plate on the left (*arrow*) characteristic of a nondisplaced Salter–Harris I fracture

epiphyseal closure a dislocation is more likely and, as in adults, posterior dislocations are more common. Acetabular rim fractures can be associated injuries, but in childhood the fracture more often is one which involves the triradiated cartilage. Avulsion injuries of the lesser and greater trochanters are not particularly common, but with the apophysis of the lesser trochanter, the findings can be chronic as part of the problem of spasticity and contractures in cerebral palsy. Unlike adults, avulsion of the lesser trochanter in a skeletally immature child should not raise suspicion of underlying metastatic malignancy.

Legg–Perthes Disease

Legg–Perthes disease or aseptic necrosis of the femoral capital epiphysis is common, but its etiology is not known. It generally is held that as many as 10 % of patients who present with symptoms initially suggesting transient synovitis actually turn out to have early Legg–Perthes disease [4]. In my experience, however, confusing the two entities is not that common, but follow-up is necessary if symptoms do not resolve and the initial diagnosis is transient synovitis.

Early on in Legg–Perthes disease, increased density and smallness of the involved femoral head occur (Fig. 9.6a). These are the earliest findings in Legg–Perthes disease, and although subchondral fractures (Fig. 9.6b) also occur relatively early, they are not nearly as common [5]. Other findings include lateral displacement of the femoral head with widening of the medial joint space and atrophy of the surrounding muscles [5]. Lateral displacement of the femur results in less pressure on the medial acetabular wall and development of the so-called teardrop sign [6] (Fig. 9.6a). However, positioning is crucial and must be near perfect to

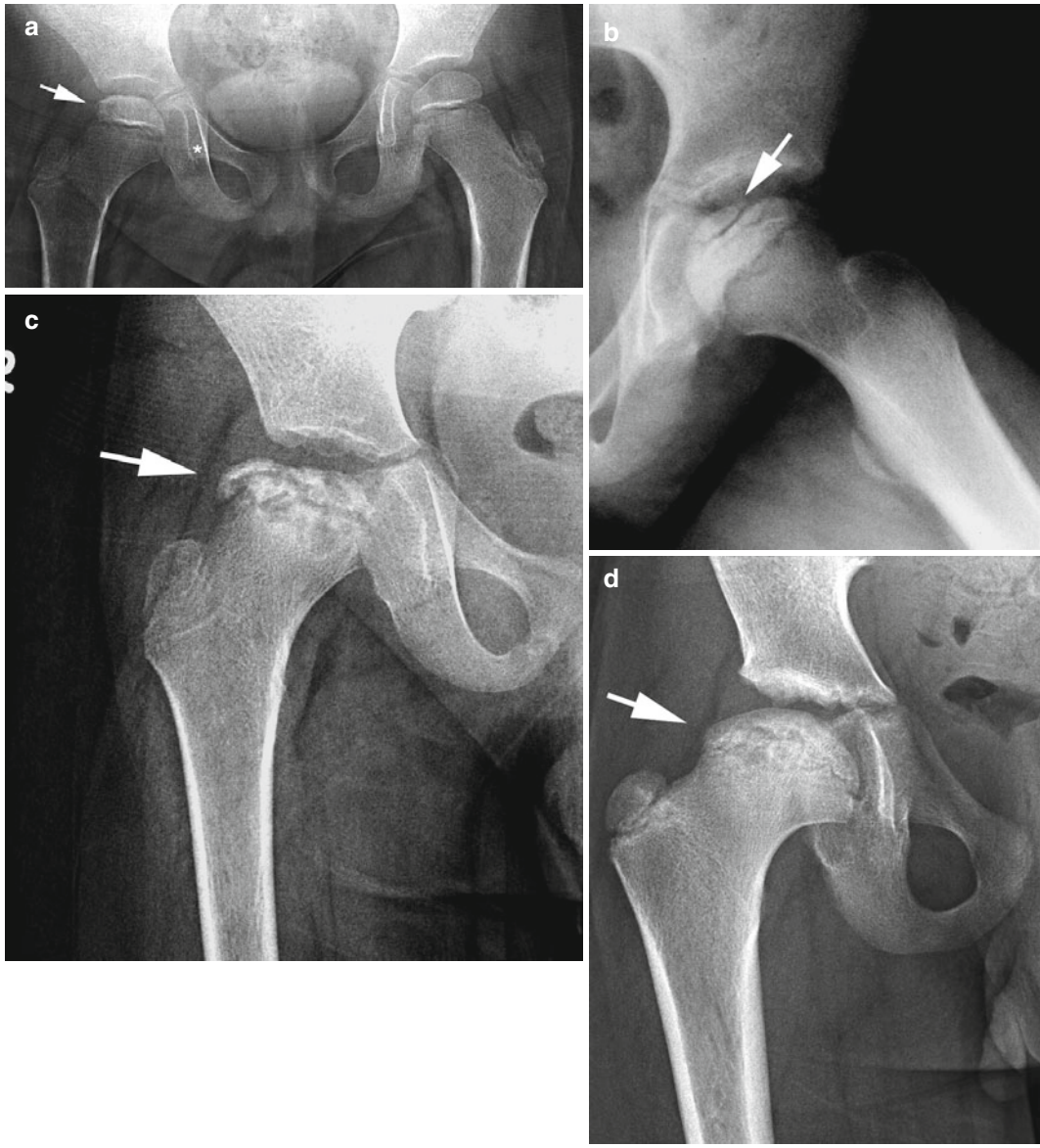


Fig. 9.6 Legg–Perthes disease. (**a**) Early changes consist of smallness and increased density of the involved femoral capital epiphysis (*arrow*). The joint space also is widened and a tear drop sign (*) is present. (**b**) Subchondral fracture (*arrow*). (**c**) More advanced changes. The femoral capital epiphysis is fragmented and partially resorbed (*arrow*). There is widening of the joint space and persistent subluxation of the hip. Also note lucent areas in the metaphysis. (**d**) Healing phase: poor outcome. Because the femoral head was not constantly located within the acetabular roof with subsequent healing, one ends up with the typical coxa magna, vara, and plana deformity

avoid misinterpretation of this finding which may appear to be present if the pelvis is rotated. Eventually the femoral head becomes more sclerotic and fragmented and finally is resorbed (Fig. 9.6c). If the femoral head is kept within the acetabulum during the healing phase, it will heal in a normal rounded fashion. However, if the femoral head remains dislocated, one will end up with the typical coxa vara, coxa magna, and coxa plana deformity (Fig. 9.6d). In addition to the foregoing findings, in many cases associated irregularities of the metaphyses [7] occur (Fig. 9.6c). These changes are secondary to reactive fibrous tissue. Generally, they are considered a poor prognostic sign.

Finally, if plain film findings are equivocal, or normal, and one still suspects Legg–Perthes

disease, one can turn to nuclear scintigraphy or MR imaging [8, 9]. There are those who believe that MR imaging is more sensitive, but nuclear scintigraphy is less expensive. With nuclear scintigraphy, one looks for photon deficiency of the femoral head, usually laterally, while with MR imaging, there is loss of the normal high signal of fatty marrow on T1-weighted images.

Aseptic necrosis also can occur with sickle cell disease and in patients on steroid therapy. Often the problem is bilateral in these patients, while with idiopathic Legg–Perthes disease, only about 10 *% of cases demonstrate simultaneous bilateral involvement*. Roentgenographically the changes are no different than in the idiopathic form, but they may be more acute in onset. In idiopathic Legg–Perthes disease, a delay in bone age also has been noted [10].

Slipped Capital Femoral Epiphysis (SCFE)

The slipped capital femoral epiphysis of childhood is another condition which can present on an acute basis. This occurs if a superimposed acute-on-chronic slip occurs (Fig. 9.7). More often, however, these patients have a history of chronic hip pain or limp for a number of months. The symptoms tend to be low grade and in some cases very minimal, with virtually no or little pain [11].

The classic early roentgenographic findings consist of smoothing of the zone of provisional calcification of the femoral head and increased lucency along with widening of the epiphyseal plate (Fig. 9.8a). Later, medial and often more pronounced posterior slippage of the epiphysis occurs, and this often is better seen on the frog-leg view (Fig. 9.8b). In addition, on frontal view, a line drawn along the outer aspect of the femoral neck can aid in determining whether the epiphysis has slipped medially, for in those cases where slippage has occurred, the line does not intersect the femoral capital epiphysis (Fig. 9.8a).

The precise cause of the slipped capital femoral epiphysis in childhood is unknown, but it probably represents a subclinical, chronic Salter–Harris type I injury. In this regard, it has been suggested that in many of these patients, the epiphyseal–metaphyseal junction is more vertical than normal, and because of this the epiphysis is more prone to slippage. Lack

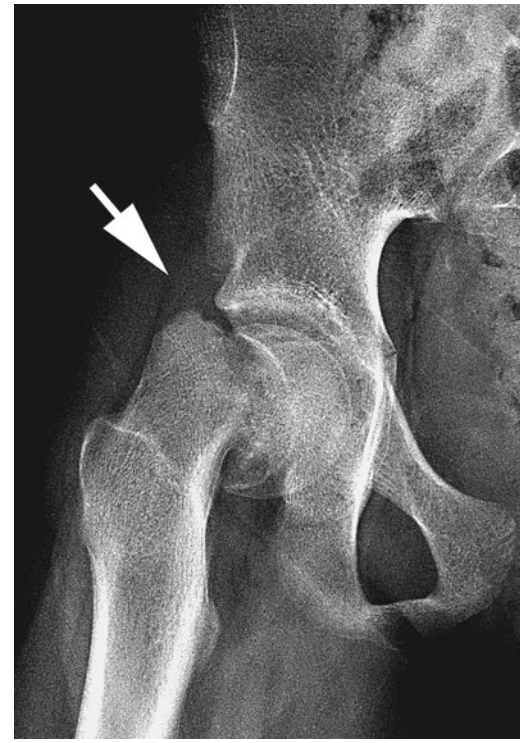


Fig. 9.7 Slipped capital femoral epiphysis: acute on chronic. Note the markedly slipped femoral capital epiphysis (*arrow*). This occurs on an acute basis, but the underlying SCFE problem probably was present for months

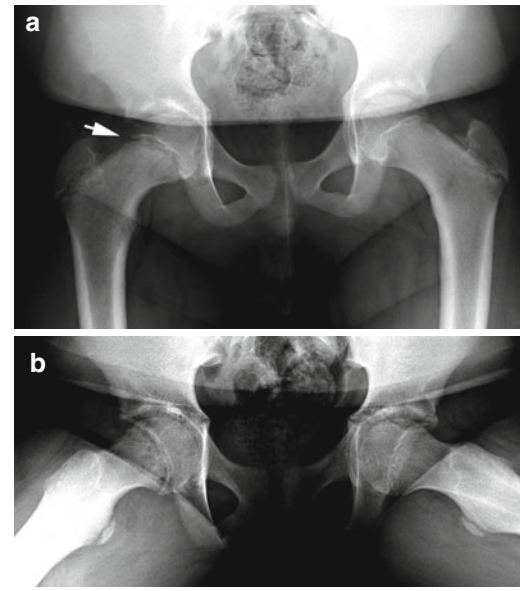


Fig. 9.8 Slipped capital femoral epiphysis: typical findings. (**a**) Note typical widening of the epiphyseal plate and increased sclerosis and smoothness of the zone of provisional calcification of the femoral capital epiphysis (*arrow*). (**b**) Frog-leg view demonstrates the slippage more clearly

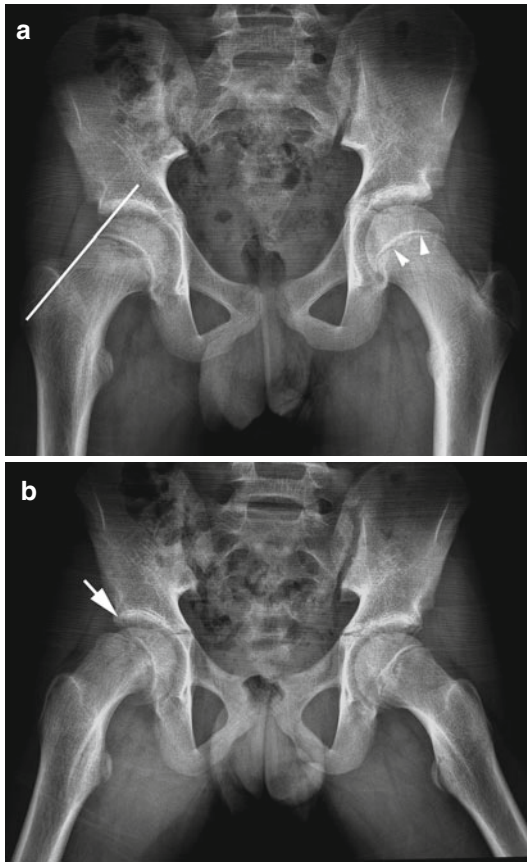


Fig. 9.9 Slipped capital femoral epiphysis classic and preslip. (**a**) Note typical findings of a slipped capital femoral epiphysis on the right. Also note that the line drawn along the outer edge of the femoral neck does not intersect the femoral capital femoral epiphysis. In addition note the increased density and concentric smoothness of the zone of provisional calcification of the femoral capital epiphysis on the other side (*arrowheads*). This represents a preslip phase. (**b**) Frog-leg view more clearly demonstrates the slipped epiphysis on the right and again demonstrates the smooth concentric zone of provisional calcification on the left

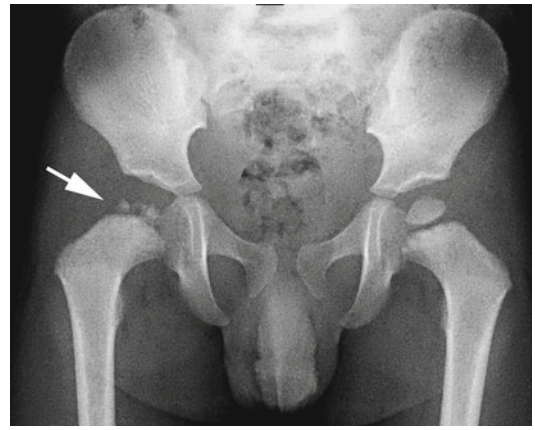


Fig. 9.10 Meyer's dysplasia. Note the small irregular femoral capital epiphysis on the right (*arrow*)

of normal anteversion also has been suggested to predispose to slippage and, of course, so has obesity. Slippage is slightly more common in males and occurs primarily in early adolescence [11]. In addition, the following additional hormonal factors have been associated: decreased growth hormone and hypothyroidism [12, 13]. Bilaterality is more common in these later cases. In idiopathic slips, bilateral disease usually is asymmetric and occurs in up to 20 % of cases, usually within 2 or 3 years of the primary slip [14]. However, in some cases one can see advanced slippage on one side and early, so-called preslippage on the other side (Fig. 9.9). In these cases, preslippage is manifested by increased sclerosis and smoothness of the zone of provisional calcification of the femoral capital epiphysis (Fig. 9.9). What happens in these case is that there is a very subtle but chronic Salter–Harris I injury and as the epiphysis slips on the metaphysis, there is trabecular shearing/compressive fracturing and healing all going on at the same time. This results in the zone of provisional calcification being very smooth and crescentic.

Finally, one must be aware of Meyer's dysplasia. In this condition the femoral heads are irregular (Fig. 9.10) and the findings mimic those of Legg–Perthes disease except that the patient is asymptomatic. Osteochondritis dissecans of the femoral head is uncommon [15].

MRI of the Hip and Thigh

MRI of the hip may be obtained in the ER setting for a child presenting with hip pain, and in this regard, it may detect an unsuspected apophyseal avulsion, soft tissue injury, or an intrinsic cause of hip pain (Fig. 9.11). Unlike adults, an occult femoral neck fracture is rarely seen.

In cases of suspected septic arthritis of the hip, as discussed earlier, the initial imaging modality of choice is ultrasound for detecting joint effusion. The final diagnosis rests on joint aspiration, but not uncommonly a child presents to the ER with hip pain and clinical signs of infection, but with no hip effusion or signs of osteomyelitis on plain

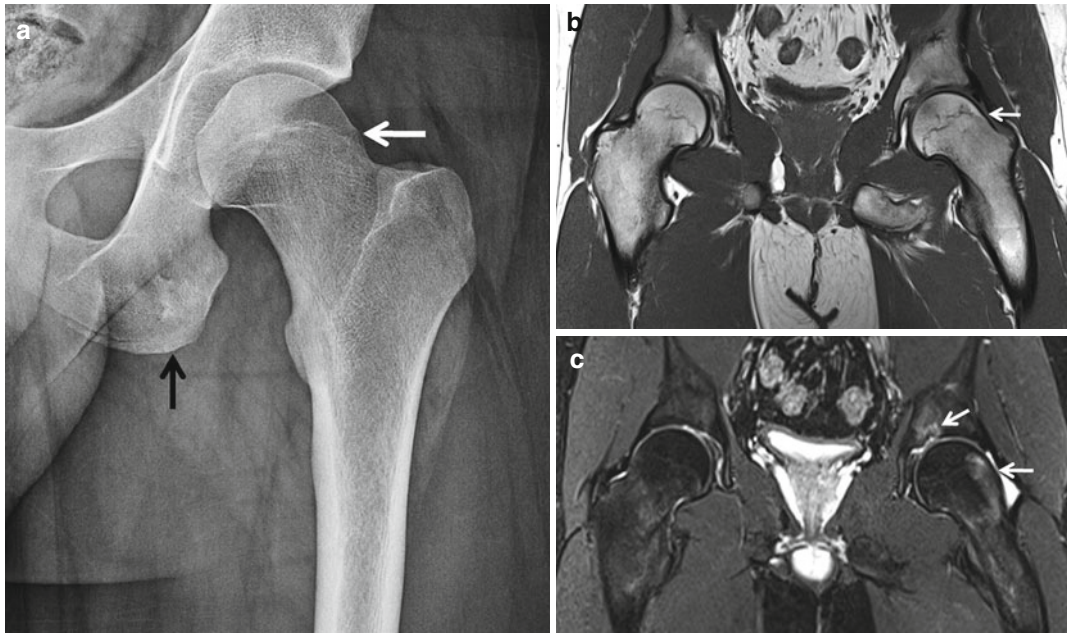


Fig. 9.11 Hip pain: value of MR. (**a**) AP radiograph of the left hip in a teenager complaining of hip pain. Hypertrophy of the ischial tuberosity is noted from an old ischial avulsion (*black arrow*). It was unclear if there was reinjury. There also is a subtle osseous epiphyseal hump present at the lateral head–neck junction (*white arrow*) suggesting CAM type femoro-acetabular impingement. MRI was ordered to define exact cause of hip pain. (**b**) Coronal T1-weighted image confirms the "gunstock deformity" of the left proximal femur with an osseous hump noted on plain films at the lateral head–neck junction (*white arrow*). Note the normal head–neck junction configuration on the right. (**c**) Coronal STIR image shows a small left hip effusion with bone contusions at the site of CAM deformity in the femur and anterior acetabular margin (*arrows*) confirming impingement as the cause of hip pain. The ischial tuberosity avulsion had healed

films. In these cases an MRI study of the pelvis, including both hips, is valuable in localizing the underlying pathology (Fig. 9.12). MRI may also be obtained for evaluation of suspected soft tissue injuries and muscle strain in the thigh (Fig. 9.13).

Femoral Shaft

Fractures of the femoral shaft are common in childhood and generally not difficult to detect. Usually they result from serious, known injuries and are of the transverse, spiral, or oblique variety. It is important to note that with femoral shaft fractures, a small degree of overriding of the fracture fragments is desirable (Fig. 9.14a). The reason for this is that the hyperemia associated with the fracture leads to accelerated growth of the femur, and because the distal femur is the fastest-growing long bone end in the body, there is overgrowth and eventual excessive lengthening of the femur. Initial overriding protects against this.

Recently, some note has been made of the fact that many times what appears to be an ordinary fractured femur in an infant is actually part of the battered child syndrome [16, 17]. The main theme of these reports is that in young infants, in whom one might not expect to see femoral shaft fractures with any degree of frequency, if any suspicion regarding the fracture arises, the possibility of the infant having been battered should be entertained. This is especially important if the oblique or transverse fracture fragments are outwardly angulated. This problem is discussed in more detail later in Chap. 12 dealing with child abuse (see Fig. 12.7). Stress [18] and bowing [19] fractures of the femur are uncommon (Fig. 9.14b).

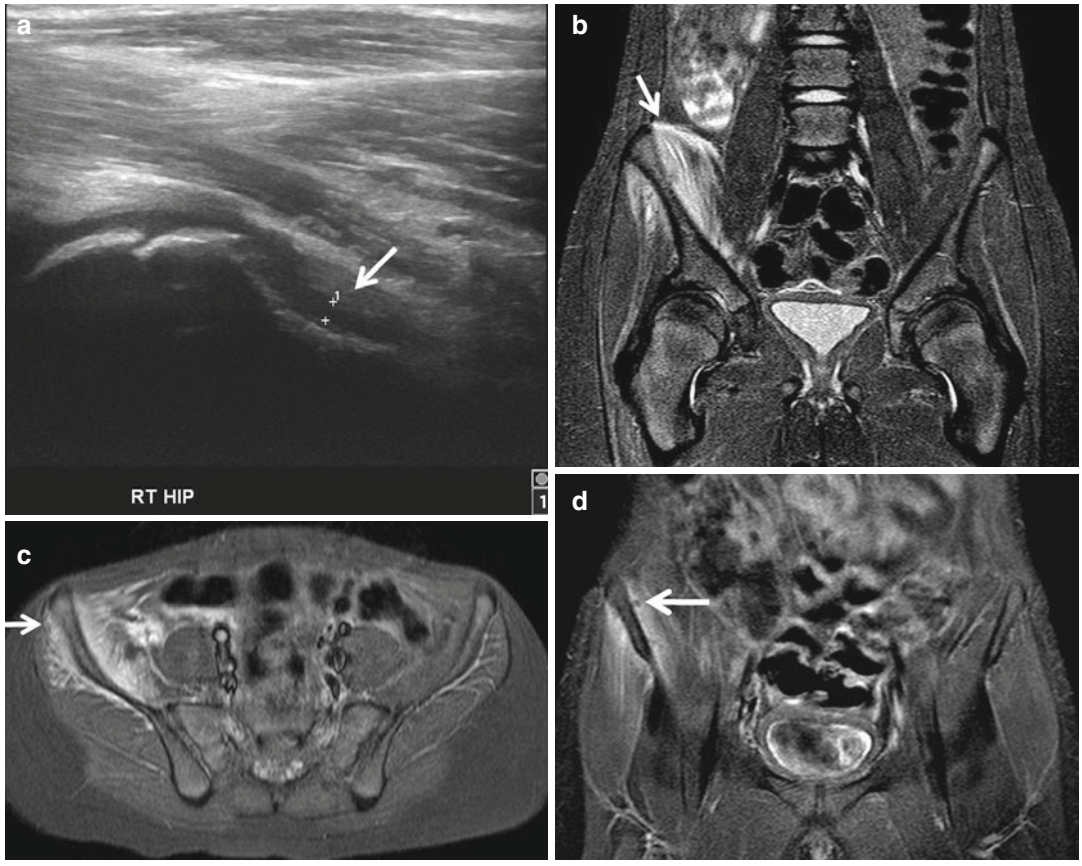


Fig. 9.12 Hip pain: value of MR. 8-year-old presenting with right hip and right lower quadrant pain. ESR and WBC count were significantly elevated. (**a**) Ultrasound of the hip shows a small right hip effusion (*arrow*); however, the clinical exam was not conclusive and another pathology was suspected. (**b**) Coronal STIR image shows diffuse edema and enlargement of the right iliacus (*arrow*) and mild edema in the gluteus minimus. (**c**) Axial post-contrast T1-weighted image with fat saturation shows diffuse enhancement of the affected muscles and indistinct cortex of the iliac bone (*arrow*) suggesting osteomyelitis. (**d**) Coronal post-contrast T1-weighted image with fat saturation shows diffuse enhancement of the affected muscles with a very small (tiny) non-enhancing abscess (*arrow*). No drainable fluid collection was seen. Final diagnosis was osteomyelitis of the iliac bone

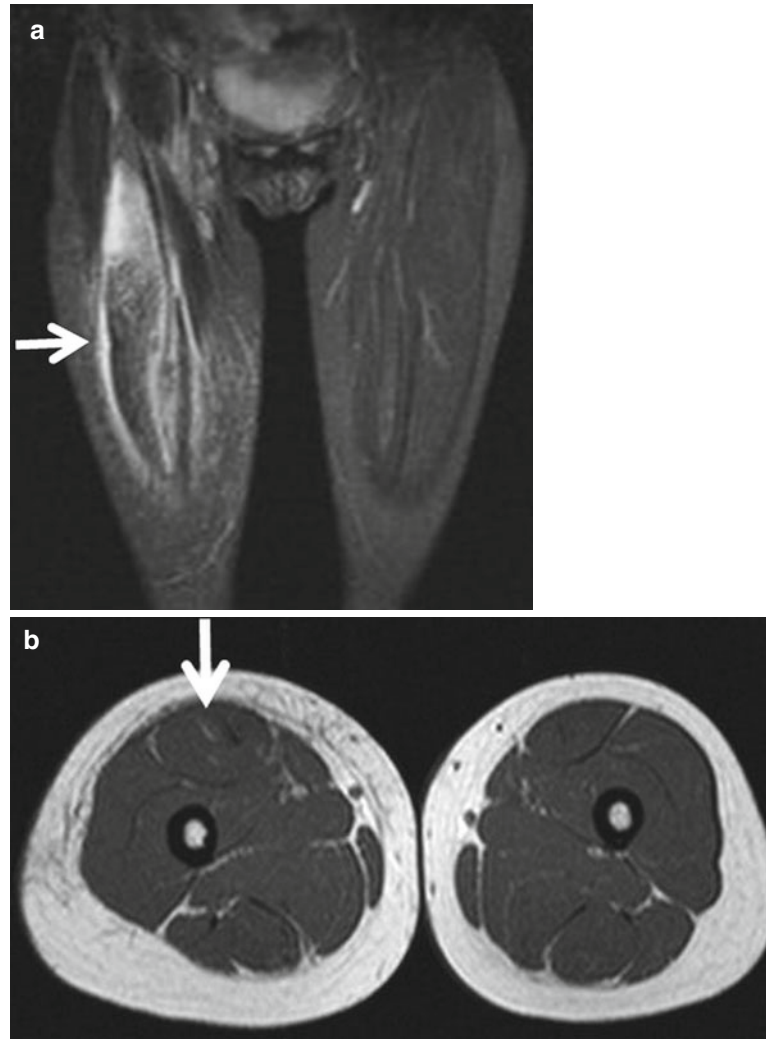
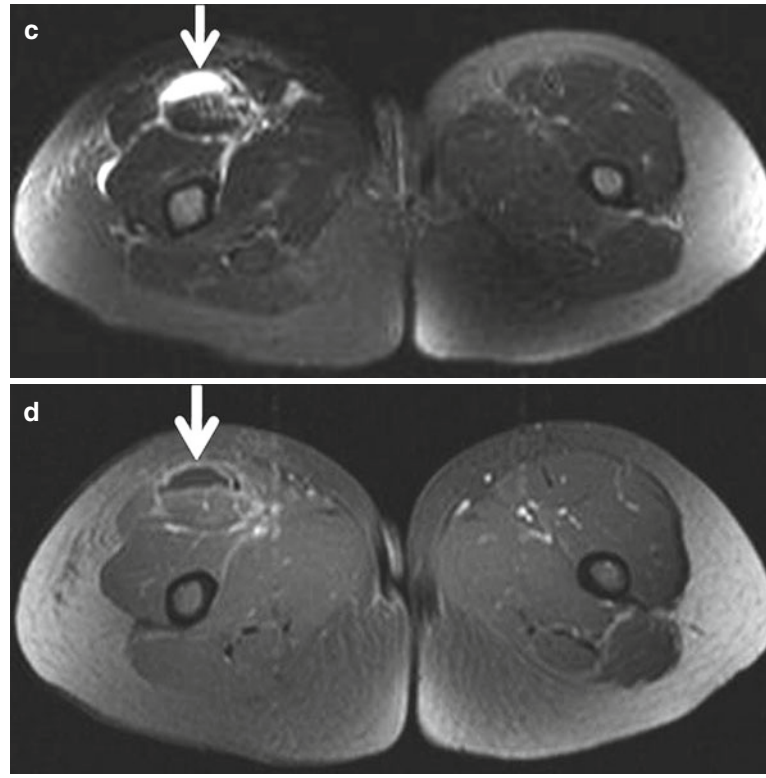


Fig. 9.13 Rectus femoris strain: value of MR. (**a**) Coronal STIR image shows diffuse edema of the right rectus femoris muscle with adjacent fluid (*arrow*). (**b**) Axial T1-weighted image shows subtle focal hyperintense signal within the enlarged muscle belly suggesting subacute hemorrhage (*arrow*). (**c**) Axial T2-weighted image with fat saturation shows focal hyperintensity within the muscle belly suggesting a partial muscle tear (*arrow*). (**d**) Axial post-contrast T1-weighted image with fat saturation confirms the low-signal partial muscle tear (*arrow*) adjacent to the central tendon

Fig. 9.13 (continued)



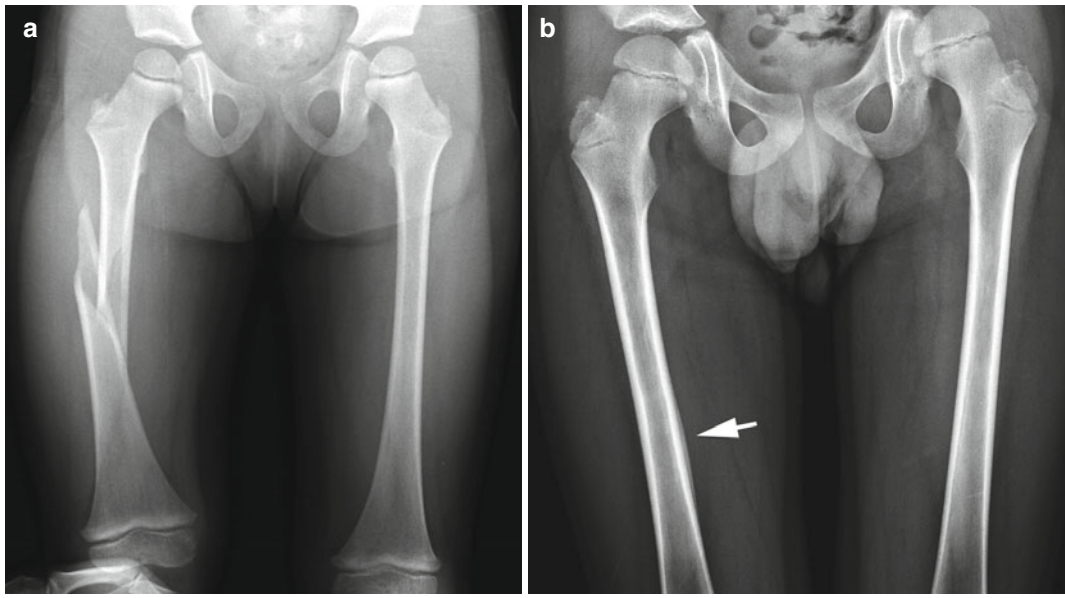


Fig. 9.14 Femoral shaft fractures. (**a**) Note the spiral midshaft femoral fracture on the right. The fracture fragments are overriding and this is desired. (**b**) Subtle periosteal new bone deposition (*arrow*) is seen along the inner cortex (*arrow*) of the right femur. These findings are typical for a stress fracture

References

1. Terjesen T, Osthus P. Ultrasound in the diagnosis and follow-up of transient synovitis of the hip. J Pediatr Orthop. 1991;11:608–13.
2. Swischuk LE. Musculoskeletal: what's different in children? Fell down the stairs two times; now limping. Emerg Radiol. 2011;18:369–70.
3. Baker JF, Leanard M, Devitt BM, Queally JM, Noel J. Traumatic hip dislocation in a 3 year-old girl. Pediatr Emerg Care. 2011;27:1178–9.
4. Erken EHW, Katz K. Irritable hip and Perthes' disease. J Pediatr Orthop. 1990;10:322–6.
5. Stansberry SD, Swischuk LE, Barr L. Legg-Perthes disease; incidence of the subchondral fracture. Appl Radiol. 1990;19:30–3.
6. Kahle WK, Colman SS. The value of the acetabular teardrop figure in assessing pediatric hip disorders. J Pediatr Orthop. 1992;12:586–91.
7. Hoffinger SA, Rab GT, Salamon PB. Metaphyseal cysts in Legg-Calvé-Perthes disease. J Pediatr Orthop. 1991;11:301–7.
8. Mitchell MD, Kundel HL, Steinberg ME, Kressel HY, Alavi A, Axel L. Avascular necrosis of the hip: comparison of MR, CT and scintigraphy. AJR. 1986;147:67–71.
9. Pinto MR, Peterson HA, Berquist TH. Magnetic resonance imaging in early diagnosis of Legg-Calve-Perthes disease. J Pediatr Orthop. 1989;9:19–22.
10. Keenan WNW, Clegg J. Perthes' disease after "irritable hip": delayed bone age shows the hip is a "marked man". J Pediatr Orthop. 1996;16:20–3.
11. Loder RT, Farley FA, Herzenbert JE, Hensinger RN, Kuhn JL. Narrow window of bone age in children with slipped capital femoral epiphyses. J Pediatr Orthop. 1996;16:20–3.
12. Loder RT, Wittenberg B, DeSilva G. Slipped capital femoral epiphysis associated with endocrine disorders. J Pediatr Orthop. 1995;15:349–56.
13. Wells D, King JD, Roe TF, Kaufman FR. Review of slipped capital femoral epiphysis associated with endocrine disease. J Pediatr Orthop. 1993;13:610–4.
14. Hernandez JA, Swischuk LE, Wallace J, et al. Slipped capital femoral epiphysis (SCFE) incidence of contralateral slip, RSNA 87th scientific assembly and annual meeting, Chicago Ill, Nov 2001, (Presented at the Scientific Assembly).
15. Wood JB, Klassen RA, Peterson HA. Osteochondritis dissecans of the femoral head in children and adolescents: a report of 17 cases. J Pediatr Orthop. 1995;15:313–6.
16. Beals RK, Tufts E. Fractured femur in infancy: the role of child abuse. J Pediatr Orthop. 1983;3:583–6.
17. Gross RH, Stranger M. Causative factors responsible for femoral fractures in infants and young children. J Pediatr Orthop. 1983;3:341–3.
18. Burks RT, Sutherland DH. Stress fracture of the femoral shaft in children: report of two cases and discussion. J Pediatr Orthop. 1984;4:614–6.
19. Cail SS, Keats TE, Sussman MD. Plastic bowing fracture of the femur in a child. AJR. 1978;130:780–2.

Knee and Leg

10

Normal Fat Pads and Soft Tissues

There are a number of normal fat pads around the knee, and all can be useful. On frontal view, these fat pads are seen adjacent to the distal femur (Fig. 10.1a) and can become obliterated with deep edema. On lateral view, similar fat pads are seen posterior to the distal femur (Fig. 10.1b). Other fat pads include the prefemoral fat pad just over the anterior surface of the distal femur, the infrapatellar or Hoffa's fat pad inferior to the patella, and the suprapatellar fat pad which exists between the insertion of the quadriceps tendon and the neck of the suprapatellar joint bursa (Fig. 10.1b). The infrapatellar fat pad commonly is obliterated by the edema associated with Osgood–Schlatter and Sinding–Larsen–Johansson disease. With prepatellar cellulitis, the soft tissues anterior to the quadriceps tendon, patella, and infrapatellar tendon become thickened and trabeculated. In the normal knee, the infra- and suprapatellar tendons usually are clearly identified (Fig. 10.1b).

Detection of Fluid in the Knee Joint

The knee joint does not widen significantly with accumulations of fluid, and thus one must depend on surrounding soft tissue and fat pad changes for the detection of fluid in the knee joint [1]. In this regard, it is the lateral view of the knee that is most useful. On this view, fluid almost always first visibly accumulates in the suprapatellar bursa, which lies behind the quadriceps tendon and in front of the prefemoral fat pad. If this occurs, the quadriceps tendon is displaced anteriorly and the fat pad posteriorly, and the fluid-filled suprapatellar bursa blends with the quadriceps tendon to make it look thicker than normal (Fig. 10.2).

Fluid in the knee also is detectable with ultrasound, CT, and MR imaging. Ultrasound, however, is noninvasive and easily demonstrates the presence of knee joint fluid. However, because plain films are so dependable, seldom is there need for any of these studies to be performed for the sole purpose of detecting fluid in the knee joint.

Injuries of the Distal Femur and Proximal Tibia and Fibula

Cortical buckle (torus) fractures around the knee are uncommon in older children because the cortices of both the distal femur and proximal tibia are sturdy. However, in infants and young children, they are common both in the distal femur and proximal tibia (Fig. 10.3). These fractures can result from simple axial loading injuries but also commonly are seen with hyperextension injuries. In this regard, in the upper tibia, buckle fracturing of the anterior tibial cortex along with an associated posterior diastatic hairline fracture is common [2–5] and often due to a trampoline-induced injury [6]. In such cases, when one falls off the trampoline, the fall is braced with the hyperextended lower extremity and stresses are

L.E. Swischuk, S.P. Jadhav (eds.), *Emergency Musculoskeletal Imaging in Children*,
DOI 10.1007/978-1-4614-7747-1_10, © Springer Science+Business Media New York 2014

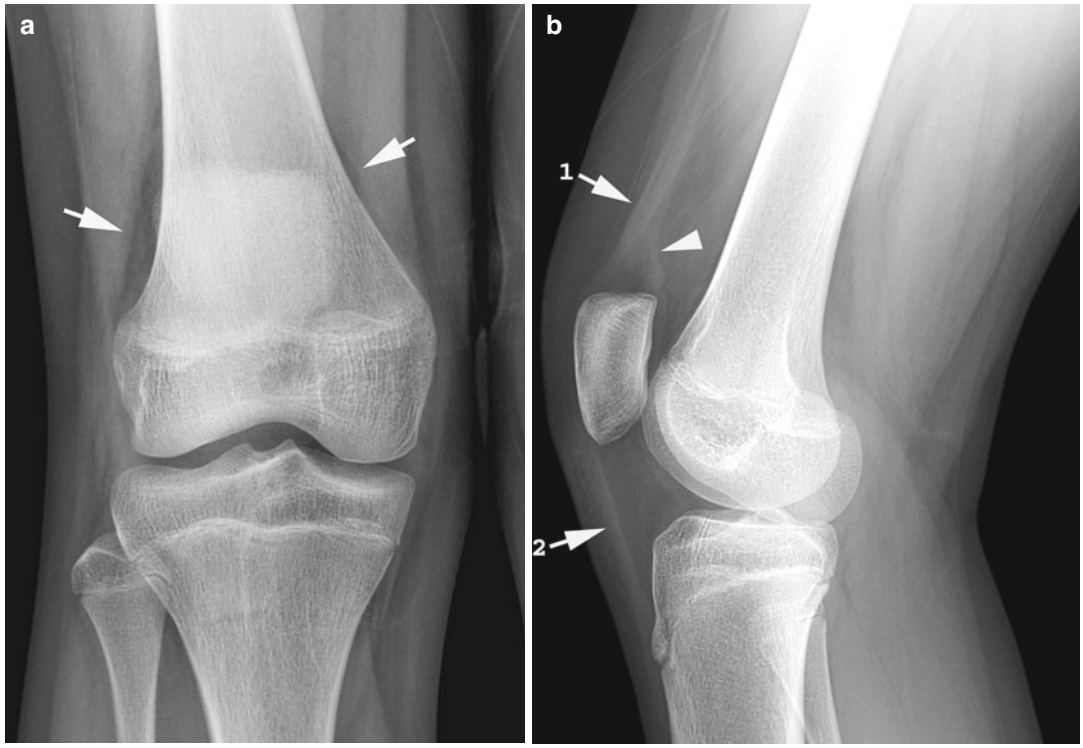


Fig. 10.1 Normal fat pads and soft tissues. (**a**) Note the normal fat pads (*arrows*) along the distal femur. (**b**) Lateral view. Note the quadriceps tendon (*1*), the infrapatellar tendon (*2*), and the neck of the suprapatellar bursa (*arrowhead*). Also note the fat pads anterior and posterior to the distal femur. The infrapatellar or Hoffa's fat pad lies directly behind the infrapatellar tendon. The small triangular-shaped suprapatellar fat pad lies between the insertion of the quadriceps tendon and the neck of the suprapatellar bursa

placed on the upper tibia (Fig. 10.4a, b). On AP view of the knee, one may see a transverse (Fig. 10.4c) or slightly oblique fracture which often is hairline. In addition, visualizing this fracture on the AP view probably occurs in less than 50 % of cases. In some cases, an associated cortical buckle fracture is seen (see Fig. 10.5c).

All of the foregoing notwithstanding, in most cases, it is the lateral view of the knee which is most informative with this fracture where the findings consist of (1) buckling of the anterior tibial cortex, (2) increased concavity of the notch for the tibial tubercle, (3) anterior tilting of the epiphyseal plate, and (4) posterior diastatic fracture (Fig. 10.4b). In many cases, these findings are very subtle and comparative views are invaluable (Fig. 10.5a, b). This fracture is very common in infants and young children, and we have arbitrarily named it the toddler II fracture and the spiral fracture described by Dunbar (see Fig. 10.28) as the toddler I fracture.

Upper tibial transverse fractures also can result from lateral forces applied to the knee, and both this fracture and the toddler II fracture can result in a valgus deformity of the tibia [7–10]. This deformity, often initially minimally present, can become more pronounced and persistent as time goes by (Fig. 10.6). For the most part, this is believed to result from the fact that there is overgrowth of the medial aspect of the proximal tibia. In this regard, it has been noted that normally there is a greater blood supply to the upper medial tibia and that, with the hyperemia associated with fractures, the growth accelerated and overgrowth occur [8, 9].

Epiphyseal–metaphyseal injuries are not that common about the knee but do occur. In gross form, they are not difficult to detect, but the more subtle, nondisplaced Salter–Harris type I and II injuries



Fig. 10.2 Joint fluid: suprapatellar bursa. Note the distended suprapatellar bursa (*arrows*) compressing the anterior femoral fat pad. It blends with the quadriceps tendon making the tendon appear thicker than normal

frequently elude initial observation. In these cases, one should be suspicious of the slightest degree of widening of the epiphyseal plate (Fig. 10.7a). Comparative views are very helpful and it must be emphasized that positioning must be accurate for the slightest malpositioning of the knee may erroneously suggest a wide epiphyseal plate.

A variation of the usually Salter–Harris fracture is the one which occurs when the proximal tibial epiphysis is totally or partially avulsed (Fig. 10.7b, c) and finally MR imaging is especially useful in detecting epiphyseal metaphyseal injuries which are occult or invisible on plain films (Figs. 10.8 and 10.9). MRI has been shown to change management in cases of epiphyseal–metaphyseal injuries by better defining the extent of the fracture and in some cases by diagnosing unsuspected fractures [11].

Stress fractures around the knee most commonly occur in the upper tibia in older children. A fracture line usually is not visible but with healing typical sclerosis and periosteal new bone deposition are seen posteriorly (Fig. 10.10a). In the early stages, these changes can be subtle, but later periosteal new bone deposition is profound, and often a more serious lesion such as a bone tumor is erroneously suggested. Less commonly stress fractures occur in the upper anterior tibia, and both of these fractures are the equivalent of the toddler II fracture seen in infants and young children. The findings in the latter fracture usually consist of focal sclerosis in the upper anterior tibia (Fig. 10.10b–d). All of these findings also can be demonstrated with CT and MR where the occult fracture line often becomes visible. MR is valuable in differentiating stress reaction from stress fracture which has therapeutic implications with stress fractures requiring longer activity modification and rest.

Although not true stress fractures, impaction fractures of the distal femurs and proximal tibia can be considered within the ball park of stress fractures. In this regard, it is the tibia more often than the femur which is involved. Most often an axial loading force is exerted on the knee, and in most cases, the plain films are basically are normal. However, MR usually demonstrates the area of impaction (Fig. 10.10e, f).

Patellar Fractures and Dislocations

Patellar fractures and dislocations are common. Overt fractures usually occur from direct blows to the patella and occasionally from acute quadriceps tendon stress-induced injuries (Fig. 10.11). In these latter cases, the proximal half or third of the patella is avulsed from the remainder of the patella, and the findings are readily recognizable.

In terms of patellar dislocations, both acute and chronic repetitive dislocations of the patella are common in childhood, but in most cases, the patella relocates before radiographs are obtained. Patellar dislocations usually result from twisting of the knee wherein the medial ligamentous stabilizers (retinacula) rupture and the medial margin

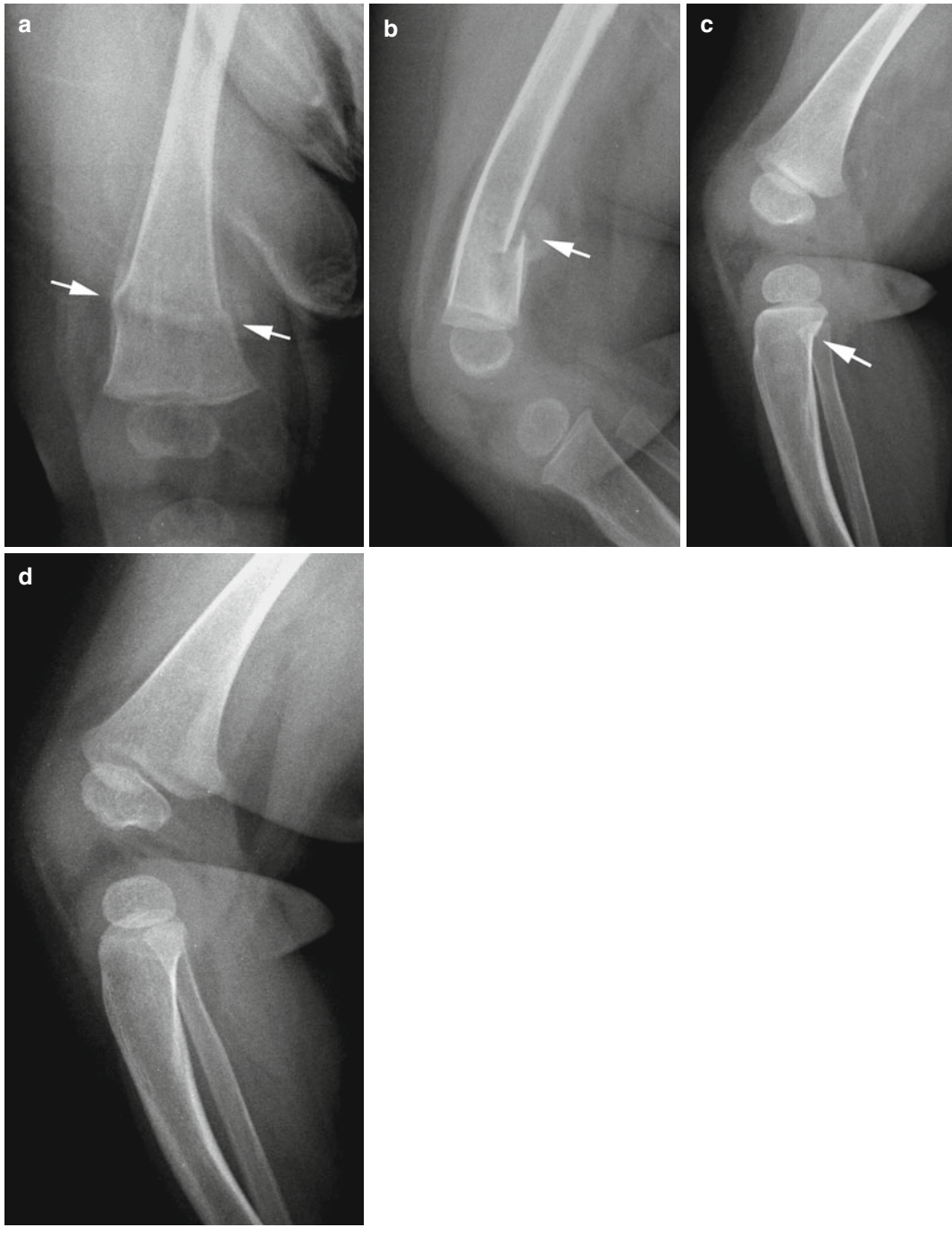


Fig. 10.3 Distal femoral and proximal tibial buckle fractures. (**a**) Note the typical impacted buckle through the distal femur (*arrows*) with early healing. (**b**) Lateral view demonstrates the same impacted fracture (*arrow*). (**c**) Note the very subtle angled buckle fracture through the posterior cortex (*arrow*) of the proximal tibia. (**d**) Normal side for comparison. Note the smooth curving appearance of the posterior tibial cortex

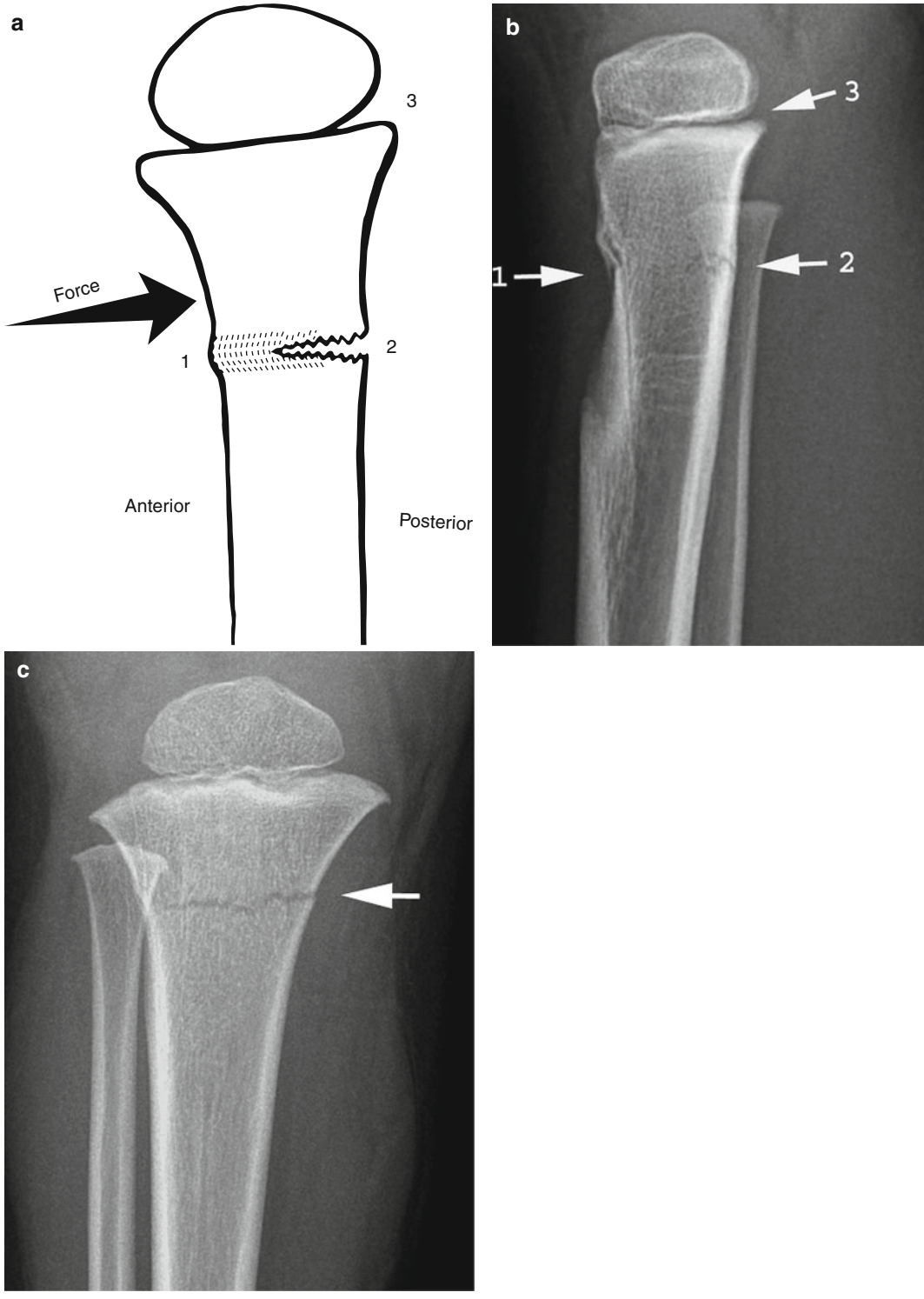


Fig. 10.4 Upper tibial impaction fracture: toddler II fracture. (**a**) Anterior compressive force is exerted on the upper tibia with hyperextension of the knee to produce: (*1*) an anterior buckle fracture, (*2*) a diastatic posterior fracture, and (*3*) anterior tilting of the epiphyseal plate. (**b**) Typical imaging findings. First note the anterior buckle fracture (*1*) and then note the subtle posterior diastatic fracture (*2*). Finally note anterior tilting of the epiphyseal plate (*3*). (**c**) Typical transverse upper tibial fracture line (*arrow*)

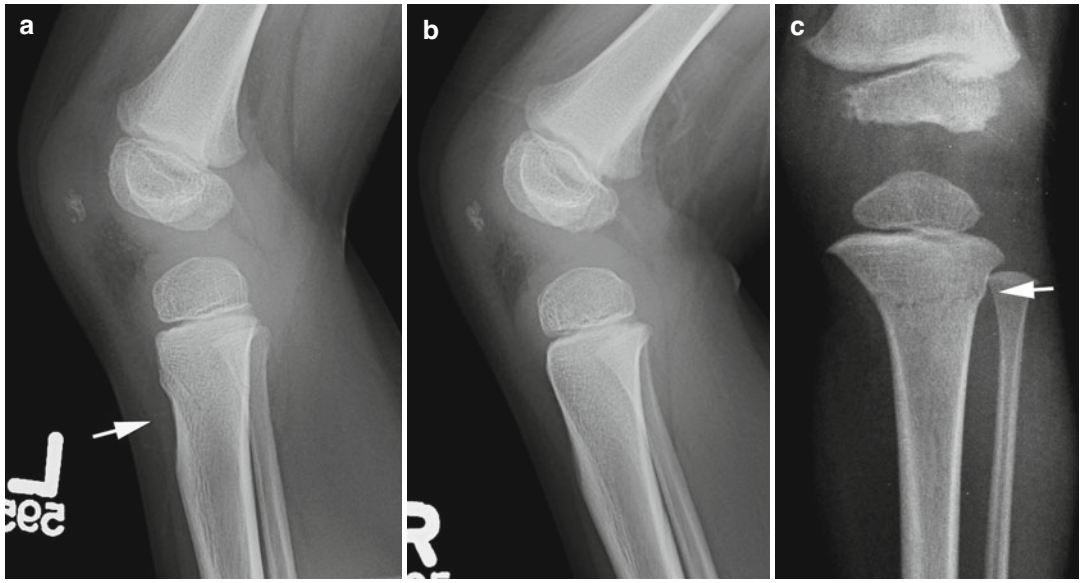


Fig. 10.5 Toddler II fracture: subtle findings. (**a**) In this patient, the main finding is increased scalloping of the concavity for the tibial tubercle (*arrow*). A minimal buckle fracture exists a little higher. (**b**) Normal side for comparison. Note the normal appearance of the cortex of the upper anterior tibia. (**c**) Another patient. Note the subtle hairline transverse fracture and the very minimal associated buckle fracture (*arrow*)

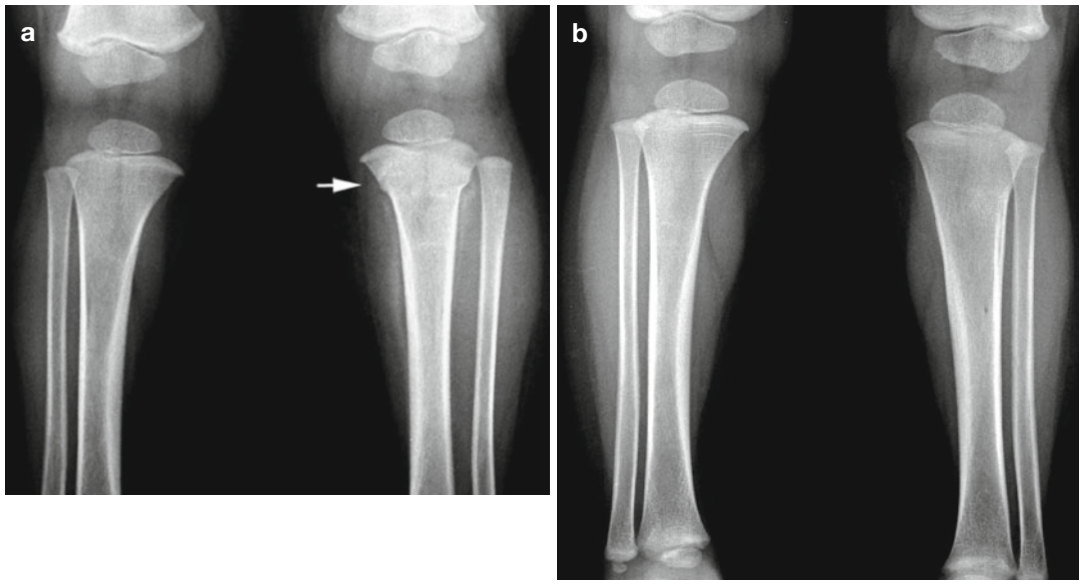


Fig. 10.6 Upper tibial fracture: valgus deformity. (**a**) Note a typical impacted buckle tibia fracture (*arrow*). (**b**) With healing, the fracture becomes obliterated, but a valgus deformity of the tibia is present

of the patella strikes against the lateral femoral condyle [12]. In some cases of patellar dislocation, an avulsed fracture fragment is seen along the medial aspect of the patella (Fig. 10.12a). Transient patellar dislocation often results in a large hemarthrosis making clinical examination difficult. Often an ACL rupture is erroneously suspected clinically, and an MRI is ordered which

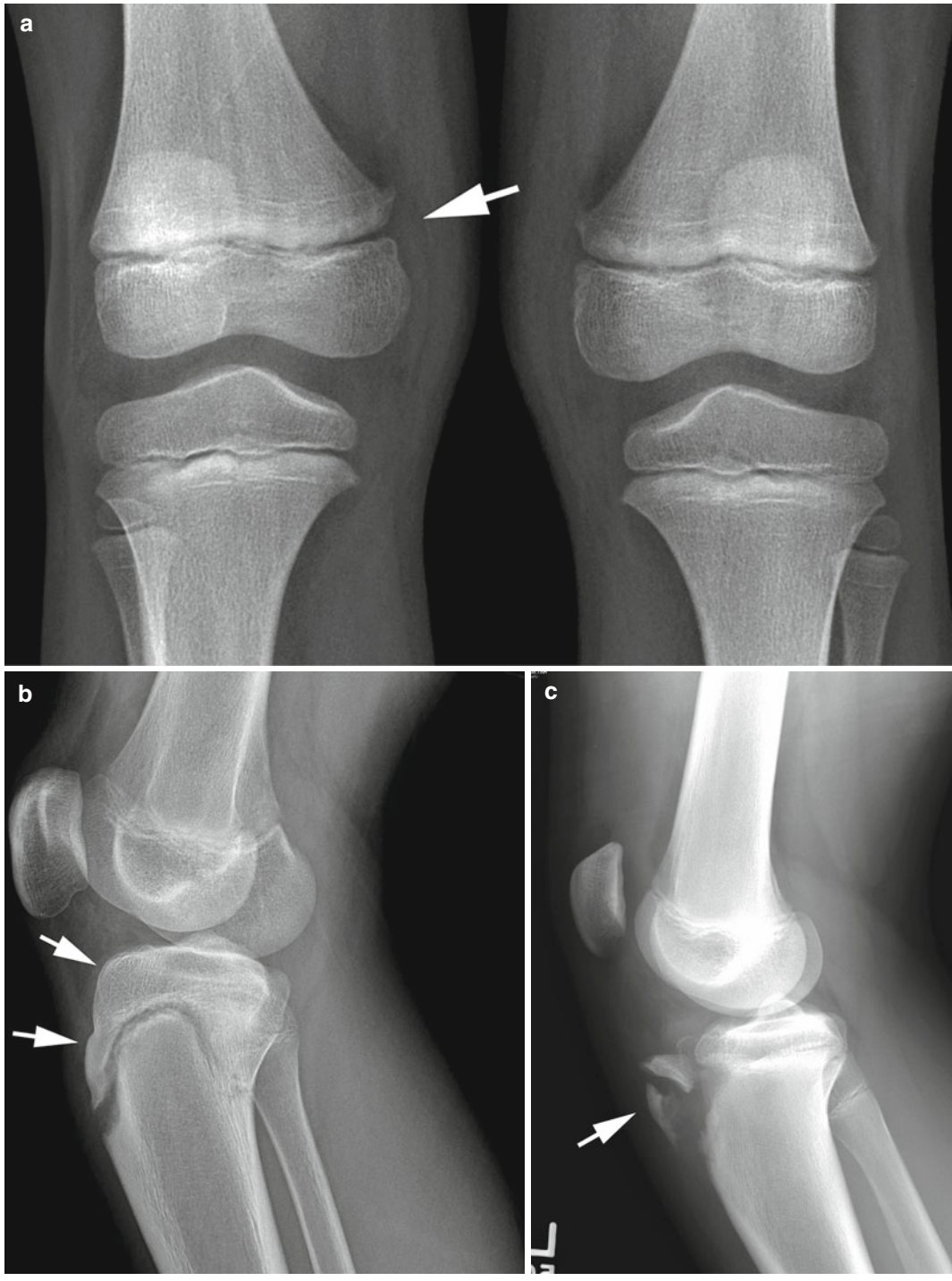


Fig. 10.7 Epiphyseal–metaphyseal fractures. (**a**) Note subtle widening of the epiphyseal plate in the right distal femur (*arrow*) constituting a minimal SH I fracture. (**b**) Tibial epiphyseal avulsion. Note the avulsed tibial epiphysis along with that portion which extends over the anterior tibia (*arrows*). There is a posterior compression fracture present also. (**c**) In this patient, only partial avulsion of the tibial epiphysis (*arrow*) has occurred



Fig. 10.8 Occult epiphyseal–metaphyseal fractures: value of MR. (**a**) Frontal radiograph of both knees is normal with no evidence of physeal widening. The patient had pain in the right knee. (**b**) Coronal STIR image in the same patient shows edema in the physis which extends into the metaphysis (*arrow*) consistent with a nondisplaced Salter–Harris I injury. (**c**) Another patient with frontal radiographs suggesting mild physeal widening in the right distal femur (*arrow*). MRI was obtained for confirmation and to exclude internal derangement of the knee. (**d**) Coronal STIR image confirms the finding of widening of the growth plate (*arrowhead*). Also note high-signal metaphyseal edema adjacent to the widening epiphyseal plate and fluid/hemorrhage extending subperiosteally along the lateral aspect of the metaphysis (*arrow*). (**e**) In this patient, the epiphyses basically were closed and the plain films were normal. On the T1-weighted image, there is irregularity along the old epiphyseal plate region (*arrow*). (**f**) Coronal STIR image demonstrates increased epiphyseal plate signal indicating a mild Salter–Harris fracture

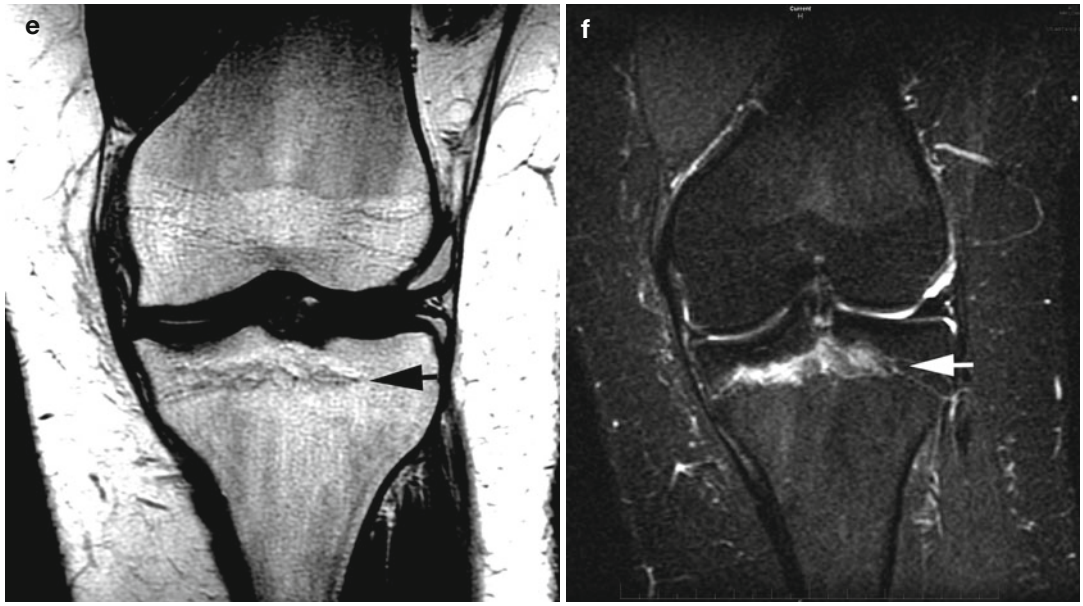


Fig. 10.8 (continued)

reveals the correct diagnosis. With MR imaging the retinacular injury, the avulsed bony fragment, and bone bruises involving the medial margin of the patella and lateral femoral condyle are readily demonstrable (Fig. 10.12b–d). Finally, it should be noted that the avulsed medial patellar fracture fragment is not mobile and usually stays in one position. In addition, it often is the only finding seen in cases of patellar dislocation with subsequent relocation.

Lateral condylar fractures resulting from patellar dislocation are less well appreciated on plain films, but in some cases, one may see the fracture donor site (Fig. 10.13a). In other cases, the avulsed bony fragment, as opposed to the medial patellar fragment, can be very mobile and can be seen anywhere within the knee joint (Fig. 10.13b, c). On subsequent MR imaging, one usually can see the fracture site and the associated bone bruise of the lateral condyle (Fig. 10.13d, e).

Patients with chronic recurrent patellar dislocation often have associated patella alta, a condition in which the patella is higher in position than normal. Abnormal tracking of the patella results, and the patellofemoral groove becomes shallow [13]. Patella alta is best seen on lateral view, but the shallow groove and associated flattening of the lateral condyle are best seen on skyline views (with 30 % flexion) of the patella. Most dislocations, whether acute or chronic, are lateral dislocations.

The role of MRI is not only to diagnose unsuspected transient patellar dislocations but also to evaluate for patellofemoral dysplasia, osteochondral fractures [14], and presence of osteochondral loose bodies. Patellar dislocations with loose bodies are usually treated surgically. Patients without loose bodies are treated non-operatively with bracing and rehabilitation.

Other avulsion fractures around the knee [15] included suprapatellar quadriceps tendon avulsions. These usually are fairly straightforward as the avulsed fracture fragment is clearly obvious. They are not nearly as common as the other two avulsion fractures/tendon injuries, that is, Sinding–Larsen–Johansson disease [16] and Osgood–Schlatter disease [17–19].

With Osgood–Schlatter disease, the infrapatellar tendon, as it inserts on to the tibial tubercle, can avulse part of the tubercle, or the tendon may simply undergo a tendon injury. Clinically, find-

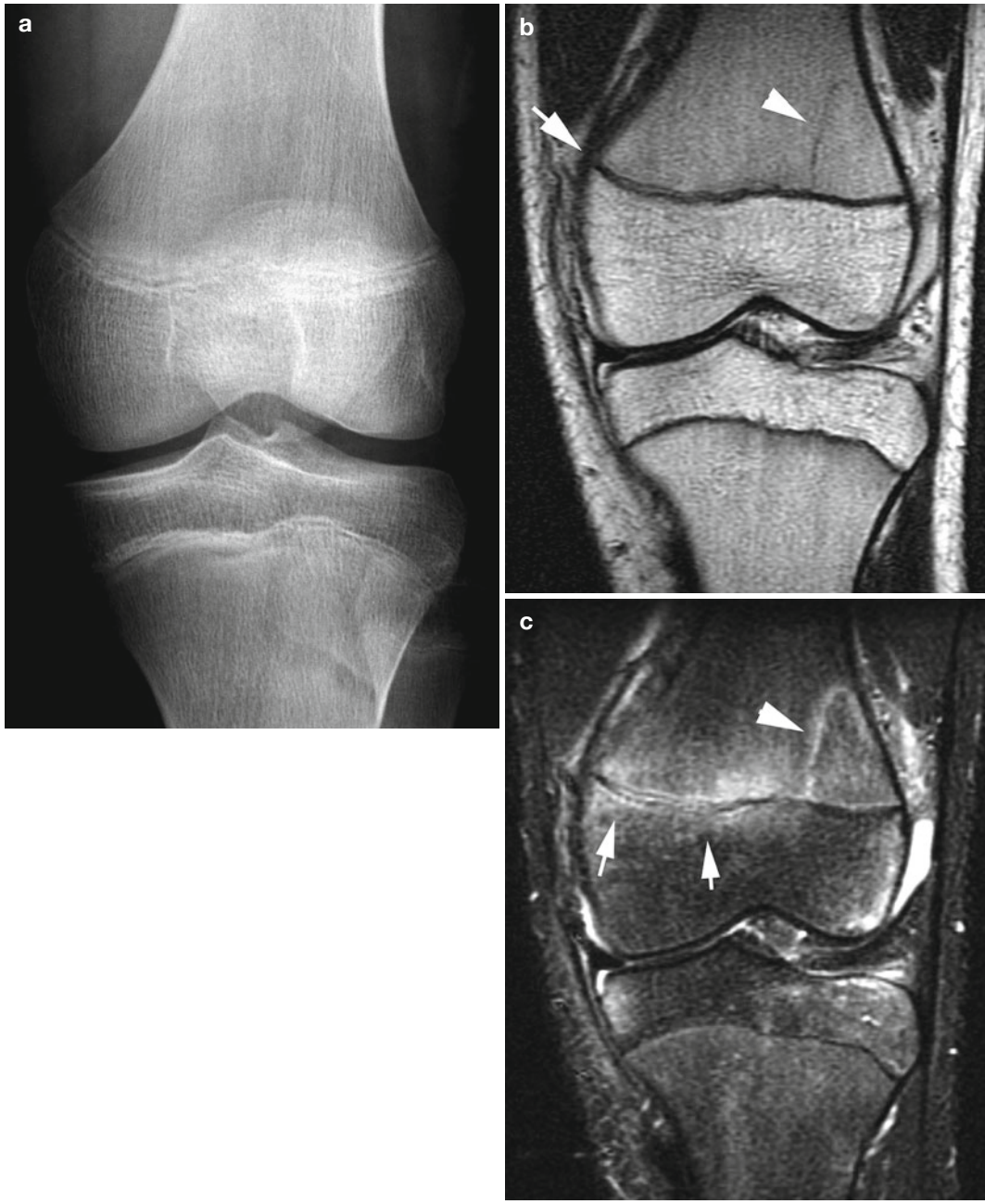


Fig. 10.9 Occult epiphyseal–metaphyseal fractures: value of MR. (**a**) Left knee pain. AP view of the left knee is normal. (**b**) Coronal T1-weighted image demonstrates a subtle Salter–Harris II fracture (*arrowhead*) and subtle widening of the epiphyseal plate medially (*arrow*). (**c**) Coronal STIR image. Note the high signal in the fracture line (*arrowhead*) of the Salter–Harris II fracture. In addition, note increased signal in the medial part of the epiphyseal plate and high signal (bone bruises) in the adjacent metaphysis and epiphysis (*arrows*). (**d**) Another patient with knee pain. Frontal and lateral views of the knee show no evidence of fracture. A small joint effusion is seen on the lateral view (*arrow*). (**e**) Sagittal T1W image shows a Salter–Harris II fracture of the distal femur (*arrow*). (**f**) Coronal STIR image shows widening of the lateral aspect of the physis (*arrow*) and adjacent high-signal metaphyseal edema. Also note metaphyseal extension of the fracture (*arrowhead*)

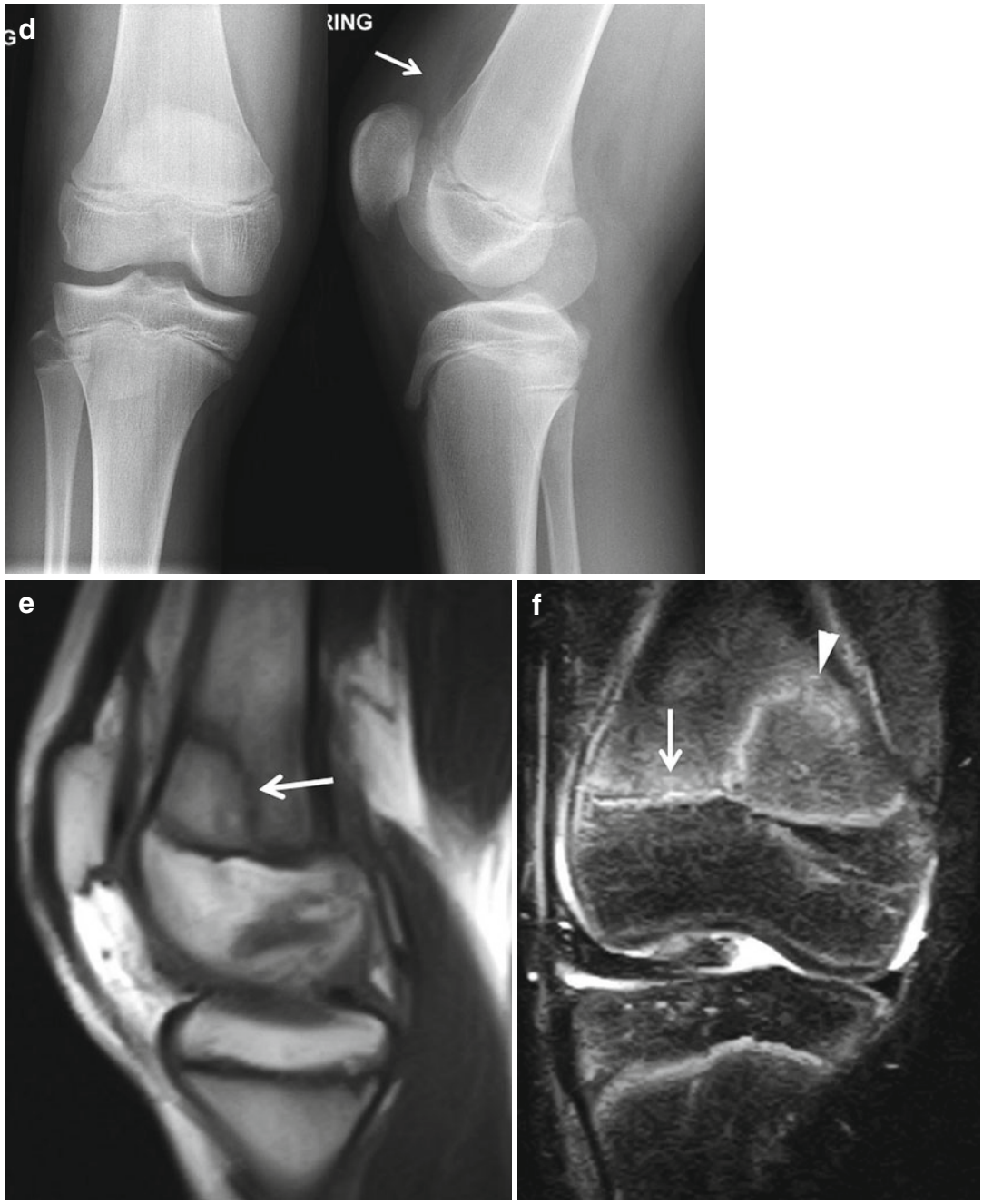


Fig. 10.9 (continued)

ings consist of pretubercular swelling and pain, and on imaging, swelling is present over the tibia tubercle. In addition the insertion of the infrapatellar tendon is edematous, and tendon itself appears swollen (Fig. 10.14a). In many cases but not all, an avulsed fracture fragment can be seen (Fig. 10.14b). With healing, one can see considerable hypertrophic bone formation (Fig. 10.15) and eventually a small acquired exocytosis. All of these configurations are virtually pathognomonic of Osgood–Schlatter disease but occasionally can be mimicked by the very rare periosteal

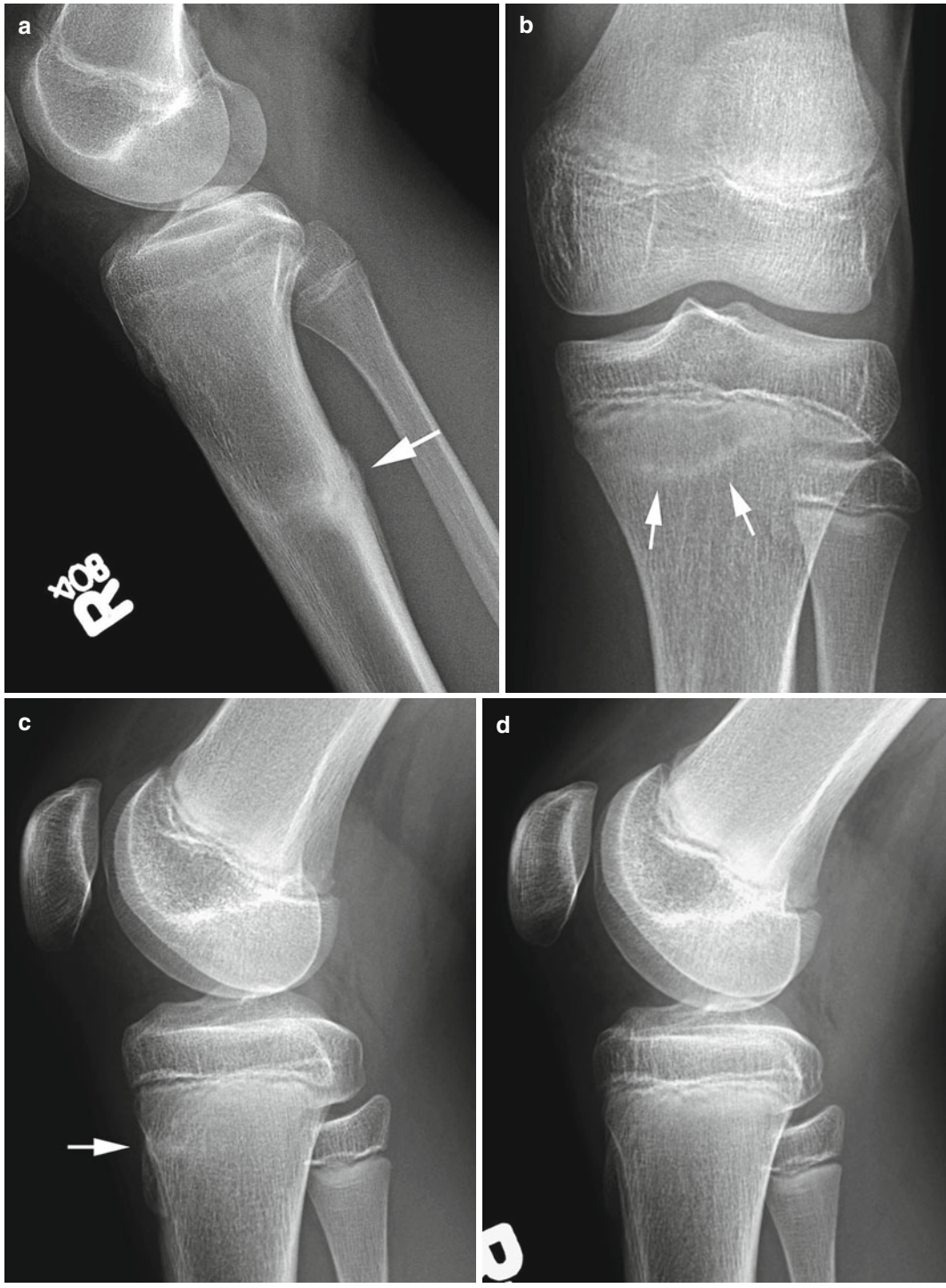


Fig. 10.10 Stress fracture. (**a**) Typical upper tibial stress fracture manifesting in cortical thickening and periosteal new bone deposition over the upper posterior tibia (*arrow*). Note that subtle sclerosis extends to the anterior cortex. (**b**) In this patient, a vague crescentic sclerotic line (*arrows*) is noted in the upper tibia. (**c**) Lateral view demonstrates that the line is secondary to an impaction stress fracture (*arrow*) of the upper anterior tibia. (**d**) Normal side for comparison. Note the normal appearance of the upper tibia with no visible sclerosis. (**e**) Compression tibial plateau. AP view of the knee is basically normal. There is minimal suggestion of a fracture (*arrow*). (**f**) Coronal T2 fat-saturated image demonstrates the compression fracture (*arrow*) of the tibial epiphysis and associated disruption of the epiphyseal plate (*arrowheads*)

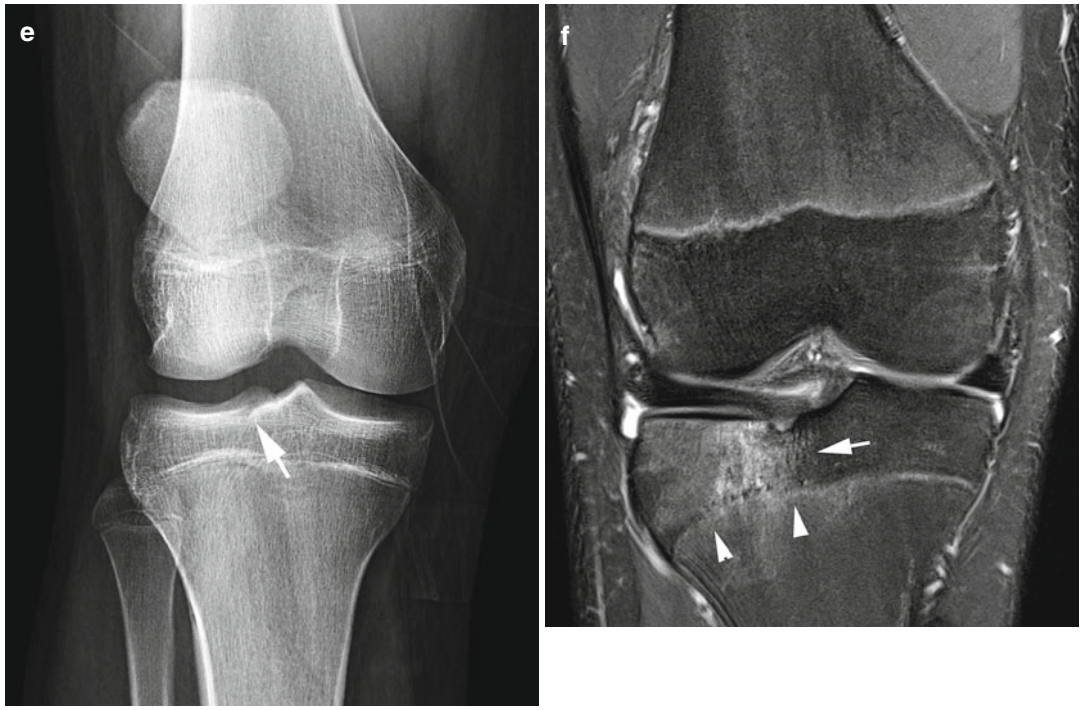


Fig. 10.10 (continued)

chondroma of the tibial tubercle [20]. This lesion is more bulky, mostly lytic, and associated with destruction of the upper tibia under the tibial tubercle.

With Sinding–Larsen–Johansson disease, the same mechanics as exists with Osgood–Schlatter disease exists, but they involved the inferior pole of the patella. The findings consist of soft tissue edema over the inferior patella, thickening of the infrapatellar tendon as it inserts into the inferior patella, and variable obliteration of the infrapatellar or Hoffa's fat pad (Fig. 10.16). In addition, one often sees the avulsed fracture fragment. With both Osgood–Schlatter disease and Sinding–Larsen–Johansson disease, MR imaging is very useful, especially if the findings are unclear on plain films (Fig. 10.17). Although the diagnosis of Osgood–Schlatter disease is clinical, imaging is often obtained to rule out other pathology (Fig. 10.18).

Sinding–Larsen–Johansson disease occurs at an age before physeal closure around the knee. After physeal closure, patellar tendonitis occurs. This is referred to as "jumper's knee" due to the fact that it occurs in teenagers involved in sports activity involving jumping (Fig. 10.19a–c). In cases of acute injuries, often a sleeve avulsion fracture occurs at the inferior patellar pole. This is usually diagnosed on radiographs. More subtle cases may need an MRI for the correct diagnosis (Fig. 10.19d, e).

Chondromalacia of the patella, often associated with chronic patellar dislocation, is a difficult diagnosis to make with certainty. It is not particularly common in children and currently is best evaluated best with MR imaging [21] where abnormal signal and variable degrees of deficiency of the cartilage on the posterior aspect of the patella are seen (Fig. 10.20). Stress fractures of the patella are uncommon, but linear stress fractures have been identified [22].

Osteochondritis dissecans of the medial femoral condyle is not common in early childhood but is common in later childhood [23]. Roentgenographically, typical findings are those of a bony defect along the anteromedial aspect of the medial femoral condyle (Fig. 10.21a, b). These lesions probably represent subchondral



Fig. 10.11 Patellar fractures. (**a**) Note the linear fracture (*arrow*) through the patella. (**b**) In this patient, two linear fractures (*arrows*) are visualized. (**c**) Patellar bone bruise. With a direct hit to the patella, increased signal in the inferior patella (*arrow*) is seen on this STIR image. (**d**) Coronal STIR image demonstrates the same increased signal (*arrow*)

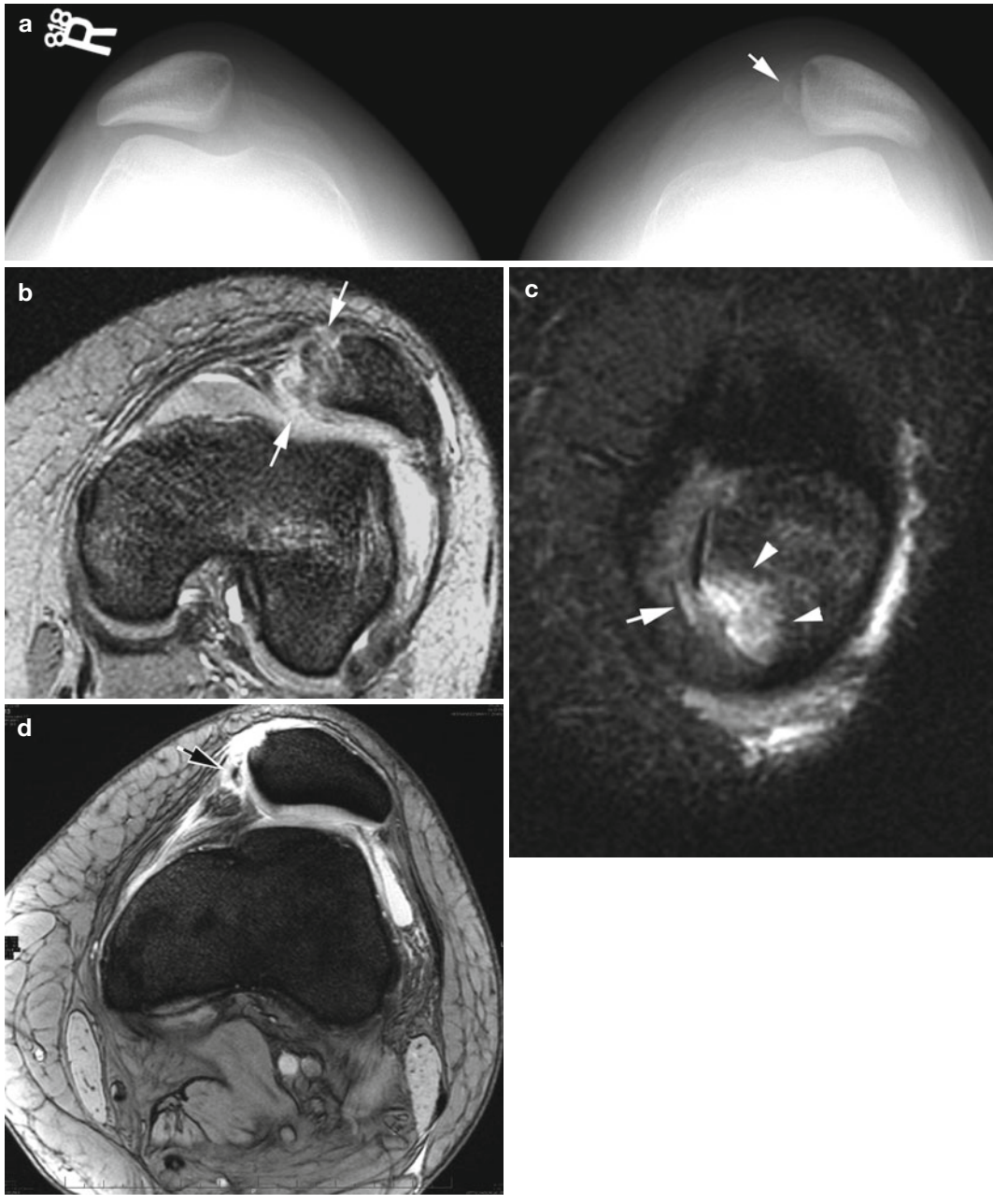


Fig. 10.12 Patellar dislocation: medial retinacular tear and fracture. (**a**) On this skyline view, note that both patellae are subluxed and that the intercondylar notches are shallow on both sides. In addition, there is a subtle avulsed medial fracture fragment (*arrow*) on the left. There also is surrounding swelling. (**b**) Axial T2 GRE study demonstrates the disrupted medial retinaculum (*arrows*). (**c**) Coronal STIR image through the patella demonstrates the avulsed fracture fragment (*arrow*) and a bone bruise in the medial patella (*arrowheads*). (**d**) Another patient. Coronal T2 view of the knee. Note the avulsed medial patellar fracture fragment (*arrow*) and the slightly disrupted medial retinaculum. The patella is subluxed

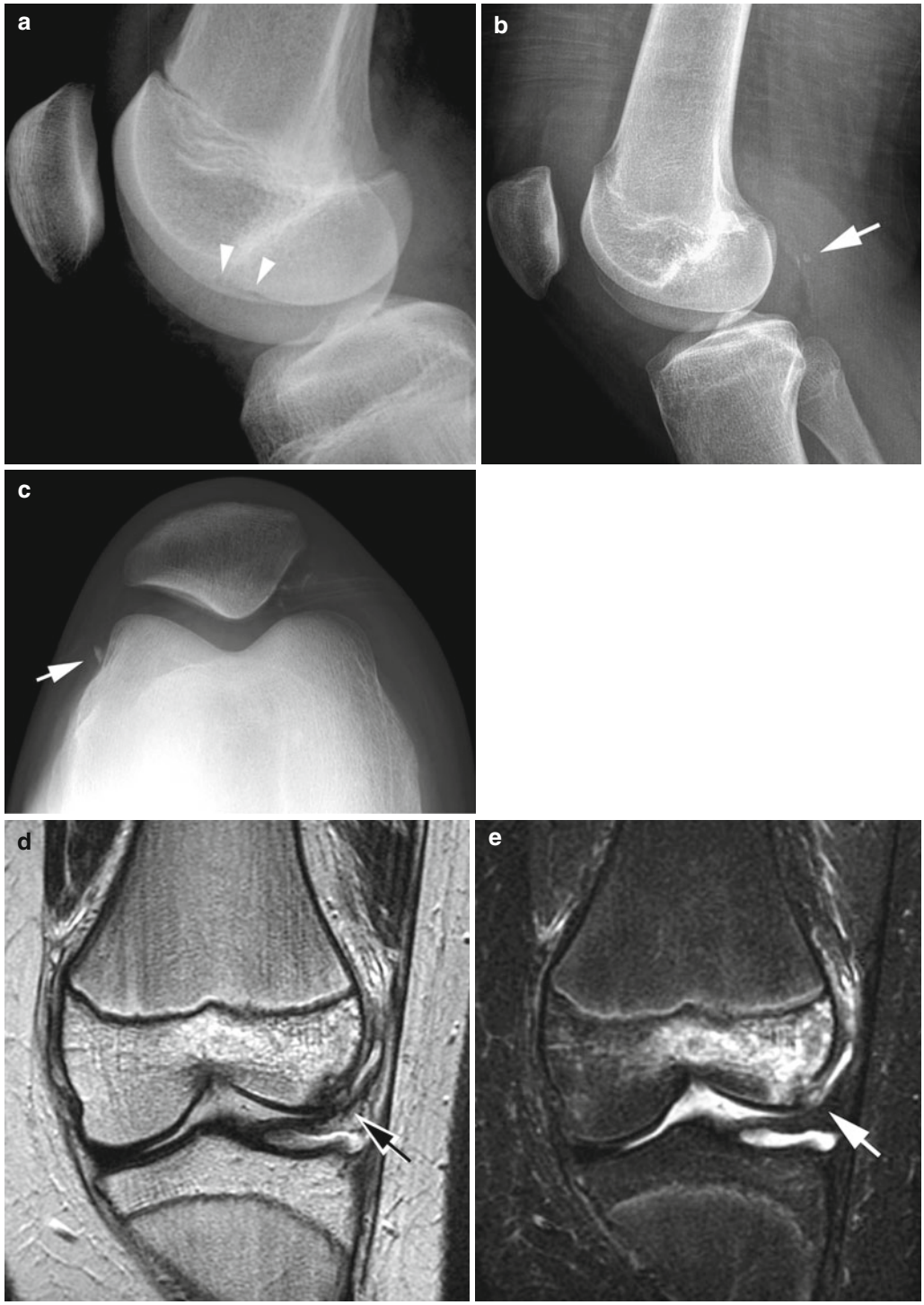


Fig. 10.13 Patellar dislocation with lateral condylar fracture. (**a**) Donor site. Note the subtle defect in surface of the lateral condyle (*arrowheads*) representing the donor site of a lateral condylar avulsion fracture. (**b**) Another patient demonstrates an avulsed fracture fragment in the popliteal bursa (*arrow*). (**c**) In this patient, the avulsed fracture fragment (*arrow*) is in the lateral joint recess. (**d**) Coronal T2 MR image demonstrates the avulsed lateral condylar fracture fragment (*arrow*). A bone bruise also is present in the lateral condyle. (**e**) Coronal STIR image demonstrates the avulsed fracture fragment (*arrow*) with surrounding edema along with a bone bruise in the lateral condyle

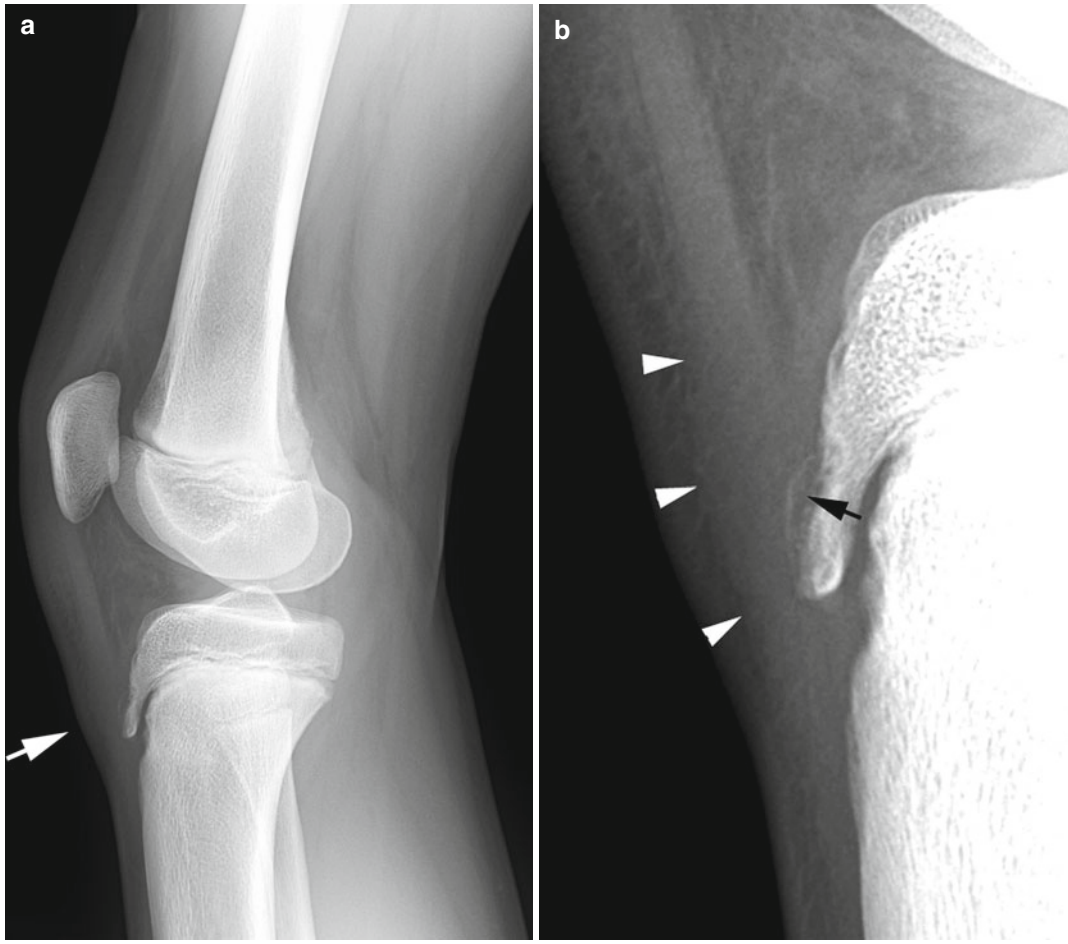


Fig. 10.14 Osgood–Schlatter disease: plain film findings. (**a**) Note soft tissue thickening and indistinctness of the infrapatellar tendon (*arrow*) as it inserts on to the tibial tubercle. A faint avulsed fracture fragment is present. (**b**) Enlarged view more clearly demonstrates the avulsed fracture fragment (*black arrow*). The soft tissue changes also again are visualized (*arrowheads*)

fractures and now are best assessed with MR imaging if there is question of instability. MR imaging clearly demonstrates whether the fragment is displaced or not displaced. Stable osteochondritis dissecans shows lack of fluid intensity deep to the lesion and intact overlying articular cartilage (Fig. 10.21c, d). Signs of instability on MRI in adults, namely, fluid intensity deep to the osteochondral fragment and cyst formation deep to the fragment (Fig. 10.21e, f), are not as reliable in children. Treatment varies from conservative management to arthroscopic fixation of unstable lesions. Loose bodies may be excised.

Meniscal and cruciate ligament injuries are not as common in early childhood as in the adolescent and young child, but they do occur. Plain film findings usually are absent, and most cases subsequently are diagnosed by MR imaging. In terms of meniscal injuries in childhood, a note about the lateral meniscus in children is in order. Often this meniscus is very large and, rather than being C-shaped, assumes a semicircular shape. Consequently, the medial aspect extends almost to the intercondylar notch, and because of this and abnormal mechanics, the meniscus is very prone to tearing. This is termed the discoid lateral meniscus and is best demonstrated with MR

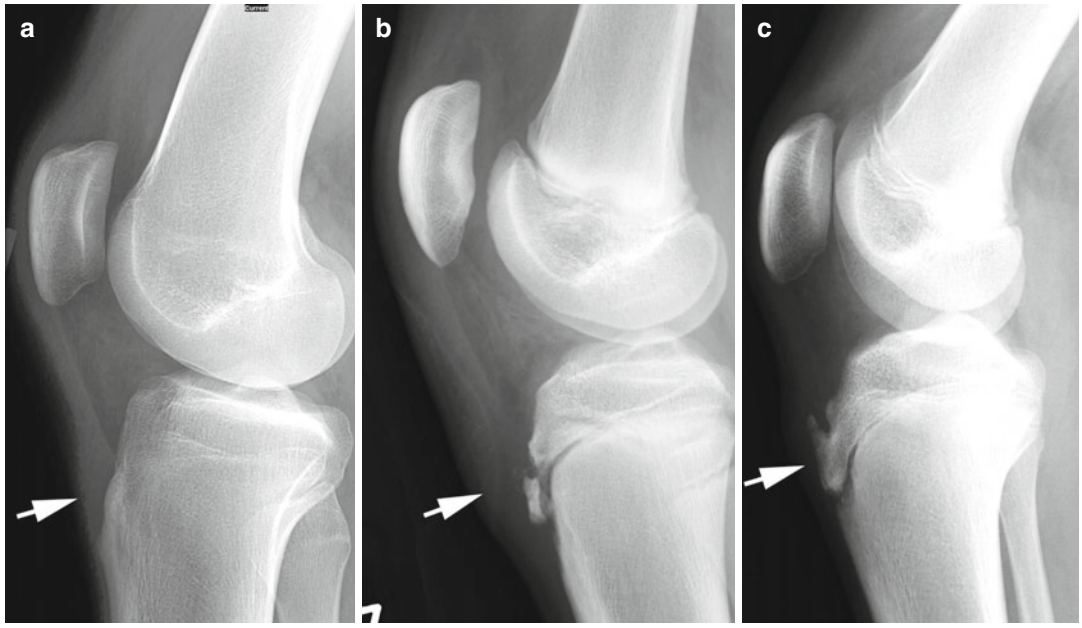


Fig. 10.15 Osgood–Schlatter disease: spectrum of plain film findings. (**a**) In this patient, only thickening of the infrapatellar tendon (*arrow*) is seen. (**b**) This patient demonstrates similar thickening of the infrapatellar tendon and surrounding tissues (*arrow*). Chronic fragmentation of the tibial tubercle is present, and there is a very small avulsion fracture off of the inferior fragment. (**c**) Healed Osgood–Schlatter disease. Note the small exostosis off of the anterior surface of the tubercle (*arrow*)

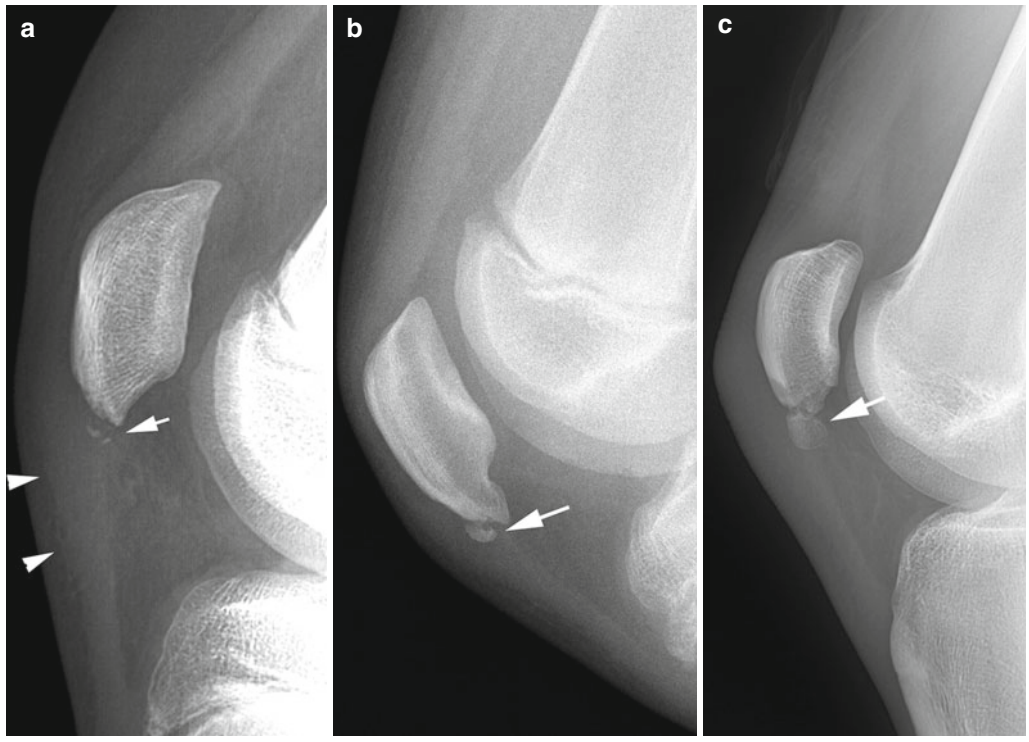


Fig. 10.16 Sinding–Larsen–Johansson disease: spectrum of findings. (**a**) Note thickening of the patellar tendon (*arrowheads*) as it inserts on to the patella. In addition, note a small avulsed fracture fragment (*arrow*). (**b**) In this patient, the avulsed fracture (*arrow*) fragment is partially healed. Tendon thickening is minimal. (**c**) In this patient with basically healed Sinding–Larsen–Johansson disease (*arrow*), there still is a little anterior soft tissue swelling

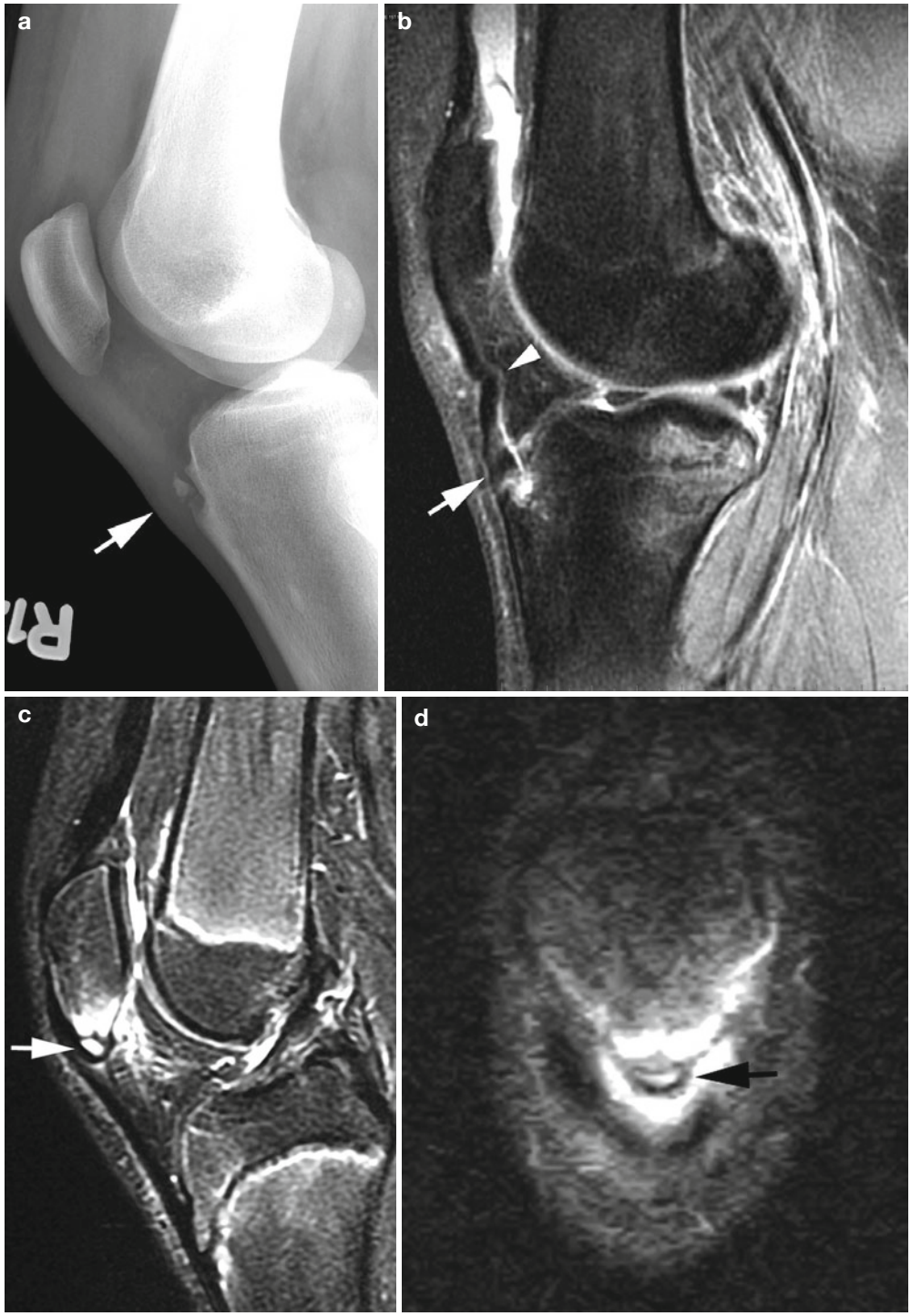


Fig. 10.17 Osgood–Schlatter disease and Sinding–Larsen–Johansson disease: MR findings. (**a**) In this patient with *Osgood–Schlatter disease*, an avulsed bony fragment is seen along with slight swelling in the area (*arrow*). (**b**) Sagittal STIR MR image demonstrates the low-signal bony fragment (*arrow*) along with some high-signal fluid posterior and inferior to the avulsed fracture fragment. The infrapatellar tendon is buckled (*arrowhead*). (**c**) *Sinding–Larsen–Johansson disease*. Sagittal STIR image of the knee. Note the high signal in the avulsed bony fragment (*arrow*); there also is high signal in the inferior patella and in the superior part of the infrapatellar fat pad. (**d**) Coronal STIR image of the patella. Note high signal in the avulsed bony fragment (*arrow*). High signal is present inferior to the fragment and in the adjacent patella

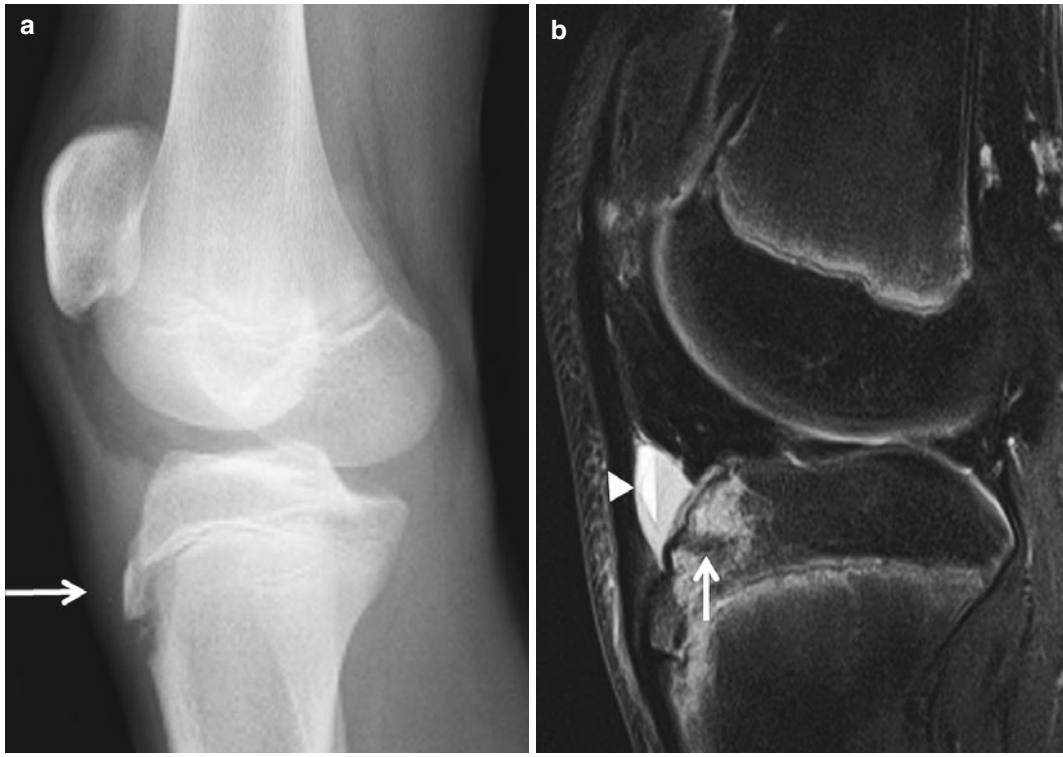


Fig. 10.18 Osgood–Schlatter mimic. (**a**) Lateral radiograph of the knee shows soft tissue swelling over the tibial tuberosity with mild fragmentation (*arrow*) suggesting Osgood–Schlatter disease. (**b**) Sagittal PD-weighted image with fat saturation shows normal patellar tendon and an incomplete fracture of the proximal tibial epiphysis (*arrow*). A blood–fluid level is present in the deep infrapatellar bursa (*arrowhead*)

imaging (Fig. 10.22a–c). The most common type of tear in a discoid meniscus is a degenerative horizontal cleavage tear. In one study [24], 69.5 % of discoid menisci demonstrated a meniscal tear at arthroscopy.

A detailed dissertation of all of the findings associated with meniscal tears and other meniscal abnormalities is beyond the scope of this book, and most are similar to the problem seen in adults. Of importance in evaluating these tears, however, is determining whether the suspected tear reaches the articular surface [25]. In addition, with bucket-handle tears, the usual bowtie configuration of the meniscus is lost [26]. Joint effusions are common as are bone bruises. Some of these findings are demonstrated in Figs. 10.22d–f and 10.23.

Anterior cruciate and, to a far lesser extent, posterior cruciate ligament tears appear the same as they do in adults. Most of these tears occur in older children, and adolescents and the findings range from ligament sprain through total rupture, with or without avulsion of the tibial tubercle. Thereafter, MR is obtained and clearly demonstrates sprains through complete tears and bone bruises (Fig. 10.24). Associated fractures can be seen involving the anterior tibial spine and the upper tibial Segond fracture (Fig. 10.25). A Segond fracture is an avulsion at the tibial attachment of the lateral capsular ligament and is associated with ACL tears in more than 90 % of the cases. ACL tears are often associated with posterolateral corner injuries.

Posterior cruciate ligament injuries are far less common. The quadriceps tendon along with the infrapatellar tendon can be injured other than when they are injured with Osgood–Schlatter or Sinding–Larsen–Johansson diseases. Very often on plain films, the fact that the tendon is disrupted is visible, but eventually the injury is defined with MR imaging. However, ultrasound also can demonstrate tears in these tendons [27].

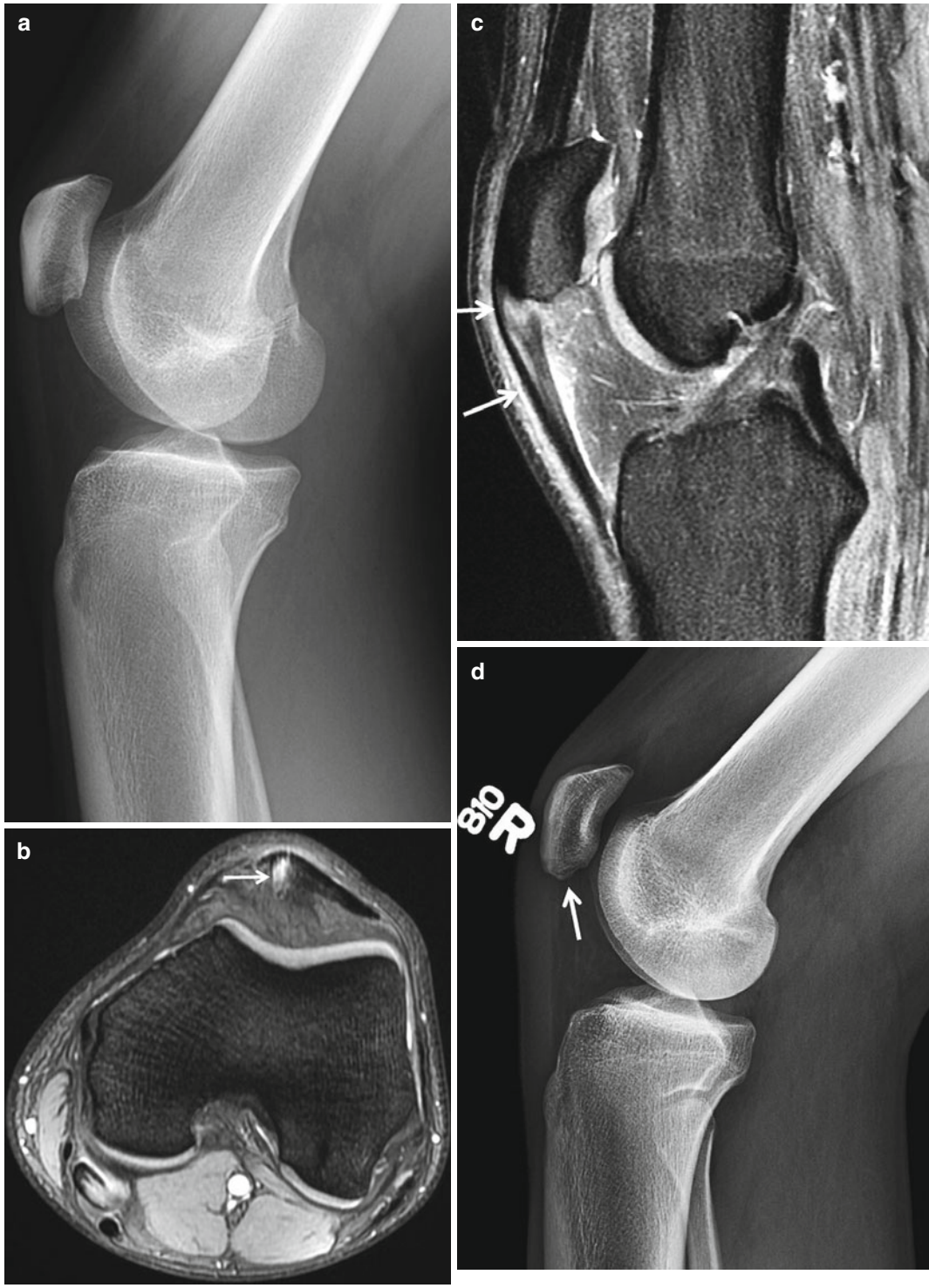


Fig. 10.19 Jumper's knee. (**a**) Normal lateral radiograph in a teenager with knee pain. (**b**) Axial T2-weighted gradient image shows a focal partial thickness tear of the medial aspect of the infrapatellar tendon (*arrow*). (**c**) Sagittal PD-weighted image with fat saturation confirms edema within and surrounding the infrapatellar tendon (*arrows*) consistent with patellar tendonitis. (**d**) Lateral radiograph in a teenager with acute onset of knee pain after an injury. This was reported as normal. On retrospect, there is suggestion of a sleeve avulsion at the inferior patellar pole (*arrow*). (**e**) Sagittal PD-weighted image with fat saturation shows the sleeve fracture and adjacent edema in the infrapatellar fat pad of Hoffa (*arrow*)

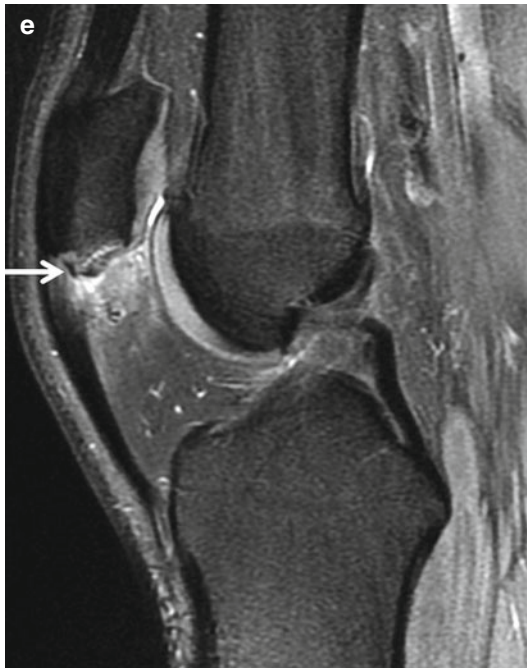


Fig. 10.19 (continued)

An uncommon problem related to trauma around the knee is rupture of the synovium of the knee joint. In such cases, chronic extrasynovial fluid collections can extend deep into the calf, and the clinical findings can be confused with deep vein thrombosis. Ultrasonography is invaluable in these cases because it demonstrates the fluid collection resulting from synovial rupture. By the same token, it is also useful in the detection of deep vein thrombosis.

MRI is also useful in certain unique situations. In case of Salter–Harris injuries that fail to reduce satisfactorily or do not heal, an MRI may show soft tissue interposition in the widened physis which needs open reduction (Fig. 10.26a, b). MRI is also indicated after knee trauma if there are symptoms of locking to evaluate for loose bodies and/or internal derangement (Fig. 10.26c, d).

Normal Findings Causing Problems

One of the more common normal findings around the knee is irregularity of the distal femur, just along the medial supracondylar ridge as seen on lateral views of the knee (Fig. 10.27a). It occurs most commonly in older children and adolescents and should not be misinterpreted as an area of osteomyelitis or a bone tumor. The irregularity occurs along the line of muscle insertion of the adductor magnus muscle [28] or the origin of medial head of gastrocnemius. There is histologic support for the concept that this lesion results from chronic avulsion [29] and, depending on the degree of healing, the lesion can appear quite ragged and even somewhat scalloped (Fig. 10.27c, d). More recently, this lesion/phenomena has been referred to as a desmoid. These irregularities also are seen on CT and MR imaging (Fig. 10.27b–e).

Benign cortical (fibrous) defects can be found in any of the long bones and frequently are multiple. However, they most commonly occur in the distal femur and proximal tibia and characteristically are eccentric and very peripheral (cortical) in location. They seldom extend beyond a half centimeter or so into the medullary cavity of the bone (see Fig. 3.5). Benign cortical defects are related to the somewhat larger benign nonossifying fibroma. This lesion also is eccentric but often more definitely corticated and larger than a benign cortical defect (see Fig. 3.5d). In a few cases, benign cortical defects appear very cystic and possess a thin outer cortex. In such cases, normal muscle pull on the cortex can cause acute avulsion and fragmentation (see Fig. 3.6).

In older children, the tibial tubercle has a normal defect along its inferior aspect. On lateral view, this defect is not difficult to interpret, but on frontal view, it can be mistaken for a lytic lesion of the knee (Fig. 10.28a, b). In young infants, the tibial tubercle is not ossified at all, and a scoop-like bony defect in the area can present a problem (Fig. 10.28c).

The patella is very prone to irregular ossification, and a number of peculiar irregularities and deformities can encountered. Some of these are very fracture-like in appearance, but very often the same configuration is present on the other side, and this solves the problem (Fig. 10.29a). Another common normal ossification anomaly of the patella is the bipartite or tripartite patella. In these cases, the extra portion of the patella usually lies in the upper outer quadrant, and very often

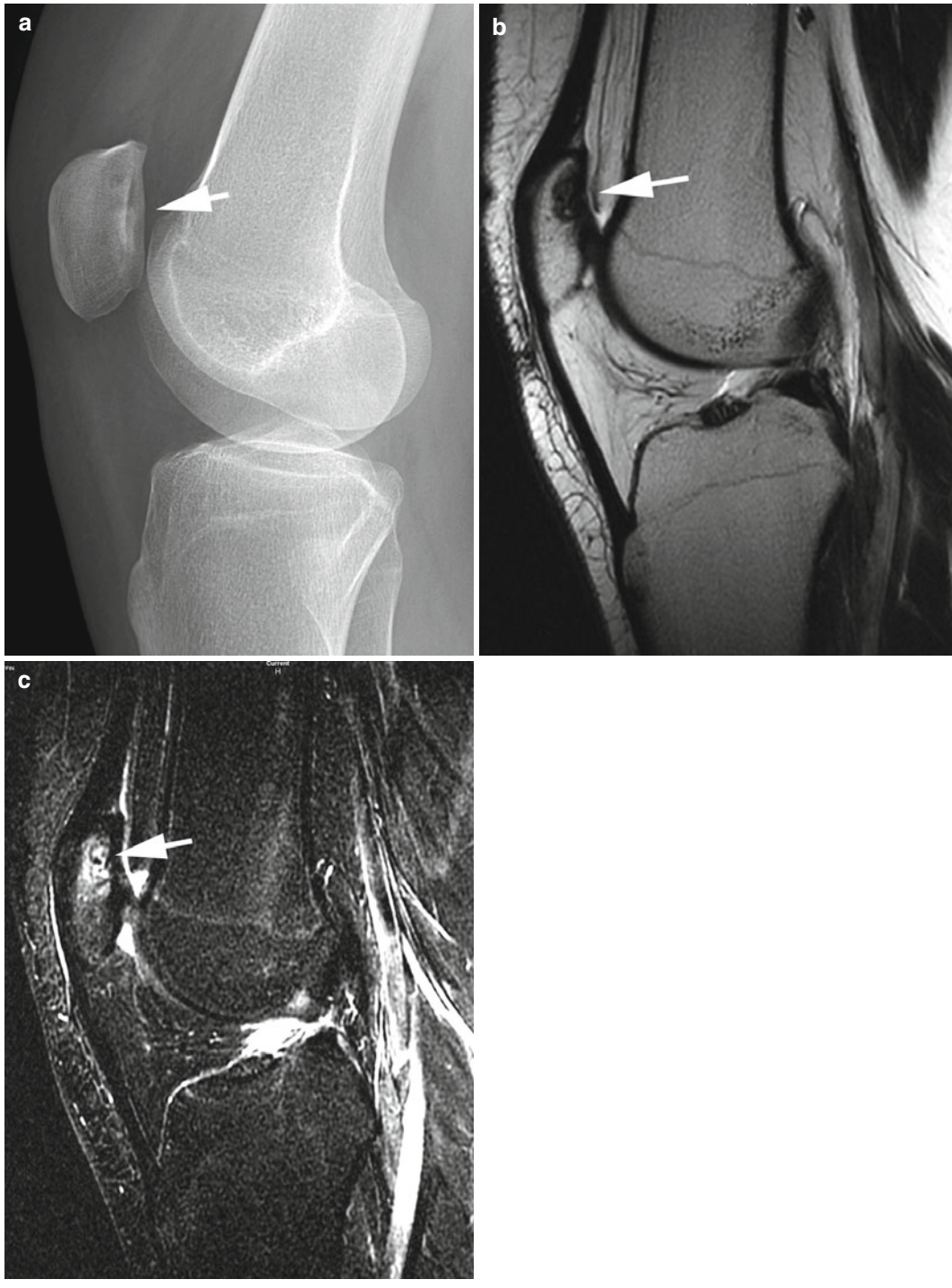


Fig. 10.20 Chondromalacia of the patella. (**a**) Note the defect (*arrow*) over the posterior surface of the patella. (**b**) T1-weighted sagittal image demonstrates low signal in the defect (*arrow*). (**c**) Sagittal STIR image demonstrates irregular (edema) increase signal around the defect (*arrow*)

the anomaly is bilateral (Fig. 10.29b). Finally, a normal dorsal defect of the patella [30, 31] should not be confused with a lesion such as osteomyelitis or osteochondritis dissecans (Fig. 10.30).

Another irregular normal ossification pattern of the patella is when there is a small fleck of bone over the anterior, usually inferior surface (Fig. 10.31a). This finding very closely mimics an avulsion fracture. However, in normal cases, there will not be any soft tissue swelling over the patella. Another finding around the knee is the fabella, a normal accessory ossification center in the gastrocnemius tendon. It is visualized on lateral view over the posterior knee.

Finally the distal femoral epiphysis frequently ossifies irregularly and can appear very disturbing to the uninitiated (Fig. 10.31b). These irregularities are common in infants and young children. Another normal finding causing problems is medial beaking of the distal femoral metaphysis,

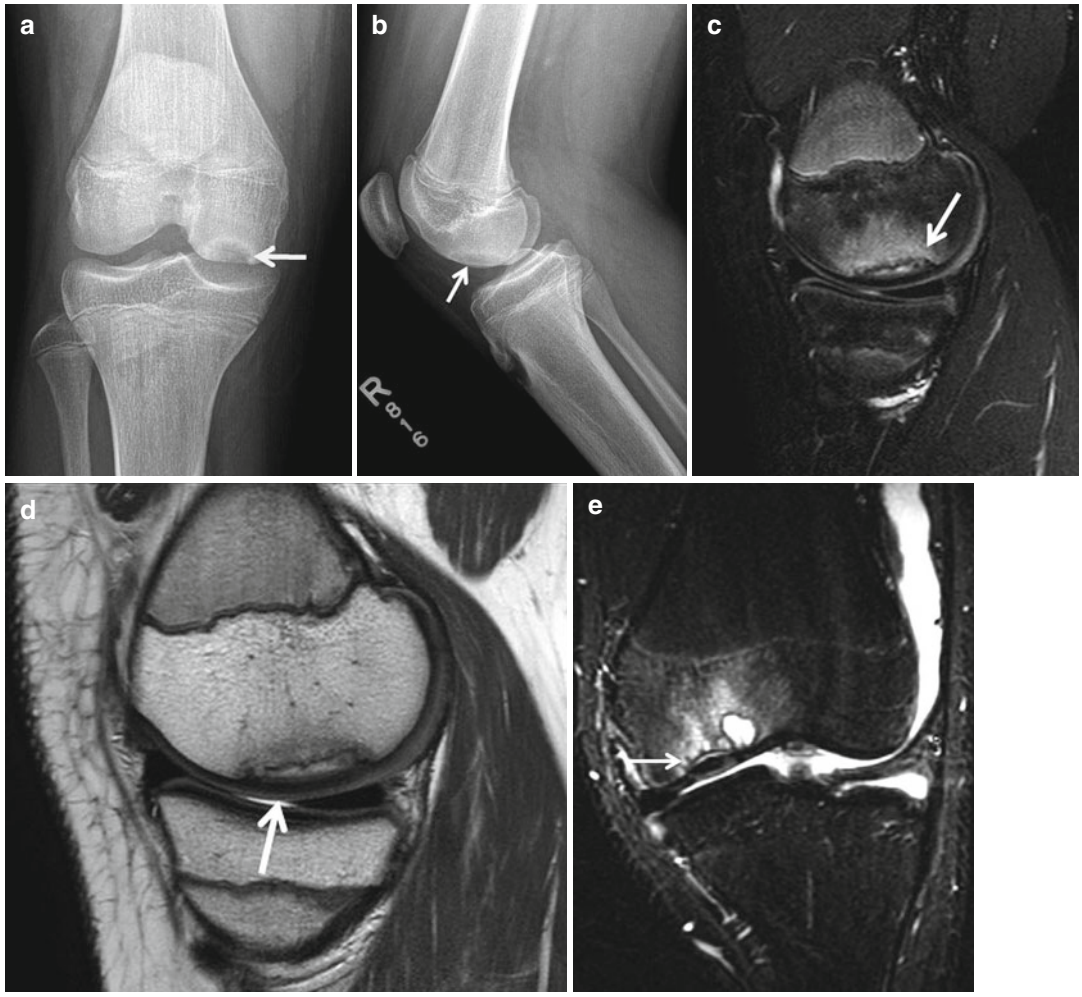


Fig. 10.21 Osteochondritis dissecans: stable. (**a**) Frontal and (**b**) lateral radiographs of the right knee show a large defect in the anteromedial femoral condyle at the articular surface (*arrows*). (**c**) Sagittal T2-weighted image with fat saturation shows edema in the OCD fragment and bone deep to it but no fluid signal at the interface (*arrow*). (**d**) Sagittal PD-weighted image shows intact overlying articular cartilage (*arrow*). (**e**) Another patient. Unstable. Coronal STIR image shows osteochondritis dissecans involving the medial femoral condyle. Note the fluid signal deep to the fragment, bone edema, as well as cystic changes suggesting instability. (**f**) The osteochondral fragment is mildly displaced posteriorly (*arrow*) on this sagittal STIR image confirming instability

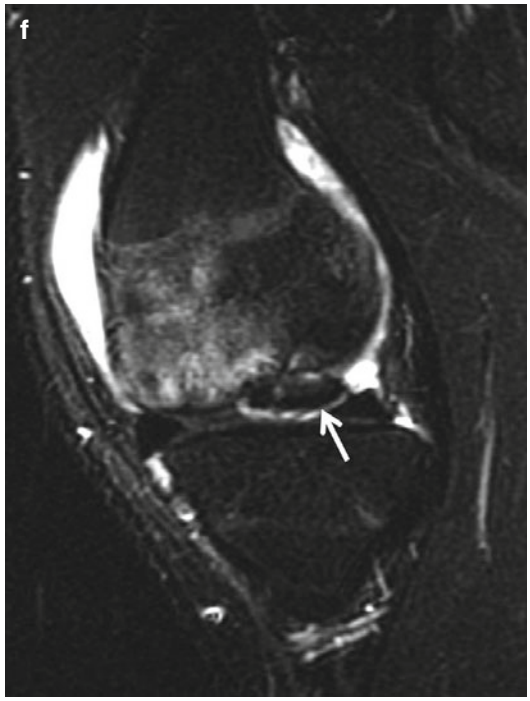


Fig. 10.21 (continued)

and occasionally the upper tibial metaphysis in patients with bowlegs. This subject is addressed (see Fig. 12.6).

Injuries of the Lower Leg (Midshafts of the Tibia and Fibula)

Overt fractures of the midshafts of the tibia and fibula are not difficult to recognize. It should be noted, however, that such fractures show a distinct tendency to occur in the tibia and less often in the fibula (Fig. 10.32), but plastic bending fractures do occur in the fibula. These fractures are more common than generally appreciated [32], and furthermore they often are subtle. Bending usually occurs inwardly, but outward bending also can occur. Overall, however, it must be remembered however that normal inward bending of the fibula is common, and therefore, comparative views are very important for the detection of the more subtle of these injuries (Fig. 10.33).

In young infants, a very common fracture of the tibia is the so-called toddler fracture [33]. This fracture characteristically is a spiral, hairline fracture and often is invisible, or nearly invisible, on initial radiographs (Fig. 10.34). It behaves almost like a stress fracture, and even in those cases where it is visible, it often appears clearer on one view than the other. In addition, one often detects this fracture somewhat fortuitously. The reason is that pain cannot be adequately localized clinically and very often ankle films are obtained rather than long bone films. In this regard, images of the ankle include an oblique view, and it is on this view that very often one can see the fracture. Another problematic finding with these fractures arises when they are seen in the healing phase where periosteal new bone deposition often first suggests a tumor such as Ewing's sarcoma (Fig. 10.35). A somewhat similar fracture has been recorded in ballet dancers [34]. Occasionally similar fractures in the tibia can be more vertical [35]. We have arbitrarily named the Dunbar toddler fracture as the toddler fracture type I and the hyperextension-induced upper tibia injury [2, 3, 36] as toddler fracture II.

Stress fractures of the tibial shaft and occasionally of the fibular shaft are not uncommon, but they occur in older children and adolescents. They usually present with focal areas of sclerosis, with or without a visible transverse fracture line (Fig. 10.36). In those cases where no fracture is seen, MR is especially useful in identifying the injury or in substantiating the fracture where plain film findings are positive (Fig. 10.36b–d).

Normal Findings Causing Problems

About the only normal finding in the midshaft of the tibia or fibula that can be confused with an underlying lesion is a normal vascular groove (Fig. 10.37). These vascular grooves appear no different from those in other long bones, but in the tibia, they can be misinterpreted as a spiral toddler type fracture.

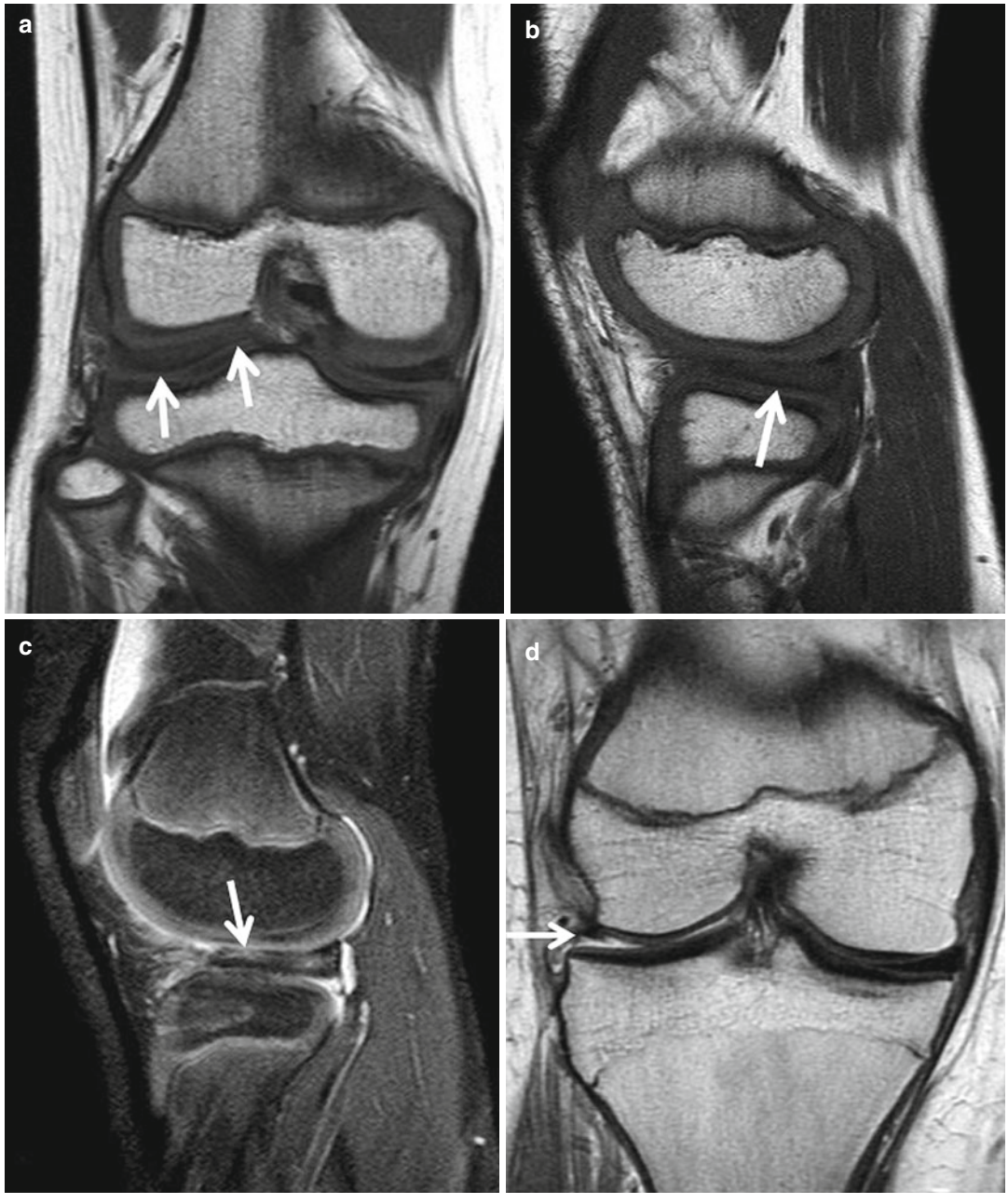


Fig. 10.22 Meniscal injuries. (**a**) Discoid meniscus with degenerative tear. Coronal PD-weighted image shows a discoid lateral meniscus reaching the intercondylar notch (*arrows*). Note the abnormal increased signal within the lateral meniscus when compared to the normal medial meniscus. (**b**) Sagittal PD-weighted image shows the discoid meniscus with abnormal increased signal (*arrow*) consistent with a degenerative tear. (**c**) Sagittal PD-weighted image with fat saturation confirms the high signal tear reaching the superior articular surface (*arrows*). (**d**) Radial tear. Coronal PD-weighted image shows absent meniscus in the region of the body consistent with a complete radial tear affecting the entire width of the meniscus. Only the lateral edge of the meniscus (*arrow*) is present. (**e**) Sagittal PD-weighted image in another patient shows a radial tear of the body of the lateral meniscus (*arrow*). (**f**) Axial GRE image in another patient demonstrates extensive radial tears of the lateral meniscus (*arrows*)

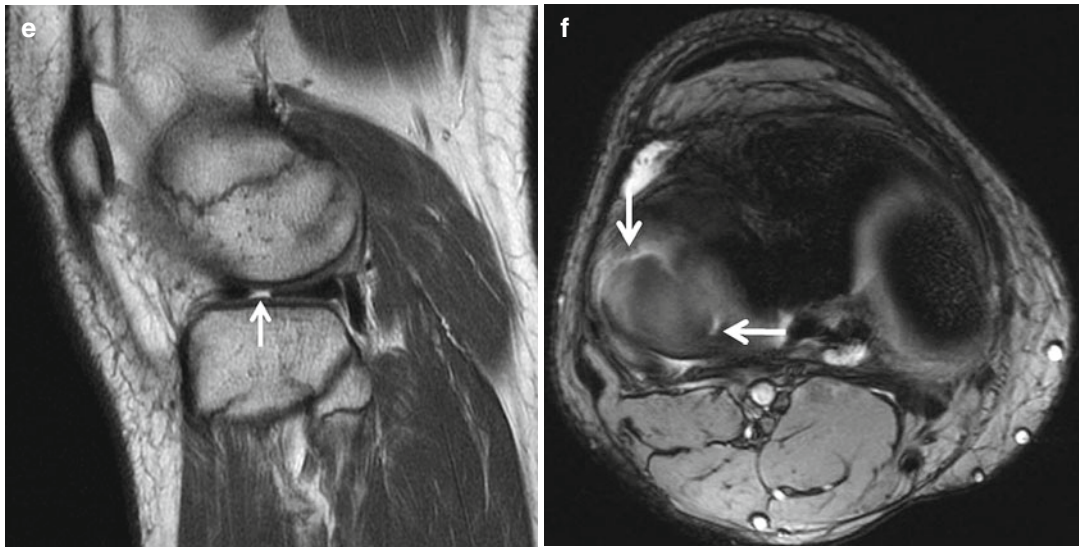


Fig. 10.22 (continued)

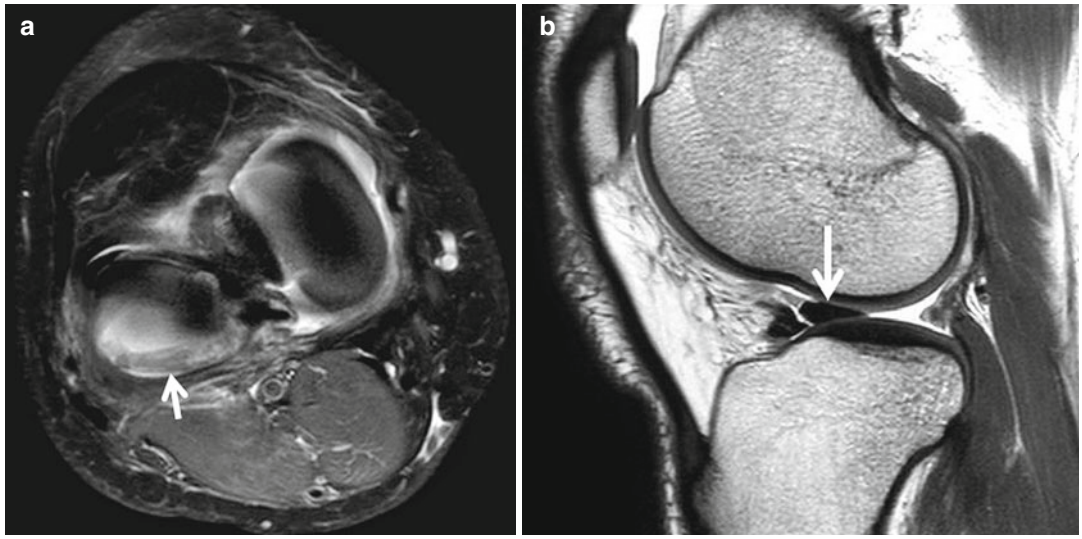


Fig. 10.23 Meniscal injuries. (**a**) Flipped meniscus. Axial T2-weighted image with fat saturation shows an absent posterior horn of the lateral meniscus (*arrow*). (**b**) Sagittal PD-weighted image shows that the posterior horn is flipped anteriorly (*arrow*) and lies posterior to the anterior horn. (**c**) Bucket-handle tear. Coronal STIR image in a 16-year-old shows a bucket-handle tear of the medial meniscus with the medial aspect of the meniscus displaced into the intercondylar notch (*arrow*). Only the peripheral portion of the meniscus remains in situ (*arrowhead*). (**d**) Sagittal T2-weighted image through the intercondylar notch shows the "double PCL sign" of a bucket-handle tear. The pseudo PCL is the displaced portion of the medial meniscus (*arrow*). A large joint effusion is also seen

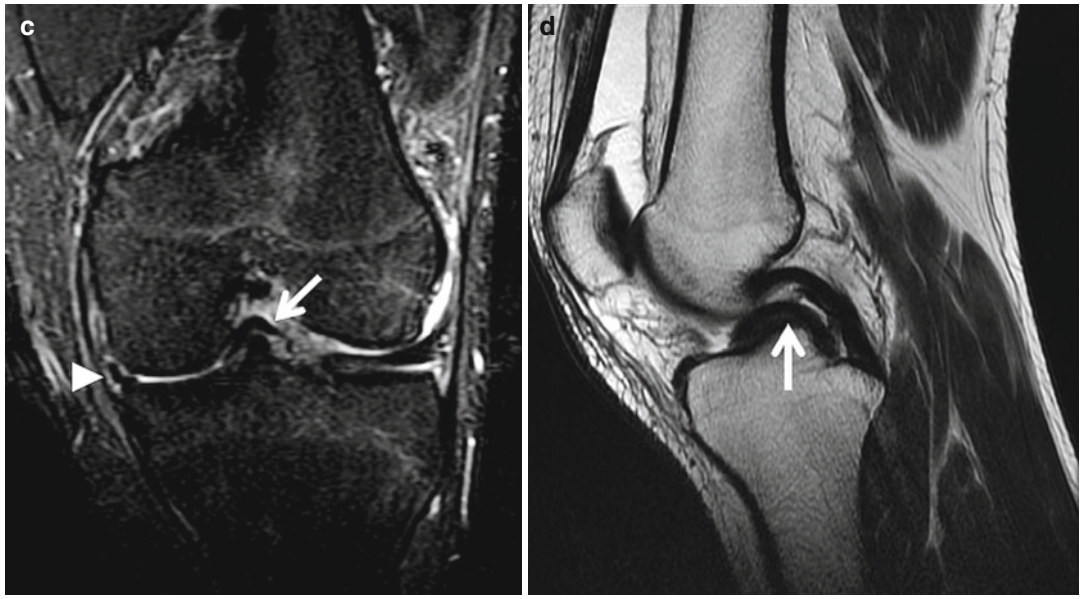


Fig. 10.23 (continued)

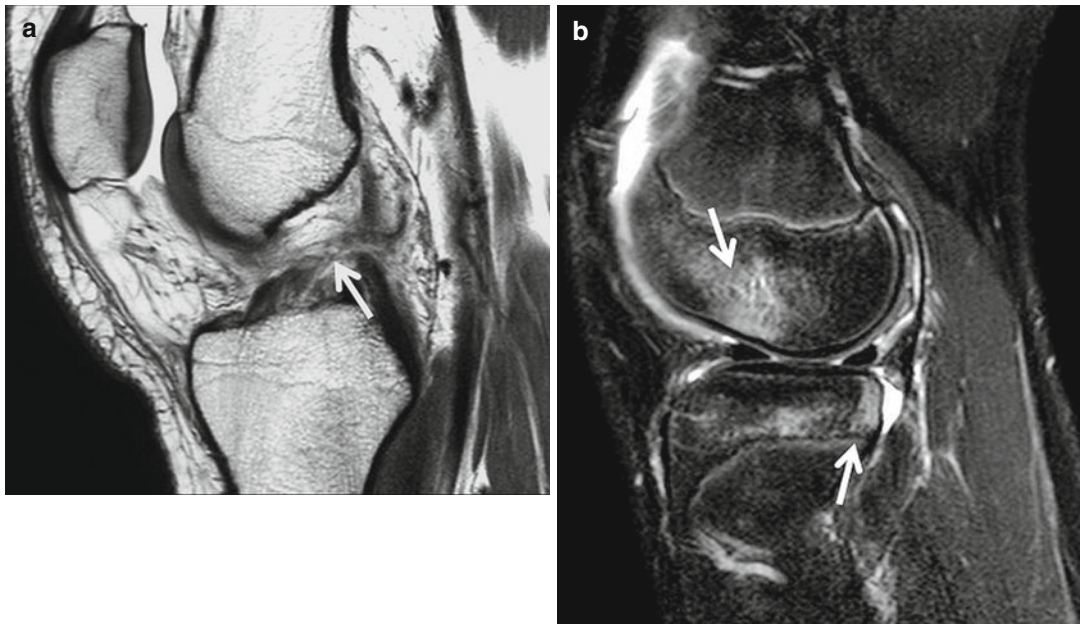


Fig. 10.24 ACL tears. (**a**) Sagittal PD-weighted image at the level of the intercondylar notch shows a complete ACL tear through its mid-substance (*arrow*). (**b**) Bone contusion pattern: anterior cruciate ligament injury. Note the classic contusion pattern consisting of posterolateral tibia and anterolateral femoral epiphyseal contusions (*arrows*)

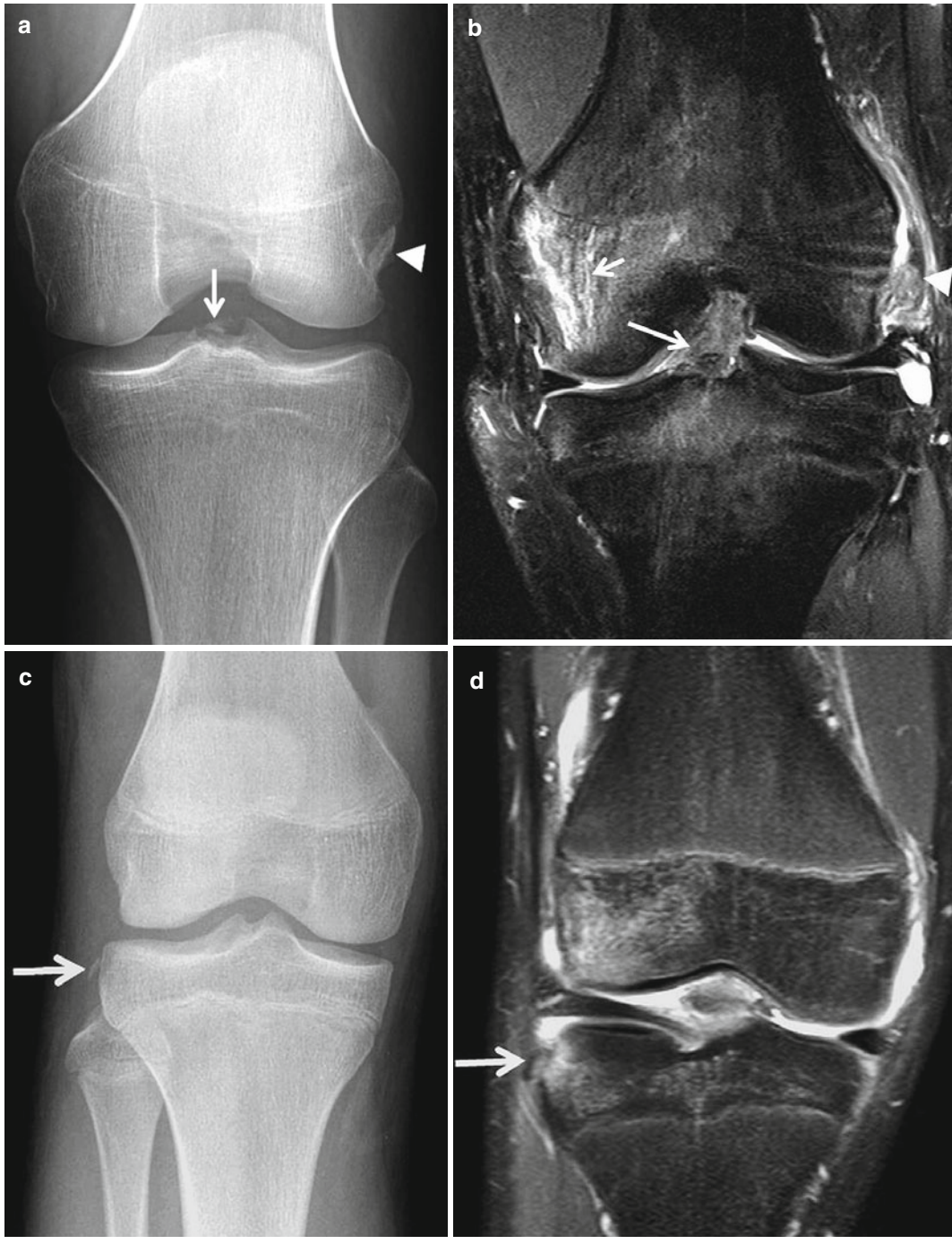


Fig. 10.25 ACL tears: associated fractures. (**a**) Anterior tibial spine fracture. Frontal radiograph demonstrates avulsion of the medial tibial spine at the tibial insertion of the ACL (*arrow*) and at the origin of the popliteus over the lateral femoral condyle (*arrowhead*). (**b**) Coronal T2-weighted image with fat saturation shows the avulsion of the tibial spine with increased signal in the ACL attached to it (*long arrow*). Popliteus avulsion is also confirmed (*arrowhead*). In addition, there is a large bone contusion in the medial femoral condyle (*short arrow*). (**c**) Segond fracture. Frontal radiograph shows a classic Segond avulsion fracture (*arrow*) from the lateral margin of the proximal tibia below the joint line. Due to a strong association of Segond fracture with ACL tear, an MRI was obtained. (**d**) Coronal PD-weighted image with fat saturation shows the Segond fracture (*arrow*). ACL tear in this patient is shown in Fig. 10.24**a**

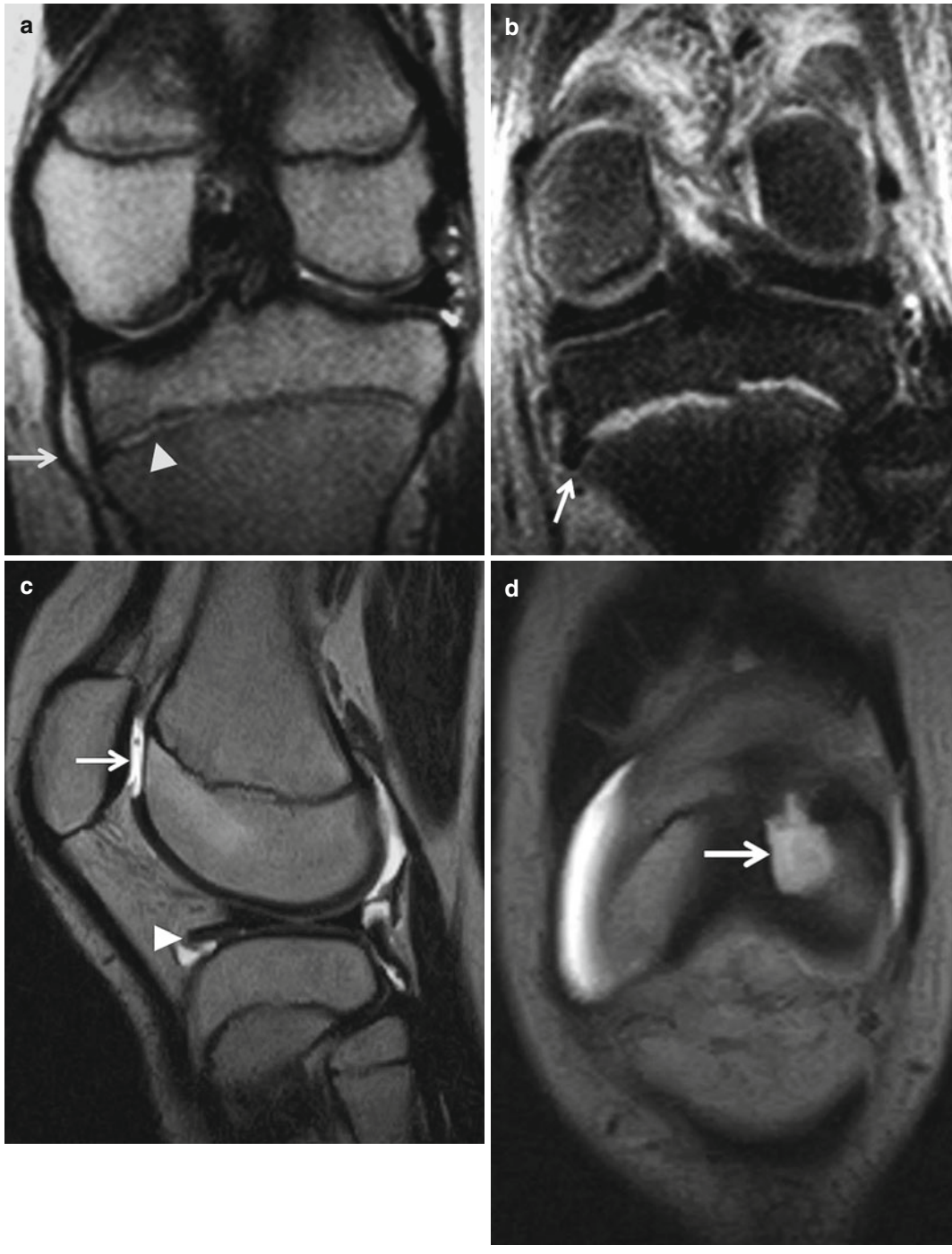


Fig. 10.26 MRI: Other uses in the knee. (**a**) Impaired Salter–Harris fracture healing. Coronal T2-weighted image shows a lax medial collateral ligament (*arrow*) suggesting a distal tear. The medial aspect of the proximal tibial physis also is widened suggesting Salter–Harris fracture (*arrowhead*). (**b**) Coronal STIR image shows torn periosteum interposed into the widened medial aspect of the tibial physis (*arrow*) preventing satisfactory reduction. (**c**) Sagittal T2-weighted image in another patient with history of blow to the knee. A large chondral defect is noted in the lateral facet of the trochlea (*arrow*) with a cartilaginous loose body (*arrowhead*) adjacent to the anterior horn of the lateral meniscus. (**d**) Coronal T2-weighted image shows the large chondral defect in the lateral facet of the trochlea (*arrow*)

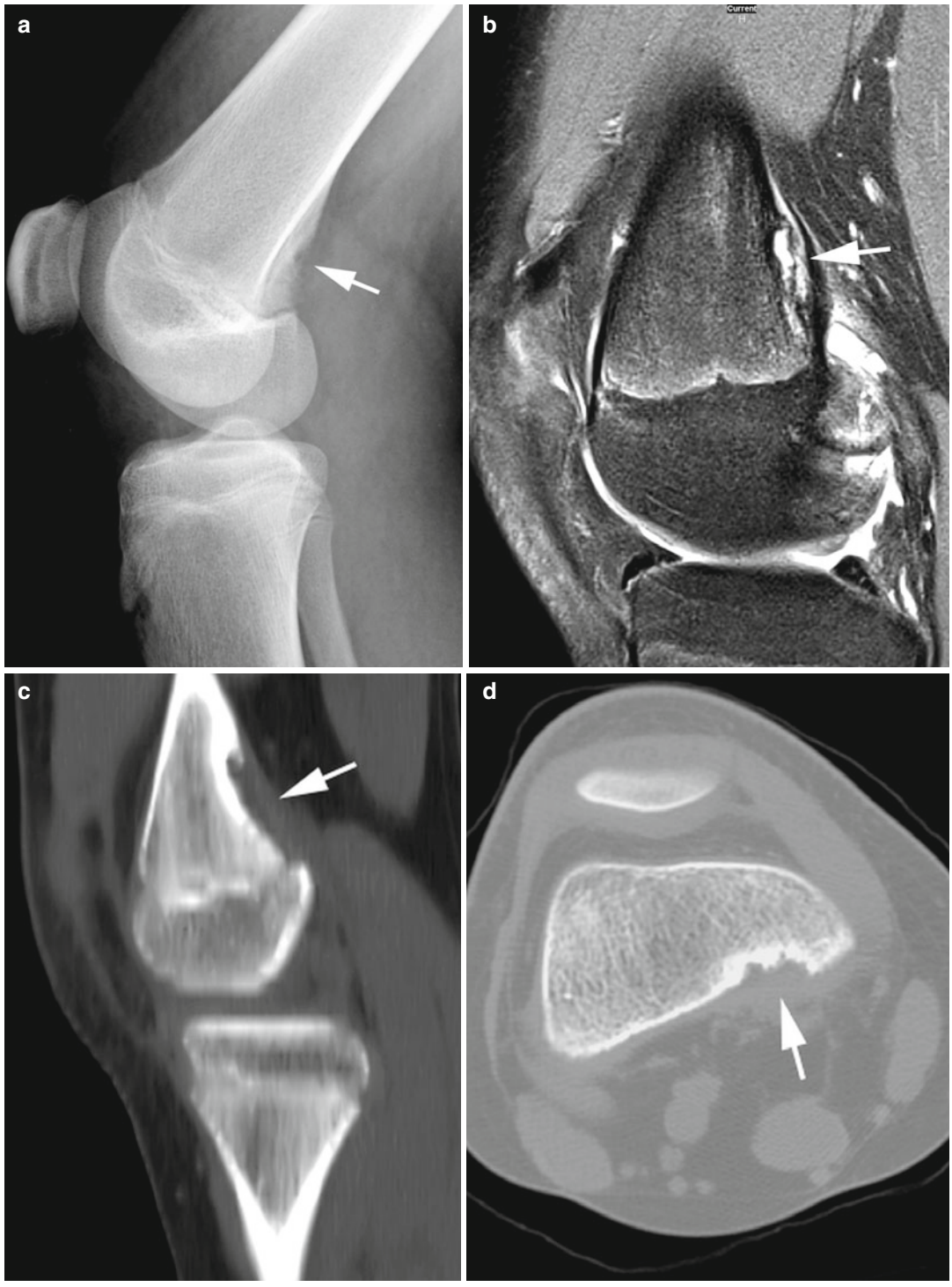


Fig. 10.27 Normal posteromedial femoral irregularity. (**a**) Note the irregular bony cortex (*arrow*) over the medial/posterior aspect of the distal femur. (**b**) Sagittal STIR image demonstrates increased signal at the site of irregularity (*arrow*). (**c**) Another patient whose sagittal CT study demonstrates a concave scooped-out area (*arrow*). (**d**) Axial view in the same patient demonstrates the same findings (*arrow*). (**e**) Axial T2 image demonstrates multiloculated increases signal in the area (*arrow*)

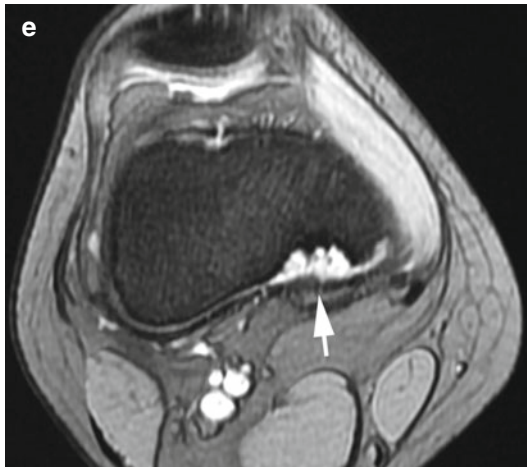


Fig. 10.27 (continued)

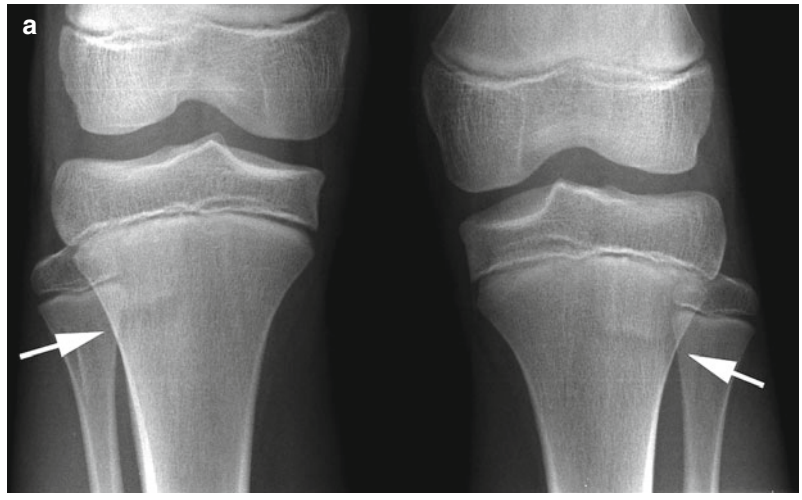
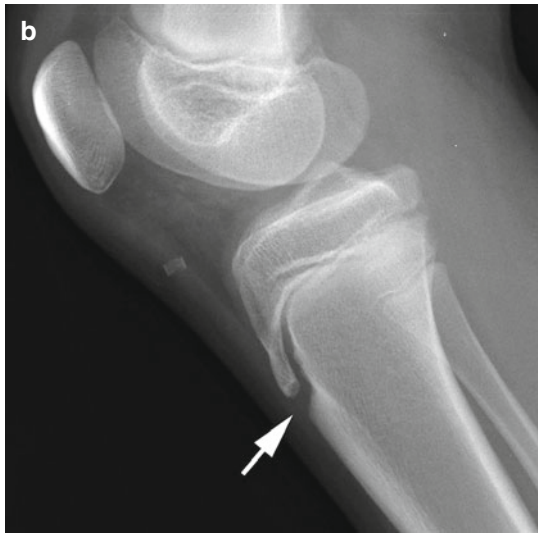


Fig. 10.28 Normal tibial tubercle: pseudofracture. (**a**) Note lucencies through the upper tibias (*arrows*) which might be misinterpreted as fractures. (**b**) Actually they represent the space between the tibial tubercle and the upper tibia (*arrow*). (**c**) Anterior scooping of the upper tibia. Anterior scooping (*arrow*) is normal. It must be differentiated from increased scooping seen with hyperextension toddler II fractures. In this regard, the absence of edema around the scooping is consistent with normality



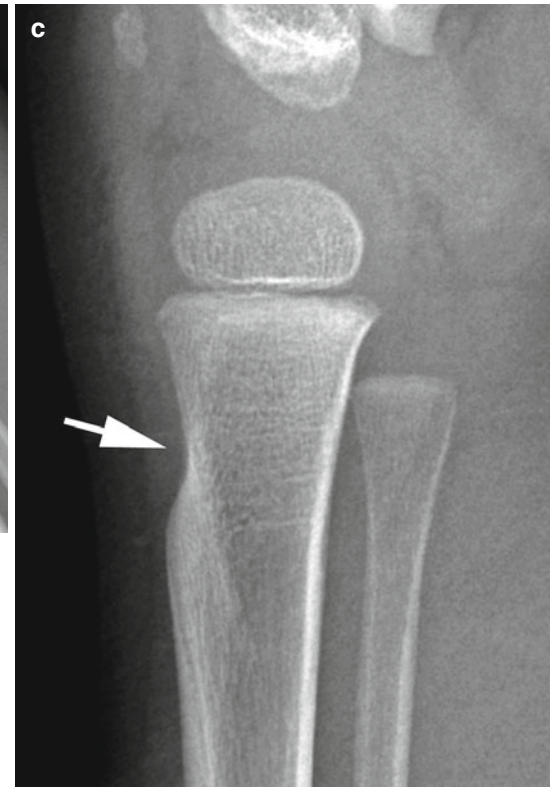


Fig. 10.28 (continued)

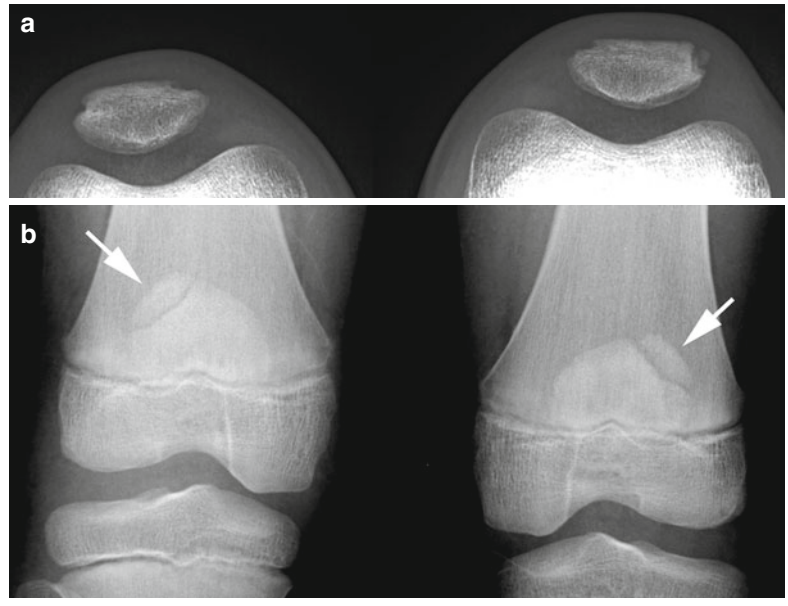


Fig. 10.29 Patella: pseudopathology configurations. (**a**) Patellar ossification irregularity. Note bilateral cortical irregularity of the patellae. On the right, the small fragment should not be misinterpreted as an avulsion fracture because there is no swelling around the site. (**b**) Bilateral typical bipartite patellae (*arrows*)

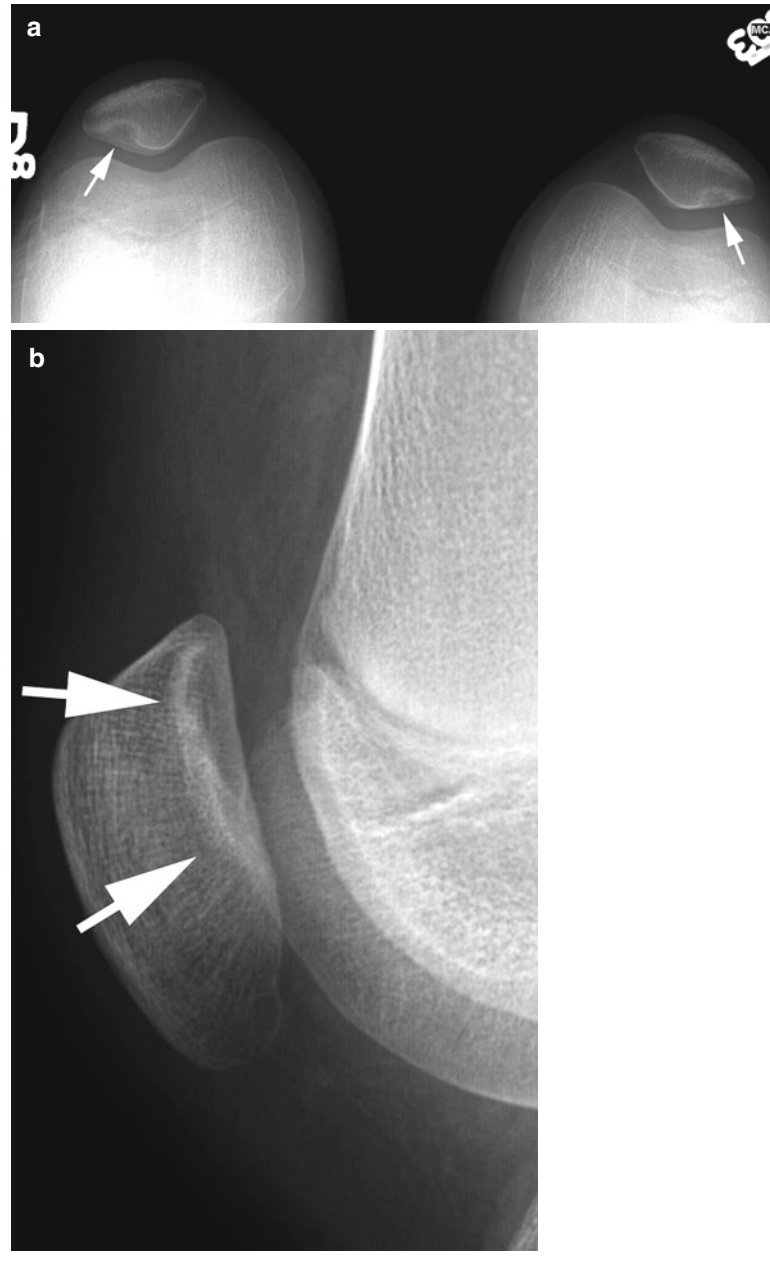


Fig. 10.30 Normal posterior defect of patella (*arrows*). (**a**) Note round defects in both patellae (*arrows*). (**b**) Lateral view demonstrates the thickened cortex through the base of the defect (*arrows*) of one in one of the patellae

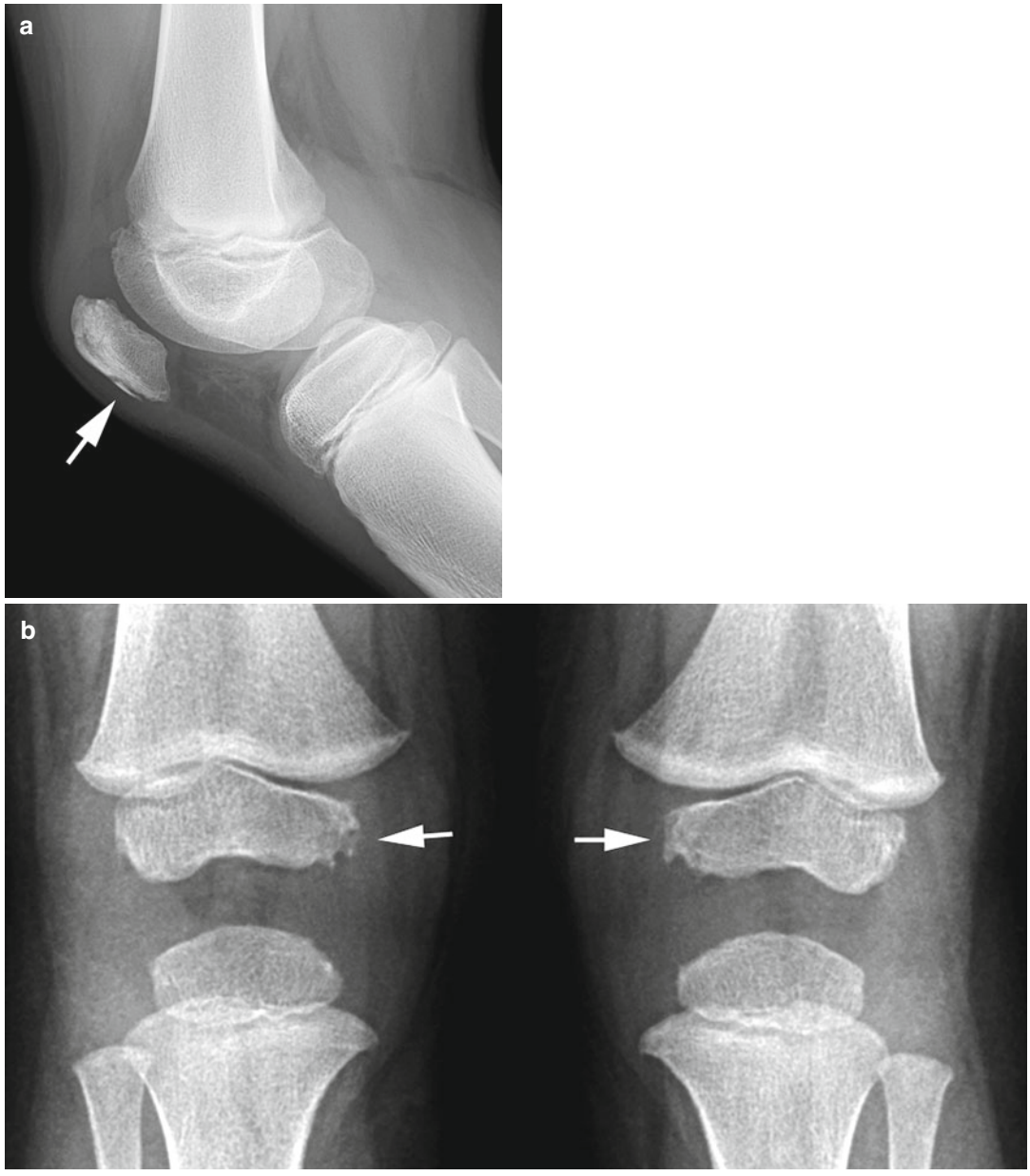


Fig. 10.31 Knee pseudofractures. (**a**) Note the secondary center (*arrow*) over the anterior patella. This is a very common finding and should not be misinterpreted for a fracture. (**b**) Irregularity of both distal femoral epiphyses, especially medially (*arrows*), is normal

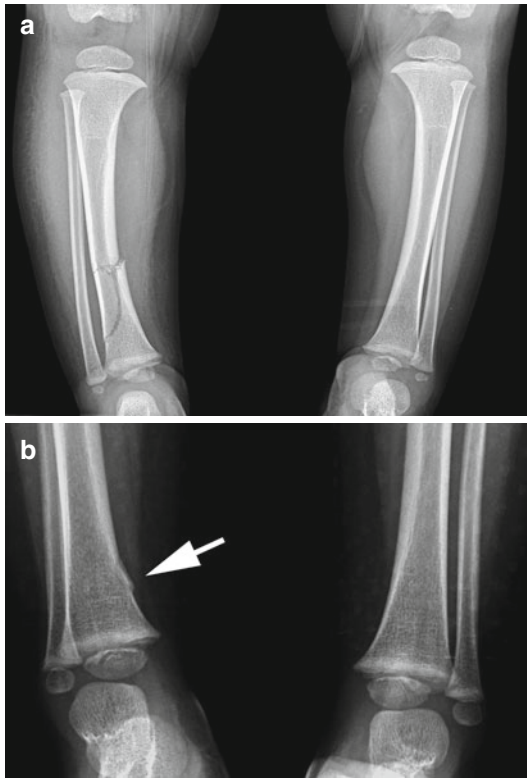


Fig. 10.32 Lower extremity fractures. (**a**) Typical comminuted tibial fracture. (**b**) Subtle buckle fracture (*arrow*) through the distal tibia

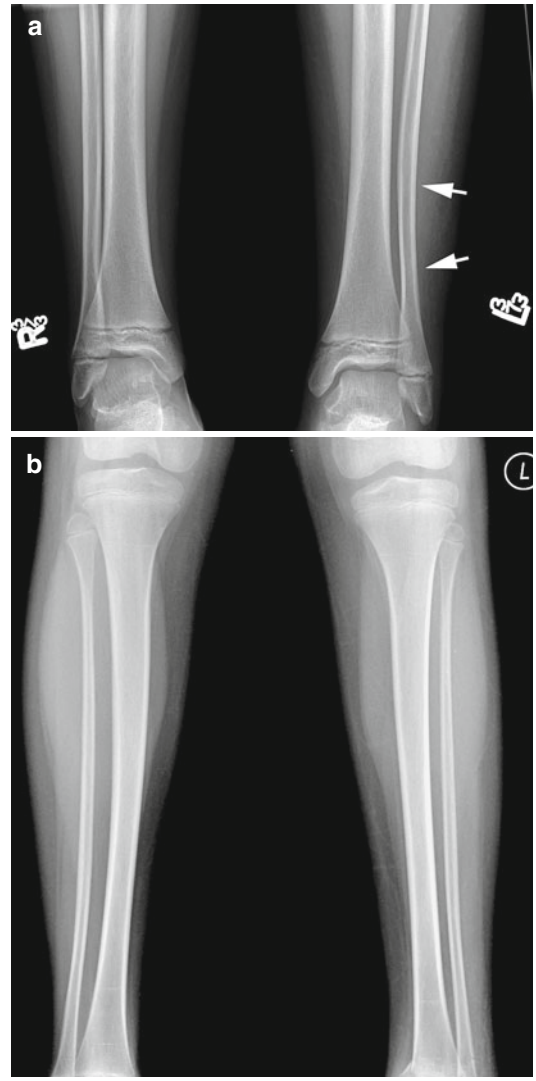
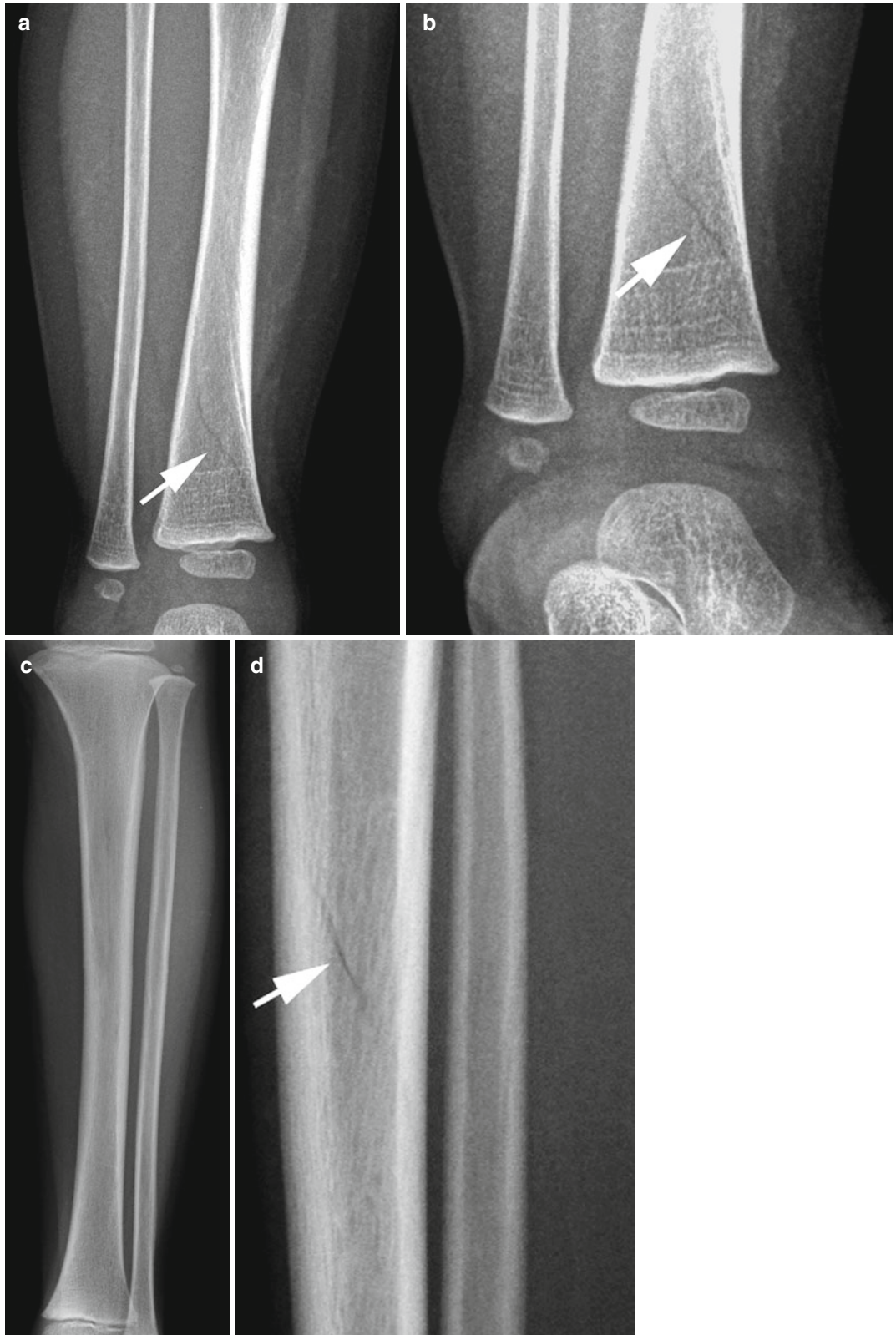


Fig. 10.33 Plastic bending fracture fibula. (**a**) Note the inward plastic bending fracture of the left fibula (*arrows*). Compare with the straight right fibula. (**b**) Normal fibula inward bending. Note that in this normal patient, both of the fibulae are inwardly bent

Fig. 10.34 Toddler fracture: type I. (**a**) Note the subtle spiral fracture (*arrow*) through the distal tibia. (**b**) Magnified view more clearly demonstrates the fracture (*arrow*). (**c**) In this patient with lower leg pain, a fracture is not clearly visualized. (**d**) However, with closer inspection and magnification, a subtle spiral fracture (*arrow*) is seen in the mid-diaphysis


a
b
c
d

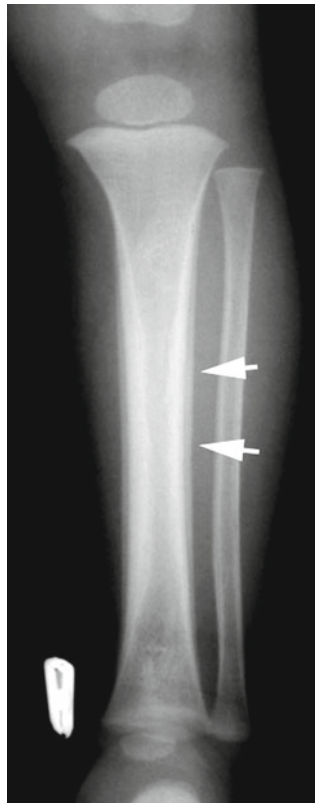


Fig. 10.35 Toddler fracture I: healing pseudotumor configuration. Note periosteal new bone deposition along the shaft of the tibia (*arrows*). This patient had a spiral fracture which was not clearly visible at this time

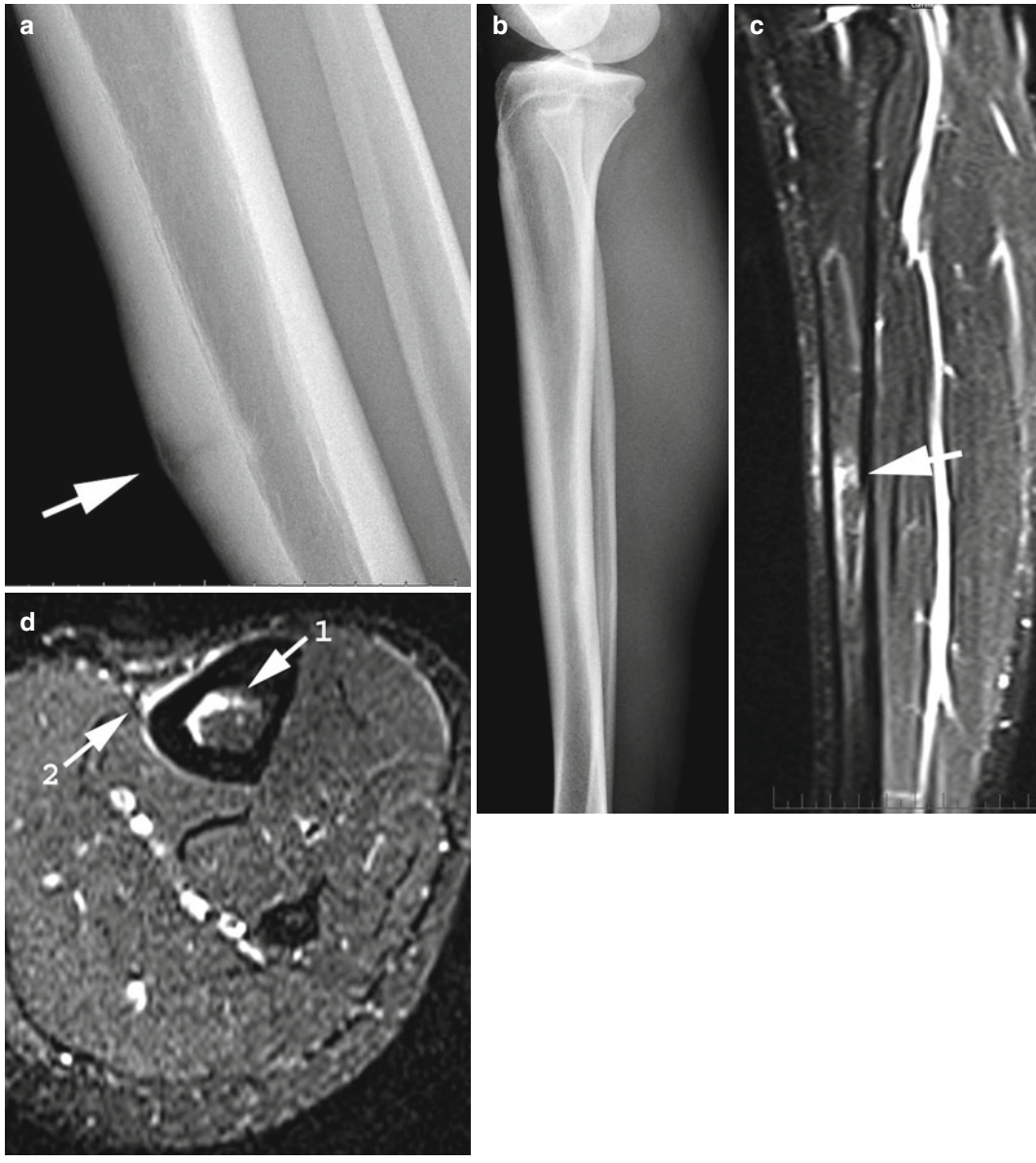


Fig. 10.36 Stress fracture: tibia. (**a**) Note anterior tibial cortical thickening and a vague, but present transverse fracture line (*arrow*). (**b**) Stress phenomenon. In this patient, mild thickening of the anterior cortex of the tibia is seen. A fracture line is not seen. (**c**) Sagittal STIR image. Note increased signal anterior to the tibia and in the marrow (*arrow*) consistent with stress reaction. (**d**) Axial STIR image. Note increased signal in the tibial marrow (*1*) and anterior to the tibial cortex (*2*)

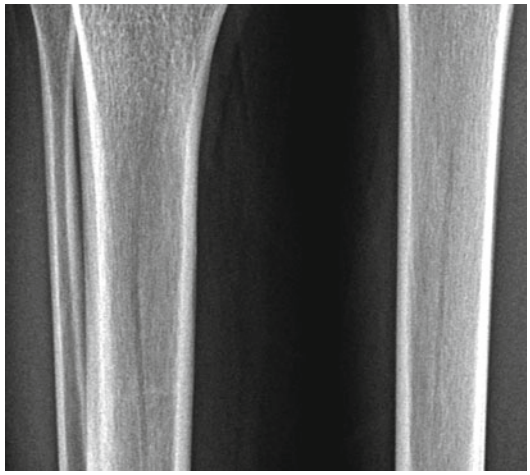


Fig. 10.37 Nutrient grooves, pseudofractures. Note bilateral basically vertical nutrient grooves in both the tibias

References

1. Hayden Jr CK, Swischuk LE. Para-articular soft tissue changes in infants and trauma of the lower extremity in children. AJR. 1980;134:307–11.
2. Swischuk LE, John SD, Tschoepe EJ. Upper tibial hyperextension fractures in infants: another occult toddler's fracture. Pediatr Radiol. 1999;29:6–9.
3. Tschoepe EJ, John SD, Swischuk LE. Tibial fractures in infants and children: emphasis on subtle injuries. Emerg Radiol. 1998;5:245–52.
4. Swischuk LE. Musculoskeletal: what's different in children? Kicked in lower right leg: now limping and refusing to bear weight. Emerg Radiol. 2012;19:273–5.
5. Swischuk LE. Musculoskeletal injury in the right let of a child who jumped a lot in a birthday party. Emerg Radiol. 2009;16:311–33.
6. Boyer RS, Jaffee RB, Noxon GW, Condon VR. Trampoline fracture of the proximal tibia in children. AJR. 1986;146:83–5.
7. Currarino G, Pinckney LE. Genu valgum after proximal tibial fractures in children. AJR. 1981;136:915–8.
8. Green NE. Tibia valga caused by asymmetrical overgrowth following a nondisplaced fracture of the proximal tibial metaphysis. J Pediatr Orthop. 1983;3:235–7.
9. Robert M, Khouri N, Carlioz H, Alain JL. Fractures of the proximal tibial metaphysis in children: review of a series of 25 cases. J Pediatr Orthop. 1987;7:444–9.
10. Zionts LE, Harcke T, Brooks KM, MacEwen GD. Posttraumatic tibia valga: a case demonstrating asymmetric activity at the proximal growth plate on technetium bone scan. J Pediatr Orthop. 1987;7:458–62.
11. Close BJ, Strouse PJ. MR of physeal fractures of the adolescent knee. Pediatr Radiol. 2000;30:756–62.
12. Diederichs G, Isserver AS, Scheffler S. MR imaging of patellar instability: injury patterns and assessment of risk factors. Radiographics. 2010;30(4):961–98.
13. Malghem J, Maldague B. Depth insufficiency of the proximal trochlear groove on lateral radiographs of the knee: relation to patellar dislocation. Radiology. 1989;170:507–10.
14. Neitosvaara Y, Aalto K, Kallio PE. Acute patellar dislocation in children: incidence and associated osteochondral fractures. J Pediatr Orthop. 1994;4:513–7.
15. Grogan DP, Carey TP, Leffers D, Ogden JA. Avulsion fractures of the patella. J Pediatr Orthop. 1990;10:721–30.
16. Sinding-Larson MF. A hitherto unknown affliction of the patella in children. Acta Radiol [Diagn] (Stockh). 1921;1:171–3.
17. Dwek JR, Chung CB. The patellar extensor apparatus of the knee. Pediatr Radiol. 2008;38:925–35.
18. Fitch RD. Tibial tubercle avulsions. J Pediatr Orthop. 1986;6:186–92.
19. Rosenberg ZS, Kawelblum M, Cheung YY, Beltran J, Lehman WB, Grant A. Osgood-Schlatter lesion: fracture or tendonitis: scintigraphic, CT, and MR imaging features. Radiology. 1992;185:583–5.
20. Kirschner SG, Pavlov H, Heller RM, Kay JJ. Periosteal chondromas of the anterior tibial tubercle: two cases. AJR. 1978;131:1088–9.
21. McCauley TR, Kier R, Lynch KJ, Jokl P. Chondromalacia patellae: diagnosis with MR imaging. AJR. 1992;158:101–5.
22. Iwaya T, Takatori Y. Lateral longitudinal stress fracture of the patella: report of three cases. J Pediatr Orthop. 1985;5:573–5.
23. De Smet AA, Fisher DR, Graf BK, Lange RH. Osteochondritis dissecans of the knee: value of MR imaging in determining lesion stability and the presence of articular cartilage defects. AJR. 1990;155:549–53.
24. Klingele KE, Kocher MS, Hresko MT, Gerbino MT, Micheli MT. Discoid lateral meniscus: prevalence of peripheral rim instability. J Pediatr Orthop. 2004;24:79–82.
25. De Smet AA, Norris MA, Yandow DR, Quintana FA, Graf BK, Keene JS. MR diagnosis of meniscal tears of the knee: importance of high signal in the meniscus that extends to the surface. AJR. 1993;161:101–7.
26. Helms CA, Laorr A, Cannon Jr WD. The absent bow tie sign in bucket-handle tears of the menisci in the knee. AJR. 1998;170:57–61.
27. Bianchi S, Swass A, Abdelwahab IF, Banderali A. Diagnosis of tears of the quadriceps tendon of the knee: value of sonography. AJR. 1994;162:1137–40.
28. Dunham WK, Marcus NW, Enneking WF, Haun C. Developmental defects of the distal femoral metaphysis. J Bone Joint Surg. 1980;62A:801–6.
29. Resnick D, Greenway G. Distal femoral cortical defects, irregularities and excavations: a critical

review of the literature with the addition of histologic and paleopathologic data. Radiology. 1982;143: 345–54.
30. Alexander JE, Seibert JJ, Aronson J. Dorsal defect of the patella and infection. Pediatr Radiol. 1987;17: 325–7.
31. Safran MR, Mcdonough P, Seeger L, Gold R, Oppenheim WL. Dorsal defect of the patella. J Pediatr Orthop. 1994;14:603–7.
32. Swischuk LE. Musculoskeletal: what's different in children? Run over by a golf cart and my leg hurts. Emerg Radiol. 2010;17:257–8.
33. Dunbar JS, Owen HF, Nogrady MB, McLeese R. Obscure tibial fracture of infants: the toddler's fracture. Can J Assoc Radiol. 1964;15:136–44.
34. Nussbaum AR, Treves ST, Micheli L. Bone stress lesions in ballet dancers: scintigraphic assessment. AJR. 1988;150:851–5.
35. Miniaci A, McLaren AC, Haddad RG. Longitudinal stress fracture of the tibia: case report. Can J Assoc Radiol. 1988;39:221–3.
36. John SD, Moorthy CS, Swischuk LE. Expanding the concept of the toddler's fracture. Radiographics. 1997;17:367–76.

Ankle and Foot

11

Ankle

Normal Soft Tissues and Fat Pads of the Ankle

In the infant and child, three fat pads around the ankle usually are visualized on lateral view. The largest is the pre-Achilles fat pad, located just anterior to the Achilles tendon, but this fat pad is not utilized for the detection of joint fluid. Rather, the anterior and posterior fat pads lying against the joint capsule are the ones that are used (Fig. 11.1a).

Detecting Fluid in the Ankle Joint

In determining whether fluid is present in the ankle joint, it is best to study the lateral view [1, 2]. On frontal view, only soft tissue swelling around the ankle is seen, but on lateral view, outward displacement of the anterior (more often) and/or posterior fat pads is seen (Fig. 11.1b). The fluid collection under the anterior fat pad has been referred to as the "teardrop" sign [2]. No joint space widening usually is seen, for the ligaments around the ankle joint are very sturdy and do not allow for much in the way of joint distraction.

Injuries of the Distal Tibia and Fibula

A variety of injuries can be sustained in the distal tibia and fibula, and most often these result from a combination of inversion, eversion, and rotational forces. In the young infant, cortical buckle (torus) fractures through the distal tibia and fibula are very common, especially the tibia (Fig. 11.2). In the older child, however, the more common injury is some type of Salter–Harris epiphyseal–metaphyseal fracture [3]. In the ankle, all Salter–Harris fractures types are common with the exception of the type V injury. With any of these fractures, if the fracture is overt, detection of the fracture is relatively easy (Fig. 11.3). However, in other cases, detecting the fracture is more difficult. The key to detecting these more subtle fractures lies in comparing the width of the epiphyseal plates in the injured ankle to those on the normal side and in assessing the soft tissues for evidence of swelling. Examples of Salter–Harris fractures are presented in Figs. 11.4 and 11.5.

The Salter–Harris type III injury is quite common in the distal tibia (Fig. 11.5). The reason for this is that the distal tibial epiphysis fuses earlier medially than it does laterally. Consequently, with an inversion injury of the ankle, there is separation of the epiphysis laterally but not medially, and then the forces are directed downward through the epiphysis and a Salter–Harris III fracture results.

This fracture often is difficult to detect on initial inspection of the AP and lateral views. On the other hand, very often it is seen on the oblique view of the ankle (Fig. 11.6). In other cases, gross displacement of the fracture can be seen (Fig. 11.7).These fractures are the childhood equivalent of the Tillaux fracture [4] and are best assessed with CT imaging (Fig. 11.8). This is

L.E. Swischuk, S.P. Jadhav (eds.), *Emergency Musculoskeletal Imaging in Children*,
DOI 10.1007/978-1-4614-7747-1_11, © Springer Science+Business Media New York 2014

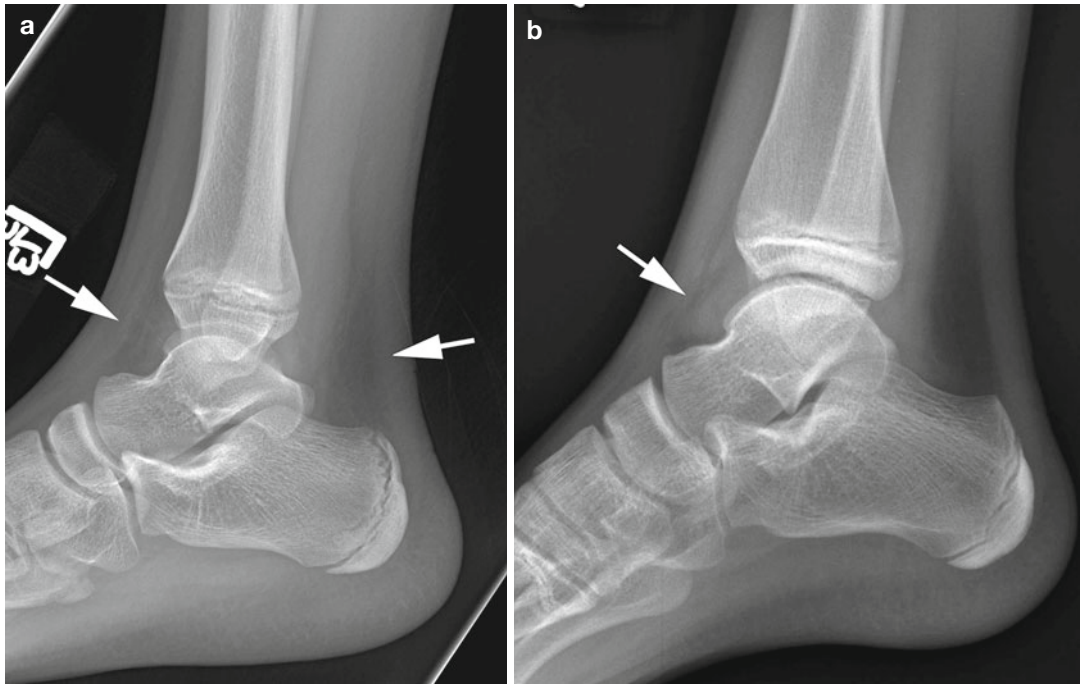


Fig. 11.1 Normal fat pads and joint fluid. (**a**) Note the normal anterior and posterior fat pads (*arrows*). (**b**) Note the teardrop sign (*arrow*) indicative of joint fluid

performed to define the degree of fracture fragment displacement and to determine whether internal fixation is required. The usual maximum allowable limit of the diastatic fracture is 3 mm.

Inversion–rotation injuries of the ankle are very common, and although in most cases they result only in a sprained ankle, in other instances, Salter–Harris injuries result. In adults, the Ottawa ankle rules can, if applied, significantly reduce the number of ankle injuries requiring radiographic examination [5]. *This also probably is true in children, but unfortunately there is no uniform adherence to these rules.*

With inversion ankle injuries, one may only see an epiphyseal–metaphyseal separation (Salter–Harris I fracture) of the distal fibula [6, 7]. In other cases, an associated tibial Salter–Harris III fracture can be seen (see Fig. 11.6), while in still other cases, both the fibular and tibial epiphyses are involved in Salter–Harris fractures (see Fig. 11.3a). In either case, however, a more serious associated fracture through the medial malleolus of the tibial can be seen (Fig. 11.9a). In still other cases, one may encounter only a small cortical avulsion off of the distal fibula (Fig. 11.9b, c). These latter fractures must be differentiated from normal accessory ossicles occurring in this area (see Fig. 11.25).

With eversion injuries, the ankle mortise often is seriously disturbed, and a wide range of relatively readily detectable injuries can be encountered (Fig. 11.10a). In other cases, only a small avulsion fracture off of the medial condyle is present (Fig. 11.10b). So-called posterior malleolar fractures actually are Salter–Harris type II epiphyseal–metaphyseal fractures, and many times the fracture is visible only on the lateral view (see Figs. 11.3b and 11.8b). This fracture is usually part of a Salter–Harris III or IV fracture and often referred to as a triradiated fracture. It is best assessed with CT scanning.

Injuries of the Tarsal Bones

Fractures and dislocations of the tarsal bones are generally less common in childhood than in adulthood. This is especially true in the infant and

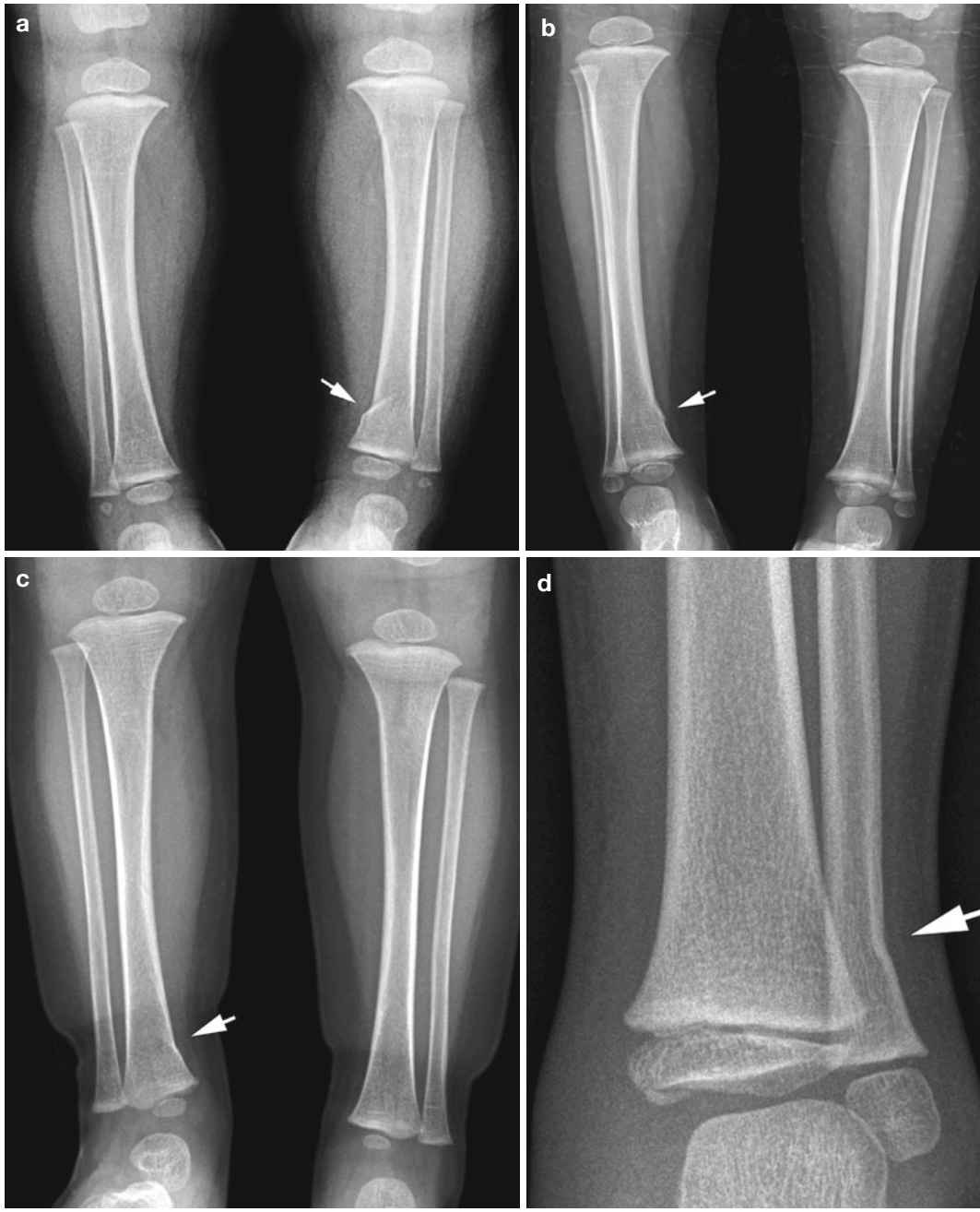


Fig. 11.2 Fractures: buckle. (**a**) Note the typical buckle fracture through the distal tibia (*arrow*). (**b**) A more subtle buckle fracture (*arrow*) through the distal tibia. (**c**) Another subtle angled buckle fracture (*arrow*) through the distal tibia. (**d**) Angled buckle fracture (*arrow*) through the distal fibula

young child. In the older child, one can encounter fractures of the navicular and talus and occasionally of the other tarsal bones. Talar fractures are probably more common than the other fractures. These fractures tend to occur through the neck of the talus and there often is rotation/dislocation of the distal fracture fragment (Fig. 11.11), and subsequent aseptic necrosis is a known complication.

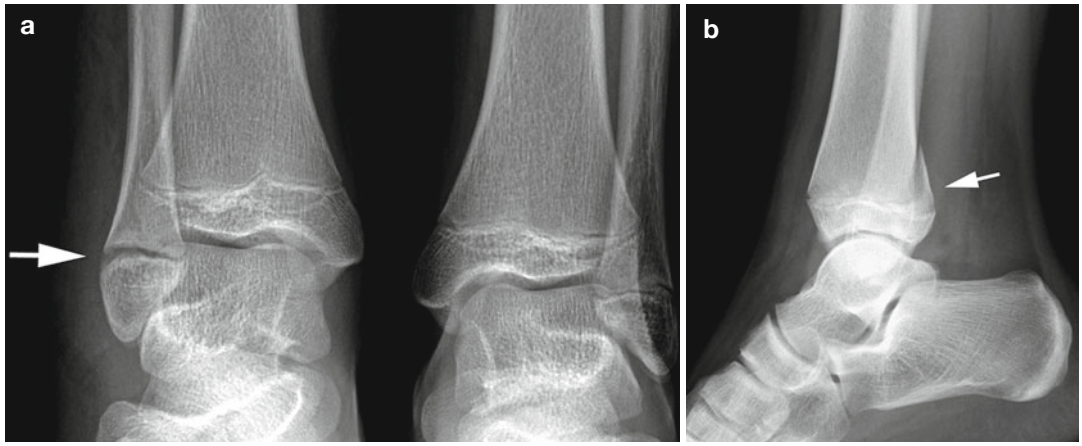


Fig. 11.3 Salter–Harris I fracture fibula. (**a**) Note the widened epiphyseal plate (*arrow*) through the right distal fibula. Compare with the other epiphyseal plates and especially the one through the normal distal left fibula. (**b**) Typical Salter–Harris II through the distal tibia (*arrow*)

The navicular bone also can be fractured, but very often it undergoes a stress/compression fracture which results in increased density (compressed trabeculae) of the navicular bone (Fig. 11.12). Less commonly they can occur through the talus. Fractures of the other tarsal bones are not rare but not common. Perhaps the cuneiform is one of the more involved bones (Fig. 11.13).

Impaction cuboid fractures are more common than generally appreciated and tend to occur in younger children and infants. They can be considered as part of the expanded toddler fracture concept [8–11] for these patients frequently present with limping; the cause of which remains unclear until the fracture is detected. As with all toddler fractures, diagnosis is a matter of knowing *what to look for and where to look for it*. In this regard, with cuboid fractures, the most significant finding is an increase in density and, in many cases, decrease in size of the cuboid bone (Fig. 11.14). At first, increased density is due to trabecular compression, but eventually, it is due to a combination of trabecular compression and new bone healing. Plain films usually suffice, but nuclear scintigraphy and MR imaging also can detect these injuries.

Fractures of the calcaneus usually result from patients jumping or falling on their heels, and many are subtle or occult [12–16]. In some cases, a clear-cut fracture line is visualized, but otherwise one must look for indirect findings such as soft tissue swelling, loss of Bohler's angle, decreased height of the calcaneus, and increased density (impaction) of the calcaneus (Fig. 11.15). Often these fractures are finally best seen on tangential views of the calcaneus.

Other fractures which can involve the calcaneus include fractures of the anterior process (Fig. 11.16) and simple buckle fractures (Fig. 11.17a). In addition, the apophysis of the calcaneus can be fractured (Fig. 11.17b, c). It is important, however, to not misinterpret normal irregularity of the normally sclerotic calcaneal apophysis for a fracture (see Fig. 11.26).

Small avulsion fractures of the various tarsal bones and other bones around the ankle also can be encountered. These are more common than generally appreciated, and although they may be visible on standard views, very often oblique views first bring these fractures to light (Fig. 11.18). Indeed, in some cases, visualization of these fractures is strictly fortuitous, and all of them must be differentiated from normal accessory ossification centers of the various bones around the ankle (see Fig. 11.25).

Tarsal bones are often the site of stress reactions and fractures. This may be a fatigue fracture (Fig. 11.19) or an insufficiency fracture from weight bearing after bone resorption secondary to immobilization.

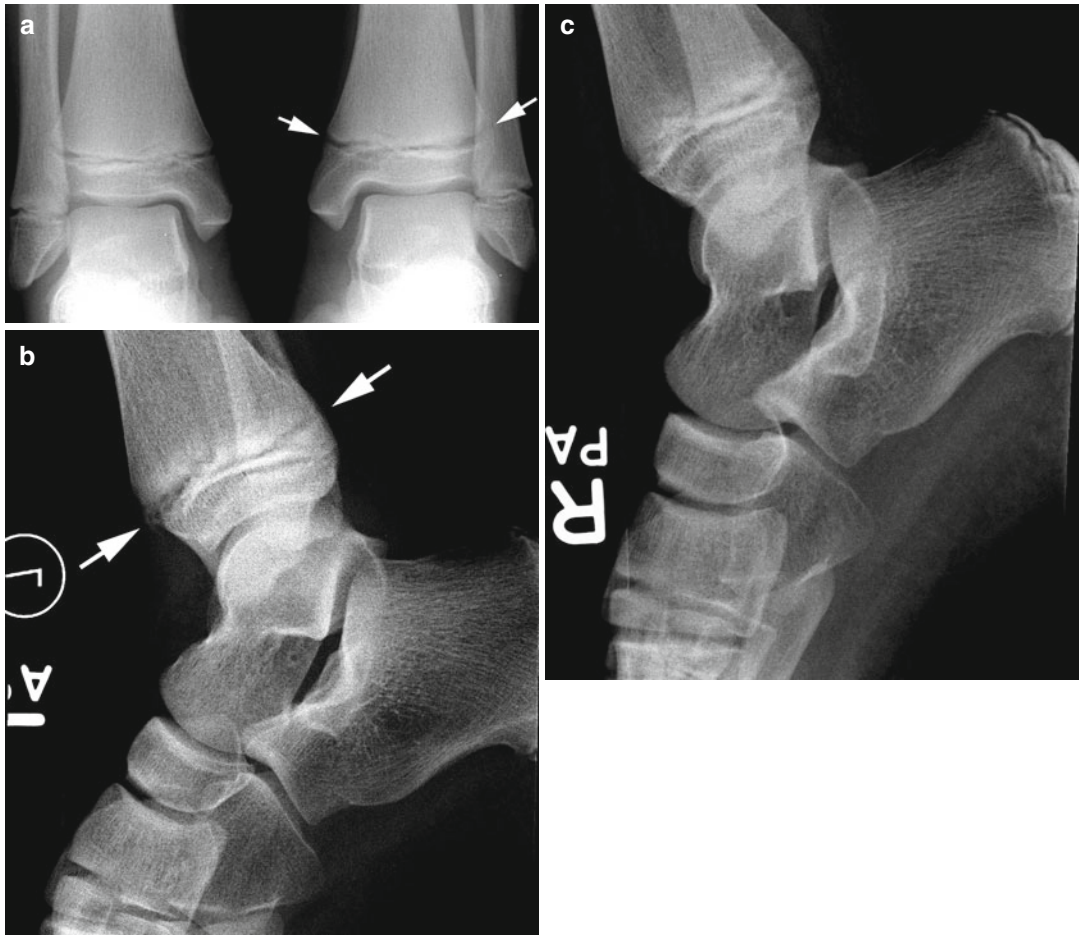


Fig. 11.4 Salter–Harris fractures: subtle findings. (**a**) Note widening of the epiphyseal plate (*arrows*) through the distal left tibia. Compare with the normal plate on the other side. The findings in the tibia are consistent with a Salter–Harris I fracture. There may be slight widening of the fibular epiphyseal plate. (**b**) Note the slightly widened distal tibial epiphyseal plate (*arrows*).The findings are subtle. (**c**) Normal side for comparison. Compare the normal epiphyseal plate with the slightly widened one seen in (**b**)

Sprained Ankle

Unlike the sprained wrist, a sprained ankle most often turns out to be nothing more than a sprained ankle. Of course, this is not to say that fractures never occur but only to point out that the high incidence of underlying fracture that accompanies wrist sprains is not present with ankle sprains. Another important aspect of a sprained ankle resulting from an inversion injury is that very often there is an associated fracture of the base of the fifth metatarsal. The peroneus brevis muscle inserts into this bone, and with inversion injuries, an avulsion fracture frequently occurs. This fracture usually is initially overlooked clinically but almost always is detectable roentgenographically (see Fig. 11.33).

Achilles Tendonitis

Children very commonly develop acute or chronic pain over the insertion of the Achilles tendon onto the calcaneus. Actually the condition represents a tenosynovitis secondary to a subclinical tendon avulsion injury in the active child [17–19]. In addition, it frequently is associated with plantar fasciitis [20], for the plantar fascia,

and Achilles tendon are a continuous membranous tendon structure wrapping around the heel. The roentgenographic findings usually consist of localized swelling over the area and thickening of the Achilles tendon and plantar fascia along with obliteration of the pre-Achilles fat pad (Fig. 11.20). Unless one appreciates this injury when a patient presents with heel pain, there is a great tendency to attribute the problem to aseptic necrosis of the normally sclerotic and irregular-appearing calcaneal apophysis. Such a diagnosis should be avoided because this is the expected appearance of the normal calcaneus (see Fig. 11.26). However, because of the sclerotic/fragmented appearance of the calcaneal apophysis, the findings frequently are attributed to Sever's disease, that is, aseptic necrosis of the calcaneal apophysis. However, it is doubtful and indeed unlikely that aseptic necrosis of the calcaneal apophysis exists. Ultrasonography and MR imaging can be used to detect plantar fasciitis and Achilles tendonitis [16–19] but usually are not required.

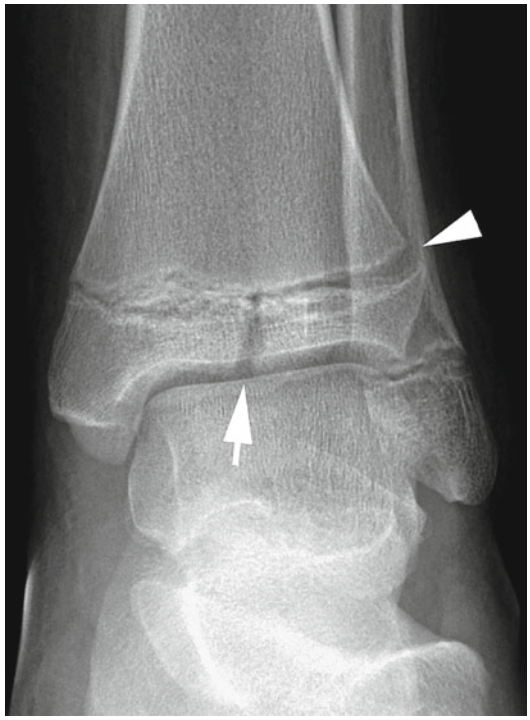


Fig. 11.5 Salter–Harris III fractures. Note the typical Salter–Harris III fracture through the distal tibia (*arrow*) and the widened tibial epiphyseal plate (*arrowhead*)

Plantar Fasciitis and Stone Bruise

Plantar fasciitis can be identified on plain films when there are thickening and indistinctness of the plantar fascia (Fig. 11.21a, b). Similarly swelling over the inferior aspect of the heal, resulting from a so-called stone bruise (stepping on a stone), can be readily detected with plain films (Fig. 11.21c). Of course MR also is useful in detecting these injuries but usually is not required.

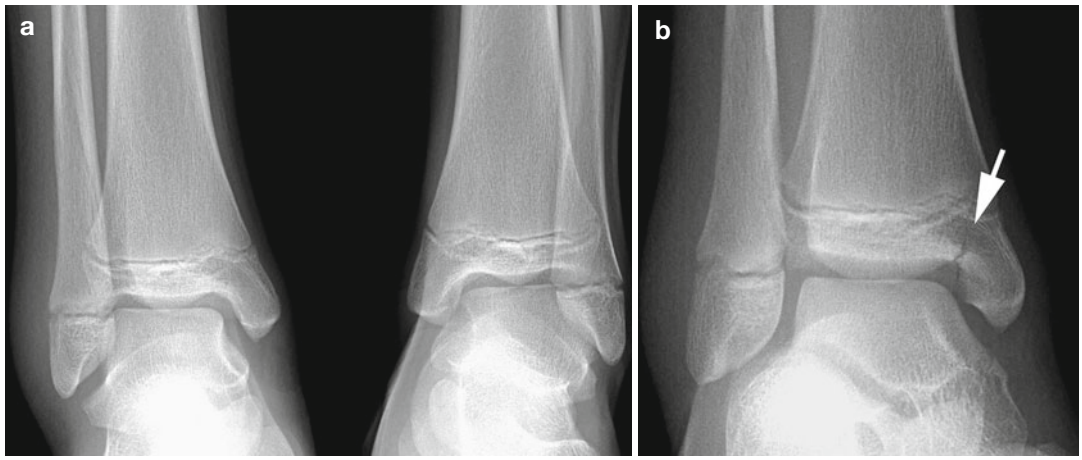


Fig. 11.6 Salter–Harris III fracture: occult on AP view. (**a**) Note swelling over the lateral malleolus and some suggestion of a minimal Salter–Harris I fracture through the distal fibula. The tibial epiphysis appears intact. (**b**) Oblique view, however, demonstrates a typical Salter–Harris III fracture (*arrow*)

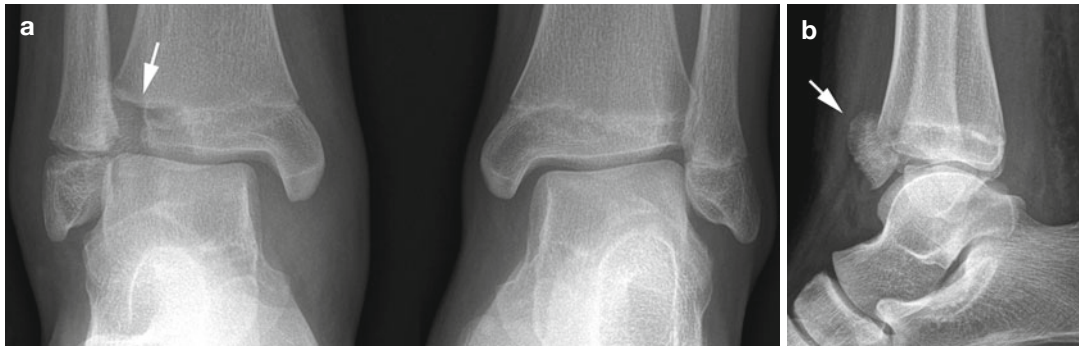


Fig. 11.7 Salter–Harris III fracture: displaced fracture fragment. (**a**) Note swelling of the ankle and a Salter–Harris I injury through the distal fibula. Also note the lucent gap (*arrow*) through the distal lateral tibial epiphysis. (**b**) Lateral view demonstrates the avulsed and displaced epiphyseal fragment (*arrow*)



Fig. 11.8 Salter–Harris III fracture: CT findings. (**a**) Coronal view. Note the Salter–Harris III fracture (*arrows*). (**b**) Sagittal view. Note the Salter–Harris III fracture (*lower arrow*) and the associated Salter–Harris II fracture (*upper arrow*). (**c**) Axial view through epiphysis. Note the widened fracture line (*arrow*)



Fig. 11.9 Eversion ankle injuries. (**a**) Note the Salter–Harris IV fracture through the medial malleolus (*arrow*). There also is a Salter–Harris I fracture through the distal fibula. Marked soft tissue swelling is seen over the lateral malleolus. (**b**) Thin avulsed sliver of bone (*arrow*) off the distal fibular epiphysis. (**c**) In this patient, a small avulsed ossicle (*arrow*) is seen off of the distal fibula

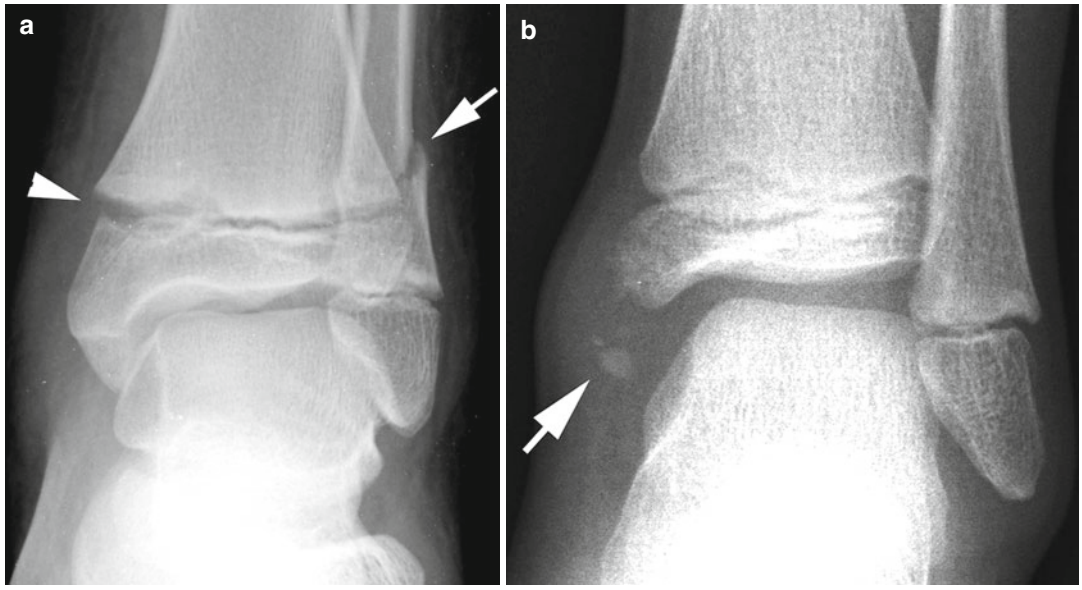


Fig. 11.10 Eversion ankle injury. (**a**) First note the widened tibial epiphyseal plate (*arrowhead*) and then the oblique fracture through the distal fibula (*arrow*). (**b**) In this patient, there is an avulsion fracture of the medial condyle (*arrow*). Significant edema supports the diagnosis

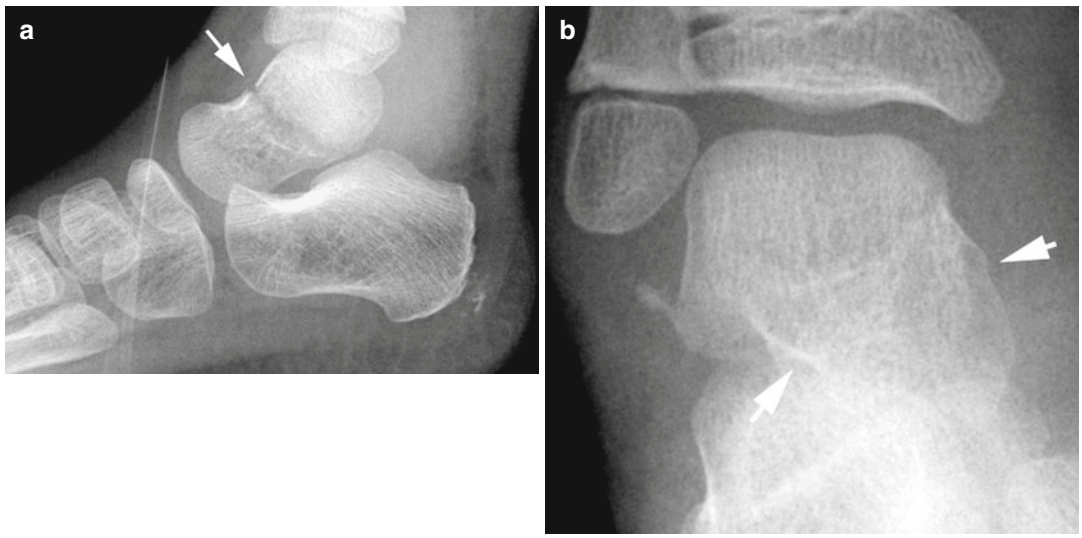


Fig. 11.11 Talar fracture. (**a**) Note the fracture (*arrow*) through the neck of the talus. The two bony fragments are of different density because there is rotation of the distal fragment. (**b**) Note the position of the distal fragment (*arrows*) consistent with rotation

Osteochondritis Dissecans of the Tarsal Bones

Osteochondritis dissecans of the tarsal bones is not particularly common in childhood but does occur and most often involves the talus [21]. The findings are similar to those of osteochondritis dissecans elsewhere in that there is a bony defect with slight peripheral sclerosis (Fig. 11.22a). An intra-articular piece of bone may or may not be

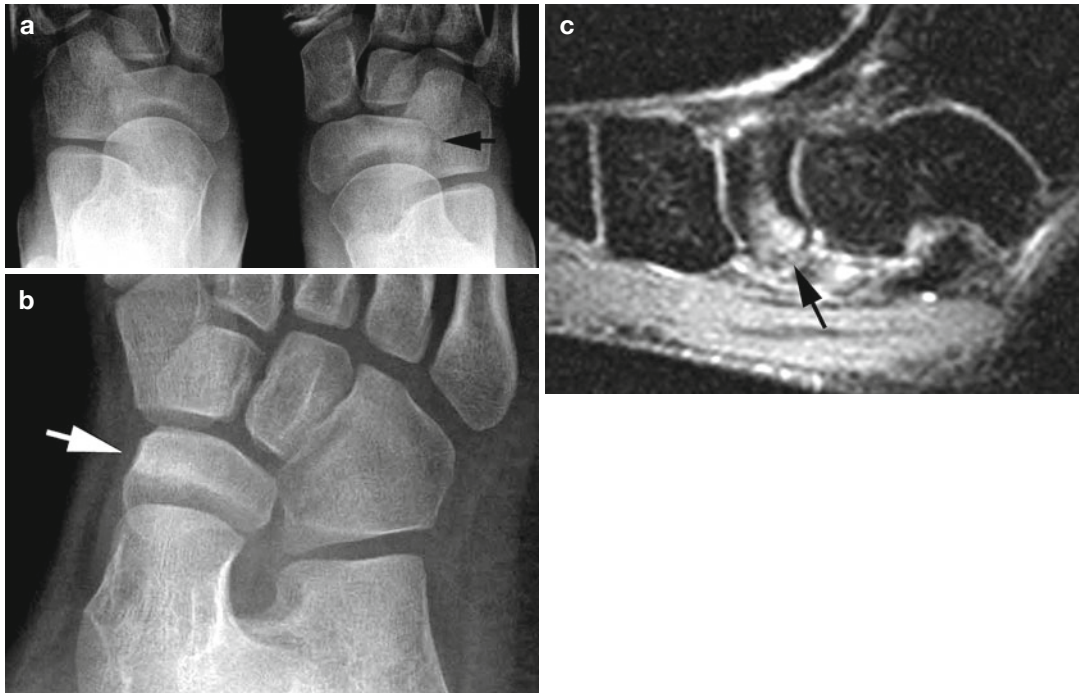


Fig. 11.12 Navicular compression fracture. (**a**) Note increased density (*arrow*) of part of the navicular bone on the right. (**b**) Oblique view confirms the increased density (*arrow*). (**c**) Another patient. MR STIR sagittal view demonstrates increased signal (*arrow*) in the navicular bone consistent with a compression fracture

visualized. It might be noted, however, that as with osteochondritis dissecans elsewhere, the lesion may or may not be symptomatic at the time of detection. MR imaging can be utilized to detect the degree of fragment displacement (Fig. 11.22b, c).

Aseptic Necrosis of the Tarsal Bones

Aseptic necrosis of the various tarsal bones can be a cause of foot pain, and in this regard, the tarsal navicular is the most commonly involved bone. Köhler's disease is the term applied to aseptic necrosis of the navicular bone, and the roentgenographic findings consist of increased density and variable fragmentation and irregularity of the bone (Fig. 11.23a, b). In addition, one can utilize the soft tissues [22] for detection or verification of Köhler's disease because the soft tissues over the aseptically necrotic bone are edematous (Fig. 11.23b). This is especially important because the tarsal navicular bone can be somewhat dense and even irregular on a normal basis (Fig. 11.23c). In such cases, there will be no swelling over the tarsal bone on lateral view.

Normal Variations Causing Problems

Numerous accessory ossicles occur in the ankle (Fig 11.24), but to illustrate all of them would be excessive. The most common are those occurring at the distal ends of the lateral and medial malleoli, the posterior aspect of the talus, and the navicular bone (Fig. 11.25). It is most important not to misinterpret these secondary ossification centers and accessory ossicles as avulsion fractures, even though avulsion of the secondary centers themselves can occur [23].

The normal, sclerotic, and often irregular calcaneal apophysis [24] is notoriously misinterpreted as being due to aseptic necrosis of the calcaneus. *Indeed, this normal appearance is often so striking that it is tempting to assign some type of pathologic condition to the bone* (Fig. 11.26). However, in such cases, adjacent soft tissue swelling will be

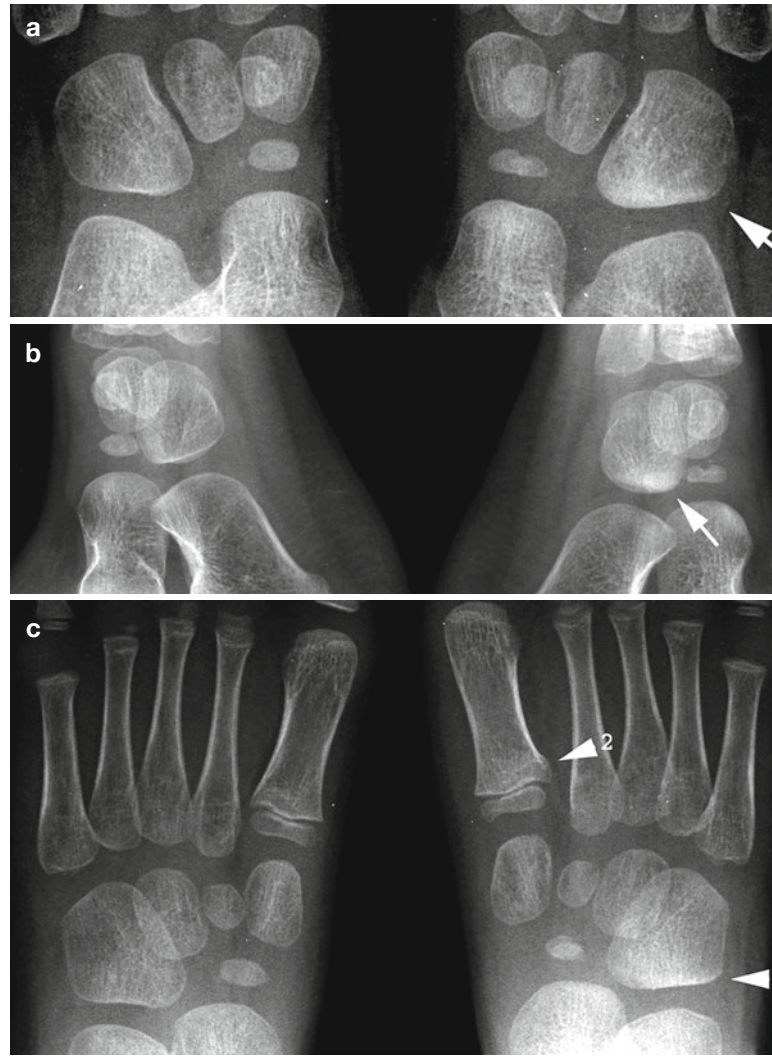


Fig. 11.13 Compression–impaction fracture cuboid bone. (**a**) Note the increased density over the lower part of the right cuboid bone (*arrow*). The cuboid bone also is a little shorter and squarer than the one on the left, all consistent with a compression injury. (**b**) Oblique view confirms the area of increased density (*arrow*). (**c**) In this patient, both types of bunk bed fractures are present. First note the area of increased density in the cuboid bone of the right (*1*). Then note the subtle buckle fracture through the base of the first metatarsal (*2*)

absent and will aid one in not over calling the finding. Finally, it should be noted that the tarsal bones in general are especially prone to irregular ossification and the findings also should also not be misinterpreted for fractures or aseptic necrosis of the tarsal bones (Fig. 11.27).

Foot

Normal Soft Tissues and Fat Pads

As in the hand, there are no particularly valuable fat pads to evaluate in the foot. Consequently, except for localized edema, there is little else to analyze.

Detecting Fluid in the Small Joints of the Foot

The detection of fluid in the small joints of the foot rests with noting soft tissue swelling around the involved joint. Occasionally, the joint space can be widened, but this is not a common finding.

Injuries of the Metatarsals and Phalanges

Dislocation of the various joints of the foot is uncommon except perhaps for dislocation of the great toe. Cortical, buckle, or torus fractures, on the other hand, are quite common, and in this

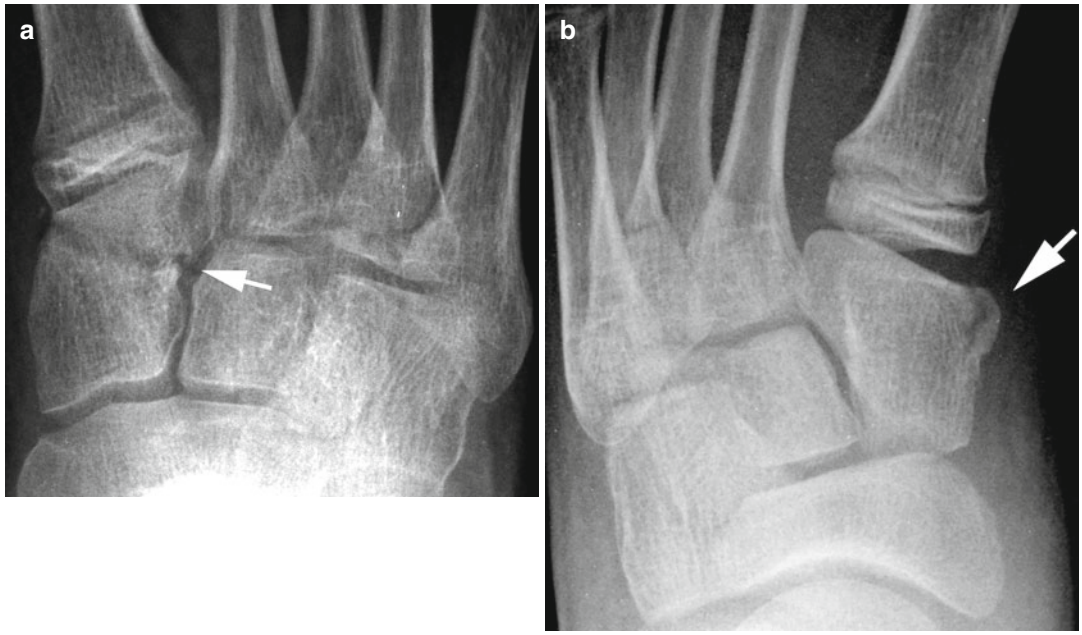


Fig. 11.14 Cuneiform fractures. (**a**) Note the avulsion-type fracture (*arrow*) through the cuneiform bone. (**b**) Another avulsion fracture (*arrow*)

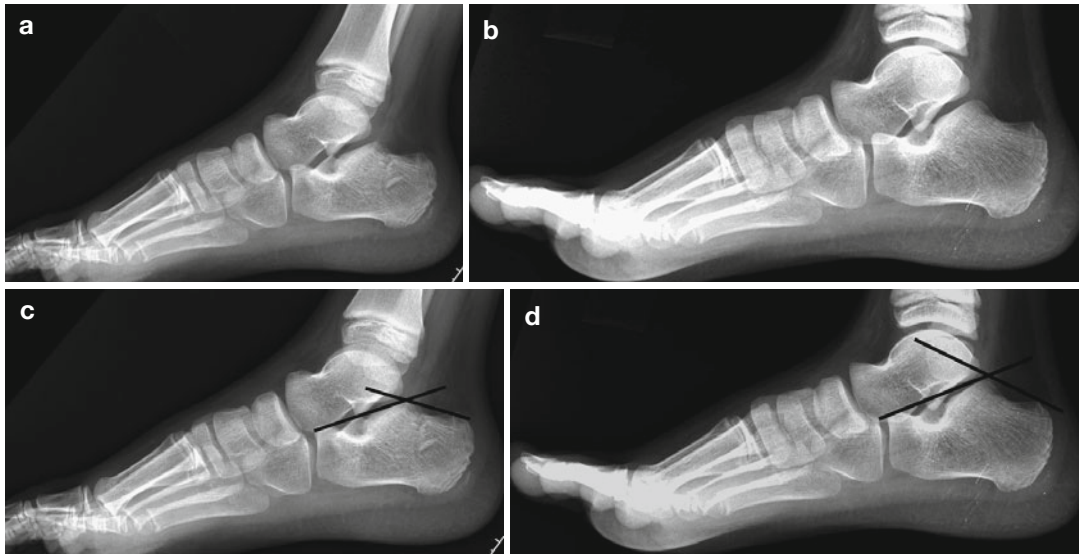


Fig. 11.15 Calcaneal fracture. (**a**) Note the slightly irregular contour of the calcaneus, a buckle fracture over the posterior inferior surface, and some increase in density. (**b**) Normal side for comparison. Note the normal appearance of the calcaneus with clearly visible trabeculae. These are not seen as clearly in Fig. 11.5a. (**c**) Bohler's angle is reduced on the affected side. (**d**) Bohler's angle is normal on the normal side



Fig. 11.16 Calcaneal anterior process fracture. (**a**) Note the avulsion fracture of the anterior process of the calcaneus (*arrow*). (**b**) Sagittal STIR MR image demonstrates the avulsed fracture fragment with internal marrow increased signal (*arrow*). There also is some increased signal in the adjacent calcaneus. (**c**) Another patient. The plain radiographs were normal in this patient. However, in a STIR MR study, sagittal plane demonstrated increased signal in the anterior process and the adjacent calcaneus (*arrows*)

regard, fractures through the metatarsals can occur through their bases, heads, or midshafts and, when overt, are not difficult to detect (Fig. 11.28). However, some of these fractures can be quite subtle [25, 26], and only telltale soft tissue edema and meticulous inspection of the films along with comparative and oblique views will allow one to detect these fractures (Fig. 11.29). Oblique views also are helpful with fractures of the toes, which generally consist of Salter–Harris and angled or ordinary buckle fractures (Fig. 11.30).

A specific fracture of the first metatarsal is the bunk bed fracture where the forefoot is jammed into the floor or ground [11, 27, 28]. This fracture is believed to be the childhood equivalent of the Lisfranc fracture [29], and although there usually is no true dislocation of the first metatarsal from the cuneiform bone (as in adults), a buckle fracture through the base of the first metatarsal is the hallmark of this fracture which again can be quite subtle (Fig. 11.31). This fracture also can be considered another form of the toddler fracture in the expanded concept of toddler fractures [11].



Fig. 11.17 Other calcaneal fractures. (**a**) Note the subtle buckle fracture (*arrow*) of the right calcaneus. (**b**) Fracture of the calcaneal apophysis (*arrow*). Note that the fracture edges are very sharp. (**c**) One month later, healing has occurred and the fracture is no longer visible. It is important to differentiate these fractures from normal fracture-like findings in the normal calcaneal apophysis. With the latter, the edges of the lucency are not sharp (see Fig. 11.26)

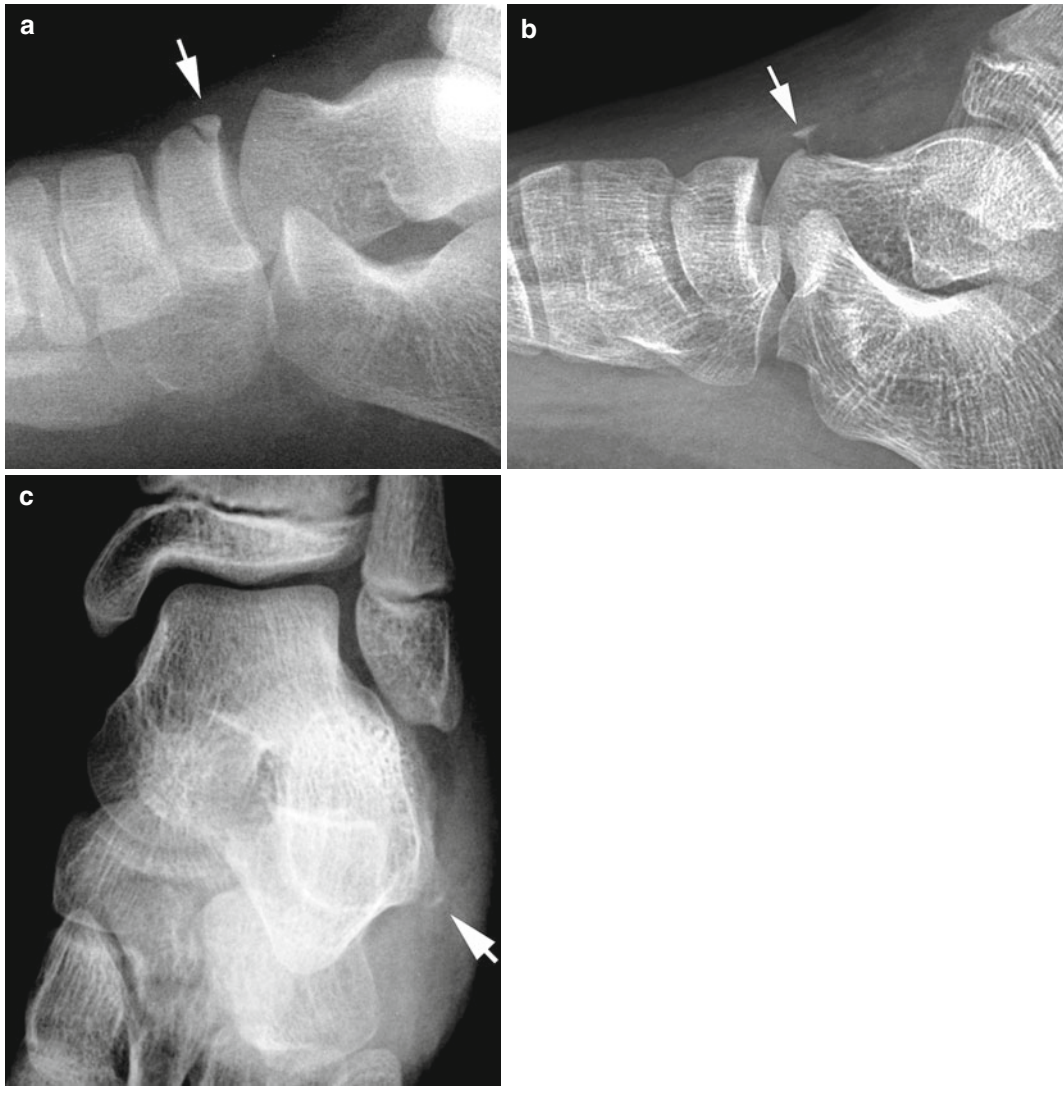


Fig. 11.18 Avulsion fractures of the ankle. (**a**) Note the subacute avulsion fracture (*arrow*) off of the tarsal navicular bone. (**b**) Acute avulsion fracture (*arrow*) off of the talus. Note adjacent soft tissue swelling. (**c**) Acute avulsion fracture (*arrow*) off of the calcaneus

Epiphyseal–metaphyseal injuries are much less common in the foot than in the hand, but they are not rare. These fractures can involve any of the bones of the foot, but the one of special importance is the Salter–Harris type I–type II fracture through the great toe [30–33]. Often these fractures are subtle but, with comparative views, are detectable (Fig. 11.32). One of the reasons that they are important is that with distal phalangeal fractures, if the nail bed is broken, then complicating osteomyelitis is a common problem.

Another specific fracture of the metatarsal bones is the one which occurs through the base of the fifth metatarsal or the so-called Jones fracture. This fracture is common and usually is sustained with inversion injuries of the ankle. It results from pulling on the base of the fifth metatarsal by the peroneus brevis muscle. Many times, however, swelling around the ankle diverts attention



Fig. 11.19 Stress fracture. (**a**) AP radiograph of the feet in a gymnast complaining of right lateral foot pain. No abnormality was seen. (**b**) Coronal STIR image of the foot shows high-signal edema in the cuboid with a hypointense fracture line distally (*arrow*). (**c**) The fracture (*arrow*) is confirmed on the T1-weighted image

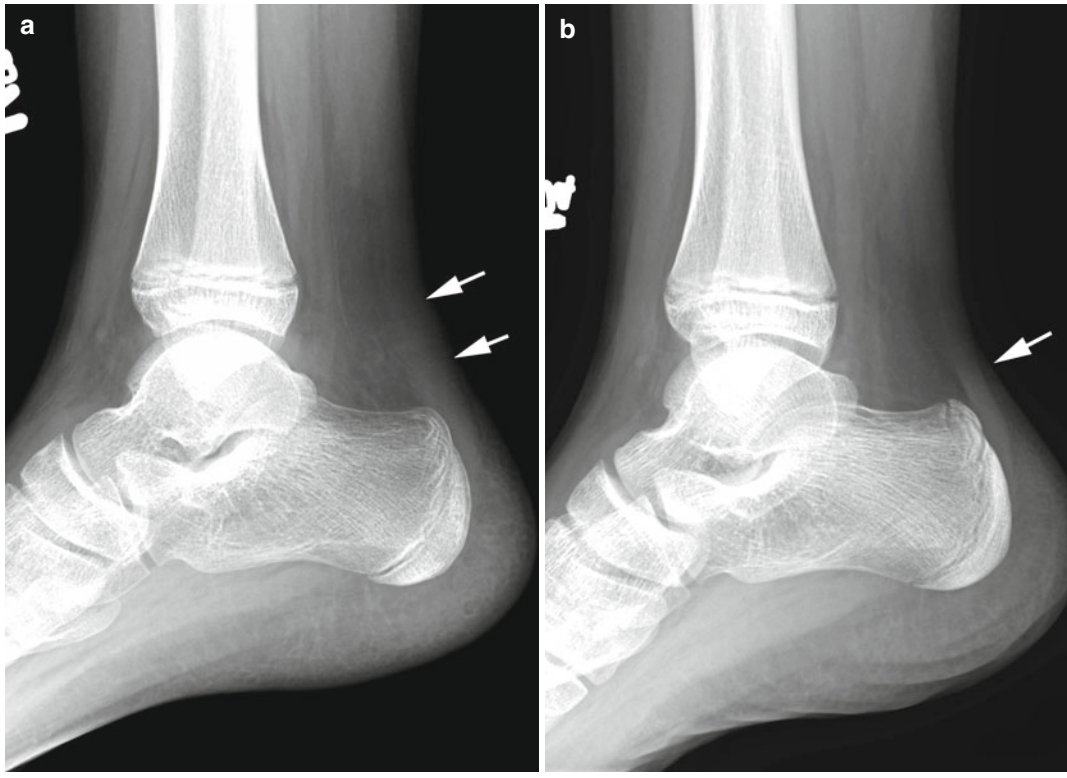


Fig. 11.20 Achilles tendonitis. (**a**) Note the indistinct margins and some thickening of the Achilles tendon (*arrows*). The pre-Achilles fat pad also is somewhat reticulated and indistinct. (**b**) Normal side for comparison. Note the normal, distinct Achilles tendon (*arrow*) and the clear pre-Achilles fat pad

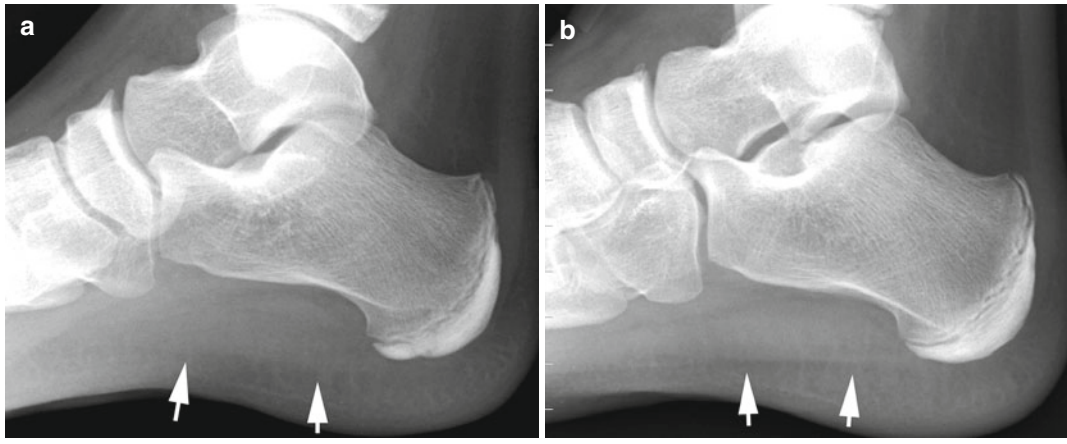


Fig. 11.21 Plantar fasciitis and stone bruise. (**a**) Note thickening and indistinctness of the plantar fascia (*arrows*). (**b**) Normal side for comparison. Note the normal distinct plantar fascia (*arrows*). (**c**) Bone bruise. Note soft tissue thickening, increased density, and indistinctness of the soft tissue structures on the right (*arrowheads*). These are findings of a stone. Compare them with the normal left side



Fig. 11.21 (continued)

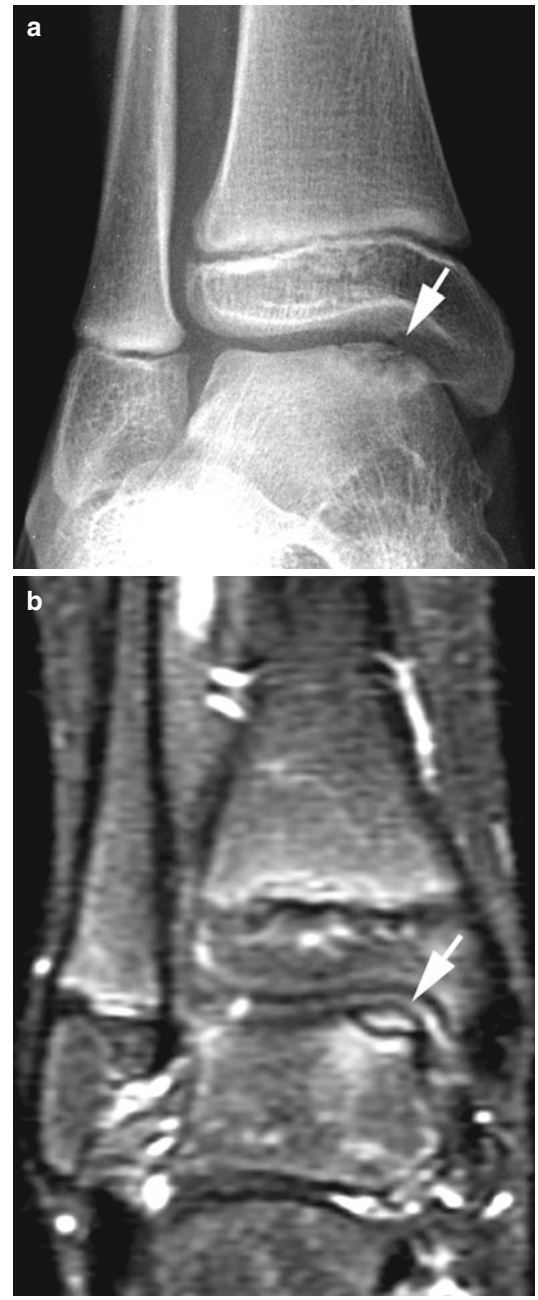


Fig. 11.22 Osteochondritis dissecans: talus. (**a**) Oblique view of the ankle demonstrates an irregular bony defect (*arrow*) over the dome of the talus. (**b**) Coronal MR STIR image demonstrates the avulsed fracture fragment with high signal (*arrow*). (**c**) Sagittal STIR image demonstrates the same fragment (*arrow*)

Fig. 11.23 Köhler's disease: aseptic necrosis navicular. (**a**) Note the small slightly dense navicular bone (*arrow*). In addition, note adjacent soft tissue edema. (**b**) Lateral ankle view. Again note the small sclerotic navicular bone but, more importantly, overlying soft tissue edema (*arrows*). (**c**) Normal irregular/sclerotic navicular bone. Note the normal appearance of the navicular bone on both sides (*arrows*). (**d**) Note normal wedge deformities of the navicular bone on both sides (*arrows*)

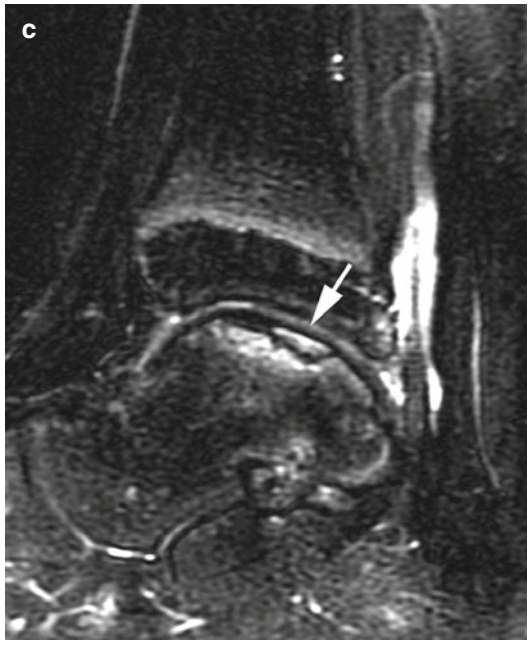
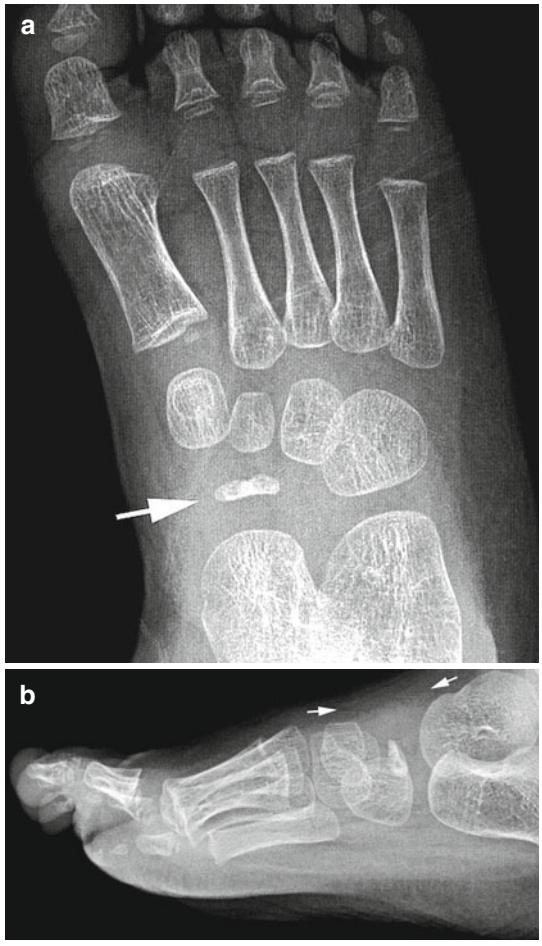
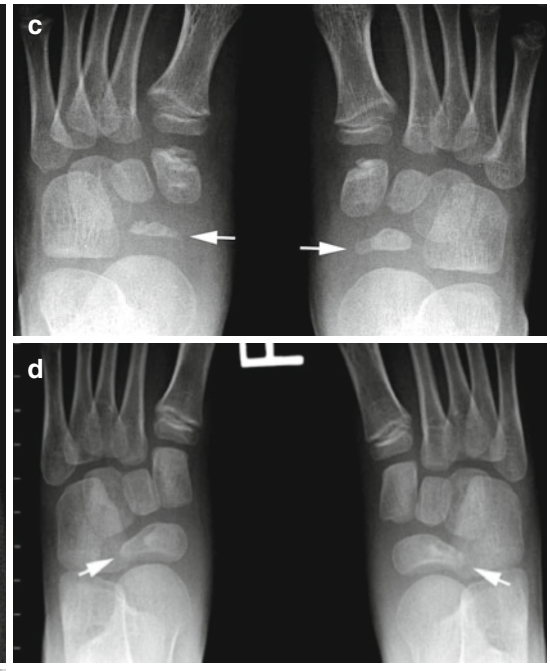


Fig. 11.22 (continued)





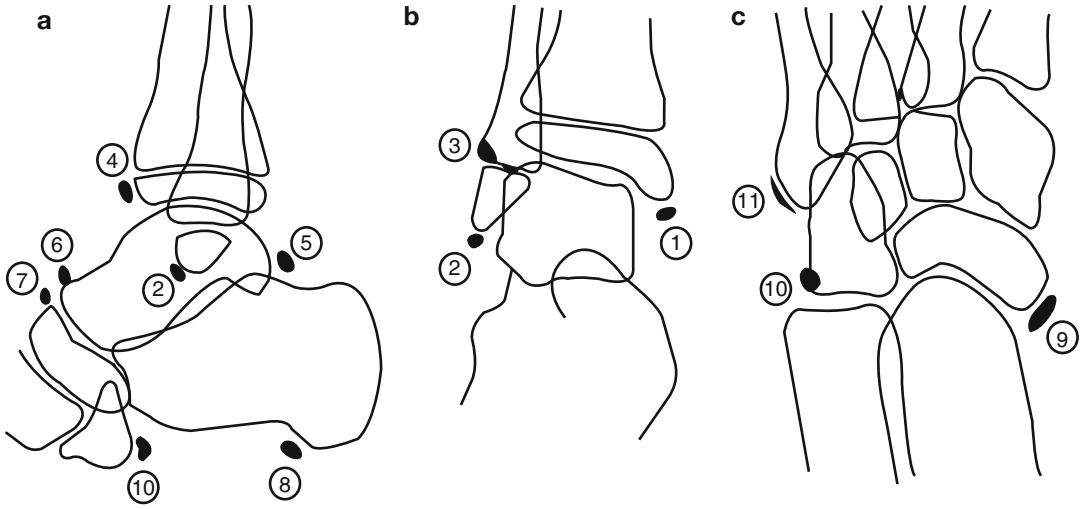


Fig. 11.24 Accessory ossicles about the ankle: diagrammatic representation. (**a**–**c**) Accessory center of medial malleolus or os subtibiale (*1*), accessory center of distal fibular epiphysis or os subfibulare (*2*), accessory metaphyseal fibular ossicle (*3*), os talotibiale (*4*), os trigonum (*5*), os supratalare (*6*), os supranaviculare (*7*), os subcalcis (*8*), os subtibiale externum (*9*), os peroneum (*10*), and os vesalianum (*11*)

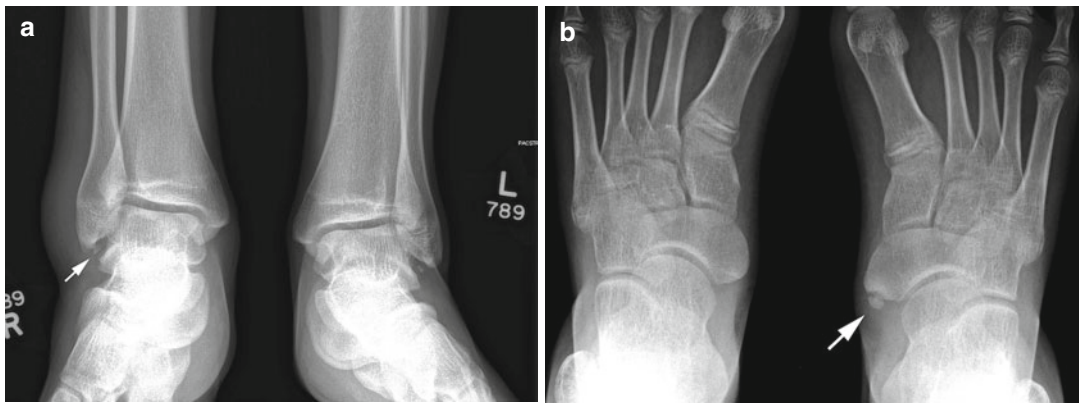


Fig. 11.25 Accessory centers: malleoli. (**a**) Note the ossicle (*arrow*) off of the right fibular epiphysis. There is a lot of soft tissue swelling, and at first, one might consider this to be an avulsion fracture. However, on the other side, the normal left side, the same ossicle is present. (**b**) Os naviculare. Note the normal Os naviculare (*arrow*) off of the navicular bone

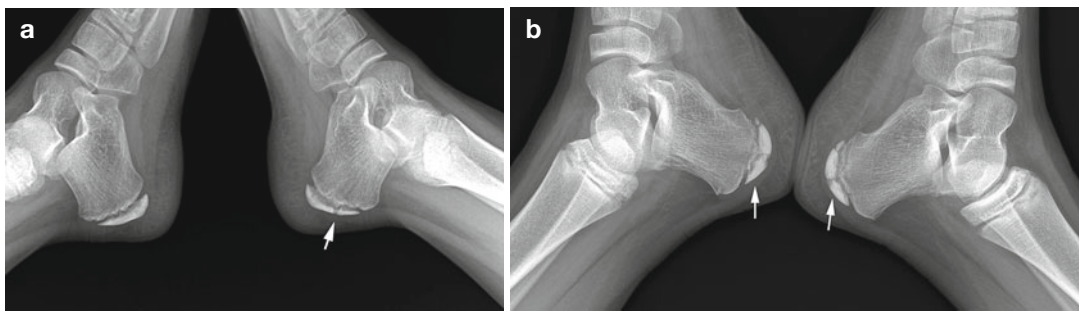


Fig. 11.26 Calcaneal apophysis: normal sclerotic/fragmented appearance. (**a**) Note the dense calcaneal apophysis on the right with a defect (*arrow*) which might at first suggests a fracture. However, note that there is no associated soft tissue swelling. (**b**) Note the very irregular and sclerotic calcaneal apophysis (*arrows*) which also is normal



Fig. 11.27 Tarsal bones: irregular ossification. (**a**) Note irregular ossification of the tarsal navicular (*arrow*). (**b**) There is irregular ossification of a number of the tarsal bones and in addition of the apophyses of the metatarsals

from this fracture, and it is not until the fracture is detected roentgenographically that the injury comes to light (Fig. 11.33).

In *differentiating fractures of the base of the fifth metatarsal from the normal os vesalianum*, it should be noted that the fractures almost always are transverse or near transverse (Fig. 11.33), while the os vesalianum usually is a longitudinal structure (Fig. 11.34a). However, the os vesalianum can be avulsed or even fractured (Fig. 11.34b). Clinically the findings are accompanied by focal tenderness over the base of the fifth metatarsal.

Miscellaneous Injuries of the Foot

Lisfranc fractures are uncommon but can be seen with epiphyseal–metaphyseal fractures (Fig. 11.35a). MRI can be useful in detecting occult fractures at the Lisfranc joint and to evaluate the integrity of Lisfranc ligament (Fig. 11.35b, c). Similarly fractures of the sesamoid bone over the great toe can be seen. These latter fractures tend to occur in older children and teenagers and need to be differentiated from the normal bifid sesamoid bone (see Fig. 11.40a). The term "turf toe" is used to describe a wide



Fig. 11.28 Metatarsal fractures: various. (**a**) Oblique spiral fracture of the fifth metatarsal (*arrow*). (**b**) Linear fracture of the first metatarsal (*arrow*). Also note the buckle fracture through the distal second metatarsal (*arrowhead*). (**c**) Subtle buckle fracture through the bases of the third and fourth metacarpals (*arrows*). (**d**) Buckle fractures through the distal ends of the third and fourth metatarsals. There probably is a minimal buckle fracture through the distal second metatarsal and a minimal angled buckle fracture through the distal fifth metatarsal. (**e**) Salter–Harris III fracture (*arrow*) of the proximal first metatarsal

spectrum of capsule-ligamentous sprains at the first metatarsophalangeal joint sustained by a hyperextension injury [33]. It is most often seen in football players. The forces that cause soft tissue injuries in turf toe also cause osseous injury primarily affecting the sesamoids but also the metatarsal head and the proximal phalanx (Fig. 11.36). Management is usually nonsurgical with varying duration of immobilization based upon the severity of injury. Early surgery for turf toe is indicated when large tendon ligament tears are present, in cases of joint instability, or when sesamoid diastasis or migration is present [34].

Stress fractures in the foot are reasonably common in the older child but not in the infant. Of these, the best known is the stress fracture of the second metatarsal, the so-called March fracture. As with any stress fracture, the fracture line may



Fig. 11.28 (continued)

be difficult to detect in its early stages, but the fracture becomes evident because it causes abundant periosteal new bone deposition. Nonetheless one may only see thickening of the cortex (Fig. 11.37a). Occult stress fractures now are readily identified with MR imaging (Fig. 11.37b, c). Stress fractures of the proximal phalanx of the great toe also have been described [35].

Another lesion in the foot that causes pain is aseptic necrosis of the second metatarsal head or Freiberg's disease. Roentgenographically, the findings range from increased sclerosis to sclerosis interspersed with focal bony resorption of the second metatarsal head (Fig. 11.38). Osteochondritis dissecans in the foot is rare but has been documented in the epiphysis of the first metatarsal [36].

Normal Findings Causing Problems

The os vesalianum, or accessory ossification center at the base of the fifth metatarsal, has been dealt with earlier in this chapter and is a common



Fig. 11.29 Metatarsal fractures: subtle. (**a**) Note suggestion of a subtle angled buckle fracture through the distal fifth metatarsal (*arrow*) on the left. There is swelling in the area. (**b**) Oblique view clearly demonstrates the buckle fracture (*arrow*). (**c**) In this patient, an oblique view demonstrates an angled buckle fracture through the distal third metatarsal and a minimal buckle fracture through the distal second metatarsal (*arrows*). Compare with the contour of the other metatarsals. (**d**) Subtle transverse buckle fracture through the second and third metatarsals (*arrows*). (**e**) In this patient, there was pain over the left forefoot. In this regard, note that the soft tissues space between the first and second metatarsal is increased consistent with edema. However, a fracture is not visualized. (**f**) Oblique view, however, demonstrates a minimal buckle fracture through the base of the second metatarsal (*arrow*). Rearrange E&F. The counterclockwise sequence is not good

Fig. 11.29 (continued)



normal finding misinterpreted as a fracture of the base of the fifth metatarsal (see Fig. 11.33). Irregular ossifications of the epiphyses or apophyses of the metatarsals and phalanges also are commonly encountered (Fig. 11.39)

The bipartite sesamoid bone of the great toe is a common normal variation frequently misinterpreted for a fracture of the sesamoid bone (Fig. 11.40a). Sesamoid bones do fracture, but a bipartite sesamoid is much more common. The sesamoid bones tend to occur over the head of the first metatarsal. Another normal finding confused with a Salter–Harris III fracture of the epiphysis of the great toe is the bipartite epiphysis (Fig. 11.40b).

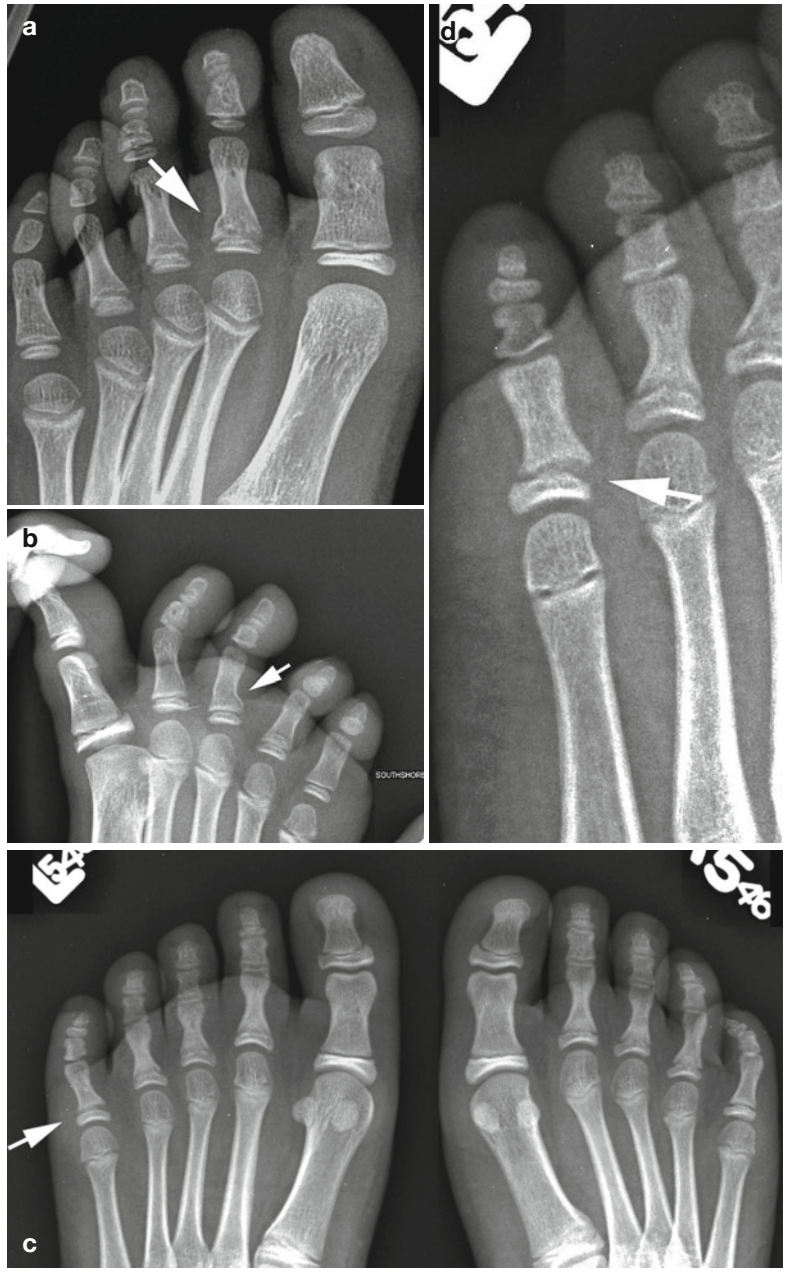


Fig. 11.30 Phalanges: various fractures. (**a**) Note the buckle fracture/Salter–Harris fracture through the base of the proximal phalanx of the second digit (*arrow*). (**b**) In this patient, an angled buckle fracture is present through the base of the proximal phalanx of the third digit (*arrow*). (**c**) This patient demonstrates a minimally displaced Salter–Harris fracture (*arrow*) through the base of the proximal phalanx of the fifth digit. (**d**) Oblique view more clearly demonstrates the fracture (*arrow*). Rearrange sequence of figs. counterclockwise arrangement is not good

Fig. 11.32 Salter–Harris I injuries of the great toe. (**a**) Note the widened epiphyseal plate (*arrow*) through the distal phalanx on the left. (**b**) A more subtle Salter–Harris I fracture (*arrow*) is seen in this patient. (**c**) This patient demonstrates Salter–Harris I fractures through both the proximal and distal phalanges (*arrows*). (**d**) Salter–Harris III fracture (*arrow*) through the base of the proximal phalanx of the first digit

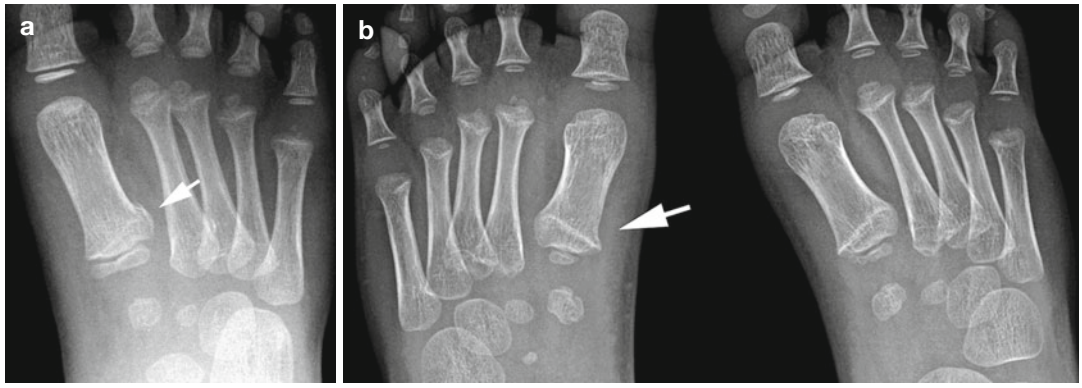


Fig. 11.31 Bunk bed fracture: first metatarsal type. (**a**) Note the buckle fracture through the proximal first metatarsal (*arrow*). (**b**) In this patient, a very subtle angled buckle fracture (*arrow*) is present through the base of the first metatarsal. Note soft tissue swelling around the metatarsal



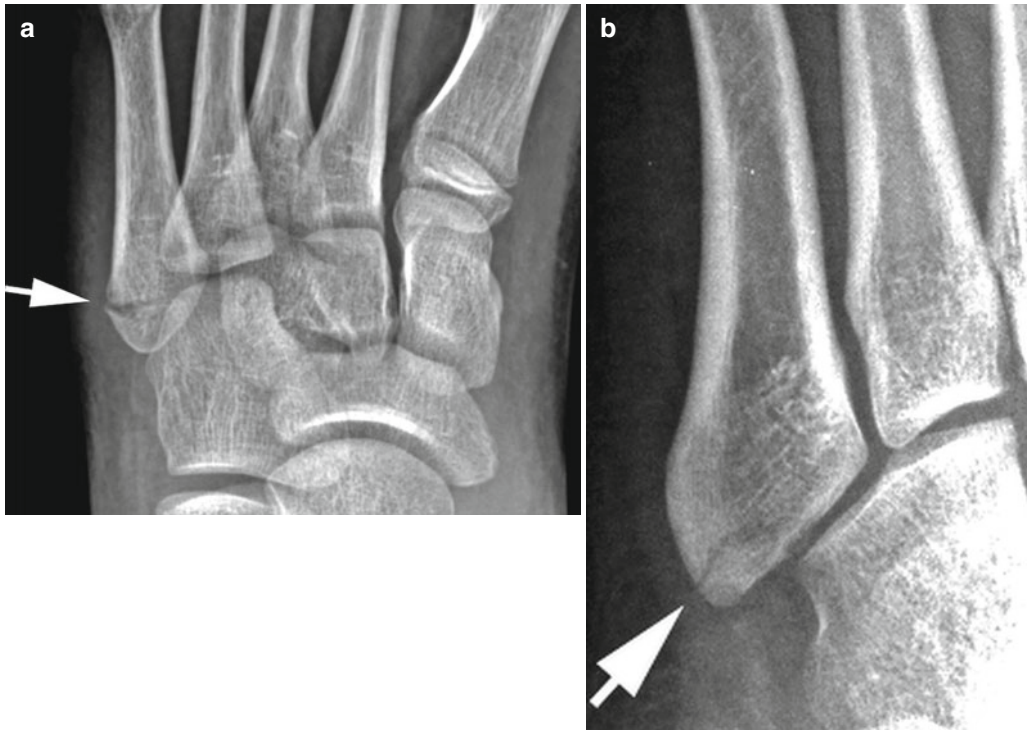


Fig. 11.33 Jones fracture. (**a**) Note the typical transverse Jones fracture (*arrow*) through the proximal fifth metatarsal. (**b**) In this patient, a more subtle fracture (*arrow*) is seen

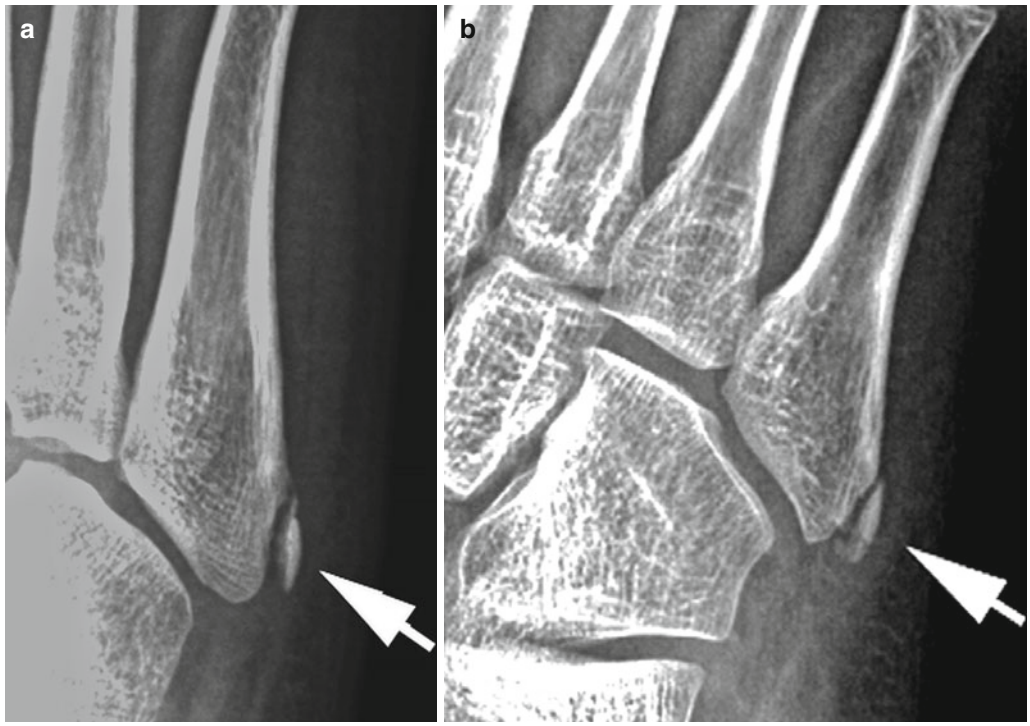


Fig. 11.34 Os vesalianum. (**a**) Note the normal appearance and position of the os vesalianum (*arrow*). (**b**) In this patient, the proximal os vesalianum is disrupted, and a subtle, transverse fracture is suggested (*arrow*)



Fig. 11.35 (**a**) Lisfranc fracture. Note separation between the first and second metatarsals (*arrow*). Then note an avulsion fracture of the cuneiform bone and an Salter–Harris I fracture through the base of the first metatarsal. (**b**) Occult fracture. AP radiograph of bilateral feet in a teenager complaining of foot pain after trauma. No fracture is seen. (**c**) Coronal STIR image of the involved foot shows high-signal edema in the base of the second metatarsal surrounding a nondisplaced fracture seen as a hypointense line (*white arrow*). Note that the Lisfranc ligament is intact (*arrowhead*)



Fig. 11.36 Sesamoid fracture and turf toe. (**a**) Note the transverse sesamoid bone fracture (*arrow*). (**b**) Another patient with a turf toe. Coronal T1-weighted image of the forefoot in a teenager with hyperextension injury of the toe shows a nondisplaced fracture of the medial sesamoid with surrounding hypointense bone edema (*arrow*). (**c**) Axial (short-axis) STIR image confirms high-signal edema in the medial sesamoid bone and also shows contusions in the head of the 1st metatarsal and distal second metatarsal (*white arrows*). Extensive surrounding soft tissue contusion is seen. Flexor hallucis longus tendon is intact (*black arrow*). (**d**) T2-weighted sagittal image shows tear of the plantar plate in the region of the medial sesamoid phalangeal ligament (*white arrow*) with resultant plantar displacement of the sesamoid away from the head of the metatarsal. (**e**) Coronal STIR image shows tear of the medial collateral ligament at its proximal insertion (*white arrow*)



Fig. 11.36 (continued)



Fig. 11.37 Stress fracture: second metatarsal. (**a**) Note thickening of the cortex (*arrows*) in this chronic stress fracture of the second metatarsal. (**b**) This patient had pain over the left forefoot. Note swelling around the first metatarsal, but a fracture is not visible. (**c**) MR, sagittal STIR MR image, demonstrates increase signal through the marrow of the first metatarsal (*arrow*) consistent with a stress reaction



Fig. 11.38 Freiberg's disease. Note impaction, slight deformity, and some increased sclerosis through the second metatarsal head (*arrow*)

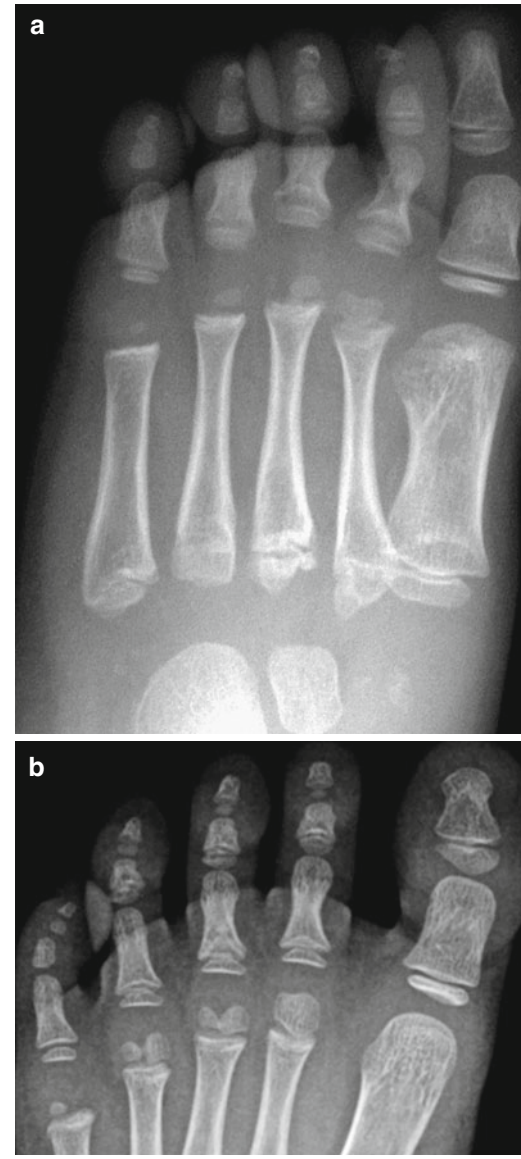


Fig. 11.39 Ossification variations of the foot. (**a**) Note the numerous irregularly ossified apophyses of the metatarsals. (**b**) Note the peculiarly shaped epiphyses, bipartite epiphyses, and cone epiphyses involving the foot

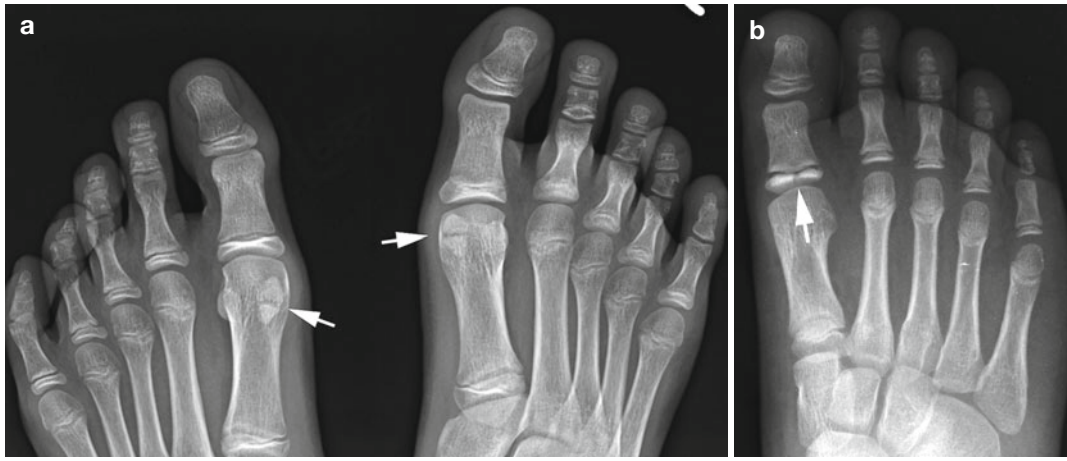


Fig. 11.40 (**a**) Bipartite sesamoid bones. Note the bilateral bipartite sesamoid bones (*arrows*). (**b**) Bipartite epiphysis. Note the bipartite epiphysis (*arrow*) through the base of the proximal phalanx of the first digit. Fractures can appear somewhat similar

References

1. Hayden Jr CK, Swischuk LE. Para-articular soft tissue changes in infections and trauma of the lower extremity in children. AJR. 1980;134:307–11.
2. Towbin R, Dunbar JS, Towbin J, Clark R. Teardrop sign: plain film recognition of ankle effusion. AJR. 1980;134:985–90.
3. Swischuk LE. Musculoskeletal: what's different in children? Swings on a rope, falls seven feet, twists ankle; ankle pain. Emerg Radiol. 2013;20:173–174. [Epub ahead of print].
4. Felman AH. Tillaux fractures of the tibia in adolescents. Pediatr Radiol. 1989;20:87–9.
5. Verma S, Hamilton K, Hawkins HH, Kothari R, Singal B, Buncher R, Nguyen P, O'Neill M. Clinical application of the Ottawa ankle rules for the use of radiography in acute ankle injuries: an independent site assessment. AJR. 1997;169:825–7.
6. Zomorrodi A, Bennett JE, Attia MW, Loiselle J, Rogers KJ, et al. Consistent between emergency department and orthopedic physicians in the diagnosis and treatment of distal fibular Salter Harris I fractures. Pediatr Emerg Care. 2011;27:301–3.
7. Chong-Han CH, Yngve DA, Lee JY, Hendrick EP, John SD, Swischuk LE. Comparison view for subtle physeal injury in the pediatric ankle. Emerg Radiol. 2001;8:207–12.
8. Bauer G, Kinzl L. Fracture of the cuboid in children: case report and review of the literature. J Pediatr Orthop. 1998;18:466–8.
9. Blumberg K, Patterson RJ. The toddler's cuboid fracture. Radiology. 1991;179:93–4.
10. John SD, Moorthy CS, Swischuk LE. Expanding the concept of the toddler's fracture. Radiographics. 1997;17:367–76.
11. Swischuk LE. Musculoskeletal: what's different in children? Being checked for cough, congestion, and also complaints of limping. Emerg Radiol. 2013;20(1):1–2.
12. Inokuchi S, Usami N, Hiraishi E, Hasmimoto T. Calcaneal fractures in children. J Pediatr Orthop. 1998;18:469–74.
13. Laliotis N, Pennie BH, Carty H, Klenerman L. Toddler's fracture of the calcaneum. Injury. 1993;24:169–70.
14. Oestreich A, Bhojwani N. Stress fractures of ankle and wrist in childhood: nature and frequency. Pediatr Radiol. 2010; 40:1387–9.
15. Schindler A, Mason DE, Allington NJ. Occult fracture of the calcaneus in toddlers. J Pediatr Orthop. 1996;16:201–6.
16. Starshak RJ, Simons GW, Sty JR. Occult fracture of the calcaneus: another toddler's fracture. Pediatr Radiol. 1984;14:37–40.
17. Heneghan MA, Wallace T. Heel pain due to retrocalcaneal bursitis-radiographic diagnosis. Pediatr Radiol. 1985;15:119–22.
18. Kainberger FM, Engel A, Barton P, Huebsch P, Neuhold A, Salomonowitz E. Injury of the Achilles tendon: diagnosis with sonography. AJR. 1990;155: 1031–6.
19. Micheli LJ, Ireland ML. Prevention and management of calcaneal apophysitis in children: an overuse syndrome. J Pediatr Orthop. 1987;7:34–8.
20. Cardinal E, Chhem RK, Beauregard CG, Aubin B, Pelletier M. Plantar fasciitis: sonographic evaluation. Radiology. 1996;201:257–9.
21. Higuera J, Laguna R, Peral M, Aranda E, Soleto J. Osteochondritis dissecans of the talus during childhood and adolescence. J Pediatr Orthop. 1998;18: 328–32.
22. Weston WJ. Köhler's disease of the tarsal scaphoid. Australas Radiol. 1978;12:332–7.

23. Ogden JA, Lee J. Accessory ossification patterns and injuries of the malleoli. J Pediatr Orthop. 1990;10: 306–16.
24. Shopfner CE, Coin CG. Effect of weight-bearing on the appearance and development of the secondary calcaneal epiphysis. Radiology. 1966;86:201–6.
25. Swischuk LE. Musculoskeletal: what's different in children, pushed by a friend, foot-rolled, now can't walk. Emerg Radiol. 2011;18:275–7.
26. Swischuk LE. Musculoskeletal: what's different in children, fell out of bed and now the right foot hurts. Emerg Radiol. 2012;19:1–4.
27. Swischuk LE. Musculoskeletal: what's different in children, jumped of bed: foot pain. Emerg Radiol. 2009;16:171–4.
28. Swischuk LE. Jumping on bed, mother hears screaming, patient on floor holding left foot. Pediatr Emerg Care. 2010;26:220–1.
29. Johnson GF. Pediatric lisfranc injury: "bunkbed" fracture. AJR. 1981;137:1041–4.
30. Swischuk LE. Musculoskeletal: what's different in children, tripped and jammed my toe. Emerg Radiol. 2010;17:1–2.
31. Swischuk LE. Musculoskeletal: what's different in children, great toe injury during soccer. Emerg Radiol. 2011;18:93–4.
32. Pinckney LE, Currarino G, Kennedy LA. The stubbed great toe: a cause of occult compound fracture and infection. Radiology. 1981;138:375–7.
33. Watson TS, Anderson RB, Davis WH. Periarticular injuries to the hallux metatarsophalangeal joint in athletes. Foot Ankle Clin. 2000;5(3):687–713.
34. Anderson RB. Turf toe injuries of the hallux metatarsophalangeal joint. In: Techniques in foot and ankle surgery. Philadelphia: Lippincott Williams & Wilkins; 2002. p. 102–11.
35. Yokoe K, Mannoji T. Stress fracture of the proximal phalanx of the great toe: a report of three cases. Am J Sports Med. 1986;14:240–2.
36. Falkenberg MP, Dickens DRV, Menelaus MB. Osteochondritis of the first metatarsal epiphysis. J Pediatr Orthop. 1990;10:797–9.

Battered Child Syndrome/ Non-accidental Trauma

12

The presentation of a battered child or a child/infant subject to non-accidental trauma is common in the emergency room setting. Very often the patient presents with a bizarre history, no history, or a suspicious history. Usually a detailed history is the true history, while a nebulous, changing, or not making sense history is suspicious. In addition, in many cases, the imaging findings are obscure or just at the edge of the film because the film was not obtained for the prime purpose of looking for fractures. For example, in the infant illustrated in Fig. 12.1, the presenting problem was that of something wrong in the abdomen. The parents claimed that every time they tried to pick up the infant, the infant cried and the abdomen seemed to be a little distended. That is all there was to the history. Because of this, a single supine view of the abdomen was obtained (Fig. 12.1). When the image was inspected, the abdomen appeared normal. There was no evidence of visceromegaly, bowel obstruction, free air, or any other intraabdominal problem. However, with closer inspection, healing rib fracture were seen in the lower ribs (Fig.12.1a, b). This case not only emphasizes that one needs to look at the corners of the films but also that one needs to look at the ribs. We have had a rule for a long time, and the rule goes as follows "if you are dealing with a potential battered child or you are dealing with an infant/young child where things do not seem to be fitting, take a second look at the ribs." It is very difficult for an infant/young child to sustain rib fractures from ordinary activity [1–4]. When present, they are a very strong signal that non-accidental trauma is at play.

Fresh rib fractures, unless some angulation of the ribs occurs, may be difficult to detect. Angulated fractures are more readily detected (Fig. 12.2a, b), and all of these rib fractures may require oblique views of the chest for full evaluation and detection. Thereafter, as the fractures heal, callus formation is deposited around the fracture, and eventually the fracture has a round "ball-like" appearance (Fig. 12.2c, d). This appearance places the fracture somewhere between 2 and 4 weeks of age. Thereafter the callus smooths out, and only a thick rib is identified (Fig. 12.2e). All in all, from fresh fracture to thick rib requires about 10 weeks [3].

Rib fractures have different mechanics at play in terms of whether they are posterior, mid, or anterior fractures [1–4]. With posterior fractures, shaking leverage against the transverse process causes the proximal rib to fracture [2]. These fractures may be difficult to detect on initial films but usually are apparent with healing (Fig. 12.3a). Fractures through the midportion of the ribs occur from squeezing and shaking and are the easiest to detect (Fig. 12.3b). With anterior rib fractures, costochondral separations occur from shaking (mainly) and squeezing. Initially very little if anything abnormal is seen, but eventually there is increased cupping and density of the anterior ribs (Fig. 12.3c). Of the three fractures, the anterior rib fractures are the most difficult to detect [4], and they are usually easier to detect on lateral chest films.

L.E. Swischuk, S.P. Jadhav (eds.), *Emergency Musculoskeletal Imaging in Children*,
DOI 10.1007/978-1-4614-7747-1_12, © Springer Science+Business Media New York 2014

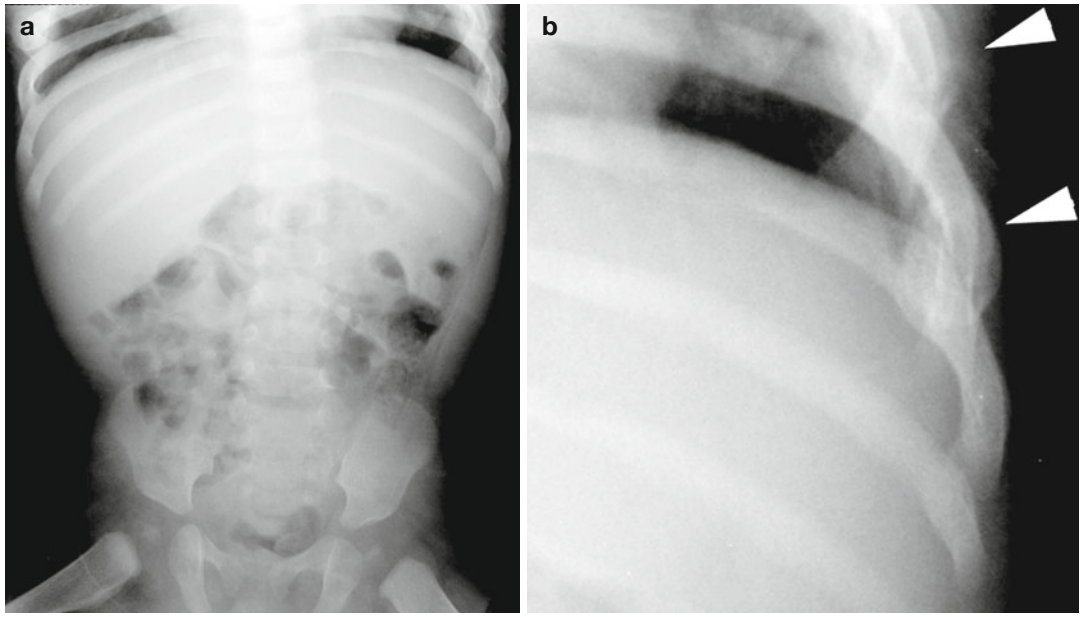


Fig. 12.1 (**a**) KUB in patient who was irritable and cranky. The abdominal findings are normal, but there is evidence of healing rib fractures bilaterally, just at the top edges of the image. (**b**) Magnified view of the left ribs demonstrates healing rib fractures (*arrowheads*)

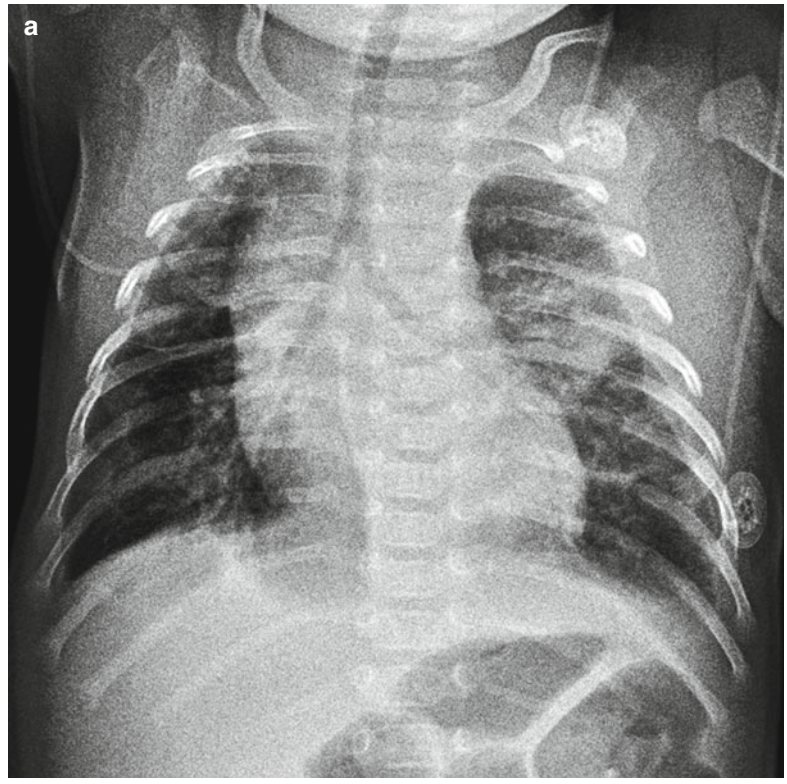


Fig. 12.2 Rib fractures: healing sequence, various patients. (**a**) In this patient, acute angled rib fractures are seen on the left. There also is some pleural thickening. All of this suggests acute injury. (**b**) Close-up demonstrates the angled rib fractures (*arrows*). (**c**) Healing phase, approximately 2 weeks. Note early callus formation around the healing rib fractures (*arrows*). (**d**) Healing approximately 4 weeks. Note the abundant target-like callus formation around the ribs. (**e**) Ten plus weeks out, only residual thickening of the ribs is seen (*arrows*)

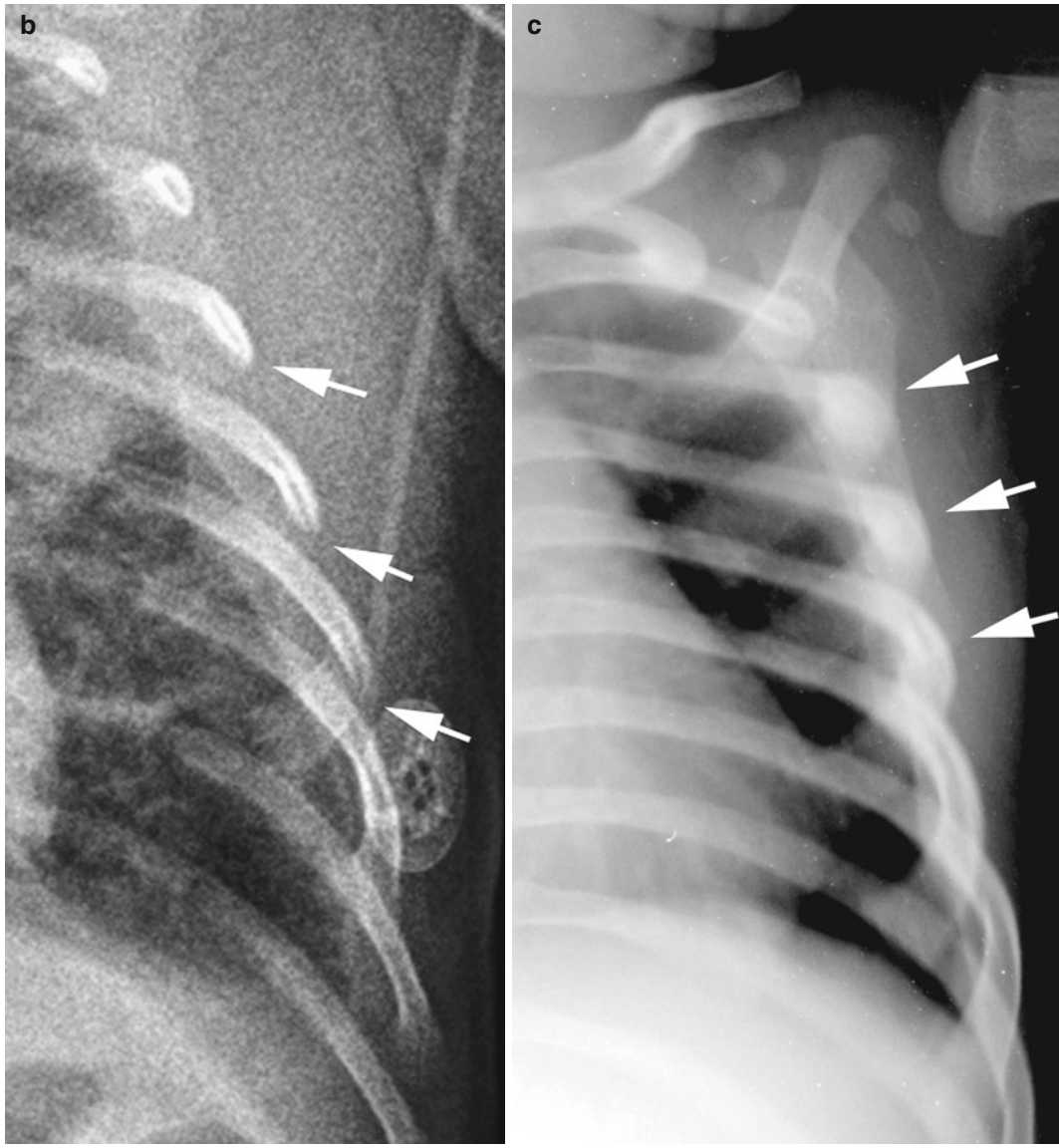


Fig. 12.2 (continued)

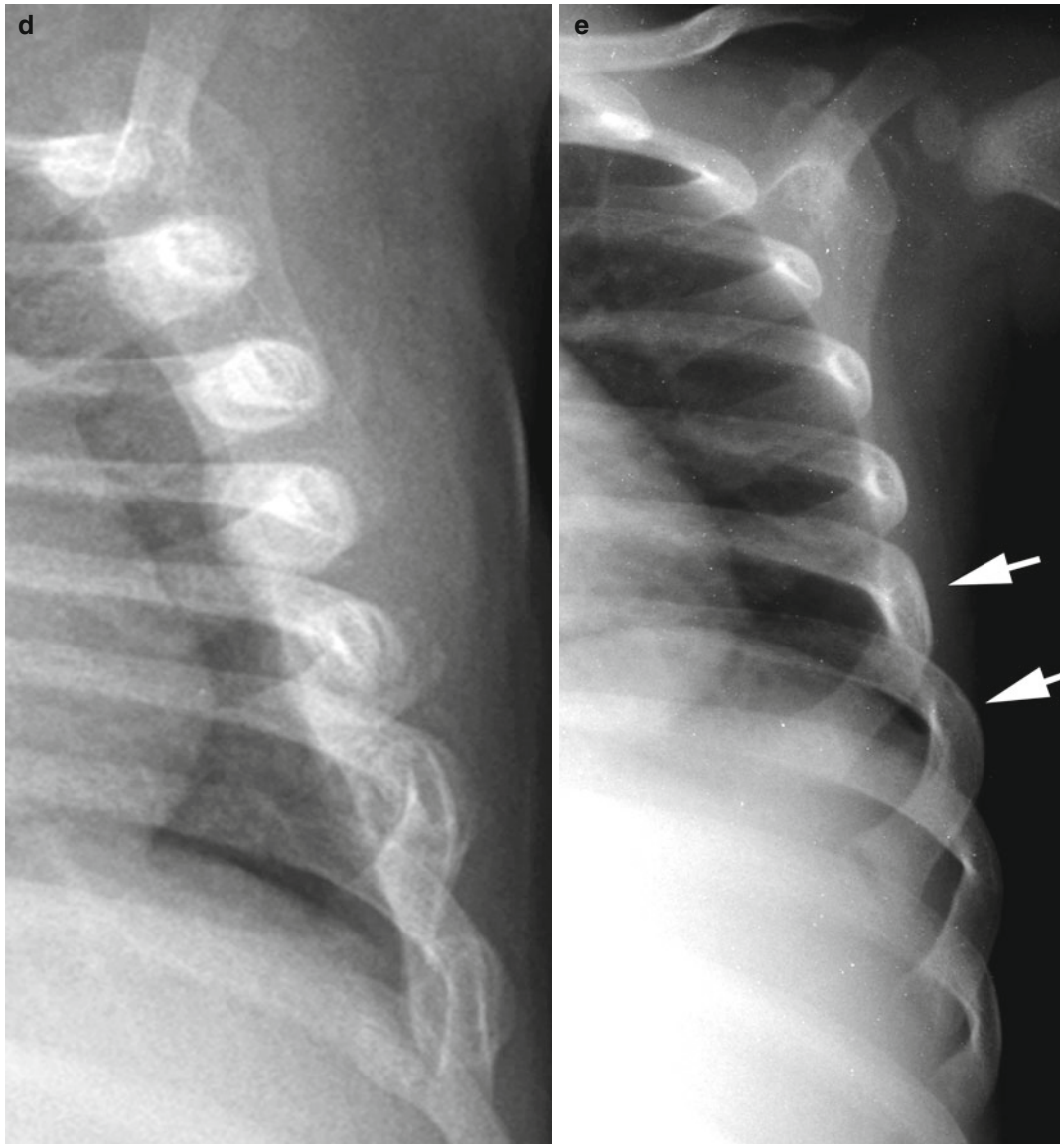


Fig. 12.2 (continued)

Next to the ribs, always look at the clavicles [3]. The reason for this is that when an infant is shaken, the hands and fingers go around the thorax and squeeze the thorax and ribs, but the thumbs are anchored over the anterior chest with their tips usually lying over the clavicles. Therefore, not only do the ribs suffer from squeezing and shaking but so do the clavicles (Fig. 12.4). The healing sequence of clavicular fractures is the same as with rib fractures, and therefore, from fracture to only a thick clavicle is about a 10-week time period.

Metaphyseal corner fractures are characteristic of the "shaken baby syndrome" [5, 6]. These fractures are basically Salter–Harris I or II fractures which occur over a 360° radius around the involved metaphysis. In other words, with shaking, there is back and forth, side to side, and rotation of the extremities around the involved joint. Because of this, a ring of bone is avulsed from

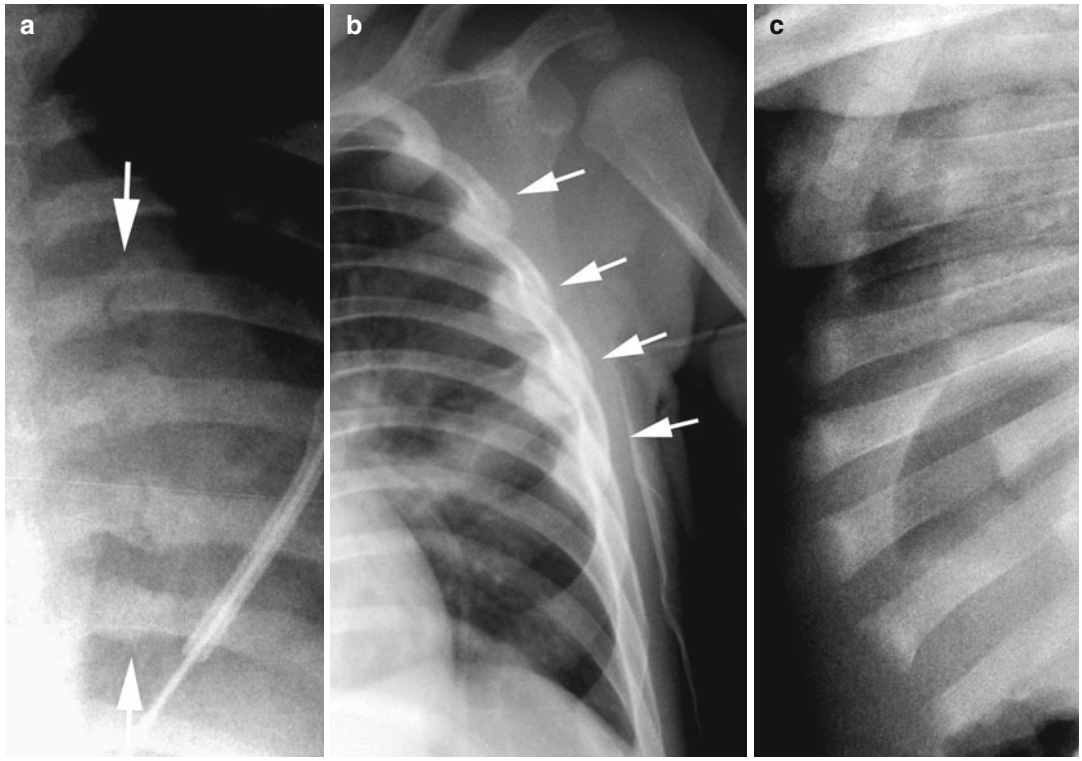


Fig. 12.3 Rib fractures: location. (**a**) Posterior rib fractures healing. There are four fractures between the *arrows*. (**b**) Lateral rib fractures healing (*arrows*). (**c**) Anterior rib fractures. Costochondral fractures manifest by increased cupping and sclerosis of the anterior ribs

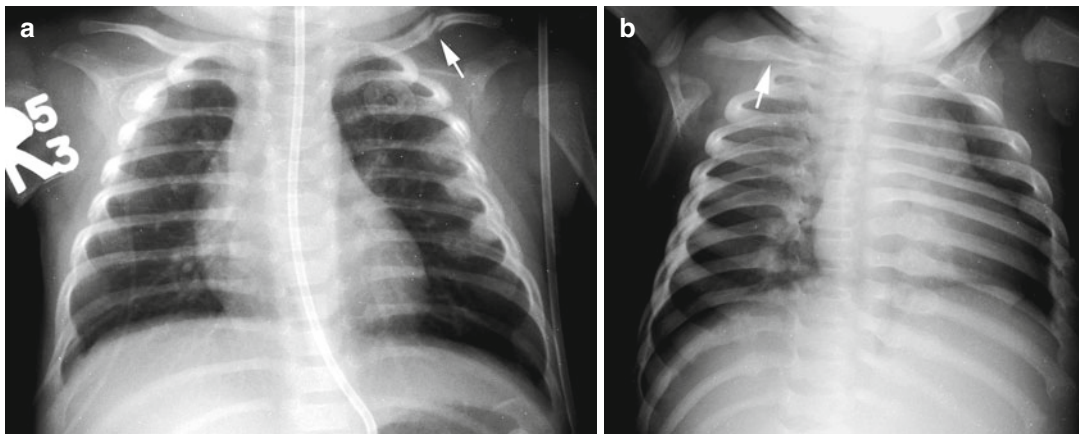


Fig. 12.4 Clavicle fractures. (**a**) Note the fresh midshaft left clavicular fracture (*arrow*). Also note subtle evidence of healing lateral rib fractures on the left, ribs two to five. (**b**) Healed clavicular fracture (*arrow*). Note the healed posterior rib fractures on the left and the right

the metaphysis. This ring of bone may be seen as an acute avulsion (Fig. 12.5d) but is more clearly visible with healing (Fig. 12.5a–c). The lesion has been referred to as the classic metaphyseal lesion (CML) [6], and although the fracture is classic for the battered child syndrome, it can be

seen under other circumstances [7, 8] including premature infants who suffer from metabolic bone diseases of the premature, rickets, neurogenic patients, and patients with physiologic bowing of the lower extremity. In all of these cases, one usually can appreciate that the underlying predisposing problem is not simple non-accidental trauma for the bones will be osteopenic (Fig. 12.5). In this regard, rickets as a condition misinterpreted for the battered child has basically been set aside [9, 10], and this also been our experience. In this regard, basically when one encounters the classic metaphyseal lesion in patients with other diseases, the patients have the severe/congenital forms of the diseases, and there will be no difficulty detecting that this predisposing condition exists. These typical corner fractures tend not to occur in the milder forms of these conditions.

Another time when the metaphyseal corner fracture can be present and be normal is in infants with physiologic bowing of the legs. Physiologic bowing is very common under 2–3 years of age and is associated with sturdy muscles. What happens is that there is pulling and stress on the medial metaphysis of the femur and often the tibia, and breaking along with corner fractures can occur (Fig. 12.6). This phenomenon occurs medially and not laterally, and therefore, if one sees beaking laterally, even in a patient with bowed legs, one should become suspicious. In addition, in patients with bowed legs, the bones are very well mineralized.

All of the foregoing has dealt with the classic presentation of the battered child syndrome. However, probably more than half of these patients suffer injury to only one extremity [3, 11–16]. Most often it is the humerus or femur that is involved, and in these cases, it is of the utmost importance to get an accurate history. If the history does not change and if it seems plausible, then one can accept the fracture as accidental. However, if the history is unclear, ambivalent, not available, etc., one needs to be very suspicious. These fractures do not result from shaking the infant. They result from fulcrum-induced forces on the extremity which result in an outwardly angled spiral or transverse fracture (Figs. 12.7 and 12.8). Indeed, we have come to treat this particular fracture configuration as very suspicious for it would be very difficult to sustain under normal circumstances, especially in the young infant. However, some of these fractures are legitimate and come with an acceptable history (Fig. 12.9).

Another fracture often coming up for consideration as possibly being due to inflicted trauma is the impaction fracture of the proximal humerus or femur (Fig 12.10). These are typical impacted buckle fractures, and if one stops to think, it would be virtually impossible for anyone to purposely inflict such a fracture on an infant. This fracture requires the abrupt blockage of the axial loading forces, such as sustained when falling on an outstretched extremity. It would be very difficult to accomplish this on purpose.

We looked at a number of our cases with such fractures and eventually determined that they were most likely legitimate. What happens in these patients is that they fall off of a couch, bed, etc. and instinctively put out their leg or their arm to break the fall. When this happens, they can sustain these fractures. At first, this finding was a surprise to us, but we now no longer consider the fracture very suspicious. This has been our conclusion and that of others [17].

Finally, a word is in order regarding two very common legitimate fractures, that is, the toddler I (tibial spiral) and toddler II (upper tibial impaction buckle) fractures. These fractures can occur in one extremity in the battered child syndrome. The toddler II fracture can result from shaking, but the toddler I (tibial spiral) fracture requires a definitive force applied to the tibia. It must be a twisting force. Nonetheless, in either case, when the fractures are bilateral and of the same age, they almost surely have been inflicted.

Skull fractures, subdural hematomas, and intercranial bleeding are a well-known part of the battered child syndrome. These areas will not be dealt with in detail in this communication. The findings usually are self-evident, and in terms of skull fractures, it is still worthwhile to obtain regular skull films and not simply perform CT studies of the head. The reason for this is that the CT studies of the head may miss horizontal fractures. Of course, these now readily can be

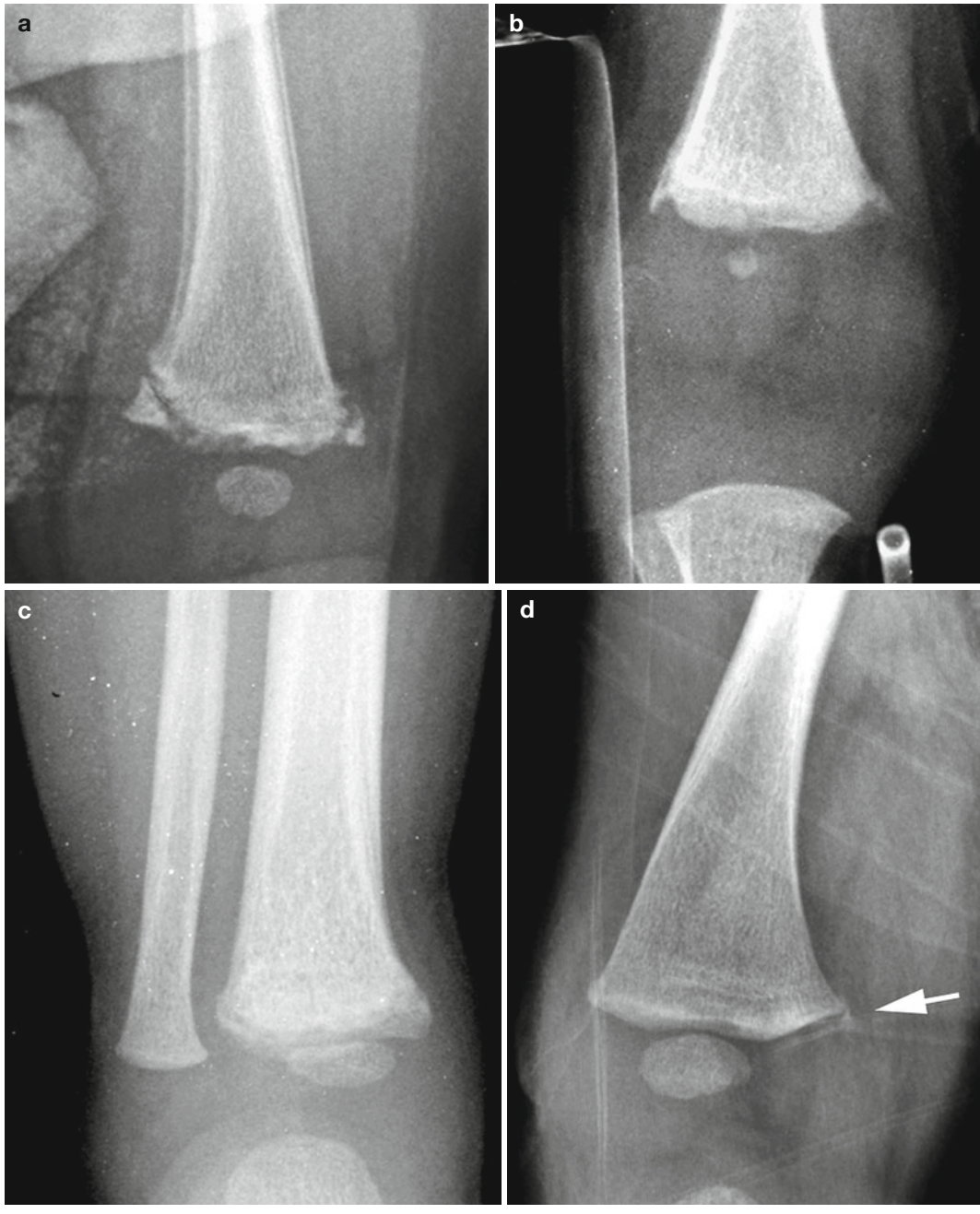


Fig. 12.5 Classic metaphyseal lesion (CML). (**a**) Typical healing epiphyseal–metaphyseal fracture with fragmentation irregularity and periosteal new-bone formation. (**b**) More advance healing leaves only residual beaking. (**c**) Healing of a minimal epiphyseal fracture. Note the irregular lucent metaphyseal edge. (**d**) Minimal ring epiphyseal–metaphyseal fracture (*arrow*)

demonstrated with 3D reconstruction of the skull (Fig. 12.11). Intraabdominal and thoracic injury is much less common.

Another group of infants who may be abused but the fact that they were abused is not appreciated on initial contact are those infants suffering

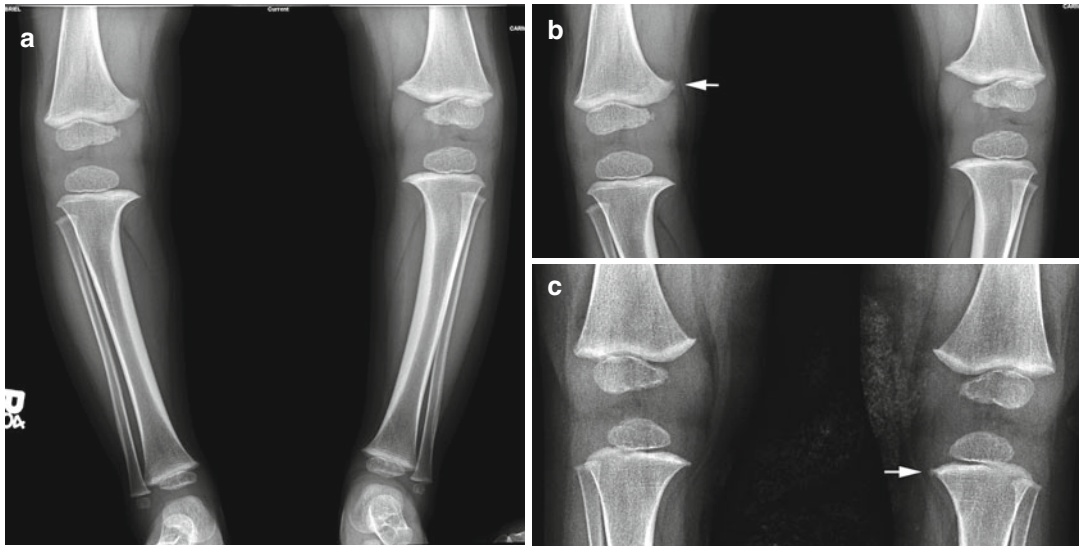


Fig. 12.6 Bowed legs and beaking. (**a**) Note bowed legs. The bones are well mineralized. There is beaking of the upper tibias and lower femurs. Some fragmentation is present through the medial right distal femoral beak. (**b**) Magnified view more clearly demonstrates the beaking irregularity on the right (*arrow*). (**c**) Another patient with beaking and some fragmentation of the upper medial tibial metaphysis on the left (*arrow*)

from the presumed sudden infant death syndrome and/or unexplained seizure activity. In most of these infants, there are no signs of head injury, and on CT studies, only brain edema seen on the brain may be normal. These patients often have been suffocated, and this is another time to take a look at the ribs and the clavicles to see if there are any fractures present.

Spine injury and intraspinal canal hemorrhage are not common but do occur [18–23], including the cervical spine where even the hangman fracture is seen [24, 25]. With the heavy head in infants, it is not a surprise that with shaking, a hangman fracture could occur. In general, spine fractures sustained in the battered child syndrome are not subtle but rather overt (Fig. 12.12). Visceral injury also can occur in the battered child syndrome.

In conclusion, the imagers role in dealing with non-accidental trauma is to know what type of fractures occur, where they occur, and what is there significance. In this regard, rib and clavicular fractures are very suspicious along with the outward angled single long bone fracture. If there is any confusion regarding the presence of entities such as rickets and metabolic bone disease, one should remember that the bones in the battered child are normally mineralized and formed.

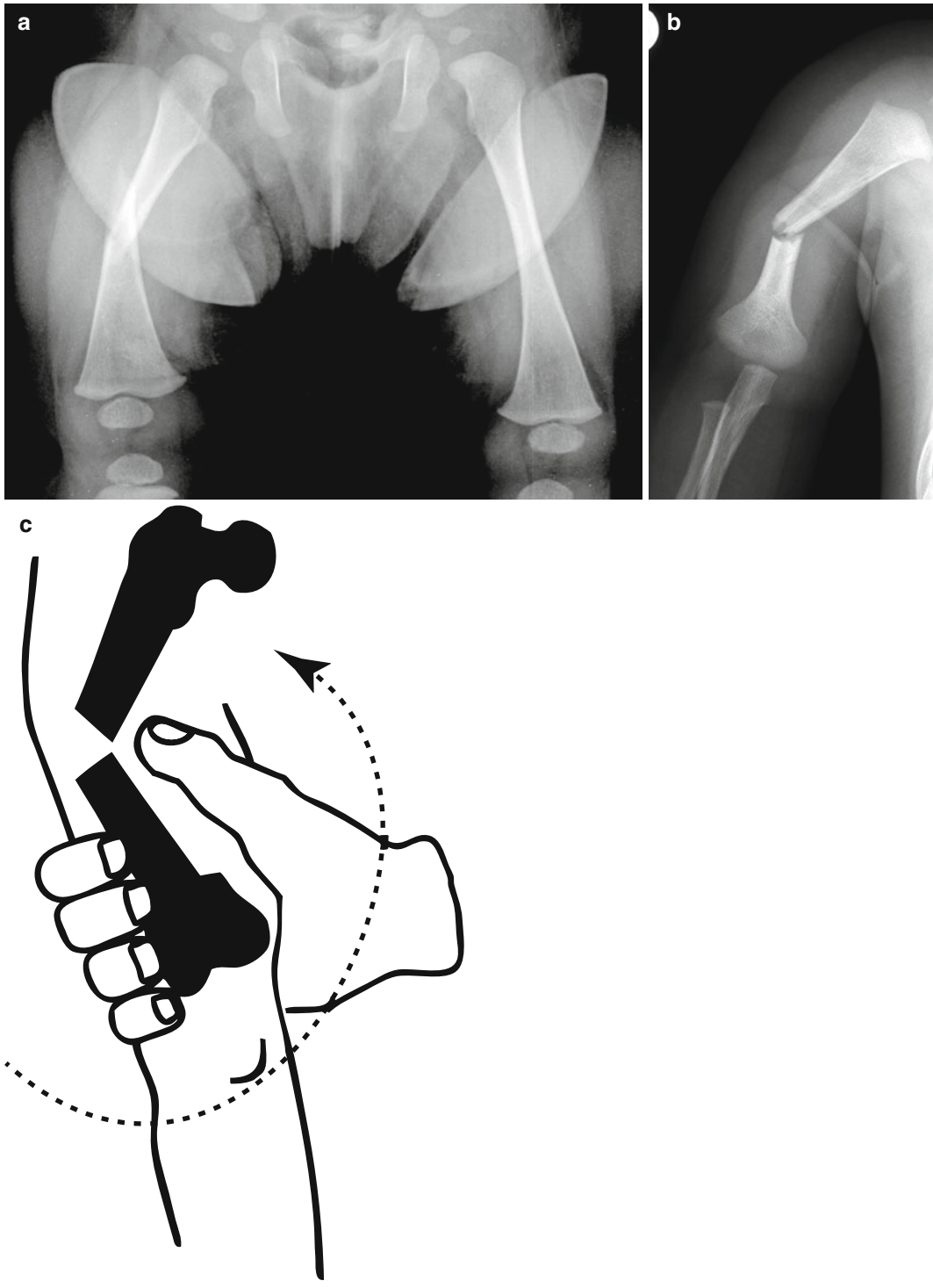
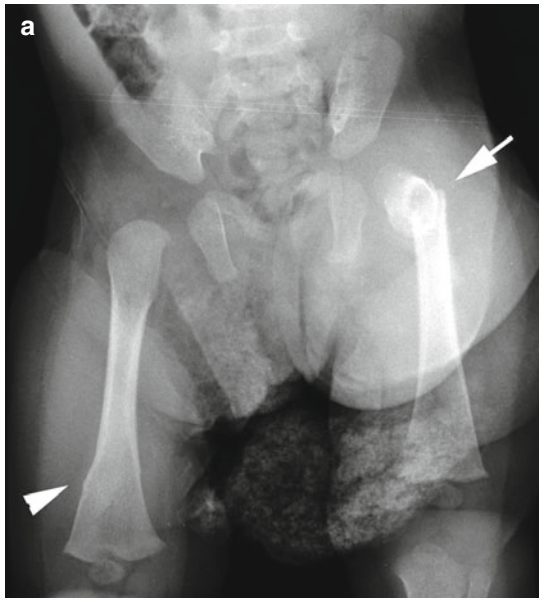


Fig. 12.7 Long bone fracture: outward angulation. (**a**) Note the spiral/oblique midshaft right femoral fracture with outward angulation of the fracture fragments. (**b**) In this infant, a transverse outwardly angled fracture is seen through the midshaft of the right humerus. (**c**) Mechanism of injury. The upper arm or leg is grabbed by the hand, and the bone is then twisted and snapped. The thumb acts as the fulcrum for the snap/fracture



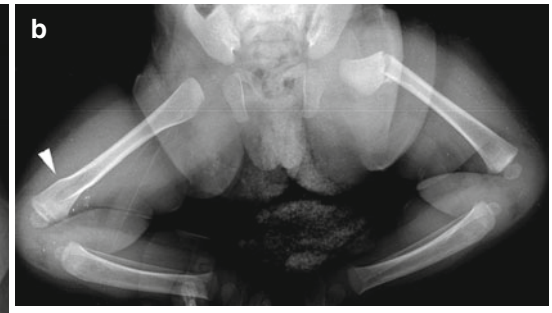
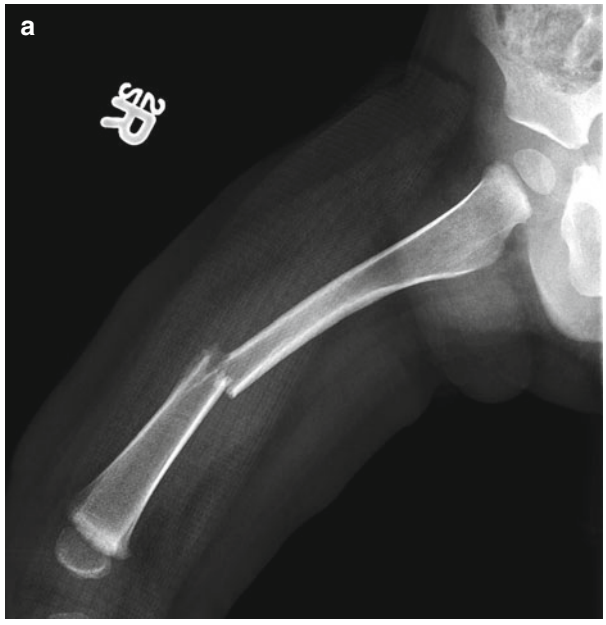


Fig. 12.8 Angled impacted upper femoral fracture. (**a**) Note the impacted outwardly angled upper femoral fracture (*arrow*). Also note a minimal buckle fracture (*arrowhead*) through the distal right femur. (**b**) Frog-leg view more clearly demonstrates the outwardly angled left femoral fracture and again demonstrates the buckle fracture of the distal right femur (*arrow*). There is some soft tissue swelling around this fracture site



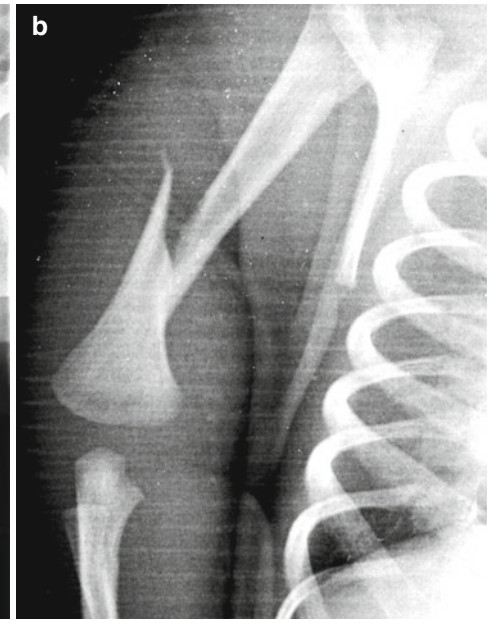


Fig. 12.9 Outward angled femoral and humeral fractures: legitimate. (**a**) Note the slightly outwardly angled transverse fracture through the midshaft of the right femur. This patient was stepped on by a horse. (**b**) Note the spiral outwardly angled fracture through the midshaft of the right humerus. This infant was grabbed by the grandmother as the baby was falling off the edge of the bed. The grandmother heard a snap and the history never changed. It is very important to get the history in these patients because it helps to determine whether the fracture is legitimate or non-accidental

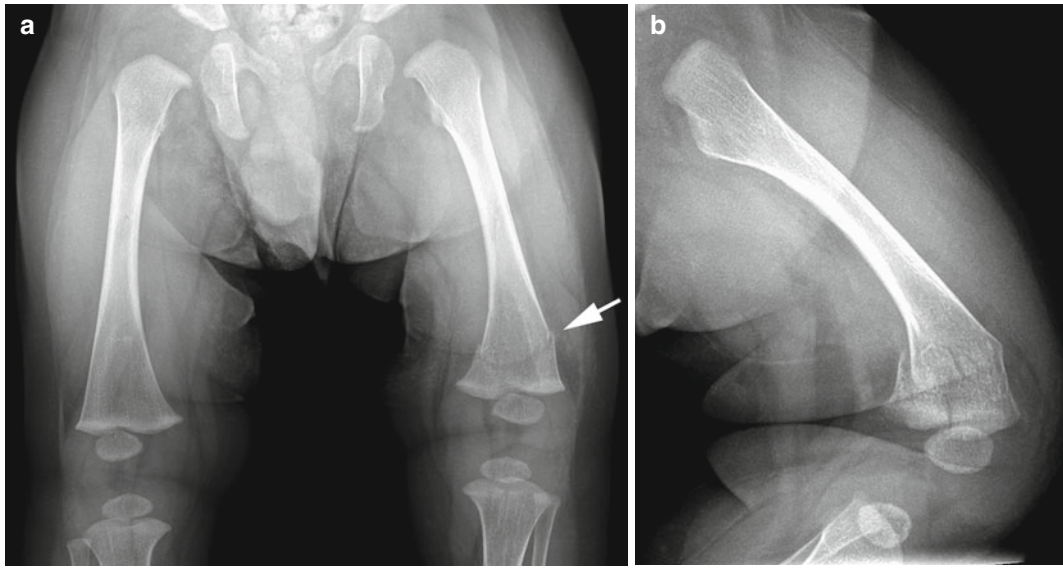


Fig. 12.10 Long bone impaction fractures. (**a**) Note the impacted buckle fracture through the distal left femur (*arrow*). (**b**) Oblique view more clearly demonstrates the extent of the fracture. These fractures, either in the femur or in the humerus, for the most part in our experience are legitimate

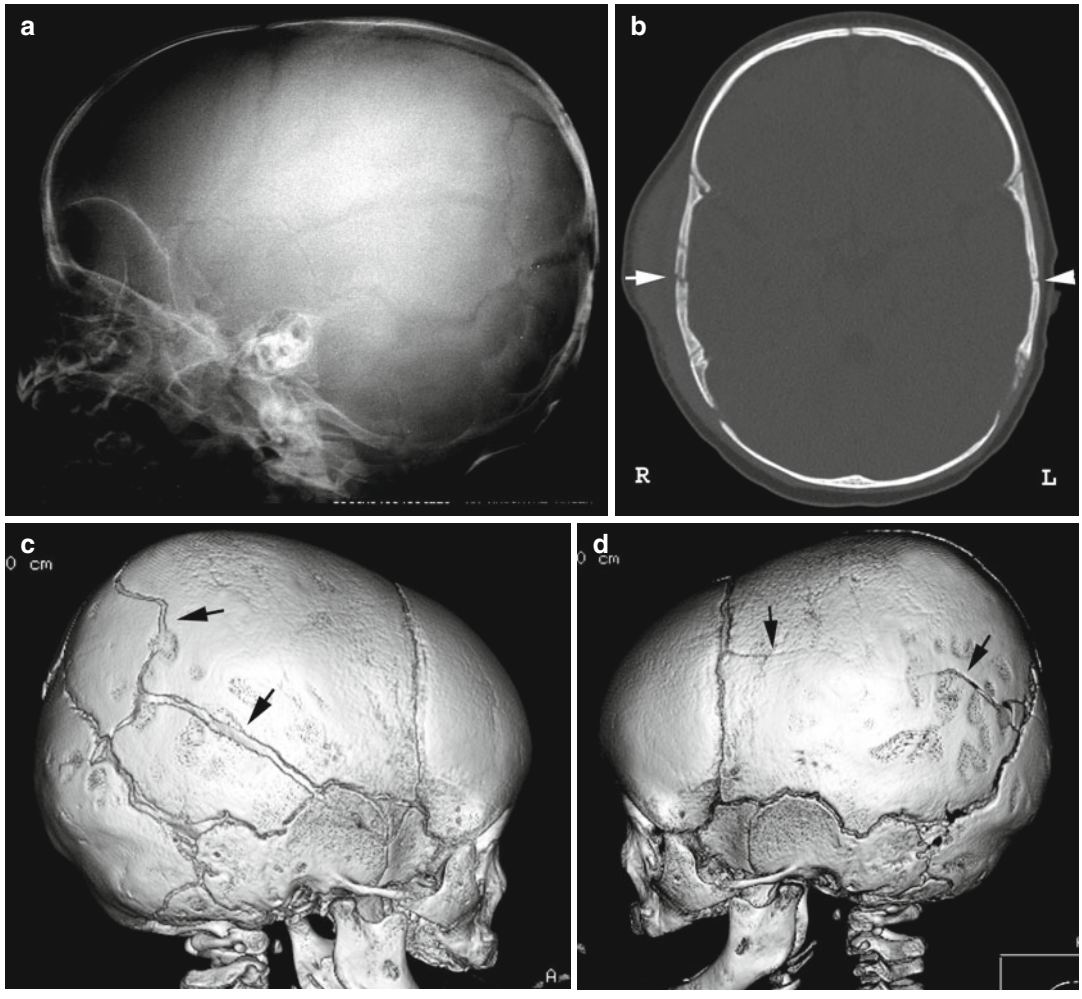


Fig. 12.11 Skull fractures. (**a**) Lateral view of the skull. Note the mid-parietal fracture with extension into the lambdoid suture and superiorly into the posterior parietal bone. (**b**) Axial CT study demonstrates the diastatic right parietal fracture (*arrow*) and an unexpected linear left parietal fracture (*arrowhead*). (**c**) 3D reconstruction clearly demonstrates the diastatic right parietal fracture (*arrows*). (**d**) 3D reconstruction also demonstrates the non-diastatic linear parietal fracture (*arrows*) on the left



Fig. 12.12 Spine fractures. Note the typical hangman fracture (*arrow*) through C2. This was an unexpected finding in a battered infant who had other skeletal findings diagnostic of non-accidental trauma

References

1. Kleinman PK, Marks Jr SC, Nimkin K, Rayder SM, Kessler SC. Rib fractures in 31 abused infants: postmortem radiologic-histopathologic study. Radiology. 1996;200:807–10.
2. Kleinman PK, Schlesinger AE. Mechanical factors associated with posterior rib fractures: laboratory and case studies. Pediatr Radiol. 1997;27:87–91.
3. Kogurt MS, Swischuk LE, Fagan CJ. Patterns of injury and significance of uncommon fractures in the battered child syndrome. AJR. 1974;121:143–9.
4. Kleinman PK, Marks SC, Adams V. Factors affecting the visualization of anterior rib fractures in abused infants. AJR. 1987;150:635.
5. Caffey J. Multiple fractures in long bones of children suffering from chronic subdural hematoma. AJR. 1946;56:163–73.
6. Kleinman PK, Marks SC, Blackbourne B. The metaphyseal lesion in abused infants: a radiologic-histopathologic study. AJR. 1986;146:895–905.
7. Kleinman PK, Sarwar U, Newton AW, Perez-Rossello JM, Rebello G, Herliczek TW. Metaphyseal fragmentation with physiologic bowing: a finding not to be confused with classic metaphyseal lesion. AJR. 2009;192:1266–8.
8. Swischuk LE. Metaphyseal corner fractures in infants: a review. Emerg Radiol. 1998;5:103–7.
9. Chapman T, Sugar N, Done S, Marasignan J, Wanbold N, Feldman K. Fractures in infants and toddlers with rickets. Pediatr Radiol. 2010;40:1184–9.
10. Schilling S, Wood JN, Levine MA, Langdon D, Christian CW. Vitamin D status in abused and non-abused children younger than 2 years old with fractures. Pediatrics. 2011;127:835–41.
11. King J, Diefendorf D, Apthorp J, Negrete VF, Carlson M. Analysis of 429 fractures in 189 battered children. J Pediatr Orthop. 1988;8:585–9.
12. Loder RT, Bookout C. Fracture patterns in battered children. J Orthop Trauma. 1991;5(4):428–33.
13. Leventhal JM, Thomas SA, Rosenfield NS, Markowitz RI. Fractures in young children: distinguishing child abuse from unintentional injuries. Am J Dis Child. 1993;147:87–92.
14. Strait RT, Siegel RM, Shapiro RA. Humeral fractures without obvious etiologies in children less than 3 years of age: when is it abuse? Pediatrics. 1995;96:667–71.
15. Dalton HJ, Slovis T, Helfer RE, Comstock J, Schuerer S, Riolo S. Undiagnosed abuse in children younger than 3 years with femoral fracture. Am J Dis Child. 1990;144:875–8.
16. Shaw BA, Murphy KM, Shaw A, Oppenheim WL, Myracle MR. Humerus shaft fractures in young children: accident or abuse? J Pediatr Orthop. 1997;17:293–7.
17. Hnaey SB, Boos SC, Kutz TJ, Starling SP. Transverse fracture of the distal femoral metaphysis: a plausible accident mechanism. Pediatr Emerg Care. 2009;25(12):840–4.
18. Carrion WV, Dormans JP, Drummond DS, Christofersen MR. Circumferential growth plate fracture of the thoracolumbar spine from child abuse. J Pediatr Orthop. 1996;16:210–4.
19. Diamond P, Hansen CM, Christoferson MR. Child abuse presenting as a thoracolumbar spinal fracture dislocation: a case report. Pediatr Emerg Care. 1994;10:83–6.
20. Gabos PG, Tuten HR, Leet A, Stanton RP. Fracture-dislocation of the lumbar spine in an abused child. Pediatrics. 1998;101:473–7.
21. Kleinman PK, Zito JL. Avulsion of the spinous processes caused by infant abuse. Radiology. 1984;151:389–92.
22. Swischuk LE. Spine and spinal cord trauma in the battered child syndrome. Radiology. 1969;92:733–8.
23. Choudhary AK, Bradford RK, Kias MS, Moore GJ, Boal DKB. Spinal subdural hemorrhage in abusive head trauma: a retrospective study. Radiology. 2012;262:216–23.
24. Rooks VJ, Sisler C, Burton B. Cervical spine injury in child abuse: report of two cases. Pediatr Radiol. 1998;28:193–5.
25. Kleinman PK, Shelton YA. Hangman's fracture in an abused infant: imaging features. Pediatr Radiol. 1997;27:776–7.

Index

A
Achilles tendon, 187
  ultrasonography and MR imaging, 188
Adenopathy, 11, 14, 16
ALPSA, 58
Ankle
  accessory ossicles, 192, 202
  calcaneal apophysis, 192, 202
  distal tibia and fibula, 183–191
  fat pads, 183, 184
  fractures, 183–188
  fluid detection, 183, 184
  Köhler's disease, 192, 200
  plantar fasciitis and stone bruise, 188, 199
    MR imaging, 188
  sprained ankle, 187, 210
  tarsal bones, 184
    aseptic necrosis, 192, 200
    factures, 186–198
    irregular ossification, 193, 203
    osteochondritis dissecans, 191, 200
Anterior labral periosteal sleeve avulsion (ALPSA), 58
Avulsion fractures
  anterior superior and inferior iliac spines, 121, 124
  elbow, 77, 85
  iliac crest, 121, 125
  ischium, 121
  tarsal bones, 186, 197
  trochanters, 121, 122, 125

B
Bankart variant, 58
Battered child syndrome
  bowed legs and beaking, 221, 224
  classic metaphyseal lesion, 221–223
  clavicle fractures, 220, 221
  KUB, 217, 218
  long bone fracture, 222, 225, 227
  metaphyseal corner fractures, 220
  outward angled femoral and humeral fractures, 222, 226
  rib fracture
    healing sequence, 217–220
    location, 221
    mechanics, 217
  skull fractures, 223, 228
  spine, 224, 229
  visceral injury, 224
Benign cortical defect, 19, 22, 24, 25
Bipartite sesamoid bones, 207, 215
Bone cyst, 19–23
  aggressive appearance, 23
  CT study, 19, 23
  fallen fragment sign, 19, 22
  metaphyseal location, 22
Bone infarction, 9, 11
Boxer's fracture, 100, 117
Buckle fractures
  angled configuration, 32, 33
  carpal bones, 93, 104
  distal radius and ulna, 95, 96
  distal tibia and fibula, 185
  elbow, 77, 82
  foot, 195
  hand, 100–114
  proximal ulna, 77, 82
  radial head angled, 71, 81
  types A and B, 31, 32

C
Carpal bones
  aseptic necrosis, 95, 106
  buckle/stress fracture, 93, 104
  dislocations, 96
    lunate and perilunate, 97
  pisiform fracture, 96
  scaphoid fracture, 93, 102
Cellulitis, 5–11
Classic metaphyseal lesion (CML), 221–223
Clavicular injuries
  acromioclavicular separations, 41, 43
  dislocations, 42
  coracoid process, 41, 43
  greenstick fracture, 41, 43
  medial dislocation, 42, 45–47
  plastic bending fracture, 41, 43
  sleeve fracture, 43, 44
Cystic hygroma, 19, 20

L.E. Swischuk, S.P. Jadhav (eds.), *Emergency Musculoskeletal Imaging in Children*,
DOI 10.1007/978-1-4614-7747-1, © Springer Science+Business Media New York 2014

D
Diametric (ring) fractures, 121

E
Elbow
  dislocation, 79
  distal humerus fractures
    lateral condylar, 63, 69–73
    medial condylar, 63, 70, 74–78
    supracondylar, 63–68
  fat pads, 61, 62
  ossification centers, 80, 87
  osteochondritis dissecans, 79, 86
  proximal radius fractures,dislocations, 74, 81
    Monteggia fracture, 71, 89
    radial head angled buckle fracture, 71, 81
    radial head impaction fractures, 71, 79–80
  proximal ulna fractures
    avulsion fractures, 77, 85
    buckle fractures, 77, 82
    coronoid process, 77, 85
    hairline fractures, 77
    transverse fractures, 75
  sail sign, 61
Eosinophilic granuloma, 19, 20, 28
Epiphyseal–metaphyseal fractures
  growth abnormalities, 34
  MRI role, 35
  types, 33–35
Epitrochlear adenitis, 11, 15
Ewing's sarcoma, 21, 165
Exostoses, 19, 26

F
Fallen fragment sign, 19, 22
Fascitis, 11–13
Femoral shaft. *See* Hip and femur
Foot
  bipartite sesamoid bones, 207, 215
  fractures, metatarsals and phalanges, 193–208
  Freiberg's disease, 214
  Jones fracture, 197, 210
  Lisfranc, 203, 211
  os vesalianum, 203, 210
  sesamoid fracture and turf toe, 203, 204, 207, 212, 213
  soft tissues and fat pads, 193
  stress fractures, 204, 213
Forearm
  bowing bones, normal, 81, 89
  greenstick, 80, 81, 88
  Monteggia fracture, 81, 89
  plastic bending fractures, 80, 81, 87, 88
  radiocapitellar line, 81
  vascular grooves, 81, 90
Fractures
  avulsion (*see* Avulsion fractures)
  boxer's, 100, 117
  buckle (*see* Buckle fractures)
  clavicular (*see* Clavicular injuries)
  condylar, lateral (*see* Condylar fractures, lateral)
  diametric (ring), 121
  elbow (*see* Elbow)
  epicondylar, medial (*see* Epicondylar fractures, medial)
  epiphyseal–metaphyseal (*see* Epiphyseal–metaphyseal fractures)
  Galeazzi's, 92, 94
  greenstick (*see* Greenstick fractures)
  humerus (*see* Upper injuries) 58–59
  Jones, 197
  lateral condylar (*see* Lateral condylar fractures)
  lisfranc, 203, 211
  medial epicondylar (*see* Medial epicondylar fractures)
  metaphyseal corner, 220
  monteggia, 71, 81, 89
  navicular compression, 186, 192
  neck, femur impacted, 45, 49
  pelvis (*see* Pelvic fractures)
  pisiform, 96
  plastic bending/bowing (*see* Plastic bending/bowing fractures)
  proximal humeral, 42, 43, 47
  proximal radiol (*see* Proximal radial fractures)
  pseudo-epiphyseal, 48
  pseudofractures (*see* Pseudofractures)
  radial head angled buckle, 71, 81
  radial head impaction, 71, 79–80
  radial, proximal (*see* Radial fractures, proximal)
  rib (*see* Rib fractures)
  sacral, 121, 122
  Salter–Harris (*see* Salter–Harris fractures)
  scaphoid, 93, 102
  scapular (*see* Scapular fractures)
  segond, 160, 169
  skull, 223, 228
  sleeve, 43, 44
  Smith's, 91, 97
  spine, 224, 229
  stress (*see* Stress fractures)
  supracondylar (*see* Supracondylar fractures)
  talar, 185, 191
  toddler (*see* Toddler fractures)
  torus, 31
  transverse, 75
  upper tibial impaction, 142, 145, 146
Freiberg's disease, 214

G
Galeazzi's fracture, 92, 94
Gamekeeper's thumb, 102
Greenstick fractures, 31, 33, 34
  clavicular, 41, 43
  forearm, 80, 81, 87

H
Hand–foot syndrome, 9, 11
Hand injuries
  aseptic necrosis, 102
  boxer's fracture, 100, 117
  buckle (torus) fractures, 100, 114, 115
  crush fracture, 100, 110
  fat pads and soft tissues, 97
  fluid detection, 100
  gamekeeper's thumb, 102
  Salter–Harris fractures, 112
  spiral fracture of phalanx/metacarpal, 110
Hemangioma, 19, 20
Hill–Sachs notch, 50–51
Hip and femur
  fat pads and joint space, 129, 130
  fluid detection in hip joint
  fractures
    femoral shaft, 135, 138
    upper femur, 129–131
  Legg–Perthes disease, 131–133
    subchondral fracture, 131, 132
    SCFE (*see* Slipped capital femoral epiphysis)
  Meyer's dysplasia, 134
  septic arthritis, 129, 130
  transient synovitis, 129, 130
  upper femur fractures, 129–131
Humerus fractures
  proximal humeral, 42, 43, 47
  shaft, 58–59

I
Infarction. *See* Bone infarction
Infection/inflammation. *See* Osteomyelitis; Pyomyositis
Infrapatellar fat pad, 141
Ischiopubic synchondrosis, 122, 127

J
Jones fracture, 197

K
Knee
  ACLtears, 160, 168
  benign cortical (fibrous) defect, 162
  fluid detection, joint, 141–143
  fractures, 143–146
    March, 204
    Stress, 143, 146
    Toddler II, 142–146
    Segond, 160
  normal pat pads and soft tissues, 141, 142
  patella
    avulsed medial fracture fragment, 146
    chondromalacia, 153, 163
    jumper's knee, 153, 161
    lateral condylar fracture, 149, 156
    medial retinacular tear and fracture, 146, 155
    meniscal and cruciate ligament injuries, 157, 166
    Osgood–Schlatter disease, 151, 157, 158 (*see also* Osgood–Schlatter disease)
    osteochondritis dissecans, 153, 164
    patella alta, 149
    Sinding–Larsen–Johansson disease, 153, 158, 159 (*see also* Sinding–Larsen–Johansson disease)
  posteromedial femoral irregularity, 162, 171
Köhler's disease, 192, 200

L
Lateral condylar fracture, 69
Legg–Perthes disease, 131–133
Lisfranc fractures, 203, 211
Little Leaguer
  elbow, medial epicondylar fractures, 71, 77
  shoulder, 48
Lymphangioma, 19, 20

M
Magnetic resonance imaging (MRI)
  epiphyseal–metaphyseal fractures, 35
  osteomyelitis, 5–7, 9, 10
  patellar dislocation, 153, 157
  pyomyositis, 16, 17
  stress fractures, 35–38
March fractures, 204. *See also* Stress fractures
Medial/anteromedial tibial syndrome, 35
Medial epicondylar fractures, 71–78
  little Leaguer's elbow, 71, 77
Metacarpals and phalanges
  aseptic necrosis, 102
  boxer's fracture, 100, 117
  buckle (torus) fractures, 100, 114, 115
  crush fracture, 100, 110
  gamekeeper's thumb, 102
  multiple fractures, 100, 117
  Salter–Harris fractures, 112
  spiral fracture of phalanx/metacarpal, 110
Metatarsals and phalanges
  epiphyseal–metaphyseal injuries, 197
  Jones fracture, 197, 210
  oblique spiral and linear fractures, 195, 204
  os vesalianum, 203, 210
  Salter–Harris III and buckle fractures, 195, 204, 208
  subtle angled buckle fracture, 206, 207
Meyer's dysplasia, 134
Monteggia fractures, 71, 81, 89
Mouzopoulos sign, 45, 51–52
MRI. *See* Magnetic resonance imaging (MRI)

N
Navicular compression fractures, 186, 192
Navicular fat pad, 91–93
Neuroblastoma, 21

Non-accidental trauma. *See* Battered child syndrome
Nonossifying fibroma (NOF), 19, 22, 24, 25
Nuclear scintigraphy
  osteomyelitis, 5
  stress fracture, 35

O
Os acetabulum, 123, 127
Osgood–Schlatter disease, 157–158
Osteochondritis dissecans, 191, 200
  elbow, 79, 86
  knee, 153, 164
  tarsal, 191, 200
Osteochondroma, 19, 26–27
Osteoid osteoma, 19, 26, 27
Osteomyelitis, 5–10
Osteosarcoma, 21
Os vesalianum, 203, 210

P
Patellar dislocation
  avulsed fracture fragment, 146
  lateral condylar fracture, 149, 156
  medial retinacular tear and fracture, 146, 155
Pelvic fractures, 121–125
  avulsion fractures, 121–125
  diametric (ring), 121
  ischiopubic synchondrosis, 122, 127
  os acetabulum, 123, 127
  pseudotumoral appearance, 122, 125
Pisiform fractures, 96
Plastic bending/bowing fractures, 31, 33, 34
  clavicle fractures, 41, 43
  forearm fractures, 80, 81, 87, 88
  leg, 176
Pyomyositis
  abscess, 11, 12
  MRI, 16, 17
  plain radiographs, 11

R
Rib fractures
  healing sequence, 217–220
  mechanics, 217

S
Sacral fractures, 121, 122
Sail sign, 61
Scaphoid fracture, 93, 102
Scapular fractures
  ALPSA, 58
  impaction healing, 54
  linear-stellate, 54
SCFE, 133–134
Segond fracture, 160, 169
Shoulder injuries
  clavicular (*see* Clavicular fractures)
  companion shadow, 42
  humerus injuries (*see* Humerus)
  joint fluid, 2, 41
  os acromiale, 58
  scapular (*see* Scapular fractures)
Sinding–Larsen–Johansson disease, 158–159
Skull fractures, 223, 228
Slipped capital femoral epiphysis, 133–134
Smith's fracture, 91, 97
Spine fractures, 224, 229
Stone bruise, 188
Stress fractures
  carpal bones, 93, 104
  distal femur, and proximal tibia, 143, 152
  foot, 204, 213
  leg, 179
  pelvic, 122
  shin splints, 35
  tarsal, 186, 198
  tibia, upper and proximal, 34, 35, 143, 152
Supracondylar fractures
  anterior humeral line, 63, 65–66
  can-opener effect, 63, 64
  plastic bending fracture, 68
  polo *vs.* hockey stick, 63, 67
  spectrum of, 63, 68
  T fracture, 63

T
Talar fractures, 185, 191
Tarsal bones
  aseptic necrosis, 192, 200
  avulsion fractures, 186, 197
  cuneiform, 186, 194
  compression-impaction fracture, 186–193
  irregular ossification, 193, 203
  osteochondritis dissecans, 191, 200
  stress fracture, 186, 198
  talar fractures, 185–191
Toddler I fracture, 165
Toddler II fracture, 141–143
Tumbling bullet sign. *See* Fallen fragment sign
Tumors. *See also* Bone cyst
  cystic hygroma, 19, 20
  Ewing's sarcoma, 165
  lymphangioma/hemangioma, 19, 20
  malignant bone tumor, 19, 20
  neuroblastoma metastases, 21
  osteosarcoma, 21
  soft tissue tumor, 19

U
Ulnar styloid tip fractures, 92, 101

V
Vacuum joint phenomenon, 123, 128

W
Wrist injuries, carpal bones
aseptic necrosis, 95, 106
buckle/stress fractures, 93, 104
dislocations (*see* Carpal bones)
fat pad and soft tissues, 91, 92
gymnast wrist, 100
pisiform fractures, 96
scaphoid fractures, 93, 102
Smith's fracture, 91, 97
ulnar styloid tip fractures, 92, 101